PB84-192020

REPORT NO.
UCB/EERC-83/19
AUGUST 1983

EARTHQUAKE ENGINEERING RESEARCH CENTER

EFFECTS OF BOND DETERIORATION ON HYSTERETIC BEHAVIOR OF REINFORCED CONCRETE JOINTS

by

F.C. FILIPPOU
E.P. POPOV
V.V. BERTERO

Report to the National Science Foundation

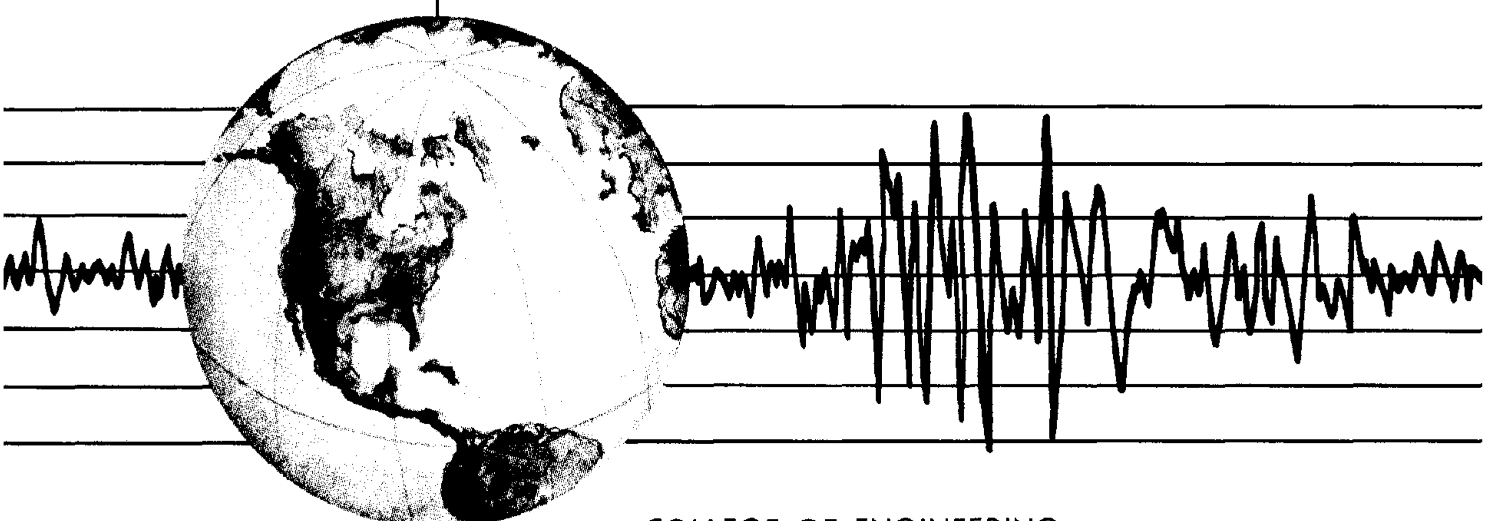

COLLEGE OF ENGINEERING

UNIVERSITY OF CALIFORNIA · Berkeley, California

For sale by the National Technical Information Service, U.S. Department of Commerce, Springfield, Virginia 22161.

See back of report for up to date listing of EERC reports.

50272-101

REPORT DOCUMENTATION PAGE	1. REPORT NO. NSF/CEE-83032	2.	3. Recipient's Accession No. PB8 4 192020

4. Title and Subtitle Effects of Bond Deterioration on Hysteretic Behavior of Reinforced Concrete Joints	5. Report Date August 1983
	6.
7. Author(s) F.C. Filippou, E.P. Popov, and V.V. Bertero	8. Performing Organization Rept. No. UCB/EERC-83/19
9. Performing Organization Name and Address Earthquake Engineering Research Center University of California 1301 South 46th Street Richmond, CA 94804	10. Project/Task/Work Unit No.
	11. Contract(C) or Grant(G) No. (C) (G) CEE81-07217
12. Sponsoring Organization Name and Address National Science Foundation 1800 "G" Street, NW Washington, DC 20550	13. Type of Report & Period Covered
	14.

15. Supplementary Notes

16. Abstract (Limit: 200 words)

The work presented in this report is concerned with developing an analytical model which describes the hysteretic behavior of reinforced concrete beam-column joints. The model takes into account the interaction of reinforcing steel and surrounding concrete through bond and the deterioration of such interaction under cyclic deformation reversals. The cyclic deterioration of bond results in relative slippage of reinforcing bars with respect to concrete thus giving rise to significant concentrated rotations at the beam-column interface. The model is presented for interior joints, its extension to exterior joints and girder inelastic regions is indicated.

17. Document Analysis a. Descriptors

b. Identifiers/Open-Ended Terms

c. COSATI Field/Group

18. Availability Statement:	19. Security Class (This Report)	21. No. of Pages
Release Unlimited		205
	20. Security Class (This Page)	22. Price

(See ANSI–Z39.18) See Instructions on Reverse OPTIONAL FORM 272 (4–77) (Formerly NTIS–35) Department of Commerce

EFFECTS OF BOND DETERIORATION ON HYSTERETIC BEHAVIOR OF REINFORCED CONCRETE JOINTS

by

Filip C. Filippou

Assistant Professor of Civil Engineering
University of California, Berkeley

Egor P. Popov

Professor of Civil Engineering
University of California, Berkeley

Vitelmo V. Bertero

Professor of Civil Engineering
University of California, Berkeley

A report on research sponsored by the
National Science Foundation

Report No. UCB/EERC-83/19
Earthquake Engineering Research Center
College of Engineering
University of California
Berkeley, California

August 1983

EFFECTS OF BOND DETERIORATION ON HYSTERETIC BEHAVIOR OF REINFORCED CONCRETE JOINTS

ABSTRACT

The work presented in this report is concerned with developing an analytical model which describes the hysteretic behavior of reinforced concrete beam-column joints. The model takes into account the interaction of reinforcing steel and surrounding concrete through bond and the deterioration of such interaction under cyclic deformation reversals. The cyclic deterioration of bond results in relative slippage of reinforcing bars with respect to concrete thus giving rise to significant concentrated rotations at the beam-column interface. The model is presented for interior joints; its extension to exterior joints and girder inelastic regions is indicated.

In Chapter 2, following the introductory material presented in Chapter 1, the analytical description of the interaction of reinforcing steel and surrounding concrete along the anchorage length of the bars is given. The relative slip of reinforcing bars with respect to the surrounding concrete results in the formation of large cracks which run perpendicular to the axis of the girder. In order to provide the necessary number of equations describing the hysteretic moment-rotation relation of a R/C member, the equilibrium of horizontal forces and bending moments has to be satisfied at the cracked reinforced concrete sections. This necessitates the development of a new cracked R/C section model which accounts for the effects of bond deterioration in the vicinity of the crack in establishing the equilibrium of steel and concrete forces at a cracked section. This model is presented in Chapter 3 along with material models describing the stress-strain relation of reinforcing steel as well as the bond stress-slip behavior under arbitrary cyclic excitations.

Details on the numerical solution algorithm are presented in Chapter 4. The algorithm consists of three nested iteration loops, which arise when the boundary value problem of Chapter 2 is solved using transfer matrices and a numerical "shooting technique".

Comparison of analytical predictions with experimental evidence from two interior beam-column subassemblages is presented in Chapter 5. Satisfactory agreement is exhibited by the proposed model. The reported results allow insight into the physical behavior of R/C beam-column joints which can lead to improvements in the earthquake resistant design of moment resisting frames.

In Chapter 6 a series of analytical parametric studies on an interior beam-column joint are reported. Parameters varied include: bond strength along anchorage length in the joint, ratio of top to bottom reinforcement, yield strength of reinforcing bars, history of loading and effects of model scale of R/C members.

ACKNOWLEDGEMENTS

The studies reported herein were conducted as part of the research supported by the National Science Foundation under Grant No. CEE 81-07217. The work described was carried out by Filip C. Filippou in partial fulfillment of the requirements for the degree of Doctor of Philosophy in Engineering and was supervised by Professors E. P. Popov and V. V. Bertero. This report essentially reproduces the first part of the dissertation.

The authors are indebted to Professors Robert L. Taylor and Beresford N. Parlett for their valuable comments in reviewing the dissertation.

The authors also express their gratitude to Dr. Rolf Eligehausen and Professor Vincenzo Ciampi for fruitful discussions on the experimental and analytical intricacies of the bond problem.

The first author would like to thank Keith Hjelmstad, Lucia Longhi, Bahram and Shahram Nour-Omid, Gordon Oliver and Juan Simo for fruitful discussions during the course of this work.

The figures have been prepared by Gail Feazell.

Table of Contents

LIST OF FIGURES

CHAPTER 1

INTRODUCTION

1.1. General

Reinforced concrete structures designed according to present building codes as moment resisting space frames, shear-walls, coupled shear-walls or any combination thereof to withstand strong earthquake motions are expected to deform well into the inelastic range and dissipate the energy input by the base motion through stable hysteretic behavior of structural components. Since inelastic deformations are typically concentrated at certain critical regions within the structure [9], the accurate prediction of the mechanical behavior of the structure during earthquake excitations depends on the development of reliable analytical models which describe the hysteretic behavior of these regions.

Ideally these models should be based on an accurate representation of material behavior taking into account the controlling states of stress or strain and identifying the main parameters which influence the hysteretic behavior of each critical region in order to predict the behavior up to failure of any structural component during the earthquake response. Such models will allow the designer to identify weak links in any initial design, which can then be redesigned to prevent premature loss of strength and stiffness, thus assuring that the structure will behave satisfactorily under severe seismic excitations by dissipating the energy input through stable hysteretic behavior of its components.

Following present earthquake resistant design philosophy the energy input by the base motion should be dissipated in the largest possible number of inelastic regions within the structure. Ductile moment resisting space frames as well as coupled wall systems are designed so that yielding starts to develop at the girder ends. Columns of a ductile moment resisting space frame should remain elastic during the earthquake response, except at the base of the building, to avoid the formation of a partial sidesway collapse mechanism. Attention is thus focused on understanding and predicting the hysteretic behavior of critical regions in girders as well as that of beam-column or girder-wall joints.

Various experimental studies of reinforced concrete structural subassemblages [9],[13], actual multistory buildings and dynamic tests of model frames have demonstrated that, when properly designed and detailed critical regions of R/C structures are subjected to severe cyclic excitations, the major concern is the deterioration of stiffness.

The principal effects of stiffness deterioration are:

(1) an increase in the flexibility and period of vibration of the virgin structure during large deformation reversals,

(2) a decrease in energy dissipation capacity,

(3) a significant redistribution of internal forces leading to excessive deformations in some regions.

Since induced seismic forces and deformations are sensitive to structural flexibility, natural period of vibration and energy dissipation capacity, stiffness deterioration modifies the overall response of the structure.

In R/C girders and beam-column joints stiffness deterioration under large cyclic excitations can be attributed to several factors. Among the most important are:

(1) Bauschinger effect of reinforcing steel,

(2) concrete cracking and splitting along reinforcing bars,

(3) cyclic deterioration of bond between reinforcing steel and surrounding concrete,

(4) shear sliding in regions with cracks running through the entire depth of the member.

(5) crushing and spalling of concrete

Except for the Bauschinger effect of reinforcing steel and the crushing of concrete all other factors are directly or indirectly related to cyclic bond deterioration between reinforcing bars and surrounding concrete.

In the case of critical regions forming at the ends or near the midspan of girders cracks appear early in the response time history. Some bond deterioration in the girder region adjacent to the crack contributes to crack opening. The deterioration of bond increases significantly, as soon as the yield strength of the reinforcement is exceeded at a cracked section. Several moment reversals cause damage of bond in the region around the crack leading to significant slippage of reinforcing bars and consequently to large concentrated rotations at the cracked section. During moment reversal the crack can remain open through the depth of the member leaving the shear to be resisted by dowel action of the reinforcement. This initiates splitting of concrete cover and shear sliding near the crack. Most importantly cyclic deterioration of shear and bond resistance mechanisms accounts for the observed stiffness deterioration in critical regions of R/C girders. The adverse effects of loading reversals on stress transfer between steel and concrete become more pronounced in beam-column and girder-wall joints. Since this study concentrates on the seismic response of R/C frames, only the problem of beam-column joints will be referred to from now on.

A number of experimental studies on the hysteretic behavior of R/C beam-column subassemblages [43,50] has shown that in moment-resisting frames, designed according to current practice, the most unfavorable bond conditions exist in interior beam-column joints leading to significant fixed-end rotations at the beam-column interfaces. This is because high beam bending moments acting at the faces of the columns cause yielding of the main rebars anchored in the joint and high joint shear forces induce cracks which damage the bond of the embedded bars. Under cyclic moment reversals, cracks across the whole beam cross section may form at both column faces. These cracks may remain open throughout most of the cyclic loading. This causes the reinforcing bars anchored in the joint to be subjected to cyclic pull from one side and push from the other thus inducing substantial bond deterioration. If, as is often the case, the width of the column is not sufficient to offer the required anchorage, the incurred bond damage leads to the eventual pull-through of the reinforcing bars. Therefore anchorage of reinforcement becomes a serious problem as it leads to substantial reduction in stiffness and energy dissipation capacity of the joints. Experimental results show that fixed-end rotations due to bond deterioration in the joint can contribute up to 50% to overall deflections of beam-column subassemblages after yielding of the reinforcement [43].

In the case of exterior beam-column joints loss of stiffness and energy dissipation capacity is also a problem. Because the main reinforcing bars of the girder are usually anchored with a 90-degree hook, these do not pull out in this case. However, large relative slippage does occur leading to significant stiffness deterioration.

It becomes apparent from the above that any analytical model for accurately predicting the hysteretic behavior of girders and beam-column joints, should include a formulation of bond stress-slip between reinforcing steel and concrete under arbitrary cyclic excitations. Moreover the analytical model should be capable of representing the physical behavior of reinforced concrete sections at discrete cracks under the combined action of bending moments and shearing forces. The discrete nature of cracks in R/C members subjected to cyclic excitations in connection with the transfer of forces between reinforcing steel and surrounding concrete appears to be of special importance since it helps to determine the length of plastic hinges in girders.

The main drawback of such a refined model is the prohibitive cost of computation, which prevents its use in earthquake response analysis of entire structures. This shortcoming notwithstanding the model can serve several important purposes:

(1) complement experimental studies by allowing inexpensive analytical "experiments" with a wide range of variation of main parameters to be conducted and thus contribute to the understanding of the significance of each of these parameters in the physical

behavior of R/C critical regions,

(2) provide valuable information for the development of simplified models, which would reproduce satisfactorily the important features of the observed response, while retaining simplicity and computational efficiency, thus facilitating their use in earthquake response analysis of structures,

(3) contribute to the needed integration of analytical and experimental studies in order to select realistic load histories for experimental investigations.

Beyond any interest to understand and predict the hysteretic behavior of R/C critical regions, there is a need to establish the relative contribution of beam inelastic regions and beam-column joints to the total energy dissipated by a structure which is subjected to severe ground shaking. It is believed that only accurate analytical models of hysteretic behavior of these critical regions can yield an answer to the above question thus helping to predict the probable nonlinear response of structures to seismic excitations and improve existing earthquake resistant design methods and code provisions.

1.2. Review of previous studies

1.2.1. Experimental studies

A large number of experimental investigations into the hysteretic behavior of R/C members, structural subassemblages and model structures has been conducted in the last two and a half decades following the First Conference on Earthquake Engineering in 1956. An extensive review of the most significant contributions has been presented in state-of-the-art reports in 1973 and 1979 by Bertero [9], [10]. Here only a small number of experimental studies concerned with the behavior of R/C beam-column joints and critical regions in girders subjected to bending with low shear will be reviewed.

Following the pioneering experimental work of Aoyama [6], Sinha et al. [41] and Agrawal et al. [3] tested a series of singly and doubly reinforced simply supported concrete beams under cyclic loading. Similar tests were performed by Park and Sampson [38] and Bertero et al. [12]. These investigations have shown that, for deformations beyond the first yielding, the behavior of critical regions subjected to moment reversals is largely controlled by the mechanical characteristics of steel and its bond to concrete. Significant bond deterioration takes place along reinforcing bars in the vicinity of cracks as moment reversals increase in number and magnitude.

Brown and Jirsa [15] subjected twelve reinforced concrete cantilever beams to reversals of overload and noted among others that the deformation of steel in the anchorage zone contributed significantly to the total deflection of the specimens.

An extensive investigation into the hysteretic behavior of half-scale R/C rectangular and T-beams was conducted by Ma, Bertero and Popov [31]. Several parameters were varied and their effect on the hysteretic behavior of the specimens was established. These included: the ratio of top to bottom reinforcement, moment to shear ratio, loading history and effect of slab.

Early experiments on the hysteretic behavior of beam-column joints were also initiated at PCA where Hanson and Connor [27] tested seven exterior connections finding their behavior in most cases satisfactory.

Following these experiments a series of interior beam to column subassemblages were tested at Berkeley by Soleimani et al. [43]. The cruciform shaped half-scale assemblies specifically designed to study the behavior of interior joints were subjected to monotonic as well as cyclic loading simulating the effect of severe seismic excitations. The results indicated that bond deterioration in the joint leads to significant fixed-end rotations influencing the subassemblage response. Similar tests were conducted at the University of Canterbury [37] and University of Texas [28], to name only a few, where however the major concern of the investigation lay with establishing the shear capacity of the beam-column panel region and arriving at a set of design recommendations which prevent shear failure of the joint. In these studies the significant contribution of reinforcing bar slippage to the overall subassemblage deflection was noted and recommendations for alleviating the problem were offered much along the lines of earlier suggestions by Bertero and Popov [13].

As a result of the knowledge gained from the above studies, further efforts were initiated to establish a bond stress-slip relationship under generalized excitations. A general review of research conducted on the subject at Berkeley was presented by Popov in Ref. [39]. A more detailed review of the bond problem is contained in Ref. [23]. Based on the results from an extensive experimental investigation Eligehausen et al. [23] formulated a general bond stress-slip relation for deformed bars embedded in well-confined concrete and subjected to generalized load histories.

1.2.2. Analytical studies

Several attempts to predict analytically the hysteretic behavior of reinforced concrete girders and beam-column joints subjected to cyclic excitations have been reported.

Early works by Aoyama [6], Agrawal et al. [3], Park and Sampson [38] employed simple beam theory and material models for reinforcing steel and concrete of various degrees of sophistication in order to predict the hysteretic moment- curvature relationship of reinforced concrete sections. Bertero and Bresler [11] were the first to discuss the possible effects of shear and bond forces on the behavior of critical regions adjacent to beam-column joints. They proposed a more accurate curvature formulation to account for slippage of reinforcing bars and considered explicitly crack opening and closing. A precise evaluation was not possible due to lack of experimental data. Brown and Jirsa [15] calculated theoretical load deflection curves for cantilever beams using an assumed curvature distribution along the span of the cantilever and including the effect of shear forces and anchorage slip by incorporating measured values.

The cost of computation associated with the above section layer models precludes their use in earthquake response analysis of structures. This fact led to the development of simplified global models describing the end moment-end rotation relation of structural members [20], [26] by assuming the inelastic behavior of girder end regions lumped into plastic point hinges or rotational springs at the ends of the member. To describe the hysteretic response of plastic hinges in R/C structures Clough [19] proposed a bilinear stiffness degrading model. Later Takeda et al. [46] introduced a more refined trilinear model accompanied by a set of sixteen rules for hysteretic behavior.

Mahin and Bertero [32] have discussed several problems which arise when lumped plasticity models are used in seismic resistant design. In particular, it was noted that such models are incapable of predicting reliably curvature and rotational ductility demands in reinforced concrete members. Anagnostopoulos [4] has presented further details on the inconsistencies of assigning proper strain hardening values to point hinge moment-rotation relations and the resulting discrepancies in curvature ductility estimates.

With the rapid development of the finite element method many investigators attempted to gain insight into the hysteretic nonlinear response of reinforced concrete members by subdividing them into a number of finite elements. The structures analyzed included simple beams, shear panels and more complicated subassemblages, usually subjected to monotonic loading only due to the prohibitive cost of computation. A few studies under cyclic loading were reported by Darwin and Pecknold [22] and Bažant and Bhat [8]. Due to the complexity of formulation and lack of experimental data, the problem of incorporating discrete cracks and an accurate bond-slip model remained unresolved. A review of the progress achieved in the finite element analysis of reinforced concrete structures is given in Ref. [1] and some recent contributions were presented at the IABSE Colloquium in Delft [2].

The attempts to derive models of hysteretic joint behavior and incorporate them in the nonlinear earthquake response analysis of structures are more recent. The proposed models can generally be divided in two groups.

The first group consists of models arrived at in connection with experiments performed on full or reduced scale beam-column joints subjected to cyclic excitations. Townsend and Hanson [49] introduced a set of polynomial expressions which represent the hysteretic behavior of beam-column connections and account for the observed stiffness deterioration. Soleimani et al. [44] introduced the concept of effective length by which the curvature at the beam-column interface is multiplied to yield the fixed-end rotation. Anderson and Townsend [5] proposed a degrading trilinear joint model whose parameters are determined to match a series of experimental results from exterior beam-column joint tests.

In general this group comprises models composed of geometric curves and a set of rules defining hysteretic behavior. They seem to agree well with the experiments they were derived from, it appears doubtful however whether they can be generalized to different configurations and other loading conditions, since the parameters defining hysteretic behavior are selected to fit obtained experimental results and are not derived from physical interpretation of the mechanisms contributing to such behavior.

The second group of joint models includes formulations derived in connection with analytical studies. These models are typically composed of a bilinear or trilinear monotonic envelope curve and an associated set of hysteretic rules defining behavior under cyclic load reversals. Otani [36] computed the characteristic points of the bilinear envelope curve by assuming that bond stresses are constant along the development length of reinforcing bars. The fixed-end rotation was found to be proportional to the square of the moment acting at the beam-column interface. Takeda's rule was used as the associated hysteretic rule. Emori and Schnobrich [25] used the same assumptions along with a trilinear envelope curve. Banon et al. [7] employed a bilinear envelope curve in connection with Takeda's hysteretic rule and included the observed pinching effect due to bond slip and shear sliding. The model was used to represent the inelastic deformations due to slippage of the reinforcement.

One inherent shortcoming of all previous models is the fact that the experimentally observed slip-through of reinforcing bars in interior joints of commonly used dimensions is not taken into account; this leads to an interaction between the two column ends so that no unique moment-rotation relationship can be derived for one end, unless the actions at the other end are accounted for. Moreover they fail to provide an understanding and analytical description of the mechanisms leading to the observed significant stiffness deterioration in R/C beam-column joints.

Recently an accurate finite element study has been reported [34]. It seems to model fairly well the behavior of beam-column subassemblages under monotonic loading with due account of shear deformations and bond slip between steel and concrete. The computational effort spent for monotonic loading is enormous so that little hope remains for an efficient description of several cycles of seismic excitation using this approach.

1.3. Objectives

The research described herein was undertaken because of the need for developing reliable analytical models to predict the hysteretic behavior of reinforced concrete structures. The research has endeavored to study the effects of reinforcing bar slippage on the hysteretic response of beam-column joints as well as inelastic regions of beams and to include these effects in earthquake response analyses of R/C moment resisting frames. An attempt is also made to model the behavior of large cracks in beams under load reversals, as they influence significantly the response of R/C members.

The objectives of the investigation reported herein can be summarized as follows:

(1) to develop an accurate model describing the behavior of beam-column joints and inelastic regions of beams under generalized excitations,

(2) to use the model in conducting a series of parametric studies in order to establish the effect of material behavior, proportioning of members and reinforcement arrangement on the response of R/C beam-column joints,

(3) to arrive at recommendations regarding the design of R/C joints which enable satisfactory hysteretic behavior to be attained,

CHAPTER 2

ANALYTICAL MODEL FOR HYSTERETIC BEHAVIOR OF REINFORCED CONCRETE MEMBERS

When medium or high rise reinforced concrete moment resisting frames are subjected to severe seismic excitations, the behavior of members in the lower parts of a building is controlled by lateral forces. In a typical lower story the combined action of high lateral loads and relatively small gravity forces gives rise to the moment distribution shown in Fig.2.1d. It is to be particularly noted that the end moments at the beam-column interfaces of an interior joint act in the same sense. Upon reversal of lateral force direction a complete reversal of bending moments takes place at the girder end regions.

In order to gain some insight into the mechanical behavior of R/C members subjected to moment reversals with low shear stresses and motivate the analytical solution to be developed in this chapter, an interior beam-column joint is chosen as a representative example (Fig.2.2). The joint is typical of the ones in the lower stories of a building, so that the end moments imposed upon it act in the same sense (Fig.2.2a).

When the joint is first loaded beyond yielding to point A (Fig.2.2b), large cracks open at both beam-column interfaces and bond is damaged along the shaded portions of the reinforcing bars (Fig.2.2c). Upon reversal of moment to point B (Fig.2.2b) cracks open on the opposite side of the girder sections indicating bond damage in their vicinity (Fig.2.2d). The old cracks may or may not close depending on the magnitude of the reversing moments and the ratio of top to bottom reinforcement, since the tensile yield force may not be sufficient to yield the bars under compression. At the beginning of reloading (point C in Fig.2.2b), previously incurred bond damage causes that only small frictional bond stresses resist reinforcing bar slip in the shaded portion of the bars (Fig.2.2e). Therefore a certain amount of slip must be overcome in these regions before larger steel stresses can build up. This phenomenon leads to the characteristic pinching effect in the hysteretic moment-rotation relation (Fig.2.2b).

In order to formulate an analytical model describing the hysteretic behavior of R/C members with due account of cyclic bond deterioration between reinforcing steel and concrete, the region of the member undergoing inelastic action is divided into a number of subregions at locations where cracks form (Fig.2.3). In members subjected to severe moment reversals with low shear stresses, cracks run almost vertically through the depth of the cross-section. The positions where cracks are expected to form are not known a priori and can be established in the course of an analysis by determining the sections where the concrete tensile strength is first exceeded. In the present model for reasons of simplicity the cracks have been assumed to run vertically across the section and form at predetermined locations. This is, strictly speaking, true only at beam-column interfaces of interior and exterior joints.

The hysteretic response of each subregion is determined by satisfying the equilibrium of horizontal forces and bending moments at both end sections and by establishing the stress transfer between steel and concrete within the region. Bond deterioration in both subregions adjacent to a crack contributes to crack opening and to the associated relative rotation of crack surfaces and has to be accounted for.

It is apparent that joint and girder regions can be modeled using the same analytical formulation, the only difference being the imposed boundary conditions.

In the present investigation the shear transfer within each subregion as well as the shear transfer at a fully cracked section is not considered. Shear transfer at cracks which remain open through the depth of a member can become an important problem and deserves a thorough investigation. Moreover moment gradients within the joint region are often large enough to cause diagonal cracking leading to shear deformations which affect the hysteretic joint behavior. Here it is assumed that the joints under consideration are properly designed and detailed to prevent diagonal cracking and preclude significant shear deformations. Although not pursued in the present study, it is believed that the inclusion of shear effects within the framework of the proposed analytical model does not present any conceptional difficulties.

As a first step towards formulating an analytical model to describe the hysteretic behavior of R/C members subdivided by cracks into several subregions, the transfer of steel stresses along a portion of a single reinforcing bar between two adjacent cracks (Fig.2.4) subjected to arbitrary load or deformation reversals will be presented. The explicit solution of the stress transfer problem within each subregion yields a steel force-slip relation at each crack bounding the subregion. The steel force-slip relations for each reinforcing layer are complemented by equations expressing the equilibrium of horizontal forces and bending moments which are established at the cracked end sections of the subregion. The resulting set of nonlinear equations describes the hysteretic behavior of the subregion under consideration and its interaction with neighboring subregions. In this manner all subregions can be assembled to yield the response of the entire member for the imposed global boundary conditions.

2.1. Model of a single reinforcing bar embedded in concrete

A portion of a single reinforcing bar between two adjacent cracks is depicted in Fig.2.4. The differential equations of bond are (Fig.2.5a),

$$A \frac{d\sigma_s}{dx} = q \, \Sigma_o \tag{2.1}$$

$$\epsilon_s - \epsilon_c = \frac{du}{dx} \tag{2.2}$$

$$\epsilon_s = f(\sigma_s) \tag{2.3}$$

$$q = \hat{q}(u) \tag{2.4}$$

where σ_s: steel stress

u : relative slip of reinforcement with respect to surrounding concrete

q : bond stress as a function of relative slip

ϵ_s: steel strain

ϵ_c: concrete strain

A : reinforcing bar area

Σ_o: reinforcing bar circumference

Eq. (2.1) represents the equilibrium of forces acting on an infinitesimal bar element of length dx, where bond stresses q are assumed uniformly distributed along the bar circumference. Eq. (2.2) is the strain-displacement relation, and Eqs. (2.3) and (2.4) are the constitutive equations. Boundary conditions are imposed at a crack only, i.e. at $x=0$ and $x=L$ in Fig.2.4.

In the present study the contribution of concrete to the relative slip in Eq. (2.2) is neglected. Uncertainties exist in assigning accurately an effective concrete area in order to compute concrete stresses and consequently strains. Moreover attention is focused on the post-yield behavior of members and notably on large inelastic excursions. In this case the deformations due to concrete strains contribute very little to the relative slip and can be neglected.

The approach for solving Eqs. (2.1)-(2.4) adopted in the present study is derived from earlier developments by Tassios and Yannopoulos [47] and more recently by Ciampi et al. [18]. Here, however, a more general approach is followed in the context of mixed finite element methods, which allows a better understanding of the approximations involved and a wider choice of numerical integration schemes depending on the accuracy desired.

Starting from Eqs. (2.1)-(2.4) a weighted residual formulation leads to the following two equations:

$$\int_L \overline{W}(x) \left[A \frac{d\sigma_s}{dx} - q(u) \Sigma_o \right] dx = 0 \tag{2.5}$$

$$\int_L \overline{V}(x) \left[\frac{du}{dx} - f(\sigma_s) \right] dx = 0 \tag{2.6}$$

where Eq. (2.3) has been used to substitute for ϵ_s in Eq. (2.2), and $\overline{W}(x)$, $\overline{V}(x)$ are weighting functions to be specified later.

Before proceeding to a solution scheme for Eqs. (2.5) and (2.6) linearization of the nonlinear functions $\hat{q}(u)$ and $f(\sigma_s)$ needs to be considered. Since the problem at hand is one-dimensional, it can be treated using either a secant or a tangent stiffness approach. In this study the incremental secant stiffness formulation has been adopted, which avoids some of the problems inherent to the tangent stiffness schemes in connection with functions of zero or negative slope like function $\hat{q}(u)$.

Introducing the relations

$$q(u+\Delta u) = q(u) + s(u)\,\Delta u \tag{2.7}$$

$$f(\sigma_s+\Delta\sigma_s) = f(\sigma_s) + t(\sigma_s)\,\Delta\sigma_s \tag{2.8}$$

and trying to satisfy Eqs. (2.5) and (2.6) for $u + \Delta u$ and $\sigma_s + \Delta\sigma_s$ leads to two simultaneous equations,

$$\int_L \overline{W}(x) \left\{ A \frac{d}{dx}(\sigma_s+\Delta\sigma_s) - \Sigma_o \left[q(u)+s(u)\,\Delta u \right] \right\} dx = 0 \tag{2.9}$$

$$\int_L \overline{V}(x) \left\{ \frac{d}{dx}(u+\Delta u) - \left[f(\sigma_s)+t(\sigma_s)\,\Delta\sigma_s \right] \right\} dx = 0 \tag{2.10}$$

which can be written as,

$$\begin{aligned} &\int_L \overline{W}(x) \left[A \frac{d}{dx}(\Delta\sigma_s) - \Sigma_o\, s(u)\,\Delta u \right] dx + \\ &\int_L \overline{W}(x) \left[A \frac{d\sigma_s}{dx} - \Sigma_o\, q(u) \right] dx = 0 \end{aligned} \tag{2.11}$$

$$\int_L \overline{V}(x) \left[\frac{d}{dx}(\Delta u) - t(\sigma_s)\,\Delta\sigma_s \right] dx + \int_L \overline{V}(x) \left[\frac{du}{dx} - f(\sigma_s) \right] dx = 0 \tag{2.12}$$

or,

$$\int_L \overline{W}(x) \left[A \frac{d}{dx}(\Delta\sigma_s) - \Sigma_o \, s(u) \, \Delta u \right] dx = R_1 \tag{2.13}$$

$$\int_L \overline{V}(x) \left[\frac{d}{dx}(\Delta u) - t(\sigma_s) \, \Delta\sigma_s \right] dx = R_2 \tag{2.14}$$

where R_1 and R_2 are the residuals of Eqs. (2.5) and (2.6) for the state (u, σ_s). In the above equations Δ denotes a finite increment of the corresponding variable, and $s(u)$ and $t(\sigma_s)$ are the incremental secant stiffnesses of the bond stress-slip and steel stress-strain relation, respectively.

Since Eqs. (2.5) and (2.6) are satisfied at each load step within a very small tolerance, R_1 and R_2 have been set equal to zero in Eqs. (2.13) and (2.14). If a refined numerical scheme is sought, the residuals of the previous step can be taken into account when solving Eqs. (2.13) and (2.14).

In order to solve Eqs. (2.13) and (2.14) for the unknown increment functions $\Delta u(x)$ and $\Delta\sigma_s(x)$ the bar is subdivided into a number of linear elements connected at nodes $1, 2, , \ldots, i, i+1, \ldots, n$ as shown in Fig.2.5b.

Functions $\Delta u(x)$ and $\Delta\sigma_s(x)$ can be discretized independently by means of shape functions $N_I(x)$ and $M_J(x)$ leading to a mixed finite element formulation [48],

$$\Delta u(x) = N_I(x) \, \Delta u_I \tag{2.15}$$

$$\Delta\sigma_s(x) = M_J(x) \, \Delta\sigma_J \tag{2.16}$$

where $\Delta\mathbf{u}$ is a vector of nodal displacement increments and $\Delta\boldsymbol{\sigma}$ a vector of nodal stress increments. Subscripts I and J refer to an arbitrary node along the bar. Summation over repeated indices of all nodal contributions is implied.

Weighting functions $\overline{W}(x)$ and $\overline{V}(x)$ can be discretized in a similar manner, i.e.

$$\overline{W}(x) = P_K(x) \, W_K \tag{2.17}$$

$$\overline{V}(x) = R_L(x) \, V_L \tag{2.18}$$

By substituting Eqs. (2.15-2.18) into Eqs. (2.13) and (2.14), the following equations result

$$W_K \int_L P_K \left[A\ M_{J,x}\ \Delta\sigma_J - \Sigma_o\ s(u)\ N_I\ \Delta u_I \right] dx = 0 \tag{2.19}$$

$$V_L \int_L R_L \left[N_{I,x}\ \Delta u_I - t(\sigma_s)\ M_J\ \Delta\sigma_J \right] dx = 0 \tag{2.20}$$

At this point specification of the shape functions becomes necessary. The choice of functions is constrained by the requirement that they render Eqs. (2.19) and (2.20) integrable, i.e. that all terms appearing in these equations be continuous functions. Another restriction is derived from the requirement that the matrices resulting from numerical integration of Eqs. (2.19) and (2.20) possess necessary and sufficient rank to allow rigid body modes and permit at the same time the solution of the system of equations. The simplest choice which satisfies the above requirements is to select constant polynomials for the weighting functions (uniform weighting) and linear polynomials for $N_I(x)$ and $M_J(x)$ due to the presence of derivatives of $N(x)$ and $M(x)$ in Eqs. (2.19) and (2.20). This choice has been adopted in this study.

In order to evaluate Eqs. (2.19) and (2.20) a numerical integration scheme needs to be selected, the choice depending on the accuracy desired. The simplest schemes yielding accuracy of order O(h), where h is the mesh size, are the one-point Gauss integration and the trapezoidal rule.

Using the trapezoidal rule to evaluate Eqs. (2.19) and (2.20) for two consecutive nodes i and $i+1$ along the reinforcing bar (Fig.2.5b) leads to the following relation

$$\begin{bmatrix} \mathbf{C}_i & \mathbf{D}_{i+1} \\ \mathbf{C}_i & \mathbf{D}_{i+1} \end{bmatrix} \begin{Bmatrix} \mathbf{z}_i \\ \mathbf{z}_{i+1} \end{Bmatrix} = 0 \tag{2.21}$$

where

$$\mathbf{C}_i = \begin{bmatrix} -\frac{1}{2}\, s_i\, \Sigma_o\, \Delta x_i & -A \\ -1 & -\frac{1}{2}\, t_i\, \Delta x_i \end{bmatrix} \tag{2.22}$$

$$\mathbf{D}_{i+1} = \begin{bmatrix} -\frac{1}{2} s_{i+1} \boldsymbol{\Sigma}_o \Delta x_i & A \\ 1 & -\frac{1}{2} t_{i+1} \Delta x_i \end{bmatrix} \tag{2.23}$$

and $\Delta x_i = x_{i+1} - x_i$. $\mathbf{z}_i^T = < \Delta u_i , \Delta\sigma_i >$ is the incremental state vector at node i, while s_i and t_i in Eqs. (2.22) and (2.23) indicate that the incremental secant stiffnesses $s(u)$ and $t(\sigma_s)$ in Eqs. (2.19) and (2.20) have been evaluated at node i.

Because of its special structure Eq. (2.21) allows to express the incremental state vector $\mathbf{z}_{i+1}$ at node $i+1$ in terms of the vector $\mathbf{z}_i$ at node i by means of a transfer matrix $\mathbf{T}_{i+1}$, namely,

$$\mathbf{z}_{i+1} = \mathbf{T}_{i+1} \mathbf{z}_i \tag{2.24}$$

where

$$\mathbf{T}_{i+1} = \mathbf{D}_{i+1}^{-1} \mathbf{C}_i \tag{2.25}$$

Substituting $\mathbf{C}_i$ from Eq. (2.22) and $\mathbf{D}_{i+1}$ from Eq. (2.23) into Eq. (2.25) and performing the necessary computations results in the explicit form of matrix $\mathbf{T}_{i+1}$

$$\mathbf{T}_{i+1} = \begin{bmatrix} a & b \\ c & d \end{bmatrix} \tag{2.26}$$

where

$$a = \frac{1}{D} \left(\frac{1}{4} s_i \, t_{i+1} \, \rho \, \Delta x_i^2 - 1 \right)$$

$$b = \frac{1}{2D} (t_{i+1} - t_i) \, \Delta x_i$$

$$c = -\frac{1}{2D} (s_i + s_{i+1}) \, \rho \, \Delta x_i$$

$$d = -\frac{1}{D} \left(1 + \frac{1}{4} s_{i+1} \, t_i \, \rho \, \Delta x_i^2 \right)$$

and

$$D = 1 + \frac{1}{4} s_{i+1} \, t_{i+1} \, \rho \, \Delta x_i^2$$

$$\rho = \frac{\Sigma_o}{A}$$

It is apparent that Eq. (2.24) is an implicit nonlinear relation, since the terms of $\mathbf{T}_{i+1}$ are nonlinear functions of the state vectors at nodes i and $i+1$. Eq. (2.24) can, however, be readily linearized by evaluating the secant stiffness terms in $\mathbf{T}_{i+1}$ at a previously converged step, as will be elaborated upon in Chapter 4.

Eq. (2.24) can be applied successively along the reinforcing bar resulting in an implicit nonlinear matrix relation between the incremental state vectors at two consecutive crack sections (Figs. 2.4 and 2.5b),

$$\mathbf{z}_n = \overline{\mathbf{T}}_n \ \mathbf{z}_1 \tag{2.28}$$

where

$$\overline{\mathbf{T}}_n = \mathbf{T}_n \ \mathbf{T}_{n-1} \ \cdots \ \mathbf{T}_2 \tag{2.29}$$

The significance of Eq. (2.28) is that it expresses in compact form the stress transfer along a reinforcing bar between two consecutive cracks. It can be used as the starting point in the development of analytical models describing the hysteretic behavior of R/C members under severe cyclic excitations.

2.2. Model of reinforced concrete members

Actual reinforcement arrangements in R/C members can be idealized as consisting of two layers of reinforcing bars, a top layer and a bottom layer, as shown in Fig. 2.6, where a subscript denotes the nodal point and a superscript designates top or bottom reinforcing layer. In this case the sum of the areas of all top or bottom reinforcing bars has to be substituted for A in all equations derived in Section 2.1 and Σ_o has to be replaced by the sum of the circumference of all bars in the corresponding layer; Eqs. (2.1)-(2.29) can thus be readily extended to express the stress transfer along a reinforcing layer instead of a single bar. They will be applied in the sequel along with global equilibrium equations to formulate the hysteretic response of interior and exterior joints, as well as beam inelastic regions.

2.2.1. Interior joints

In the case of interior joints (Fig.2.6) it follows from the definition given at the beginning of this chapter that the entire joint is made up of one subregion only, since it is assumed that the joint is of sufficient size and is properly detailed to prevent internal cracking. Moreover it has been observed in experiments that well defined cracks form at the beam-column interfaces of any interior joint subjected to severe cyclic moment reversals.

In the derivation to follow it is assumed that all reinforcing bars are continuous through the joint.

Eq. (2.28) can be applied to both reinforcing layers in the joint to describe the transfer of forces in its interior and directly relate the unknown incremental state vectors at its boundaries. The relevant equations for the bottom and top reinforcing layers, respectively, are:

$$\mathbf{z}_n^b = \overline{\mathbf{T}}_n^b \mathbf{z}_1^b \tag{2.30}$$

$$\mathbf{z}_n^t = \overline{\mathbf{T}}_n^t \mathbf{z}_1^t \tag{2.31}$$

In Eqs. (2.30) and (2.31) a superscript denotes top or bottom reinforcing layer and a subscript designates the end section. Eqs. (2.30) and (2.31) are complemented by global equilibrium conditions formulated at the boundaries of the joint (Fig.2.6). Equilibrium of horizontal forces requires that

$$\sigma_1^t A^t + \sigma_1^b A^b + C_1 = 0 \tag{2.32}$$

$$\sigma_n^t A^t + \sigma_n^b A^b + C_n = 0 \tag{2.33}$$

while equilibrium conditions for bending moments calculated about the bottom reinforcing layer require that

$$\sigma_1^t A^t d' + M_{C_1} = M_n \tag{2.34}$$

$$\sigma_n^t A^t d' + M_{C_n} = M_n \tag{2.35}$$

where d' is the distance between the reinforcing layers, C_1 and C_{ll} are concrete compressive forces and M_{C_1} and $M_{C_{ll}}$ is the concrete contribution to the section moments M_1 and M_{ll}, respectively.

The computation of the concrete forces C at the section of interest will be elaborated upon in Section 3.3. At this point it can be stated that C is a function of the state vectors of both reinforcing layers on either side of the crack, i.e.

$$C = \hat{C}\,(\sigma^b, \sigma^t, w^b, w^t) \tag{2.36}$$

or equivalently,

$$C = \hat{C}\,(\epsilon^b, \epsilon^t, w^b, w^t) \tag{2.37}$$

where w^b and w^t are the crack widths at the level of the bottom and top reinforcing layer, respectively, and are composed of the relative slip of reinforcing bars on either side of the crack (Fig.2.7a). To account for the fact that contact of the crack surfaces during crack closure is controlled by the crack width at the top and bottom of the section, w' and w'' respectively (Fig.2.7b), rather than by w^t and w^b, w' and w'' are monitored in order to establish the moment of crack closure. The relation between w^t and w^b on the one hand and w' and w'' on the other will be introduced in Section 3.3. Thus, it is more appropriate to say that C is a function of w' and w'' which, in turn, are related to w^t and w^b.

Apart from the obvious dependence of the concrete force on the strain distribution at the section of interest, the dependence on w' and w'' can be justified by considering that the crack width at the top or bottom of the section at the beam-column interface determines whether the crack is open or closed. Clearly, the contribution of concrete to the equilibrium of horizontal forces and bending moments is equal to zero if the crack remains open during the imposed load or deformation increment.

Thus the criterion of crack closure, which has been introduced in Eq. (2.37), is independent of steel strains, in contrast to previous studies, and solely depends on relative slip between reinforcing bars and surrounding concrete at the crack. Details and experimental evidence of the introduced formulation are deferred until Section 3.3.

Eqs. (2.32)-(2.35) can be rewritten in incremental form by substituting $\sigma+\Delta\sigma$ for σ, $C+\Delta C$ for C and $M+\Delta M$ for M and considering that the equilibrium at the previous load step has been satisfied within a very small residual, which is neglected, resulting in

$$\Delta\sigma_1^t A^t + \Delta\sigma_1^b A^b + \Delta C_1 = 0 \tag{2.38}$$

$$\Delta\sigma_n^t A^t + \Delta\sigma_n^b A^b + \Delta C_n = 0 \tag{2.39}$$

$$\Delta\sigma_1^t A^t d' + \Delta M_{C_1} = \Delta M_1 \tag{2.40}$$

$$\Delta\sigma_n^t A^t d' + \Delta M_{C_n} = \Delta M_n \tag{2.41}$$

After expanding Eqs. (2.30)-(2.31)

$$\Delta u_n^b = t_{11}^b \, \Delta u_1^b + t_{12}^b \, \Delta\sigma_1^b \tag{2.42}$$

$$\Delta\sigma_n^b = t_{21}^b \, \Delta u_1^b + t_{22}^b \, \Delta\sigma_1^b \tag{2.43}$$

$$\Delta u_n^t = t_{11}^t \, \Delta u_1^t + t_{12}^t \, \Delta\sigma_1^t \tag{2.44}$$

$$\Delta\sigma_n^t = t_{21}^t \, \Delta u_1^t + t_{22}^t \, \Delta\sigma_1^t \tag{2.45}$$

it becomes apparent that the hysteretic response of the joint is described by the time history of eight increments at the boundaries of the joint, (Fig.2.8), which can be uniquely determined at each load step from the eight nonlinear equations written above.

The numerical scheme to efficiently solve the above system of nonlinear equations is presented in Chapter 4.

The form of Eqs. (2.38)-(2.45) seems to suggest that end moment increments ΔM_1 and ΔM_n represent the imposed boundary conditions leading to a numerical loading scheme with force control. However, due to history dependent strength and stiffness deterioration associated with reinforcing bar slippage through the joint, numerical tests with deformation control appear to be a more appropriate choice. This led to a procedure of imposing two slip increments, one at each boundary of the joint, as the necessary boundary conditions in the case of interior joints.

2.2.2. Exterior joints

Significant differences with respect to reinforcement arrangement exist between interior and exterior joints leading to somewhat different global equilibrium equations and a different set of boundary conditions in the two cases.

In the case of exterior joints it is common design practice to anchor all reinforcing bars of the girder framing into the column by means of 90^o hooks (Fig.2.9a). An extensive experimental study into the bond behavior of hooked bars in R/C joints, conducted by Eligehausen et al. [24], revealed that the behavior of hooked anchorages in confined concrete can be described analytically by replacing the hook by an equivalent anchorage length of $l'_d = 5\, d_b$ extending beyond the beginning of the hook (Fig.2.9b), where d_b is the bar diameter. In addition, a bond stress-slip relation based on a different monotonic envelope curve is assigned to the hook-equivalent portion of the bar. Based on the above conclusions the actual system (Fig.2.9a) can be considered analytically equivalent to the simplified system shown in Fig. 2.9b, on which the following derivations are based.

In contrast to interior joints only one girder end moment is applied on exterior joints, acting at section n as indicated in Fig. 2.9b. The second boundary of the joint region lies within the joint at section 1, coinciding with the end of reinforcing bars rather than with the physical boundary of the joint panel region (Fig.2.9b).

It is clear that Eqs. (2.38) and (2.40), representing the global equilibrium of horizontal forces and bending moments at section 1 are not applicable in this case. Since the number of unknown increments at the boundaries of the joint remains the same as in the case of interior joints, two boundary conditions need to be imposed at section 1 to replace the global equilibrium equations.

Considering that no end forces can be present at the free end of anchored bars, leads to two conditions

$$\sigma_1^b = 0 \tag{2.46}$$

$$\sigma_1^t = 0 \tag{2.47}$$

which allows to conclude that

$$\Delta\sigma_1^b = 0 \tag{2.48}$$

$$\Delta\sigma_1^t = 0 \tag{2.49}$$

at all times.

Eqs. (2.42)-(2.45) can thus be simplified by setting equal to zero the stress increments at section 1 yielding four equations,

$$\Delta u_n^b = t_{11}^b \, \Delta u_1^b \tag{2.50}$$

$$\Delta\sigma_n^b = t_{21}^b \, \Delta u_1^b \tag{2.51}$$

$$\Delta u_n^t = t_{11}^t \, \Delta u_1^t \tag{2.52}$$

$$\Delta\sigma_n^t = t_{21}^t \, \Delta u_1^t \tag{2.53}$$

which are complemented by Eqs. (2.39) and (2.41) expressing the equilibrium of forces and moments at section n.

For reasons elaborated upon in the previous section a deformation increment at section n rather than the end moment increment ΔM_n is chosen to represent the imposed excitation, leading to six nonlinear equations in six unknown increments. The numerical scheme to efficiently solve the above system of equations, although very similar to the solution scheme for interior joints, involves some simplifications which will be presented in Chapter 4.

2.2.3. Beam inelastic regions

Several complications arise when attempting to arrive at a strictly consistent formulation of hysteretic behavior of beam inelastic regions. These complications are largely connected to the fact that the locations where cracks will form are not known a priori and therefore a subdivision of the girder inelastic region into several subregions, as described at the beginning of this chapter, is only possible during the course of computations. In addition, the assumption that the cracks form perpendicular to the axis of the girder is only approximately true.

It is the intention of this section to show that the analytical prediction of hysteretic behavior of beam inelastic regions can be accomplished within the framework of the proposed analytical model, once the position of cracks in the final cracking stage of the girder is known, and if it can be assumed with sufficient accuracy that the cracks run perpendicular to the girder axis. Moreover an attempt is made to describe the mechanical behavior of the cracked girder suggesting the refinements needed to arrive at a better model in future studies.

A part of a beam inelastic region in its final cracking stage is shown in Fig. 2.10a. The final cracking stage indicates that no additional cracks will form between the existing cracks, due to the fact that maximum concrete tensile stresses, which may build up between cracks through bond, remain smaller than the tensile strength of concrete in the ensuing time history analysis (Fig.2.10c).

Under the assumption that cracks run perpendicular to the axis of the girder in the inelastic region shown in Fig. 2.10a, a simple comparison between Figs. 2.11 and 2.6 suffices to bring to light the similarities in the behavior of an interior joint and a beam inelastic region, the only difference being the sense of moments applied at the boundaries of the subregions.

Following the above conclusion all formulas derived in Section 2.2.1 can be used to describe the hysteretic behavior of girders subjected to cyclic moment reversals beyond the final cracking stage, provided that the initial location of cracks is known. In particular, Eqs. (2.38)-(2.45) suffice to determine the eight unknown increments, once two load or deformation increments, one at each boundary, are specified as boundary conditions.

Numerical complications arise in the case of beam inelastic regions due to the fact that a loading scheme using deformation control, as in the case of joints, is not feasible. This is attributable to the fact that it is not easily possible to assign rotations along the span of the girder. By contrast moments can be computed with the aid of simple statics. Thus ΔM_{I} and ΔM_{II} in Eqs. (2.40)-(2.41) represent the imposed excitation in the case of beam inelastic regions leading to a numerical loading scheme with force control.

The implementation of the inelastic region model described above within the framework of the present study is rather straightforward. The limitation of the model lies in the fact that the location of cracks within the beam inelastic region has to be known a priori. It is possible, however, to remove this limitation in future studies and develop an analytical scheme for predicting the hysteretic behavior of girders up to the final cracking stage, and determining the location of cracks at that instant. A way of accomplishing this is indicated below.

Clearly, the final crack position depends on the time history of bond deterioration along the beam reinforcing bars and can only be approximated beforehand with the use of empirical expressions based on experimental results. In order that a refined analytical model be capable to predict the development of cracks along the girder under cyclic moment reversals, it should follow the transfer of steel stresses into the surrounding concrete, thus establishing the distribution of concrete stresses along the reinforcing bars (Fig.2.10c). To do so, Eqs. (2.1)-(2.4) have to be complemented by the following two equations,

$$\frac{d\sigma_s}{dx} A_s = \frac{d\sigma_c}{dx} A_c \tag{2.54}$$

$$\sigma_c = \hat{\sigma}\,(\epsilon_c) \tag{2.55}$$

where Eq. (2.54) expresses the equilibrium of forces along an element of infinitesimal length dx, shown in Fig. 2.12, while Eq. (2.55) is the constitutive equation for concrete.

Uncertainties arise in choosing an effective concrete area A_c around a layer of reinforcing bars. Moreover it becomes apparent that the addition of two equations to the initial set of four increases the computational effort.

Beyond the inclusion of Eqs. (2.54) and (2.55) the analytical model should be capable of automatically generating a girder subdivision into new subregions as additional cracks form, creating new boundaries as described in the introduction to this chapter.

Obviously the above refinements to the proposed model do not introduce any conceptional difficulties. However, they introduce a significant increase in the complexity of the model resulting in increased computational effort. These refinements will not be pursued here.

CHAPTER 3

MATERIAL MODELS

Before proceeding to the presentation of a numerical scheme for efficiently solving the nonlinear system of equations pertinent to the case under consideration, it is necessary to discuss the different models that can be used in Eqs. (2.3) and (2.4) for describing the material constitutive relations for steel stress-strain and bond stress-slip. In addition, a model for cracked R/C sections with an appropriate concrete stress-strain relation needs to be introduced for computing the concrete contribution to the equilibrium of forces and bending moments in Eqs. (2.38)-(2.41).

3.1. Steel stress-strain relation

Before proposing a material model to describe the hysteretic behavior of reinforcing bars under generalized strain histories some preliminary remarks are in order.

The range of cyclic strain history, which reinforcing bars are likely to be subjected to, differs significantly from that of structural steel members in that compressive strains are not as large as tensile strains. This is caused by an interplay of bond deterioration and crack closure, which prevents reinforcing bars from excessive yielding in compression before spalling of concrete cover has occurred. As long as a section is uncracked or the crack previously formed is closed and the concrete cover has not spalled, compressive forces are largely carried by concrete, while, in case that the crack is open, bond deterioration in the vicinity of the crack prevents any large force build-up in reinforcing bars. This results in small negative steel strain increments and consequently in small compressive steel stress increments. In either case bars under compression hardly ever enter into the compressive strain range before the concrete cover has spalled. Thus cyclic strain histories of reinforcing bars tend to center about an ever increasing tensile plastic strain.

Another important consideration in the search for an appropriate model is its numerical efficiency. As it will become apparent in Chapter 4, a large number of iterations, and consequently evaluations of any steel stress-strain function, is performed at each load step. This necessitates the use of a simple material model. Counteracting the need for simplicity is the requirement of accuracy, which is based on the observation that cracks running through the depth of the member can remain open during moment reversals, causing the hysteretic response of the section to be solely controlled by the behavior of reinforcing steel. In particular, the Bauschinger effect has to be accounted for. This fact destroys any hope for successfully using a simple bilinear model in any but a monotonic loading case. Obviously, the above requirements call for a compromise between simplicity and accuracy.

There is a host of nonlinear analytical models published in the literature. To a large extent they are devised to represent the cyclic behavior of structural steel thus failing to take advantage of the special strain history of reinforcing steel in reducing the complexity of the model. The most successful among them fall in the group of variable parameter models, with the parameters of the model varying with strain history. Within this group one can distinguish three different formulations:

(a) an explicit algebraic equation for stress in the form (Ref. [33])

$$\sigma = \hat{\sigma}(\epsilon) \tag{3.1}$$

(b) an implicit algebraic equation of the form (Refs. [3],[31],[38])

$$f(\epsilon, \sigma) = 0 \tag{3.2}$$

(c) a first order differential equation of the form (Ref. [21])

$$\frac{\partial \sigma}{\partial \epsilon^p} = E^p = f(\sigma) \tag{3.3}$$

where ϵ^p is the plastic strain. ϵ denotes the steel strain, σ denotes the steel stress and E^p denotes the plastic modulus.

Option (a) seems to be the most attractive since it strikes a good balance between simplicity and accuracy for the problem at hand. Based on results presented in two recent studies, [18], [45], it was concluded that the explicit formulation originally proposed by Giuffré and Pinto and later implemented in Ref. [33] offers numerical efficiency, while agreeing very well with experimental results from cyclic tests on reinforcing steel bars.

The model, as presented in [33] takes on the form

$$\sigma^* = b\,\epsilon^* + \frac{(1-b)\,\epsilon^*}{\left(1+\epsilon^{*R}\right)^{\frac{1}{R}}} \tag{3.4}$$

where

$$\epsilon^* = \frac{\epsilon-\epsilon_r}{\epsilon_o-\epsilon_r} \tag{3.5}$$

and

$$\sigma^* = \frac{\sigma-\sigma_r}{\sigma_o-\sigma_r} \tag{3.6}$$

Eq. (3.4) represents a curved transition from a straight line asymptote with slope E_o to another asymptote with slope E_1 (lines (a) and (b), respectively, in Fig.3.1). σ_o and ϵ_o are stress and strain at the point where the two asymptotes of the branch under consideration meet (point A in Fig. 3.1); similarly, σ_r and ϵ_r are stress and strain at the point where the last strain reversal with stress of equal sign took place (point B in Fig. 3.1); b is the strain hardening ratio, that is the ratio between slope E_1 and E_o and R is a parameter which influences the shape of the transition curve and allows a good representation of the Bauschinger effect. As indicated in Fig. 3.1, (ϵ_o, σ_o) and (ϵ_r, σ_r) are updated after each strain reversal.

R is considered dependent on the strain difference between the current asymptote intersection point (point A in Fig.3.2) and the previous load reversal point with maximum or minimum strain depending on whether the corresponding steel stress is positive or negative (point B in Fig.3.2). The expression for R takes the form suggested in Ref. [33]:

$$R = R_o - \frac{a_1 \xi}{a_2 + \xi} \tag{3.7}$$

where ξ is updated following a strain reversal (Fig.3.2). R_o is the value of the parameter R during first loading and a_1, a_2 are experimentally determined parameters to be defined together with R_o. The definition of ξ remains valid in case that reloading occurs after partial unloading (Fig.3.3).

The model, as described by Eqs. (3.4)-(3.7), adheres to the original formulation by Giuffré and Pinto and differs from the one proposed by Ciampi et al. in Ref. [18], where the denominator of Eq. (3.5) is set equal to twice the yield strain. This yields slight inaccuracies in the representation of the cyclic behavior of reinforcing steel.

Some clarification is needed in connection with the set of rules for unloading and reloading which complement Eqs. (3.5) and (3.6), allowing for a generalized load history. If the analytical model had a memory extending over all previous branches of the stress-strain history, it would follow the previous loading branch, as soon as the new reloading curve reached it (curve (a) in Fig.3.3). This would require that the model store all necessary information to retrace all previous reloading curves which were left incomplete. This is clearly impractical from a computational standpoint. Memory of the past stress-strain history is therefore limited to a predefined number of controlling curves, which in the present model include,

(1) the monotonic envelope,

(2) the ascending upper branch curve originating at the reversal point with smallest ϵ value,

(3) the descending lower branch curve originating at the reversal point with largest ϵ value,

(4) the current curve originating at the most recent reversal point.

Due to the above restrictions reloading after partial unloading takes place along curve (b) rather than curve (a) as shown in Fig. 3.3. However, the discrepancy between the adopted analytical model and the actual behavior seems acceptable, since the case depicted in Fig. 3.3 is the most unfavorable one. The observed satisfactory behavior of the analytical model can be mainly attributed to the manner of formulating the parameter ξ, which determines the curvature of the transition curve between the initial (elastic) and final (yield) asymptote. The hysteretic response of the adopted steel model under different load histories is shown in Fig. 3.4, which closely resemble those found in experiments.

The above implementation of the model corresponds to its simplest form, as proposed in Refs. [18] and [33]: elastic and yield asymptotes are assumed to be straight lines, the position of the limiting asymptotes corresponding to the yield surface is assumed to be fixed at all times and the slope E_o remains constant (Fig.3.1).

In spite of the simplicity in formulation, the model is capable of reproducing well experimental results with strain histories typical of structural steel, i.e. strain excursions of equal magnitude in tension and compression. Its major drawback stems from the its failure to allow for isotropic hardening. This fact can be of importance when modeling cyclic behavior of reinforcing bars in R/C members, as can be explained with the aid of Fig. 3.5. A typical stress-strain diagram for a bottom reinforcing bar is shown in Fig. 3.5. Since the ratio of bottom to top reinforcement is usually on the order of 50%, every time the top layer is subjected to significant tension the bottom layer reaches yielding. The presence of isotropic strain hardening can have a pronounced effect on the strain developed in the bottom bars during crack closure. At a stress σ_1 which satisfies equilibrium (Fig.3.5) the corresponding strains of the two models differ significantly (strains ϵ'_1 and ϵ''_1 in Fig.3.5). Since crack closure depends on bond stress-slip rather than steel strain, it becomes apparent that completely different steel strains will result in the two cases in the bottom reinforcing bars when the crack closes. The importance of the instant of crack closure on the hysteretic response of R/C members requires the use of a more refined model than the one originally presented in Refs. [18] and [33].

The proposed model accounts for isotropic strain hardening by shifting the position of the yield asymptote before computing the new asymptote intersection point following a strain reversal (Fig.3.5). The shift is effected by moving the initial yield asymptote through a stress shift σ_{st} parallel to its direction (Fig.3.5). This idea was introduced by Stanton and Mc Niven in Ref. [45]. They imposed both, a strain and a stress shift, on the monotonic envelope curve to arrive at a very accurate representation of hysteretic steel behavior under generalized strain histories. The expressions describing the functional relationship between stress or strain shift and certain parameters of strain history were obtained using system identification. The simplification introduced in this study, compared to the model presented by Stanton and Mc Niven, lies in the assumption that the monotonic envelope can be approximated by a bilinear curve, which simplifies the yield asymptotes to straight lines. Thus the form and simplicity of the originally proposed model is retained, while a substantial improvement in results is achieved.

The imposed stress shift of the yield asymptotes depends on several parameters of strain history. As suggested in Ref. [45], the main parameter is the sum of the absolute values of plastic strains up to the most recent strain reversal. Because of differences in the formulation of the steel model between the present study and that in Ref. [45] and the fact that the relations given in Ref. [45] are not in dimensionless form, it was decided to choose the maximum plastic strain as the main parameter on which the yield asymptote shift depends. The proposed relation takes the form,

$$\frac{\sigma_{st}}{\sigma_y} = a_3 \left(\frac{\epsilon_{\max}}{\epsilon_y} - a_4 \right) \tag{3.8}$$

where $\epsilon_{\max}$ is the absolute maximum strain at the instant of strain reversal, ϵ_y, σ_y are, respectively, strain and stress at yield, and α_3 and α_4 are experimentally determined parameters.

The model used in this study was implemented using the following parameter values:

$$R_o = 20$$

$$a_1 = 18.5$$

$$a_2 = 0.15$$

$$a_3 = 0.01$$

$$a_4 = 7$$

With the exception of the last two parameters all values were taken from Ref. [33].

Comparison of analytical with experimental results obtained from cyclic tests on reinforcing bars (Ref.[31]) is shown in Figs. 3.6 and 3.7. Fig. 3.6 depicts a stress-strain history typical of top reinforcing bars where yielding in compression is very limited. Fig. 3.6a presents the experimental results, while Figs. 3.6b and 3.6c show the analytical results for a model with and without isotropic strain hardening respectively. Similar results are presented in Fig. 3.7 for a stress-strain history typical of bottom reinforcing bars. The accuracy achieved with the model which includes isotropic strain hardening is seen to be very satisfactory. At the same time the model is almost as simple and computationally efficient as the one which does not allow for isotropic strain hardening.

3.2. Bond stress-slip model

An accurate formulation of the bond stress-slip relation between reinforcing bars and surrounding concrete under random cyclic excitations is of great importance to any analytical model attempting to describe the hysteretic response of reinforced concrete members. Difficulties facing experimentalists regarding simulation of actual bond conditions in structures, considerable scatter of results and inherent inaccuracies of data reduction delayed the development of a general model. A thorough experimental investigation on the behavior of anchored bars subjected to cyclic load reversals was presented by Viwathanatepa et al. in Ref. [51]. This study was recently complemented by Eligehausen et al. in Ref. [23]. In this case the investigation was conducted on short bar embedment lengths in confined concrete regions. Loading and boundary conditions existing in interior and exterior joints of moment resisting frames were simulated. The influence of a number of parameters, such as bar diameter, concrete strength and transverse confining pressure, on the local bond stress-slip relation was established.

Based on the results of this study a general analytical model was proposed in Ref. [23]. The model is valid for a wide range of slip values which are of interest in seismic response analyses of structures and exhibits satisfactory agreement with experimental results. This model will be briefly reviewed here. More details are presented in Ref. [23]. Some modifications, which are deemed necessary, are introduced and the extension of the local bond stress-slip relation to cover actual bond conditions in structural members is presented in detail.

The description of the local bond stress-slip relation between reinforcing bars and surrounding concrete consists of the following parts:

(1) two monotonic envelopes, one in tension and one in compression, which are updated at each slip reversal as a function of incurred damage (curves (a) and (b) in Fig.3.8),

(2) a typical unloading-reloading path described by the current frictional bond resistance q_f, an unloading curve (c) and a reloading curve (d), along with a set of rules for unloading and reloading in the case of incomplete cycles (Figs.3.8 and 3.9),

(3) a set of functional relations which allow updating the monotonic envelope values and the frictional bond resistance as a function of incurred damage.

The simplified monotonic envelope, shown in Fig 3.8, simulates the experimentally obtained curve under monotonically increasing slip. It consists of an initial nonlinear relationship $q = q_1 (u/u_1)^{\alpha}$, valid for $u \leqslant u_1$, followed by a plateau $q = q_1$ for $u_1 \leqslant u \leqslant u_2$. For $u \geqslant u_2$, q decreases linearly to the value of ultimate frictional bond resistance q_3 at a slip value of u_3. This value is assumed to be equal to the clear distance between lugs of deformed bars. In the case of well confined regions identical envelopes apply to tension and compression, i.e. to the case of the bar being pulled or pushed. Otherwise two different envelope curves have to be specified.

After imposing a load reversal at an arbitrary slip value (point A in Fig.3.8), unloading takes place along a steep straight line up to the point where the frictional bond resistance q_f is reached (point B). Further slippage in the same direction takes place along a curve described by a fourth degree polynomial (curve (d)) until reaching the point on the reduced envelope curve (point C) which has a slip value equal to the maximum or minimum slip imposed during previous cycles. Beyond that point a bond stress-slip relationship similar to the virgin monotonic envelope but with reduced values of q is followed (curve (e)). This curve is called "reduced envelope". In case that no slip has been previously imposed in one direction, reloading takes place along a horizontal line until reaching the reduced envelope (curve (f)). If the slip imposed in one direction does not exceed the maximum slip attained during previous cycles, a typical cycle follows the path depicted in Fig. 3.9.

The reloading curve proposed here differs from the one introduced in Ref. [23]. A comparison of the two models is shown in Fig. 3.10. When applying these two different relations to compute the response of a single reinforcing bar embedded in well confined concrete and subjected to cyclic excitations, significant deviations in the reloading curves arise (Figs. 3.11a and b). The model used in this investigation indicates a gradual increase in the force carried by the bar, whereas the model in Ref. [23] does not show any increase until reaching the maximum slip value imposed during previous cycles. By comparing the analytical response with experimental results, shown in Fig. 3.11c, it is seen that the present model compares more favorably. Moreover the revised model has the computational advantage of having a nonzero stiffness at any slip value. This fact was found essential to the stability of the numerical scheme which will be presented in Chapter 4.

Updated envelope curves are obtained from the monotonic envelope by reducing the characteristic bond stresses q_1 and q_3 by a factor, which is formulated as a function of a parameter, called the "damage parameter" d. The relation proposed in Ref. [23] has the form

$$q_1(N) = q_1(1-d) \tag{3.9}$$

where q_1 is the characteristic value on the virgin envelope curve and $q_1(N)$ is the corresponding value after N cycles. For no damage, $d = 0$, the reduced envelope curve coincides with the monotonic envelope curve. For complete damage, $d = 1$, signifying that bond is completely destroyed. The damage parameter d was assumed in Ref. [23] to be a function of the total energy dissipated. The proposed relation (Ref. [23]) has the form

$$d = 1 - e^{-1.2\left(\frac{E}{E_o}\right)^{1.1}} \tag{3.10}$$

where E is the total energy dissipated and the normalizing energy E_o corresponds to the energy absorbed under monotonically increasing slip up to the value u_3 (see Fig.3.8).

An additional relation is used in establishing the frictional bond resistance q_f, which depends upon the previous peak slip value $u_{\max}$ and relates q_f to the ultimate bond resistance $q_3(N)$ of the corresponding reduced envelope curve. For subsequent cycles between fixed values of slip, q_f is further reduced by multiplying its initial value with a factor which depends on the energy dissipated by friction alone. Explicit expressions for the above relations are given in Ref. [23].

It is important to realize that the concept of relating damage to one scalar quantity, like the normalized dissipated energy, provides the basis for a relatively easy generalization of local bond behavior to cover random excitations. Moreover the bond stress-slip model can be used without any modification over a wide range of parameter values. Typical parameters include bar diameter, concrete strength, degree of confinement and transverse pressure due to axial loads. It should be noted in this context that, with the exception of the characteristic values of the monotonic envelope curve, all expressions describing the model are cast in dimensionless form. Thus only the characteristic values of the pertinent envelope curve are needed in order to establish the hysteretic bond stress-slip relation under any conditions. These values can be based on experimental results or, alternatively, on suggestions, presented in Ref. [23] which are summarized below.

Well confined concrete. The condition of well confined concrete is present when a further increase in the amount of transverse reinforcement does not result in significant improvement of the local bond stress-slip behavior. This is depicted in Fig. 4.11 of Ref. [23].

In the case of well confined concrete regions identical envelopes apply to tension and compression, i.e. to the case of the bar being pulled or pushed. The following set of characteristic monotonic envelope values represents average bond conditions for #8 reinforcing bars in well confined concrete with concrete cylinder strength equal to $30\, N/mm^2$:

$$\begin{aligned} u_1 &= 1.0\ mm \\ u_2 &= 3.0\ mm \\ u_3 &= 10.5\ mm \\ q_1 &= 13.5\ N/mm^2 \\ q_3 &= 5.0\ N/mm^2 \\ \alpha &= 0.40 \end{aligned}$$

Due to inevitable scatter of experimental results the values of q_1, q_3 and α may well vary up to $\pm 15\%$.

(1) The influence of concrete strength can be taken into account by multiplying q_1 and q_3 with the factor $\sqrt{f'_c/30}$ where f'_c is the concrete compressive strength in N/mm^2. Furthermore the value of u_1 should be reduced approximately in proportion to $\sqrt{30/f'_c}$ [23].

(2) If the clear spacing between bars is smaller than $4\, d_b$, where d_b is the bar diameter, q_1 and q_3 should be reduced using the information given in Fig. 4.15 of Ref. [23].

(3) The influence of external transverse pressure (e.g. axial compressive column forces) can be taken into account by increasing q_1 and q_3 according to Fig. 4.17 of Ref. [23].

(4) If #6 or #10 bars are used, it is recommended to increase or decrease, respectively, q_1 by 10% [23].

(5) If the related rib area α_{SR} differs from the value 0.065, its influence should be taken into account by modifying u_1 and q_1 using the data given in Fig.2.4 of Ref. [23].

(6) The given values for u_1, u_2 and u_3 should be multiplied with the factor $c_1/10.5$, where c_1 is the clear spacing between lugs, but this modification should not be greater than $\pm 30\%$.

(7) The unloading slope is equal to $180\,N/mm^2$ for #8 bars. It should be modified in the same way as q_1 for different conditions.

Unconfined concrete. Unconfined concrete occurs in the column cover region of interior and exterior joints in R/C frames (Fig.3.12). It is possible to generalize the local bond stress-slip relation for confined concrete to cover conditions in unconfined concrete regions by introducing following modifications (Fig.3.12):

(1) a different monotonic envelope is specified for positive slip values than for negative slip values, i.e. for the case that the bar is pulled and the case that the bar is pushed, respectively,

(2) the normalizing energy E_o used in the computation of damage is chosen to be the largest between E_o^+ and E_o^-, which are, respectively, the areas under the monotonic envelopes for positive and negative slip values up to slip value u_3. To take into account different rates of damage in the two directions of loading, the pertinent total dissipated energies E, used to compute the reduced envelopes, are multiplied by an amplification factor β, which is different for the two cases. Similar rules for computing damage apply to the friction part of the curves.

The following envelope values are suggested for #8 bars in unconfined concrete with cylinder strength equal to $30\,N/\,mm^2$ (Ref. [23]):

Envelope values for the case that the bar is pulled (Fig.3.12)

$$u_1 = 0.3\ mm$$

$$u_2 = 0.3\ mm$$

$$u_3 = 1.0\ mm$$

$$q_1 = 5.0\ N/\,mm^2$$

$$q_3 = 0$$

$$\alpha = 0.40$$

Envelope values for the case that the bar is pushed (Fig.3.12)

$$u_1 = 1.0\ mm$$

$$u_2 = 3.0\ mm$$

$$u_3 = 10.5\ mm$$

$$q_1 = 20.0\ N/\,mm^2$$

$$q_3 = 7.5\ N/\,mm^2$$

$$\alpha = 0.40$$

The same modifications as in the case of confined concrete apply for different bar diameter and concrete strength. More details may be found in Ref. [23].

Hooks in confined concrete. Identical envelopes apply in tension and compression. The following envelope values have been suggested in Ref. [24] for #8 bars in concrete with cylinder strength equal to $30\,N/\,mm^2$:

For hooks bent against the direction of casting,

$$u_1 = 1.0\ mm$$

$$u_2 = 3.0\ mm$$

$$u_3 = 100.0\ mm$$

$$q_1 = 22.0\ N/mm^2$$

$$q_3 = 4.0\ N/mm^2$$

$$\alpha = 0.20$$

For hooks bent in the direction of casting the same values can be used, except for $u_1 = 2\ mm$.

3.3. Reinforced concrete section model

By examining Eqs. (2.38)-(2.45) or (2.50)-(2.53) it becomes apparent that, with the exception of the concrete contribution to the equilibrium of horizontal forces and bending moments at the end sections of the subregion, all increments describing the hysteretic response refer to reinforcing steel. This is a consequence of neglecting the influence of concrete deformations along the reinforcing bar, as was already pointed out in Section 2.1. Nonetheless the problem of steel and concrete interaction has to be taken into account at the cracked end sections; some means of relating steel variables to corresponding concrete variables has to be found in order to compute the concrete compressive forces and concrete bending moments necessary to satisfy equilibrium.

A way of accurately solving this intricate problem is by means of a three-dimensional finite element analysis. Two particular aspects of the problem can be tackled in this manner:

(1) the transfer of bond stresses from the concrete region surrounding the reinforcing bars into the rest of the reinforced concrete member, and

(2) the contact problem at the crack. Due to bar slippage giving rise to crack opening and closing, generally only a part of the cracked section is in contact and transfers forces. On the other hand across an open crack only steel forces act. Tracing the time history of the contact area during the hysteretic response of a cracked R/C section is a rather complicated problem requiring the use of contact elements.

Solving the problem of steel and concrete interaction by means of finite elements requires a tremendous amount of computation, rendering the analysis of any R/C member model prohibitively expensive. For this reason it was decided to adopt a considerably simpler approach for modeling a cracked concrete section. This approach consists of a layer section model which explicitly addresses the problems mentioned above and incorporates their effect into the model.

In any layer model of a reinforced concrete section the relative contribution of steel and concrete to force and moment resultants is determined in three steps. First, steel strain increments or total strains at the top or bottom reinforcing layer are related to concrete strain increments or total strains at the same level. In the next step the distribution of concrete strain increments or total strains over the height of the cross-section is assumed. Finally, a concrete stress-strain relation connects concrete strains to stresses in each layer and allows computation of the concrete contribution to the relevant section forces and moments. The presentation of a new concrete section model will proceed in precisely the same order.

3.3.1. Cracked section model

Most analytical investigations dealing with the hysteretic behavior of reinforced concrete members ([8],[22],[38]) are based on a smeared crack approach and have extended the assumptions of continuum theory for homogeneous materials to reinforced concrete, which is a composite material.

As a first step, compatibility of strains between reinforcing steel and surrounding concrete at the section of interest is assumed, relating steel and concrete strains in a very simple manner. This assumption implies perfect bond between steel and concrete along the reinforcing bars. For uncracked sections such an assumption agrees sufficiently well with experimental evidence. For cracked sections however the very occurrence of a crack indicates local bond damage in the vicinity of a crack as well as loss of compatibility between steel and concrete strains.

In the next step the distribution of concrete strains over the height of the cross-section is usually taken to be linear, based on Bernoulli's assumption of plane sections remaining plane after deformation. The validity of this assumption in the case of computing the average curvature along a region of the girder between two consecutive cracks remains unclear. Experiments and accurate finite element analyses can answer the above question with confidence.

The assumptions of strain compatibility and linear strain distribution lead to a simple and straightforward way of computing the concrete forces at the section of interest.

Another problem inherent to all previous studies concerns crack closing and activation of concrete under cyclic load reversal. Because bond stress-slip between reinforcing bars and surrounding concrete is not explicitly taken into account, crack widths cannot be estimated and traced as a function of time. Because of this limitation smeared crack models employ a strain quantity normal to the crack as a means of controlling the contribution of concrete to the section forces and moments ([8],[22]). Therefore, the concrete at the level of a reinforcing layer is assumed to pick up stresses normal to the crack only when the concrete strain at the same level becomes less than the strain at which the crack has opened (Ref.[8],[22]). Because of the assumed compatibility between steel and concrete strains, this requires that the steel be subjected to *compressive* strains before the crack can close. As experimental evidence suggests [37], (Fig.3.13), this is not the case and reinforcing steel strains hardly enter into the compressive range.

Understanding the mechanical behavior at a cracked R/C section can yield insight into some of the problems and help in developing a reliable section model.

After the bottom reinforcing bars are subjected to tensile forces of significant magnitude, bond between steel and concrete in the immediate vicinity of the crack is damaged and a large crack forms at the lower end of the section (Fig.3.14a). Upon reversing the moment compressive stresses in the bottom reinforcing bars build up quickly, because the area of bottom reinforcement is usually only about half that at the top and the compressive force carried by the bottom bars has to balance alone the increasing tensile force in the top bars due to the bottom crack being open (point B). Soon the bottom bars yield in compression and strain hardening sets in. At some point along the strain hardening branch (Fig.3.14e) the compressive force carried by the steel can no longer be resisted by frictional bond stresses alone, forcing the bottom bars to slip and close the crack before the steel strains enter into the compressive strain range (point B' in Figs. 3.14d and e). Once the crack has closed the major part of the compressive force is supplied by concrete in contact rather than the bottom steel, resulting in a rather small compressive steel strain increment (Point C). This fact explains why, at cracked sections subjected to large deformation reversals, tensile plastic strains imposed during previous cycles are not recovered during moment reversal and steel strains tend to center about an ever increasing plastic tensile strain (Fig.3.13).

It thus becomes apparent that several assumptions used in the available analytical models of cracked reinforced concrete sections [8,31,38] contradict physical evidence. This contradiction manifests itself in the sharp slope discontinuity exhibited by the analytical moment-curvature relation of a section with unequal amounts of top and bottom reinforcement (Fig.3.15), as well as by a delayed crack closure when a section is subjected to several load reversals between fixed rotation values (Fig.3.16).

Both facts have been recognized in a recent study (Ref.[14]) and have been accounted for by means of a modified concrete stress-strain relation. The proposed relation is extended into the tensile strain range using smooth functions to simulate gradual crack closing at an earlier moment than anticipated by models based on strain compatibility. Experimental evidence from cyclic tests on cracked girders is presented, which supports the latter fact. In spite of some satisfactory results this approach does not consider the physical mechanism at play and circumvents the actual problem.

This brief review of previous studies leads to the conclusion that two aspects of the behavior of cracked R/C sections deserve thorough investigation: strain compatibility between reinforcing steel and concrete and the criterion of crack closure.

Due to bond deterioration under severe cyclic excitations, relative slippage between reinforcing bars and surrounding concrete takes place in the vicinity of a crack. Once relative slippage sets in, the assumption of strain compatibility becomes untenable and the problem of relating steel and concrete strains at the cracked R/C section arises. It seems, at first, that, by explicitly incorporating the interaction between steel and concrete along the bar circumference, Eqs. (2.54)-(2.55), into the differential equations of bond, the problem could be resolved. However, Fig. 3.17 indicates that this is not the case. After several load reversals bond in the immediate vicinity of the crack is completely destroyed. As long as the crack is open, the concrete at the crack does not carry any stress. When the crack closes (Fig.3.17) the two surfaces of the crack are pressed together by arch action. This arch action is supported by stress transfer along the bar a distance away from the crack. Only two-dimensional finite element analysis can capture this effect and estimate the concrete stresses at the crack. By contrast, the one-dimensional model discussed in Chapter 2 will indicate an absence of any concrete stresses at the crack.

A possible solution to the above problem can be arrived at by assigning a relation between steel and concrete strains based on physical reasoning and experimental results. Experimental results pertaining to this question have been obtained in Ref. [12], where concrete stress-strain histories near a cracked R/C section are reported. One example from this work is shown in Fig. 3.18. The concrete stress-strain histories shown suggest that, during cycles of moment reversals, *strain increment compatibility* exists between steel and concrete in the immediate vicinity of the crack, as long as the crack is closed or concrete unloading takes place. After unloading and reloading in the opposite direction, reinforcing bars are subjected to tensile strain increments while concrete strains around the crack remain "frozen". Upon moment reversal, stress transfer between steel and concrete is reestablished only after the crack has closed again.

These findings can be readily explained on the basis of cyclic bond deterioration in the vicinity of the crack. After imposing several load reversals in the post-yield range, bond is completely destroyed near the crack. As long as the crack is open, no stress transfer takes place and the concrete at the crack remains "frozen" in a state that corresponds to complete unloading of concrete stresses in all section layers. Once the crack closes again, arch action supported by stress transfer between steel and concrete a certain distance away from the crack where bond is still intact activates the concrete at the crack (Fig.3.17).

The question of crack closure is rather simple, in spite of the fact that no analytical model can properly capture the gradual closing of a rough cracked surface.

Since relative slippage of reinforcing bars with respect to concrete is explicitly included in the model presented in Chapter 2, it is possible to estimate the crack width at the level of the top and bottom reinforcing layer by adding up the slip of the reinforcement on either side of the crack. Based on the estimate of crack width at the level of the top and bottom reinforcing layer it is then possible to approximately determine the crack width at the top and bottom of the cross section by assuming some simple extrapolation rule (Fig.2.7b). In this study a linear extrapolation rule was used which results in the following relations:

$$w' = w^t \frac{d' + d_1}{d'} - w^b \frac{d_2}{d'} \tag{3.11}$$

$$w'' = w^b \frac{d' + d_2}{d'} - w^t \frac{d_1}{d'} \tag{3.12}$$

where

$$w^b = u_l^b + u_r^b \tag{3.13}$$

and

$$w' = u_l' + u_r' \tag{3.14}$$

w denotes crack width and u relative bar slippage. Subscripts indicate left or right crack surface and superscripts top or bottom reinforcing layer (Fig.2.7a). w' and w'' are the crack widths at the top and bottom of the cross section, respectively (Fig.2.7b).

Once crack width at the upper and lower part of the cross-section can be traced in time, it is plausible to base the criterion of crack closure on crack width rather than steel strain in the reinforcement crossing the crack. Thus the criterion of crack closure takes on the form,

$$w' \leqslant a \tag{3.15}$$

$$w'' \leqslant a \tag{3.16}$$

It is simplest to assume that the crack is closed when the crack width is smaller than zero. Some experimental evidence presented in Ref. [14] seems to suggest however that a in Eqs. (3.15) and (3.16) might be a function of, among others, maximum crack width attained during the time history,

$$a = \hat{a}\,(w_{\max}) \tag{3.17}$$

This can be seen from Fig. 3.19, where the ratio of crack width at closure to maximum previous crack width is plotted versus crack width. Physical reasoning supports this idea by considering that shear sliding depends on crack width. Shear sliding moves the rough surfaces of a crack relative to each other, so that they no longer fit and contact is established earlier (Fig.3.20).

Because of the above reasons it was decided to assume the following crack closure criterion,

$$a = 0.10\, w_{\max} + \frac{0.125}{w_{\max}} \tag{3.18}$$

which compares reasonably well with sparse experimental data available (Fig.3.19). More experimental studies on the subject are needed.

The above discussion and experimental findings motivated the proposed concrete section model which consists of the following steps:

(1) A concrete section is subdivided into a number of layers. The number of layers, as pointed out by Stanton and Mc Niven in Ref. [45], should be large enough to minimize any numerical inaccuracies when using the midpoint rule to evaluate the sum of layer forces and moments. The subdivision is performed such that the top and bottom reinforcing bars lie in the middle of a concrete layer. These two concrete layers will be called in the following top and bottom concrete layers, respectively, although they are not the outermost layers. Different material laws can be assigned to each layer, taking into account the distinct behavior of concrete cover and that of concrete confined by stirrup-ties.

(2) At the end of each iteration of the nonlinear system of equations presented in Chapter 2, the increments of steel strain and stress as well as the increments of slip of reinforcing bars relative to concrete are known at each crack.

(3) The current value of crack width at the top and bottom reinforcing layer is determined based on Eqs. (3.13) and (3.14).

(4) The crack closure criterion, Eqs. (3.15)-(3.18), establishes whether the crack is open or closed at the top and bottom of the cross-section.

(5) If the crack at, say, the bottom of the cross-section is open, *no* compatibility of strain increments between reinforcing steel and surrounding concrete is assumed at the bottom reinforcing layer. In this case the concrete strain increment at the bottom concrete layer is assumed to be equal to zero. If the crack is found closed at the bottom of the cross-section, *complete* compatibility of strain increments between reinforcing steel and surrounding concrete is assumed at the bottom reinforcing layer. Similar

considerations apply for the top concrete layer, where the concrete strain increment is independently established based on whether the crack at the top of the section is open or closed.

(6) Concrete strain increments at the top and bottom concrete layers are added to previous total strains yielding current total concrete strains.

(7) In order to compute the strain increments in the remaining concrete layers a strain distribution over the height of the cross-section needs to be assumed. In this study a linear strain distribution between the controlling strains at the top and bottom concrete layers is assumed. The controlling strain at the top or bottom concrete layer is equal to the reinforcing steel strain at that level if the crack is open. It is set equal to the total concrete strain at that level in case that the crack is closed.

(8) Concrete strains and consequently strain increments are computed at the midpoint of each layer.

(9) Based on the corresponding material law (Fig.3.21), the stress at each concrete layer is computed and the contribution of each layer to the section forces and moments is determined. Section forces and moments are found by summation over all layers.

Two aspects of the proposed section model distinguish it from the previous studies:

(a) strain compatibility between reinforcing steel and surrounding concrete at the level of reinforcement is replaced by *conditional strain increment compatibility.* Compatibility of strain increments holds true only if the crack at that level is closed. In case that the crack is open the concrete strains remain unchanged at each load step,

(b) As a consequence of assumption (7) and the fact that reinforcing steel strains are not equal to total concrete strains at the same level, plane sections are not assumed to remain plane after deformation.

It is believed that the above assumptions describe better the observed mechanical behavior of R/C sections, because they account explicitly for the fact that interaction between steel and concrete depends on bond. Moreover the model retains the computational efficiency of simpler models, since its basic assumptions can be implemented without major numerical difficulties.

3.3.2. Concrete stress-strain relation

In order to compute the concrete stress in each layer, a material law describing the concrete stress-strain relation under arbitrary cyclic strain histories is needed.

There is some uncertainty as to the influence of the concrete model on the overall behavior of R/C members subjected primarily to bending. Some investigators have concluded that a crude concrete model suffices to accurately predict experimental results. This might be true in the case of monotonic loading and cyclic loading restricted to small excitations. It is not true, however, in the case of severe cyclic loading. The results of this study indicate that the strength deterioration of R/C members subjected to large cyclic excitations depends largely on the capacity of confined concrete to sustain stresses in the strain range beyond the maximum strength. This requires the use of a refined concrete model.

The model implemented in this study can be outlined in the following steps:

(1) the monotonic envelope curve (a) (Fig.3.21) is based on studies by Kent and Park in Ref. [30], which were recently generalized by Scott et al. in Ref. [40]. It consists of three regions (Fig.3.21):

$$\epsilon_c \leqslant \epsilon_o \qquad \sigma_c = K f'_c \left[2\left(\frac{\epsilon_c}{\epsilon_o}\right) - \left(\frac{\epsilon_c}{\epsilon_o}\right)^2 \right] \tag{3.19}$$

$$\epsilon_o \leqslant \epsilon_c \leqslant \epsilon_u \qquad \sigma_c = K f'_c \left[1 - Z\,(\epsilon_c - \epsilon_o) \right] \tag{3.20}$$

$$\epsilon_u < \epsilon_c \qquad \sigma_c = 0.2\, K f'_c \tag{3.21}$$

where

$$\epsilon_o = 0.002\,K$$

$$K = 1 + \frac{\rho_s f_{yh}}{f'_c}$$

$$Z = \frac{0.5}{\dfrac{3+0.29 f'_c}{145 f'_c - 1000} + \dfrac{3}{4}\rho_s \sqrt{\dfrac{h'}{s_h}} - 0.002\,K}$$

ϵ_o is the concrete strain at maximum stress, K is a factor which accounts for the strength increase due to confinement, Z is the strain softening slope, f'_c is the concrete compressive cylinder strength in MPa, f_{yh} is the yield strength of stirrups in MPa, ρ_s is the ratio of volume of hoop reinforcement to volume of concrete core measured to outside of stirrups, h' is the width of concrete core measured to outside of stirrups, and s_h is the center to center spacing of stirrups. In the case of concrete confined by stirrup-ties, ϵ_u is determined from Eq. 3.20 by setting $\epsilon_c = \epsilon_u$ and $\sigma_c = 0.2\,K\,f'_c$, and solving for ϵ_u noting that Z is known. In the case of concrete cover, suggestions for the value of ϵ_u range from 0.004 to 0.005. In this study ϵ_u was assumed to be equal to 0.005. By inserting this value for ϵ_u into Eq. (3.20) and assuming again $\sigma_c = 0.2\,K\,f'_c$ the value of Z can be determined.

(2) The tensile strength of concrete is neglected, since it only influences the response of a R/C section during cycles prior to cracking. Once cracking has taken place the tensile strength has negligible influence on the behavior of a cracked section.

(3) Unloading from a point A on the envelope curve takes place along a straight line connecting the point at which unloading occurred to a point B on the strain axis given by the following equation proposed by Karsan and Jirsa in Ref. [29],

$$\frac{\epsilon_t}{\epsilon_o} = 0.15\left(\frac{\epsilon_r}{\epsilon_o}\right) + 0.10\left(\frac{\epsilon_r}{\epsilon_o}\right)^2 \tag{3.22}$$

where ϵ_r is the strain at which unloading takes place (Fig.3.21).

(4) Once unloading is completed, the model "freezes" at the strain corresponding to zero stress, until the crack closes again and compressive strain increments are imposed. This is a consequence of the proposed section model and is based on experimental evidence shown in Fig. 3.18.

(5) When imposing compressive strain increments while the crack is closed, reloading takes place along the previous unloading path (curve (b) in Fig.3.21). In reality unloading and reloading follow nonlinear paths which together form a hysteresis loop. This was neglected here for reasons of simplicity, since it has a minor influence on the hysteretic response of the member.

(6) To account for crushing of concrete cover the strength in a cover layer is reduced to $0.2f'_c$ once the compressive strain exceeds the value of 0.005, as indicated in Fig.3.21.

(7) To account for splitting of concrete cover, the concrete strength in the cover layers is reduced to zero once the cumulative sum of steel tensile strain increments exceeds a limit value, which is set equal to 0.10. This value was established after a series of numerical studies, since no experimental evidence is presently available on this question. This reduction is not indicated in Fig. 3.21.

CHAPTER 4

NUMERICAL SOLUTION PROCEDURE

To determine the hysteretic response of each subregion, be it an interior or exterior joint, be it a part of the inelastic region of a girder, the solution to the pertinent system of nonlinear equations is required. In the case of interior joints and beam inelastic regions eight equations in eight unknown increments arise, while six equations in six unknowns remain in the simpler case of exterior joints. Because the solution to the former case is considerably more involved, it will be presented first and elaborated upon in detail. The solution to the simpler case can then be introduced as a simplification of the general algorithm in a rather straightforward manner.

4.1. General case

The general case for determining the hysteretic response of a subregion requires the solution of the nonlinear system of equations (2.38)-(2.45) derived in Chapter 2, which apply to interior joints and beam inelastic regions. The difference between the case of interior joints and that of beam inelastic regions lies in the sense of bending moments acting at the boundaries of the subregion as well as in the selection of the imposed excitations. In the case of interior joints deformation increments are specified at each boundary, whereas bending moment increments are imposed in the case of beam inelastic regions. The solution algorithm will be presented for interior joints. A similar approach applies in the other case.

The nonlinearity of the system of equations (2.38)-(2.45) is "hidden" in the coefficients of transfer matrix $\bar{\bar{\mathbf{T}}}_n$ in Eqs. (2.30) and (2.31), which are nonlinear functions of both incremental state vectors $\mathbf{z}_1$ and $\mathbf{z}_n$. This means that all coefficients in Eqs. (2.42)-(2.45) are nonlinear functions of the unknown increments at the boundaries of the joint and the apparent simplicity of the system of equations is deceptive. Before introducing an efficient scheme for solving the above system of equations it is instructive to examine an entirely different approach.

One can start from Eq. (2.21) and assemble all equations for nodes $1, 2, \ldots, i, i+1, \ldots, n$ in both reinforcing layers. After introducing two global equilibrium equations at each boundary of the subregion, the nonlinear equation system takes the form

$$\mathbf{A}(\mathbf{x}) \cdot \mathbf{x} = \mathbf{b} \tag{4.1}$$

where $\mathbf{x}$ is the vector of unknown increments and $\mathbf{A}$ is the nonlinear stiffness matrix of the subregion. The disadvantage of this approach lies in the fact that the dimension of the resulting nonlinear matrix $\mathbf{A}(\mathbf{x})$ is equal to $2n+2$, where n is the total number of nodes within the subregion. For example, in the case of interior joints with a column width on the order of 450 *mm* the necessary number of nodes in each layer is about 25 resulting in a matrix of dimension equal to 102.

Solving such a large system of nonlinear equations is clearly impractical. Moreover considerable numerical difficulties are encountered due to very small stiffness coefficients arising in connection with the bond stress-slip relation.

A better approach for the numerical solution of the problem at hand is to attempt to solve iteratively one equation at a time. To do so, the boundary value problem needs to be transformed into an initial value problem by implementing a "shooting" technique. In order to demonstrate this transformation, Eqs. (2.42)-(2.45) are treated for a moment as if they were linear.

As was already pointed out in Chapter 2, in the case of interior joints the imposed excitation consists of two deformation increments, one at each joint boundary. Because of the sense of the applied end rotations, the deformation increments are known at diagonally opposite corners of the joint panel region, i.e. the imposed increments are either Δu_1^b and Δu_n^t *or* Δu_1^t and Δu_n^b (Fig.4.1). As an example consider the former case, the latter being entirely similar. In order to express explicitly the incremental state vector of the top reinforcing layer at section 1, Eq. (2.31) is inverted to yield

$$\mathbf{z}_1^t = \left(\overline{\mathbf{T}}_n^t\right)^{-1} \mathbf{z}_n^t = \overline{\mathbf{P}}_1^t \mathbf{z}_n^t \tag{4.2}$$

or explicitly

$$\Delta u_1^t = p_{11}^t \, \Delta u_n^t + p_{12}^t \, \Delta \sigma_n^t \tag{4.3}$$

$$\Delta \sigma_1^t = p_{21}^t \, \Delta u_n^t + p_{22}^t \, \Delta \sigma_n^t \tag{4.4}$$

where

$$\overline{\mathbf{P}}_1^t = \begin{bmatrix} p_{11}^t & p_{12}^t \\ p_{21}^t & p_{22}^t \end{bmatrix}$$

The same relation can be arrived at by inverting Eq. (2.24)

$$\mathbf{z}_i^t = \left(\mathbf{T}_{i+1}^t\right)^{-1} \mathbf{z}_{i+1}^t = \mathbf{P}_i^t \mathbf{z}_{i+1}^t \tag{4.5}$$

and applying Eq. (4.5) successively along the nodes of a layer

$$\mathbf{z}_1^t = \overline{\mathbf{P}}_1^t \mathbf{z}_n^t \tag{4.6}$$

where

$$\overline{\mathbf{P}}_1^t = \mathbf{P}_1^t \mathbf{P}_2^t \cdots \mathbf{P}_{n-1}^t \tag{4.7}$$

It should be noted that Eqs. (4.3) and (4.4) replace Eqs. (2.44) and (2.45) in the nonlinear system of equations. On substituting Eqs. (2.43) and (4.4) into Eqs. (2.38) and (2.39) yields

$$(p_{21}^t \, \Delta u_n^t + p_{22}^t \, \Delta \sigma_n^t) \, A^t + \Delta \sigma_1^b A^b + \Delta C_1 = 0 \tag{4.8}$$

$$\Delta \sigma_n^t A^t + (t_{21}^b \, \Delta u_1^b + t_{22}^b \, \Delta \sigma_1^b) \, A^b + \Delta C_n = 0 \tag{4.9}$$

Recalling that Δu_1^b and Δu_n^t are given, only two unknowns remain in the above equations, namely $\Delta \sigma_1^b$ and $\Delta \sigma_n^t$. All coefficients, including compressive force increments ΔC_1 and ΔC_n, are implicit nonlinear functions of $\Delta \sigma_1^b$ and $\Delta \sigma_n^t$ in a manner to become apparent below. With this in mind Eqs. (4.8) and (4.9) can be simply written as

$$g_1(\Delta\sigma_1^b, \Delta\sigma_n^t) = 0 \tag{4.10}$$

$$g_2(\Delta\sigma_1^b, \Delta\sigma_n^t) = 0 \tag{4.11}$$

Eqs. (4.10) and (4.11) are the result of transforming the boundary value problem, expressed by Eqs. (2.38) through (2.45), into an initial value problem using Eqs. (4.3), (4.4), (2.42) and (2.43). In the process of the transformation the above relations were treated as being linear and explicit. Because they are implicit, nonlinear relations, a whole sequence of iterations along each of the reinforcing layers is needed, before the coefficients of transfer matrices $\overline{\mathbf{P}}_1$ and $\overline{\mathbf{T}}_n$ in Eqs. (4.8) and (4.9) can be determined and the two unknowns $\Delta\sigma_1^b$ and $\Delta\sigma_n^t$ can be solved for.

To demonstrate the procedure, consider for a moment that the current iterate of $\Delta\sigma_1^b$ is known. Since Δu_1^b is also known, Eq. (2.24), written for i=1, can be iterated upon to compute the incremental state vector at the next node, noting that the coefficients of matrix $\mathbf{T}_{i+1}$ are functions of both $\mathbf{z}_i$ and $\mathbf{z}_{i+1}$. In the same manner one advances successively along the bottom reinforcing layer by solving iteratively for the unknown increments of one node at a time. This allows one to establish all incremental state vectors of one layer and at the same time compute the coefficients t_{21}^b and t_{22}^b of matrix $\overline{\mathbf{T}}_n^b$ in Eq. (4.9). Since the process has to be repeated for each iterate of $\Delta\sigma_1^b$ until Eqs. (4.10) and (4.11) are satisfied within a prescribed tolerance, it is called the "shooting" technique.

The same procedure is followed for the top reinforcing layer by starting from section n (Fig.4.1b). The displacement increment Δu_n^t, which is known, and the current iterate on the value of $\Delta\sigma_n^t$ are inserted into Eq. (4.5), which is solved iteratively for $i=n-1$. Proceeding backwards along the top layer and iterating upon the unknown increments of one node at a time using Eq. (4.5), allows to determine all incremental state vectors of the top layer and compute the coefficients p_{21}^t and p_{22}^t of matrix $\overline{\mathbf{P}}_1^t$ in Eq. (4.8).

So far it is not clear how the coupled system of nonlinear equations, Eqs. (4.10) and (4.11), can be satisfied by proceeding in the manner described above and "shooting" through the top and bottom reinforcing layers. An additional numerical scheme is needed in order to satisfy the coupled system of nonlinear equations. An efficient procedure for numerically solving this problem consists of an accelerated version of the Gauss-Seidel algorithm for nonlinear equation systems (Ref. [35]). This version is illustrated with the aid of Fig. 4.2 and the use of Eqs. (4.10) and (4.11), rewritten in terms of general unknown increments Δv and Δw, where Δv stands for $\Delta\sigma_1^b$ and Δw stands for $\Delta\sigma_n^t$ and

$$g_1(\Delta v, \Delta w) = 0 \tag{4.12}$$

$$g_2(\Delta v, \Delta w) = 0 \tag{4.13}$$

As Fig. 4.2 shows, Eqs. (4.12) and (4.13) describe geometrically the traces of surfaces g_1 and g_2 on the coordinate plane of the two unknowns. These traces reveal that Eq. (4.10) is very sensitive to changes in variable $\Delta\sigma_n^t$, whereas it remains insensitive to changes in $\Delta\sigma_1^b$. Exactly the opposite occurs with Eq. (4.11). This fact is due to the presence of coefficients p_{22}^t and t_{22}^b in Eqs. (4.8) and (4.9), which tend to have rather large values. These values are the result of multiplication of transfer matrix coefficients along the whole length of a layer between cracks. The large values of p_{22}^t and t_{22}^b are a curse and a blessing at the same time; a curse, because they make iterating on the sensitive variable extremely tedious and a blessing because they essentially uncouple the two global equilibrium equations (4.10) and (4.11).

The proposed scheme consists of the following steps, which are graphically illustrated in Fig. 4.2:

(1) Select two starting values $\Delta v^{(0)}$ and $\Delta w^{(0)}$ for the iteration variables (point O).

(2) Keeping $\Delta v^{(0)}$ constant, iterate on Δw establishing a value $\Delta w^{(1)}$ which satisfies Eq. (4.13) (point A).

(3) Keeping $\Delta w^{(1)}$ constant, iterate on Δv establishing a value $\Delta v^{(1)}$ which satisfies Eq. (4.12) (point B).

(4) Repeat steps (2) and (3) using $\Delta v^{(1)}$ and $\Delta w^{(2)}$ instead of $\Delta v^{(0)}$ and $\Delta w^{(1)}$ to establish $\Delta w^{(2)}$ and $\Delta v^{(2)}$, respectively (points C and D).

(5) Compute the intersection of secants to the traces passing through the four points A, B, C and D established in the previous steps. The coordinates of the intersection point E yield new starting values for the unknown increments.

(6) Repeat steps (2) through (5) until convergence occurs within a prescribed tolerance.

Steps (2) through (5) make up one iteration loop. Convergence is checked at each step by computing the difference between current and last iterate of both iteration variables. Convergence is achieved when

$$|\Delta v^{(i)} - \Delta v^{(i-1)}| \leqslant TOL\, |\Delta v^{(i)}| \tag{4.14}$$

and

$$|\Delta w^{(i)} - \Delta w^{(i-1)}| \leqslant TOL\, |\Delta w^{(i)}| \tag{4.15}$$

The specified tolerance is on the order of 10^{-3} to 10^{-4}. Due to Eqs. (4.12) and (4.13) being almost uncoupled one or two iteration loops suffice to achieve the desired tolerance. Because convergence is checked at each step, the loop does not have to be completed before the convergence criterion is satisfied.

It is noted that each step of the global iteration scheme to satisfy Eqs. (4.12) and (4.13) involves iterating on *one variable* only. As was pointed out, each such iteration consists of "shooting" through the corresponding reinforcing layer by starting at the joint end opposite to the one at which it is attempted to satisfy equilibrium. Each "shooting" process in turn entails a series of iterations at each node of the corresponding reinforcing layer, in order to satisfy the implicit nonlinear equations (2.24) or (4.5).

In conclusion, the numerical solution of the problem expressed by Eqs. (2.38)-(2.45), is accomplished by three nested iteration processes, as shown in Fig. 4.3 and summarized below:

(1) Loop (A) aims at satisfying *both* nonlinear equilibrium equations (4.8) and (4.9) simultaneously.

(2) Loop (B) aims at satisfying only *one* equilibrium equation at a time by iterating on *one* variable which lies at the opposite end of the joint panel region. This is achieved by "shooting" through the corresponding reinforcing layer.

(3) Loop (C) attempts to advance from node i to node $i+1$ or node $i-1$, depending on the direction of "shooting", by iteratively satisfying Eq. (2.24) or Eq. (4.5).

Details on the algorithm used in loops (B) and (C) along with a discussion of some numerical problems and their solution will be presented in Section 4.3. The question of estimating good initial iteration values in order to start applying the algorithm in each loop is discussed in Section 4.4.

In an attempt to avoid an excessive number of iterations in any loop, an upper limit on this number is imposed. The upper limit for loop (A) is three iterations, while loops (B) and (C) were restricted to twenty and fifty iterations respectively. Once the upper limit is exceeded, automatic subdivision of step size of both iteration variables in Eqs. (4.10) and (4.11) is performed, and the whole process is restarted. The necessity of step subdivision arises only about once in every hundred load steps.

4.2. Numerical scheme for exterior joints

The numerical scheme for solving Eqs. (2.39), (2.41) and (2.50)-(2.53), which pertain to exterior joints, presents some differences from the scheme presented in the previous section for interior joints. The most important difference is the fact that the total number of equations is reduced by two, which simplifies the solution considerably. In addition, the boundary conditions imposed at section 1 (Fig.4.4) differ from the boundary conditions specified in the case of interior joints, suggesting a different choice of iteration variables.

As was already pointed out in Section 2.2.2, no forces are present at the free end of bars anchored in exterior joints leading to the condition that

$$\Delta\sigma_1^b = 0 \tag{4.16}$$

and

$$\Delta\sigma_1^t = 0 \tag{4.17}$$

at all times during the response. Since one variable is already known in each reinforcing layer at section 1, it appears advantageous to select the slip increments Δu_1^b and Δu_1^t at the same section as the main iteration variables. Upon substituting Eqs. (2.51) and (2.53) into Eq. (2.39) one obtains

$$t_{21}^t \, \Delta u_1^t \, A^t + t_{21}^b \, \Delta u_1^b \, A^b + \Delta C_n = 0 \tag{4.18}$$

One slip increment at section n, namely Δu_n^b or Δu_n^t, represents the imposed excitation (Fig.4.4). Therefore one slip increment can be eliminated from Eq. (4.18) by using either Eq. (2.50) or Eq. (2.52), depending on the sense of the applied end moment. In order to conform to the scheme used in the case of interior joints, the slip increment on the tension side of end section n is considered known (Fig.4.4). Assuming, for example, that Δu_n^t is given, Eq. (2.52) can be substituted into Eq. (4.18) to yield

$$\frac{t_{21}^t}{t_{11}^t} \Delta u_n^t A^t + t_{21}^b \, \Delta u_1^b \, A^b + \Delta C_n = 0 \tag{4.19}$$

Eq. (4.19) now contains only one unknown variable, Δu_1^b, and can be solved iteratively. The case where Δu_n^b is known is treated analogously.

It is interesting to note at this stage that the set of equations describing the response of exterior joints reduces to two *uncoupled* nonlinear equations, Eqs. (2.52) and (4.19), in contrast to two *coupled* equations in the case of interior joints.

In deriving the above numerical scheme all equations were treated as if they were linear. Since they are actually implicit nonlinear equations, the solution scheme again requires using the current iterate of Δu_1^b or Δu_1^t to "shoot" through the top or bottom reinforcing layer in an effort to satisfy the boundary conditions at the other end (section n). Each process of "shooting" through entails a series of iterations to satisfy Eq. (2.24) at each node along the corresponding reinforcing layer.

Since Eqs. (4.19) and (2.52) are uncoupled, they can be solved independently. Thus iteration loop (A) degenerates into having to complete loop (B) twice, once in order to satisfy Eq. (2.52) and the second time in order to satisfy Eq. (4.19) using the results of Eq. (2.52). In each case loop (C) is used to advance from node i to node $i+1$ by iteratively satisfying Eq. (2.24). The nested structure of the algorithm for exterior joints is shown in Fig. 4.5.

4.3. Solution algorithm for a nonlinear equation

In the previous sections no mention was made of the actual algorithm employed in iteration loops (B) and (C). In each case a nonlinear equation in one unknown increment has to be solved. In general, any such nonlinear equation can be written as

$$f(x) = 0 \tag{4.20}$$

To solve Eq. (4.20) several alternatives are possible. It is important to note, however, that Eq. (4.20) is solved $n-1$ times during each iteration loop (B), where n is the number of discretization points along each reinforcing layer. The large number of iterations involved mandates the use of an efficient numerical scheme.

The secant method at first sight appears attractive. It has a satisfactory rate of convergence (being not much slower than that of Newton-Raphson's method) and does not require direct evaluation of derivatives. This approach requires two initial approximations, but only one function evaluation is made per step. Given the nonlinear equation $f(x)=0$, and two initial approximations to the solution x^0 and x^1, a sequence of approximations is recursively computed from the expression

$$x^{n+1} = x^n - f(x^n)\frac{x^n - x^{n-1}}{f(x^n) - f(x^{n-1})} \tag{4.21}$$

The geometrical interpretation of Eq. 4.21 is that x^{n+1} is determined as the abscissa of the point of intersection of the secant through $(x^{n-1}, f(x^{n-1}))$ and $(x^n, f(x^n))$ and the x axis. The iteration is stopped when a value x^{n+1} is found such that the residual $f(x^{n+1})$ is less than a prescribed tolerance. A disadvantage of the secant method is that it is not guaranteed to converge for all initial values and for any shape of function $f(x)$ near zero.

For all real continuous functions $f(x)$, a variant of the secant method, known as Regula Falsi, is always convergent, provided that the initial approximations x^0 and x^1 are such that $f(x^0)\cdot f(x^1) < 0$. In this case the secant passes through $(x^n, f(x^n))$ and $(x^m, f(x^m))$, where m is the largest index $m < n$ for which $f(x^n)\cdot f(x^m) < 0$ (Fig.4.6a). Regula Falsi has unfortunately a rate of convergence which is much slower than the conventional secant method.

Therefore, before selecting an algorithm, it is important to examine more closely a typical graph of the residual function $f(x)$. Fig. 4.6a shows a graph of the residual function $f(x)$ as it typically arises in iteration loops (B) and (C). From this graph it becomes clear, that, since the function is not monotonic near the root, great caution has to be exercised during the iterations, to guarantee convergence to the root. Since the secant method does not converge in this case, the Regula Falsi method must be used. To implement this procedure, two starting values are needed, such that $f(x^0)\cdot f(x^1) < 0$ (Fig.4.6a). An efficient method for selecting two starting values which bracket the solution will be presented in the next section. Once the two starting values are chosen, the algorithm unfolds in the fashion described previously.

Since the Regula Falsi method has a slow rate of convergence, it is important to employ an acceleration scheme, such that the rate of convergence approaches that of the secant method. The acceleration scheme is used, whenever consecutive iterates fall on the same side of the root of Eq. (4.20). Suppose for example that $f(x^{n+1}) \cdot f(x^n) > 0$. A modified step is then completed, whereby the next iterate x^{n+2} is taken as the intersection of the secant through $(x^{n+1}, f(x^{n+1}))$ and $(x^{n-1}, \alpha f(x^{n-1}))$ and the x-axis, where α $(0 < \alpha < 1)$ is a parameter (Fig.4.6b). If after a modified step with $\alpha = \alpha_o$, still $f(x^{n+2}) \cdot f(x^{n+1}) > 0$, the secant through $(x^{n+2}, f(x^{n+2}))$ and $(x^{n-1}, \alpha_o^2 f(x^{n-1}))$ is used in the next step. Generally, α is set equal to $(\alpha_o)^k$ until there is a change of sign in the residual $f(x)$. The convergence rate of the accelerated version of Regula Falsi was found to be satisfactory using a value of $\alpha_o = 0.5$. Furthermore, no convergence problems were encountered in applying this procedure in all but very few cases, which will be discussed in Section 4.5.

4.4. Procedure for establishing initial iteration values

As has been pointed out, two initial values are necessary to start the Regula Falsi algorithm for solving the nonlinear equations encountered in the iteration loops (B) and (C). In establishing the initial iteration values the equations derived in Chapter 2 can be used. Eqs. (2.28) and (4.6) can be readily linearized about the previous load step. This is essentially accomplished by using the state vectors at the previous converged load step to determine the stiffness coefficients in matrices $\overline{\mathbf{T}}_n$ and $\overline{\mathbf{P}}_1$. Thus all coefficients in Eqs. (2.42), (2.43), (4.3) and (4.4) are known, allowing one to arrive at approximate values for the main iteration variables. Assuming, for example, that $\Delta\sigma_1^b$ and $\Delta\sigma_n^t$ are the main variables for the load step under consideration, the other variables in Eqs. (2.38) and (2.39) can be eliminated with the aid of Eqs. (2.43) and (4.4) to yield Eqs. (4.8) and (4.9). Assuming for a moment that ΔC_1 and ΔC_n are known, Eqs. (4.8) and (4.9) constitute two linear equations in the two unknowns $\Delta\sigma_1^b$ and $\Delta\sigma_n^t$. Solving the above system of equations yields an initial estimate for the main iteration variables, which lies, in general, sufficiently close to the actual solution of the nonlinear equation system, Eqs. (4.8) and (4.9), which result when the coefficients in these equations are regarded as nonlinear functions of the current state vectors. Once initial estimates for the main iteration variables are known, Eqs. (2.28) and (4.6) can be used in linearized form to establish first estimates of iteration variables at each node along the corresponding reinforcing layer. Thus the procedure first determines the initial estimates of iteration variables for loop (B) and then goes on to determine the corresponding initial values of loop (C) based upon the estimates for loop (B).

An estimate of ΔC_1 and ΔC_n can be arrived at through several alternatives. One alternative is to assume that the concrete compressive forces do not change during the load increment and consequently that ΔC_1 and ΔC_n are equal to zero. Another possibility is to set the concrete force increments equal to the increments at the previous load step. Finally a more involved, and consequently more accurate alternative, is to establish a first estimate of the main iteration variables by one of the above methods and use it to approximate ΔC_1 and ΔC_n, whereupon an improved second estimate can be found. This choice was adopted in this study, yielding satisfactory initial estimates, with the exception of cases where the crack at the beam-column interface is about to close or considerable bond deterioration has taken place. For these cases, the initial estimates are not near the final solution. Even in these cases the Regula Falsi algorithm does not have any difficulties in converging to the correct solution, requiring however a larger number of iterations.

Once one initial estimate of the iteration variable is known (e.g. x^o in Fig.4.6a), it is inserted into the nested loop algorithm (A)-(B)-(C) yielding a residual $f(x^o)$ for Eq. (4.8) or Eq. (4.9), since these are obviously not satisfied. Then this first estimate is multiplied by a factor close to unity and the process is repeated (x^1 in Fig. 4.6a). If the new residual has a different sign than the first one, two initial iteration values bracketing the solution are known and the algorithm can be started (Fig.4.6a). If, on the other hand, the new residual has the same sign, a search is started to find a second initial estimate having a residual of different sign than the previous one. Typically, two or three trials suffice to satisfy this condition, where after the accelerated Regula Falsi algorithm described in Section 4.3 is started.

4.5. Some special problems and their solution

Some problems which are encountered in the process of solving the nonlinear system of equations pertinent to the case under consideration are discussed in this section. They arise in connection with the material models which were described in the previous chapter and are not associated with the numerical scheme presented above.

The first problem occurs when attempting to satisfy Eq. (2.24), which describes the equilibrium of forces and the kinematics of deformation between nodes i and $i+1$ along a reinforcing layer. After writing out Eq. (2.24) the following relations result

$$\frac{\Delta q_i + \Delta q_{i+1}}{2} \Sigma_o - (\Delta\sigma_{i+1} - \Delta\sigma_i) A = 0 \tag{4.22}$$

$$\Delta u_{i+1} - \Delta u_i = \frac{\Delta\epsilon_{i+1} + \Delta\epsilon_i}{2} \tag{4.23}$$

Suppose now that the increments of stress and slip are known at node i. Fig. 4.7 depicts the hysteretic bond stress-slip relation for node $i+1$ showing that two equilibrium positions (points A and B) are possible when the current slip value of node $i+1$ is near the end of the reloading branch: one with a small increment of slip (point A) and another with a larger slip increment (point B). As shown in Fig. 4.7, the bond stress in the second case is slightly higher due to slightly higher steel stresses that have to be balanced at node $i+1$. These stresses are associated with larger strain increments resulting from the larger slip increment $u''_t - u_{t-\Delta t}$. The possibility of two equilibrium positions (points A and B) means that the nonlinear residual function $f(x)$ has two roots. In such a case it is impossible to guarantee that the algorithm will converge to the correct solution. Since this, however, takes place at the innermost loop (C), it is possible to let the immediately higher iteration loop (B) detect any wrong solution by controlling whether the resulting residuals in loop (B) fit in the pattern of previously computed ones. This is readily done, because an incorrect solution at some node along the reinforcing layer produces extremely large residuals in loop (B). In any case a good initial estimate of the iteration variable usually prevents the algorithm from converging to the wrong root in all but a few cases.

The second problem is associated with the concrete section model and the instant of crack closure at the joint end sections. As was elaborated upon in Section 3.3, concrete strain increments are added to the previous total concrete strains only after the crack has closed. This fact implies compatibility of strain increments between reinforcing steel and surrounding concrete after crack closure.

Assume now that the crack is open at some load step and closes during the next load or deformation increment. This means that the crack is closed only during part of the deformation increment (Fig.4.8a). If steel strain increments associated with the imposed deformation increment were considered compatible to the corresponding concrete strain increments during the entire step, a discontinuity in the residual function $f(x)$ would result, as depicted in Fig. 4.8b. It is therefore important that the exact moment of crack closure be determined when iterating on the global equilibrium equations, and that strain increment compatibility be established only for that portion of the entire step for which the crack is closed.

This is automatically accomplished during iteration loop (B) by storing the maximum steel strain increment for which the crack remains open and subtracting it from all steel strain increments for which the crack is closed before computing the resulting concrete strain increments. This essentially means that the residual function $f(x)$ automatically adjusts itself during the course of iterations to accommodate the fact that concrete strain increments necessary for computing ΔC in Eqs. (4.8) and (4.9) have to be referred to the deformation state at crack closure (Fig. 4.8a).

The described method proved very efficient in preventing any convergence problems during crack closure, while retaining computational simplicity.

4.6. Computer program JOINT

A computer program called JOINT which determines the hysteretic response of interior or exterior joints and beam inelastic regions was developed. The program implements the analytical model presented in Chapter 2 along with models of hysteretic material behavior as elaborated upon in Chapter 3. The nested loop algorithm described above is used to solve the resulting system of nonlinear equations.

The program is divided into independent units which are schematically shown in Fig. 4.9. Each unit is in turn divided into subroutines. This systematic structure facilitates modification of material models without interfering with the input-output subroutines or the solution algorithm of the program.

Following information is used as input to the program:

(1) topology of the subassemblage along the longitudinal axis,

(2) load history data,

(3) material parameters for steel stress-strain, bond stress-slip and concrete stress-strain models,

(4) section dimensions, top and bottom reinforcement data (area and bar circumference), position of reinforcing layers,

(5) material-element correspondence along reinforcing layers,

(6) maximum allowable number of iterations in each loop,

(7) name of file which contains the output data and can be processed to obtain a graphic representation of results,

The output consists of time histories of steel strain, bar slip, steel and bond stress along the top and bottom reinforcing layer of the subregion, as well as time histories of concrete strain and stress, crack width, moment, and concentrated rotation at cracked sections.

CHAPTER 5

COMPARISON BETWEEN ANALYTICAL RESULTS AND EXPERIMENTAL EVIDENCE

In this chapter a comparison of analytical predictions based on the proposed model with experimental evidence will be presented and commented upon. The experimental evidence stems from a series of tests on half-scale beam-column subassemblages specifically designed to study the behavior of interior joints under severe cyclic excitations. The cruciform shaped assemblages (Fig.5.1) were proportioned and detailed so as to minimize diagonal shear cracking and preclude significant shear deformations in the joint panel region. Moreover the shear-span ratio of the girders limited the development of significant shear stresses in the beam inelastic regions. Since the design of the subassemblages was based on a strong column-weak beam design philosophy, the columns remained essentially elastic during the entire load history and all inelastic action was concentrated in the interior joint and in the beam inelastic regions. Because of the above considerations, the design of the specimens satisfied the assumptions of the analytical model stated in the introduction to Chapter 2. Thus the experimental evidence derived from these tests offers an ideal opportunity to establish the validity of the proposed model.

5.1. Test specimens

In the series of tests reported in Refs. [42], [43] and [50], the specimens referred to in the following, carried the names BC3 and BC4. The cruciform shaped half-scale beam-column subassemblages, shown in Fig. 5.1, modeled a part of a 20-story reinforced concrete ductile moment-resisting frame at the third floor level. Both specimens had identical configuration and dimensions consisting of two 9 in. by 16 in. girders and a 17 in. by 17 in.

square column. In both specimens the main longitudinal reinforcement of the girders consisted of four #6 bars at the top and three #5 bars at the bottom. Thus the area of reinforcement at the bottom was about half that at the top following common design practice. The mechanical properties of concrete used in casting the specimens were established on the basis of standard concrete cylinder tests and are depicted in Fig. 5.2a. The mechanical characteristics of reinforcing bars were determined from machined test specimens and are shown in Fig. 5.2b. The two subassemblages were subjected to entirely different load histories: specimen BC4 was subjected to a single large displacement reversal simulating the effect of a very severe pulse-like seismic excitation; this kind of load history can also be used in establishing the monotonic moment-rotation envelope curve for the joint end sections; specimen BC3 was subjected to a large number of deformation reversals of gradually increasing magnitude.

Strains in the reinforcement were measured by weldable gages. The gages on the beam longitudinal reinforcement were placed in the girder end region just outside the column faces, so that their presence would not disturb the bond condition of the reinforcing bars anchored in the joint. Four precision linear potentiometers were used to measure bar slippage at the four corners of the joint panel region. These were rigidly connected to steel pins soldered to the reinforcing bars adjacent to the beam-column interfaces. Four additional potentiometers were used to measure the sizes of the large beam-column interface cracks. As pointed out in Ref. [50], measurements at the interface crack were necessary, first, in order to compute the slippage of reinforcing bars relative to the surrounding concrete at the beam-column interface, and secondly, in order to provide an alternative determination of fixed-end rotations due to slippage of the bars in the connection.

The question of determining the fixed-end rotation at the beam-column interface requires a thorough discussion. It is possible to compute the fixed-end rotation based on the end slip of reinforcing bars which results due to bond deterioration within the joint only. In this case the contribution of the relative slip between reinforcing bars and girder end region is not included in the fixed-end rotation, but is taken into account when computing the inelastic rotations in the girder end region. The fixed-end rotation is then based on the following relation:

$$\Theta_{FE} = \frac{u^t - u^b}{d'} \tag{5.1}$$

where u is the relative slip between reinforcing bars and surrounding concrete at the beam-column interface resulting from bond deterioration in the joint only. A superscript denotes top or bottom reinforcing layer and d' is the distance between the top and bottom reinforcing bars.

Alternatively, the contribution of relative slip between reinforcing bars and surrounding concrete in the girder end region to the rotation at the beam-column interface can be taken into account by determining the fixed-end rotation on the basis of the relation

$$\Theta_{FE} = \frac{w^t - w^b}{d'} \tag{5.2}$$

where w is the crack width at the top or bottom reinforcing layer (Fig.2.7).

In Ref. [50] fixed-end rotations were measured on the basis of Eq. (5.1) and the contribution of the relative slip which arises in the girder inelastic region was included in the girder rotations. In order to be able to directly compare analytical with experimental results the same formulation was used in the following studies. The advantage of this approach lies in the fact that attention is confined to the interaction between reinforcing steel and concrete in the joint only leading to considerable simplification in the computations. The disadvantage is that Eq.(5.1) yields erroneous results as soon as bond is completely damaged within the joint region and the bars start slipping through the joint. In this case the bars can still be anchored in the girder end region adjacent to the joint. Because bond is completely damaged in the joint, the crack at the beam-column interface on the push-in side of the bars quickly closes during reloading. This process gives rise to large end slip values on the pull side of the bars, which are underestimated by Eq. (5.1), where the relative slip between reinforcing bars and surrounding concrete in the girder end region is not taken into account. Neglecting the influence of the girder end region usually leads to a sharp drop in the strength of the joint as soon as bond is completely damaged in the joint. This decrease in strength is due to spalling of concrete cover in the girder end region and is in reality much more gradual.

For the above reasons the results to be presented in the next two chapters remain valid only as long as bond is not completely damaged in the joint. As soon as anchorage failure initiates in the joint, the fixed-end rotations are underestimated and the decrease in strength is overestimated. The instant of complete bond damage along the bars anchored in the joint will be called in the following "joint anchorage failure". It should be kept in mind, however, that "joint anchorage failure" does not imply complete anchorage failure and collapse of the subassemblage.

5.2. Comparison and discussion of results

5.2.1. General

Before proceeding with the discussion of results, it is necessary to consider the data which are needed as input to the computer program JOINT. Apart from the imposed deformation time history, the material mechanical characteristics for reinforcing steel and confined and unconfined concrete, as well as bond stress-slip envelopes along the top and bottom reinforcing bars anchored in the joint have to be specified.

The specification of material mechanical characteristics for steel and concrete is based on the information given in Chapter 3 and on the data given in Fig. 5.2. The descending slope Z of the concrete stress-strain relation in the strain softening range (Eq.3.20) and the strength increase factor K in Eqs. (3.19)-(3.21) are determined from the amount of confinement supplied by stirrup-ties in the girder end region. The beam stirrup-ties consisted of #2 bars spaced at 3.5 in. center-to-center.

The specification of bond stress-slip envelope curves along the bars anchored in the joint requires some clarification. As was pointed out in Section 3.2, the characteristic values of the monotonic envelope curves can be based on suggestions presented in Ref. [23]. For the sake of completeness these suggestions were summarized at the end of Section 3.2, where two different envelope curves were presented in the case of interior joints: one pertaining to well confined concrete in the joint core region and the other pertaining to unconfined concrete in the column cover (see also Fig.3.12). The dividing line between the two cases can not be sharply defined in a joint panel region. Therefore it is suggested to assume a gradual transition between the region of well confined concrete and the region of unconfined concrete. In summary, the following regions have been assumed in this study (Fig.5.3):

(1) unconfined concrete extends 1 d_b into the column cover region on both ends of the joint, where d_b is the reinforcing bar diameter,

(2) transition region between unconfined and confined concrete extends 2 d_b from the end of the unconfined region on both ends of the joint,

(3) the remaining column core region is considered as confined concrete region.

The above recommendations regarding the extent of the unconfined concrete region as well as the transition region are derived from the dimensions of the pull-out cone. More details are presented in Refs. [23] and [50]. Due to the limited number of tests on single reinforcing bars embedded along the entire width of the column and subjected to cyclic excitations, the above suggestions are tentative and need to be confirmed by further experimental evidence.

5.2.2. Specimen BC4

Experimental and analytical results for specimen BC4 are presented first. To avoid ambiguity, the beam on the left of the column is referred to as "west beam". Similarly, the beam to the right of the column is referred to as "east beam" (Fig.5.4). For reasons of consistency, relative slip values are defined as positive if the reinforcing bars move in the positive x-direction relative to the surrounding concrete (Fig.5.5). This implies that bar pull-out on the west beam side is associated with negative slip values, while positive slip values represent bar pull-out on the east beam side. As noted previously, the fixed-end rotations predicted by the analytical model are determined on the basis of Eq. (5.1) in order to facilitate a comparison with experimental results.

Analytical and experimental results for specimen BC4 are presented in Figs. 5.6-5.9. First, the global behavior of the beam-column joint is exhibited by means of the moment-rotation relation at the two end sections of the joint. The results of two analytical solutions are compared with experimental evidence: the first analytical solution is based on a bilinear steel stress-strain model while the second is based on Menegotto-Pinto's steel model which accounts for the Bauschinger effect. Then the local behavior of the joint is investigated more closely by studying the hysteretic relation between end moment and relative slip as well as the relation between end moment and reinforcing steel strain at the two end sections of the joint. In addition, the distribution of steel strain, steel stress, relative slip and bond stress along the top and bottom reinforcing layers in the joint panel region is presented at the end of each deformation excursion. Regarding the analytical predictions on the local behavior, only the results which are based on the nonlinear steel model are presented. In order to be able to relate the results pertaining to the local behavior of the interior joint, shown in Figs. 5.7-5.9, to those on the global behavior depicted in Figs. 5.6a and b, corresponding load points are identified by capital Roman letters. Joint end moments are considered as positive when acting counterclockwise. This sign convention is also shown on all figures where the fixed-end rotation is denoted by Θ_F.

Figures 5.6a and b show the hysteretic moment-fixed-end rotation relation for the west and east beam sides of the joint of specimen BC4, respectively. Since there is very little difference between the results of the two analytical models in the case of the west beam, only the analytical predictions which are based on the nonlinear steel model are presented in Fig.5.6a. It is noted that the analytical model represents satisfactorily the experimentally observed behavior. In the case of Fig. 5.6b, which depicts the moment-rotation relation at the east beam-column interface, noticeable deviations appear between the results of the two analytical models during reloading after the first unloading. By contrast, no difference exists in the behavior of the two models during the reloading phase following the second unloading. In the case of the first reloading, the damage of bond in the joint panel region is limited and the behavior of the joint end section during reloading is controlled by the hysteretic behavior of steel. This happens because the crack at the beam-column interface is open through the whole depth of the beam section. Clearly, neglecting the Bauschinger effect in this case causes significant deviations between predicted and actual response. In the case of the second reloading, the previously inflicted bond damage is quite substantial causing the bars to slip freely through the joint. In this case the behavior of the joint end section is controlled by the hysteretic behavior of bond and the inclusion of the Bauschinger effect does not affect the results very much. The substantial loss of strength of the joint after two severe deformation reversals is evident in Fig. 5.6b (point C). This is due to complete bond damage in the joint panel region which leads to joint anchorage failure.

Figure 5.7 depicts analytical and experimental results of the end moment-relative slip relation at the four corners of the joint panel region. As pointed out in Chapter 4 the boundary conditions in the case of interior joints are imposed by specifying slip increments Δu_1^b and Δu_n^t or Δu_1^t and Δu_n^b depending on the sense of the applied end moments. This explains why the analytical pull-out values at the instant of load reversal coincide with experimental data (Fig.5.7). By contrast, the push-in values in Fig. 5.7 are determined by the analytical joint model and, therefore, only approximate the experimental results. This fact accounts for the small deviations between analytical and experimental fixed-end rotations at the instant of load reversal (Fig.5.6). As can be seen in Fig. 5.7, the experimental moment-slip history is well represented by the analytical model. In particular the closing process of the bottom crack, Fig. 5.7a, characterized by the abrupt change of stiffness in the moment-slip curve, is satisfactorily predicted. Clearly, no analytical model can possibly describe the gradual crack closing process, which is due to the presence of concrete rubble and the effects of shear sliding at the crack interface. Nonetheless it is important that the model predicts accurately the instant of crack closure. This seems to be the case with the proposed model.

It is to be noted that the upper crack on the east beam side remains open at load point B (Fig.5.7d). At the same time the bottom crack opens to a width of 8 mm (Fig.5.7c). This fact is explained in detail later in connection with results for specimen BC3. It is important to note at this stage, however, that, while the crack at the beam-column interface remains open across the whole depth of the beam section, the shear is transferred across the interface only by dowel action of the beam reinforcing bars. This can lead to significant shear sliding and inflict additional bond damage in the vicinity of the crack.

Fig. 5.8 shows the moment-strain relation at the four corners of the joint panel region. In this case the experimental results can only be compared qualitatively, since, as reported in Ref. [50], the steel strains have been measured by 9 in. long strain gages. The measured strains thus represent *average* strains over the length of 9 in. and cannot be directly compared to analytically predicted strains which are computed at the location of the beam-column interface. As the distribution of steel strains along reinforcing bars in cracked R/C members clearly indicate, steel strains decrease very quickly away from the location of a crack. Analytical predictions compare nonetheless satisfactorily with experimental results in a qualitative sense. In Fig. 5.8a the characteristic change in curvature of the moment-strain relation when the crack starts to close is described quite well by the model. Similarly, Fig. 5.8d shows good qualitative agreement between analytical and experimental results regarding the strain at the top reinforcing layer at load point B. These results seem to support the assumptions of the concrete section model regarding partial compatibility of strains between reinforcing steel and surrounding concrete at the crack, which were presented in Section 3.3.

Figure 5.9 depicts the distribution of steel strain, steel stress, relative slip and bond stress along the top and bottom reinforcing bars anchored in the joint. The distributions are plotted at the end of each deformation excursion, i.e. at load points A, B and C in Fig.5.6. It is observed in Fig. 5.9a that even at the end of the first large excursion into the inelastic range there is a certain amount of slip-through of the bottom reinforcing bars along the entire anchorage length. It is thus important to recognize that there exists an interaction between the two end sections of the joint, established by the rigid body motion of the anchored bars. This interaction becomes more pronounced as the number and magnitude of slip reversals at the joint end sections increases, as can be seen in Figs. 5.9b and 5.9c. At load point C the slip-through of the bottom reinforcing bars amounts to 0.5 *mm* indicating considerable bond damage, which leads to the loss of strength of the joint observed in Fig.5.6b. The observed interaction between the two joint end sections destroys any hope for modeling the moment-fixed-end rotation relation of one joint end section independently from the other.

5.2.3. Specimen BC3

Analytical results for specimen BC3 are presented in Figs. 5.10-5.18. In this case experimental evidence is limited to moment-rotation relations at the two end sections of the interior joint, denoted, as before, west and east beam, and to slip values attained at the four corners of the joint panel region at the moment of load reversal. The same order of presentation as in the case of specimen BC4 is followed. Only the analytical results which are based on the nonlinear steel model are discussed. In the case of several cycles of deformation reversals the use of a bilinear steel model leads to inaccuracies and should be avoided.

First, the global behavior of the interior joint is presented by means of the hysteretic moment-rotation relation at the two beam-column interfaces, shown in Figs. 5.10-5.12. Fig. 5.10 depicts the analytically predicted moment-fixed-end rotation relation of the joint end sections up to rotation values of 0.01 rad. Fig. 5.11 on the other hand shows the moment-fixed-end rotation relation until the moment that, due to pull-out of the bars in the bottom reinforcing layer, "joint anchorage failure" is initiated. At the same time, as shown in Fig. 5.11b, considerable loss of strength of the joint takes place due to complete damage of bond along the bottom reinforcing layer. In order to facilitate a comparison of analytical results with experimental evidence, single moment-rotation loops are selected from Fig. 5.10 and plotted individually in Fig. 5.12.

The local behavior of the interior joint is studied by means of the relation between end moment and relative slip as well as the relation between end moment and reinforcing steel strain at the beam-column interfaces, shown in Figs. 5.13-5.14. Also, the steel stress-strain time history in the top and bottom reinforcing bars is depicted in Fig.5.15. The distribution of steel strain, steel stress, relative slip and bond stress along the top and bottom reinforcing layers in the joint panel region is presented at the end of the four last deformation excursions before anchorage failure. In order to be able to associate the results pertaining to the local behavior of the interior joint, shown in Figs. 5.13-5.16, to those on the global behavior depicted in Figs. 5.10-5.12, corresponding load points are identified by capital Roman letters (K,L,M and N). Joint end moments are considered as positive when acting counterclockwise. This sign convention is also shown on all figures.

The comparison of single moment rotation loops, shown in Fig. 5.12, leads to the conclusion that the analytical model predicts satisfactorily the response of the joint even under rather large deformation reversals. Several important parameters of hysteretic joint behavior such as stiffness and strength of the joint, energy dissipation capacity and moment of crack closure are described adequately. As already noted in the case of specimen BC4, the instant of crack closure is characterized by a sharp change of stiffness in the analytical moment-rotation relation. By contrast the experimental results show a much more gradual closing process, a fact attributed to the presence of concrete rubble and the effects of shear sliding at the crack interface.

As seen in Figs. 5.10-5.12, the moment-rotation hysteresis loops demonstrate differences in joint behavior under positive and negative end moments. By noting the sign convention for end moments which was defined above and the fact that, following common design practice, the area of the bottom reinforcing layer is about half the area at the top layer, two cases of joint behavior can be distinguished:

(1) the top reinforcing layer is subjected to tensile forces,

(2) the bottom reinforcing layer is subjected to tensile forces.

In the first case the crack sooner or later closes. The moment-rotation relation exhibits a small stiffness between points I_1 and I_2 in Fig. 5.12a while the crack remains open. Once the crack closes at point I_2, the stiffness of the joint increases considerably due to the contribution of concrete in contact at the crack interface. In the second case the beam-column interface crack remains open through the whole depth of the beam cross-section until the load is reversed again. The joint end moment is thus resisted by a steel-couple force at the top and bottom reinforcing layer. This fact is reflected in the shape of the moment-rotation relation between points J_1 and K in Fig. 5.12a, which essentially follows the stress-strain relation of reinforcing steel. The difference between moment-rotation and steel stress-strain relation is due to slip of reinforcing bars as the steel forces build up, causing the moment-rotation stiffness to be smaller than the stiffness indicated by the steel stress-strain relation.

In order to investigate the effect of crack closure more accurately, the relation of end moment versus relative slip of reinforcing bars at the four corners of the joint panel region, shown in Fig. 5.13, is examined. It is noted that the crack at the bottom of the beam section at the beam-column interface closes every time the bottom reinforcing bars are subjected to compressive forces (Figs. 5.13a and c). As can be seen in Figs. 5.14a and c as well as Fig. 5.15a, which show the relation between end moment and steel strain and the relation between steel stress and steel strain, respectively, the tensile forces developed in the top bars suffice to yield the bottom bars in compression; therefore, the bar pull-out imposed during the previous half cycle is overcome and the crack closes. Figs. 5.13b and d by contrast show that the crack at the top of the beam section at the beam-column interface does not close when the top reinforcing bars are subjected to compressive forces. Since the area of the bottom reinforcing layer is only about half that of the top layer, the tensile yield force developed in the bottom bars does not suffice to yield the top bars in compression (Figs. 5.14b and d and Fig. 5.15b). As a consequence, the slip of the top bars due to pull-out introduced during the previous half cycle is not overcome and the crack at the top of the section remains open (e.g. point M in Fig. 5.13b). At the same time the crack at the bottom of the same section is wide open due to pull-out associated with the imposed tensile forces in the bottom reinforcing bars (point M in Fig. 5.13a). Thus the crack at the beam-column interface remains open through the whole depth of the beam cross-section until the load is reversed again. This has important consequences in seismic resistant design; while the crack remains entirely open, the shear force at the beam-column interface is resisted only by dowel action of the longitudinal reinforcing bars; this leads to additional deterioration of stiffness associated with splitting of concrete along the reinforcing bars and acceleration of bond damage in the vicinity of the crack.

Figure 5.14 depicts the relation of end moment versus steel strain at the four corners of the joint panel region. It is seen that once the crack closes at the bottom of the beam end sections the major part of the tensile force that develops in the top bars is resisted by the concrete in contact rather than the bottom reinforcing bars. This leads to rather small steel strain increments beyond the point of crack closure and to the characteristic change in curvature of the moment-steel strain relation at the instant of crack closure.

By comparing the steel stress-strain histories in the top and bottom reinforcing bars (Figs. 5.15a and b), it becomes apparent, that the uneven distribution of steel area between the top and bottom reinforcing layer, which is common design practice, leads to considerable cyclic strain reversals in the bars of the weaker layer. As already pointed out, this is due to the bottom reinforcing bars yielding in compression whenever the top bars are subjected to tensile stresses. By contrast, the cyclic strain reversals in the bars of the strong layer are less pronounced, since the top bars do not yield in compression when they are subjected to compressive stresses. Therefore the previously accumulated plastic strain set is not recovered and the cyclic strain history of the top reinforcing bars tends to center about an ever increasing tensile plastic strain, a well known experimental fact.

The distribution of steel strain, relative slip, steel stress and bond stress along the anchorage length of the top and bottom reinforcing bars is depicted in Fig. 5.16 at different moments of the load history. Several such distributions pertaining to the bottom reinforcing bars are compiled in Figs. 5.17 and 5.18 in order to facilitate a comparison of the distribution of the above variables with increasing magnitude of deformation reversals. Capital Roman letters denote the different load reversal points which are identified in Figs. 5.10, 5.11 and 5.13a and c. Several observations can be made:

(1) since the area of the bottom reinforcing layer is only about half the area of the top layer, the cyclic reversals of steel strain and relative slip are more pronounced at the bottom layer. This leads to accelerated bond damage along the bottom reinforcing

bars anchored in the joint. Eventually the damaged bond cannot transfer the steel forces and the bottom bars slip through the joint as a rigid body (Figs. 5.16d and 5.17b). Thus functional failure of the interior joint always initiates along the weaker reinforcing layer,

(2) by considering the distribution of steel strains along the width of the joint it becomes apparent that a large portion of each reinforcing layer remains elastic during the entire load history (Figs. 5.17a and 5.18a). The observed slippage of reinforcing bars at the end sections of the joint results from the plastic deformations in the column cover regions and from the relative slip of the elastic portion of the bars (see Figs. 5.17b and 5.18b). The contribution of elastic deformations in the bars to the relative slip at the ends of the joint is relatively insignificant. Therefore, the relative slip of the elastic portion of the bars with respect to the surrounding concrete is largely "rigid body slip" and will be denoted as such below,

(3) it is to be noted that even under small inelastic deformation reversals there is a certain amount of constant bar-slip extending over the entire width of the joint (see Figs. 5.17b and 5.18b). This movement of the bars as a rigid body leads to an interaction between the forces and deformations at the two beam-column interfaces of the interior joint. This interaction becomes very pronounced under large deformation reversals (compare e.g. an almost constant slip of 1 *mm* at load point M in Fig.5.18b) and should not be neglected in any studies which attempt to describe the hysteretic behavior of interior joints,

(4) it is interesting to note that the distribution of bond stress is nearly constant over the core region of the joint leading to an almost linear distribution of steel stresses in this region (see Figs. 5.17c and d and 5.18c and d).

A question of considerable interest in understanding the hysteretic behavior of R/C beam-column joints can be addressed with the aid of Fig. 5.19, where the envelope curve obtained under monotonic loading is superimposed on the hysteretic curves resulting from cyclic loading. Note that all these curves have been obtained analytically. It is seen that in general the cyclic envelope values are smaller than the corresponding monotonic envelope values. It can also be noted that the strength increase of the joint due to strain hardening of reinforcing steel is relatively small under cyclic loading resulting in a very small strain hardening ratio in the cyclic moment-rotation relation. To determine why the cyclic envelope values remain smaller than the monotonic envelope values, the strains in the reinforcing bars can be compared at load points with equal fixed-end rotation values. Two such load points are, for example, point A in Fig. 5.6b and point L in Fig. 5.11a. The corresponding steel strain values are shown in Figs. 5.8d and 5.14b, respectively. It is seen that the strain under monotonic loading is larger thus resulting in larger steel forces and consequently moments. By contrast, the corresponding relative slip of reinforcing bars in the same layer is slightly larger under cyclic loading, as can be seen from Figs. 5.7d and 5.13b (points A and L, respectively). The above observations indicate that the same amount of relative slip or, for that matter, fixed-end rotation at the beam-column interface results in different steel strains at the ends of the joint. This is due to the different amount of rigid body slip of reinforcing bars through the joint as a consequence of different load histories. Severe cyclic load reversals lead to more bond damage than monotonic loading of the same severity of deformation thus giving rise to larger rigid body slip values, as can be seen in Figs. 5.9a (for point A) and 5.16b (for point L). In conclusion, it becomes apparent that it is not possible to accurately define a single moment-fixed end rotation envelope curve which could be used in analytical studies regarding the influence of joint behavior on the seismic response of R/C frames. The actual envelope curve is a function of load history.

CHAPTER 6

PARAMETRIC STUDIES ON AN INTERIOR JOINT

The purpose of this chapter is to present a number of parametric studies on the hysteretic behavior of an interior beam-column joint which were conducted with the aid of the proposed analytical model. Although the studies are confined to an interior joint only, it is believed that many of the conclusions arrived at in this chapter also pertain to exterior joints and critical regions in girders whose behavior is substantially affected by bond deterioration. In conducting these studies attention was focused on establishing the significance of each parameter rather than covering a large set of parameter values, because this suffices to derive qualitative design recommendations independently from the dynamic characteristics of the structure and the ground motion. A more thorough investigation can then relate the results of dynamic response analyses of several structural systems subjected to a number of ground motions with parametric studies on beam-column joints covering a large set of parameter values. In this manner it will be possible to arrive at specific recommendations regarding the design of interior and exterior beam-column joints which are likely to be subjected to large deformation reversals. This step, however, requires rather extensive analytical studies and is beyond the scope of this investigation.

This chapter concentrates on qualitatively and quantitatively describing the influence of several important parameters on the hysteretic behavior of an interior beam-column joint. Results on the significance of individual parameters are presented in Sections 6.1-6.6. These are then summarized and compared in Section 6.7, where conclusions regarding the significance of each parameter on the hysteretic behavior of interior beam-column joints are also presented.

6.1. General

Because the experimental evidence presented in Chapter 5 refers to half-scale interior beam-column joints, the parametric studies reported here were conducted on a half-scale joint. In this manner some of the results and conclusions of Chapter 5 can be more fully evaluated in the light of the evidence presented below. The fact that a half-scale joint has been selected for this study does not necessarily impose a limitation on the presented results, since attention is focused on the relative performance of the same beam-column joint under a variation of parameters. In order, however, to determine the significance of the developed procedures to actual situations, a full scale beam-column joint has also been investigated. The comparison of results between half and full scale joints is particularly important in establishing the scaling effect, if any, in structural subassemblages whose response is affected by cyclic bond deterioration. Such investigation can contribute to correctly interpreting experimental evidence from reduced scale R/C subassemblages.

The dimensions and reinforcing arrangement of the half scale interior beam-column joint, which is the subject of the following parametric investigation were presented in Fig. 5.1. As shown in Fig. 5.2b the yield strength of the main reinforcing bars was 71 ksi, which corresponds to $489\,MPa$. Four #6 bars were placed in the top reinforcing layer and three #5 bars in the bottom. In accordance with Chapter 5 average bond conditions were assumed and the characteristic values of the monotonic bond stress-slip envelope curve suggested in Chapter 3 were adhered to. These suggestions require a maximum bond strength of $16.2\,MPa$ in the confined column core region.

6.2. Variation of bond conditions

The sensitivity of the hysteretic behavior of beam-column joints to variation in the characteristic strength values of the monotonic bond stress-slip envelope curve is of considerable importance. First, because, as noted in Ref. [23], there is considerable scatter in the experimentally determined bond strength along the short embedment length of a deformed bar anchored in well confined concrete. Secondly, because the quality of construction in the field can substantially affect the quality of bond in the joints. For these reasons the characteristic strength values of the monotonic bond stress-slip envelope were reduced by 15% along the whole embedment length of the bars anchored in the joint. This reduction in bond strength still lies within the normal scatter of experimental results (Ref. [23]). To simulate bond conditions as they might result under poor construction practice, a reduction of the characteristic bond strength values by as much as 50% might be needed. Here, only the 15% reduction of bond strength was considered.

Figure 6.1a and b shows the hysteretic moment-rotation relation at the beam-column interfaces of the interior joint. The sign convention adopted in Chapter 5 is retained, along with the designation of the beams as west and east beam. Figure 6.1 is plotted to the same scale as Fig. 5.10, so that a direct comparison of results is facilitated. By comparing the hysteretic behavior of the interior joint resulting from a reduction in bond strength by 15% (Fig.6.1) to that of the same joint under average bond conditions (Fig.5.10), it is apparent that the reduction in bond strength leads to a more pronounced pinching of the hysteretic loops. Moreover, certain portions of the reloading curves exhibit zero stiffness indicating that the bars slip freely through the joint. This effect leads to a substantial reduction in energy dissipation capacity. More comments on the relative behavior of the interior joint under a reduction in bond strength will be presented in Section 6.7.

6.3. Ratio of top to bottom reinforcement

The ratio of the total area of reinforcing bars placed in the bottom layer to that of the top reinforcing layer plays an important role in the hysteretic behavior of R/C members. For this reason current codes on seismic resistant design stipulate that this ratio should not be less than 50%. Based on a number of tests on R/C subassemblages, Bertero and Popov suggested in Ref. [13] that this ratio be increased to 75%. In order to quantitatively investigate the effect of the ratio of top to bottom reinforcement, the girder reinforcement passing through the joint was changed, so that the area of the bottom reinforcing layer is equal to the area of the top layer. The dimensions of the joint and the material data were kept the same as those of specimen BC3. To avoid that yielding of the girders on both sides of the column will also induce yielding of the column, the sum of the girder yield moments in the same direction of bending at both ends of the joint has to be less than the yield capacity of the column. Thus in placing equal amount of reinforcement in the top and bottom reinforcing layer, an effort was made to keep the sum of girder yield moments in the same direction of bending the same as in specimen BC3. As a result, four #5 bars were placed in each reinforcing layer resulting in a total area of 800 mm^2 per layer. By contrast, the total reinforcing areas for specimen BC3 were 1136 mm^2 and 600 mm^2 for the top and bottom layer, respectively.

The hysteretic behavior of the interior beam-column joint is presented in Figs. 6.2a, b, c and d. The moment-fixed end rotation relation for the west beam-column interface is depicted in Figs. 6.2a and b. Figure 6.2a plots the moment-rotation time history up to rotation values of approximately 0.01 rad, while Fig. 6.2b shows the moment-rotation time history up to the point at which the bottom reinforcing bars slip through the joint which, however, is not discernible in the figures. Figures 6.2a and b can be directly compared with Figs. 5.10a and 5.11a, respectively, since these are plotted to the same scale.

The hysteretic loops show remarkably little pinching in the case of equal amount of top and bottom reinforcement, resembling the ideal behavior assumed in Clough's hysteretic model. Stable hysteretic behavior is sustained until anchorage failure of the bottom reinforcing bars takes place in the joint. Anchorage failure is understood to mean complete damage of bond along the reinforcing bars anchored in the joint. As a consequence, the steel forces can not be transferred within the joint panel region and a reduction in strength results, since the possibility of anchorage in the girder end region is not included in the analysis. As illustrated in Fig. 6.2b, there is a slight increase in strength of the joint associated with the strain hardening of reinforcing bars. By contrast, Fig. 5.11a indicates a decrease in end moment with increasing fixed-end rotation on the strong side of the joint. This effect is due to significant bond deterioration in particular along the bottom bars anchored in the joint.

In order to explain the stable hysteretic behavior in the case of equal amount of top and bottom reinforcement, Figs. 6.2c and d are prepared which show the hysteretic relation between end moment and relative slip at the west beam-column interface. It is seen that the crack at the interface closes every time the reinforcing bars at the corresponding layer are subjected to compressive forces. This happens because the tensile yield force of each layer suffices to yield the other layer in compression and close the crack. When the area of the bottom reinforcing layer is less than the area at the top layer, the crack can remain open through the whole depth of the girder section at the beam-column interface (Fig.5.13b). This fact induces two detrimental effects, which accelerate the stiffness deterioration of the joint: first, the shear forces across the interface crack are resisted only by dowel action of the main reinforcing bars crossing the crack. This induces shear sliding and splitting of concrete cover. Secondly, under these circumstances the reinforcing bars anchored in the interior joint are subjected to cyclic pull from one side and push from the other. This accelerates the deterioration of bond in the interior of the joint. The delayed deterioration of bond in the case of equal amount of top and bottom reinforcement is demonstrated by the steeper reloading stiffness in Fig. 6.2b, as compared to the reloading stiffness of specimen BC3 in Fig. 5.13a.

It can be concluded from the above that the ratio of top to bottom reinforcing area has a significant influence on the hysteretic behavior of R/C beam-column joints. The performance of these joints under severe deformation reversals can be improved by requiring that the area of reinforcement at the bottom of the girder is set equal to the area at the top. In this respect it should be noted that the lateral resistance of the structure can be maintained without increasing the total amount of reinforcement, provided that the serviceability requirements are not violated at the ends of the girders.

6.4. Variation of yield strength of reinforcement

Varying the yield strength of reinforcement can significantly affect the hysteretic response of R/C members whose behavior is controlled by bond deterioration. Reducing the yield strength of reinforcing bars and keeping the section moment at the end of the joint constant results in a larger number of bars in each reinforcing layer. This leads to an increase in the total circumference of reinforcing bars as the latter is directly related to the number of bars in a layer. It is the increase in the ratio of the total bar circumference to the total cross-sectional area of the bars that considerably improves bond conditions in a beam-column joint. Precisely the same effect can be arrived at by keeping the yield strength of the reinforcement constant and reducing the diameter of the reinforcing bars anchored in the joint, leading again to an increase in the number of bars in each layer. On the other hand, as noted in Ref. [23], the effect of bar diameter on the bond stress-slip envelope curve is only minor, provided that the clear distance between the bars is larger than $4\,d_b$, where d_b is the reinforcing bar diameter. In practical situations the clear distance between reinforcing bars usually amounts to less than $4\,d_b$ and this fact has to be taken into account by reducing the bond stress-slip envelope curve according to Section 3.2. Because of the above reasons it is the number of bars in each layer that affects the hysteretic behavior of joints the most.

In an effort to investigate this effect the yield strength of reinforcement was reduced to $326\,MPa$. In order to keep the girder end moments unchanged with respect to specimen BC3, six #6 bars were placed at the top of the girder section, whereas one #4 and four #5 bars were placed at the bottom, resulting in a total area of reinforcement of $1704\,mm^2$ at the top and $929\,mm^2$ at the bottom. Thus $|M_y^+| + |M_y^-|$ remains the same as in specimen BC3. It is to be noted that the ratio of top to bottom reinforcement was kept the same as in specimen BC3, so as to exclude this effect from the results.

The hysteretic behavior of the interior beam-column joint is depicted in Figs. 6.3 and 6.4. Figure 6.3 plots the moment-fixed end rotation time history for west and east beam column interface of the joint. The time history for fixed-end rotation values up to approximately 0.01 rad is shown in Figs. 6.3a and b, while the entire time history is illustrated in Figs. 6.3c and d. Figures 6.3a and b can be directly compared with Figs. 5.10a and b, whereas Figs. 6.3c and d correspond to Figs. 5.11a and b. Figure 6.4 plots the relation between end moment and relative slip at the west beam-column interface of the joint and corresponds to Figs. 5.13a and b.

It is apparent from Figs. 6.3 and 6.4 that the reduction in yield strength of reinforcing bars and the associated increase in the number of bars in each reinforcing layer significantly improves the hysteretic behavior of the joint. The pinching of the loops is less pronounced than that of specimen BC3, particularly in the later stages of the load history, and the reloading stiffness before crack closure is larger. This indicates better conditions of bond and a delayed bond deterioration as compared to specimen BC3. However, as Fig. 6.4a indicates, the crack at the top of the beam-column interface remains open, when the top reinforcing bars are subjected to compressive forces. In such cases the crack remains open across the whole depth of the section at the interface until the moment is fully reversed. This indicates that the problem of shear transfer at the beam-column interface may be critical, as long as the ratio of bottom to top reinforcing area does not approach unity.

6.5. Variation in history of loading

The effect of history of loading on the hysteretic behavior of R/C members has been noted by several investigators in the past. Bertero states in Ref. [9] that the experimental studies on R/C subassemblages must consider different load histories. For example, a large deformation reversal might cause sufficient damage so as to substantially reduce the moment-rotation stiffness of the joint during subsequent deformation reversals of smaller magnitude. To investigate this effect specimen BC3 was subjected to an entirely different load history than the one considered in Chapter 5, which consisted of a number of deformation reversals of gradually increasing magnitude. In this study the interior joint was subjected to a severe deformation cycle, followed by two cycles of smaller magnitude, at the end of which the magnitude of deformation reversals was gradually increased until the bottom reinforcing bars slipped through the joint.

The results of the effect of history of loading are presented in Figs. 6.5a and b, which depict the hysteretic moment-rotation relation at the west and east beam-column interface, respectively. No discernible difference between the hysteresis loops in Fig. 6.5 and those in Figs. 5.10 and 5.11 is observed. It is noted, however, that fewer large cycles suffice to initiate joint anchorage failure along the bottom reinforcing bars. More details are presented in Section 6.7 where the total energies dissipated by the interior joint under different load histories are compared.

6.6. Effects of scale on hysteretic behavior of joints

One of the important questions in the investigation of the hysteretic response of R/C members, whose behavior is controlled by bond deterioration is how to interpret experimental evidence from reduced scale specimens in predicting the physical behavior of full-size members. This is of particular importance in the case of beam-column joints, whose hysteretic behavior is substantially affected by cyclic bond deterioration along the bars anchored in the joint. An answer to the above question would clarify whether there exists a scaling law which relates experimental results from reduced scale reinforced concrete subassemblages to the response of full-size members.

To investigate the effects of scale on the hysteretic behavior of interior beam-column joints, specimen BC3 has been increased in size to that of a full scale subassemblage by multiplying the design variables through the corresponding scaling factors. Because of the restriction in the choice of reinforcing bar diameter imposed by industrially available sizes, the scaling factor for area of reinforcement was only approximately satisfied. By using three #10 bars at the bottom and two #11 and three #10 bars at the top the total area of bottom reinforcement was 2457 mm^2 and that of the top reinforcement was 4469 mm^2. In selecting these bars an effort was made to keep the ratio of top to bottom reinforcement the same as in specimen BC3. All other linear dimensions of the full-scale model were double those of specimen BC3.

The hysteretic behavior of the full-scale model is presented in Fig. 6.6 with the aid of the moment-rotation relation at the west and east beam-column interface of the interior joint. In order to be able to directly compare Figs. 6.6a, b, c and d with the corresponding relations pertaining to the half-scale interior joint, namely Figs. 5.10a, b and Figs. 5.11a and b, respectively, the end moments of the full-scale model have been reduced by the factor 8 which represents the moment scaling factor between full-scale and half-scale models. By contrast, the fixed-end rotations remain unchanged between full and half-scale models, since a dimensionless quantity should transform like a constant. To facilitate a comparison of results corresponding load points have been designated by capital Roman letters.

By comparing Figs. 6.6a and b with Figs. 5.10a and b, respectively, it is seen that the behavior of the full-scale model is similar to the hysteretic behavior of the half-scale model for rotation values up to 0.01 rad. This similarity between the full and half-scale models is lost at large rotation values, as can be seen in Figs. 6.6c and d, which depict the complete moment-rotation time history of the interior joint until the bottom reinforcing bars slip through the joint. The slip-through of reinforcing bars is strikingly visible in Fig. 6.6d. In this context it should be mentioned that both models are subjected to identical fixed-end rotation time histories, which consist of rotation reversals of gradually increasing magnitude. By comparing these figures with Figs. 5.11a and b, it is apparent that the bottom reinforcing bars of the full-scale model slip through the joint at a smaller fixed-end rotation than those of the half-scale model. This difference is particularly striking when comparing

Fig. 6.6d with Fig. 5.11b, which show that the slip-through of the bottom bars of the full-scale model takes place at a rotation of 0.012 rad, whereas the half-scale model withstands one more large deformation cycle before the bottom bars slip through the joint at a rotation of 0.017 rad.

The observed difference regarding the instant of slip-through of bottom reinforcing bars between full and half-scale models can be readily explained by investigating the bond stress-slip behavior in the two cases. Since fixed-end rotations are defined by Eq. (5.1) as a ratio of distances, such quantities being dimensionless variables do not change with scale. Thus a rotation of, say, 0.01 rad in the full-scale model should correspond to a rotation of exactly the same magnitude in the half scale model. Since, however, the distance between top and bottom reinforcing layer in the half-scale model is only half the respective distance in the full-scale model, for the same amount of end slip the fixed-end rotation in the half-scale model is twice that in the full-scale model. This is one of the reasons for the observed differences in hysteretic behavior. Assume, for example, that the distance between top and bottom reinforcing layer is 322 *mm* in the half-scale model and, consequently, 644 *mm* in the full-scale model. These values correspond to the values used in the examples studied. In this case a fixed-end rotation of 0.01 rad is associated with a pull-out slip of approximately 3.2 *mm* in the half-scale and 6.4 *mm* in the full-scale model, respectively. In spite of the fact that the bond strength of the bond stress-slip envelope curves for the reinforcing bars of the full- and half scale model differ by as much as 20%, Fig. 3.8 indicates that the discrepancy in the observed hysteretic behavior between full- and half scale model derives from the different degree of bond damage which results from a relative slip of 8 *mm* in the full-scale model as compared to the damage associated with a slip of 4 *mm* in the half-scale model assuming that the fixed-end rotation is the same in both models. It should be noted at this stage that the question of dependence of the bond stress-slip envelope curve on the diameter of reinforcing bars is the source of some controversy among researchers in the field. The conclusions of this study are based on experimental evidence presented in Ref. [23]. According to these results it seems that the slip value u_3 at which the descending portion of the bond stress-slip envelope curve reaches the frictional bond resistance depends only on the lug distance of reinforcing bars. The lug distance however does not necessarily increase linearly with increasing bar diameter. This fact in connection with the bond stress-slip model presented in Section 3.2 leads to the observed discrepancies in the hysteretic load-deformation behavior between full- and half scale models, unless special care is taken to scale the bond stress-slip behavior appropriately.

The results presented in Fig. 6.6 seem to indicate that reduced scale models of R/C subassemblages whose hysteretic behavior is controlled by bond deterioration, can overestimate the energy dissipation capacity of the subassemblage. In the case of beam-column joints which are subjected to severe deformation reversals, fixed-end rotations derived from tests on reduced scale specimens should be judged with caution. In this respect it might be wiser to compare relative slip values instead of fixed-end rotations between reduced and full-scale models. In spite of the fact that relative slip has the dimension of length and should be scaled proportionately to the scale of the models, the bond damage introduced along the bars anchored in the joint directly depends on the value of relative slip imposed at the ends of the joint. Because results should be compared on the basis of equal amount of induced damage, relative slip values should be kept constant between reduced and full-scale models. This, in turn, implies that *fixed-end rotations cannot be directly compared between reduced and full-scale models.*

6.7. Comparison of parametric studies

In order to be able to compare the hysteretic behavior of all cases presented in the previous sections, some means of evaluating the performance of the interior beam-column joint in each case has to be found. This performance function must be expressed in dimensionless form, so that cases with various strength and stiffness can be directly compared. In this study the total energy dissipated by the interior joint until the moment that the bottom reinforcing bars slip through the joint, is chosen as a measure of performance. This energy is measured by computing the energy enclosed in the moment-fixed end rotation hysteretic loops at both beam-column interfaces. It is, then, normalized by the maximum elastic energy that can be absorbed by a joint, again determined from the moment-fixed end rotation relation at the beam-column interfaces. This leads to the following definition,

$$\sum E^* = \frac{\sum E}{M_y^+ \theta_y^+ + M_y^- \theta_y^-} \tag{6.1}$$

where $\sum E^*$ is the normalized total dissipated energy, $\sum E$ is the total energy dissipated at both beam-column interfaces, M_y^+ (M_y^-) is the yield moment in the positive (negative) direction of bending and θ_y^+ (θ_y^-) is the corresponding fixed-end rotation.

As a measure of the severity of hysteretic requirements which are imposed on the interior joint the cumulative fixed-end rotation ductility is selected. It is defined as:

$$\sum \mu_{c\theta}^{\bullet} = \sum \frac{|\theta^+|}{\theta_y^+} + \sum \frac{|\theta^-|}{\theta_y^-} \tag{6.2}$$

where $\mu_{c\theta}$ is the cumulative fixed-end rotation ductility, and as above, θ^+ is a positive and θ^- a negative fixed-end rotation, respectively.

The relation between normalized total dissipated energy and cumulative fixed-end rotation ductility is believed to be a good indicator of the hysteretic behavior of subassemblages. This relation is depicted in Fig. 6.7 for the parametric studies on an interior beam-column joint presented above. The numbers on the curves denote the different cases studied and correspond to the second digit of the sections in this Chapter. Curve 1 corresponds therefore to specimen BC3, curve 2 is associated with a reduction in bond strength by 15% and so forth. All curves are terminated at the point at which slip-through of bottom reinforcing bars takes place, which occurs when bond is completely damaged along the bottom reinforcing bars *in the joint.* This does not imply complete collapse of the subassemblage, since the bars can be anchored in the girder end region on the other end of the joint, provided that no instability due to P-Δ effect occurs. As already noted, the influence of the girder end region is not included in this investigation.

It is seen in Fig. 6.7 that the instant of slip-through of the bottom reinforcing bars greatly varies between the different cases. Particularly striking is the difference between half-scale model under average bond conditions (curve 1) and half-scale model under a reduction in bond strength of 15% (curve 2). It is concluded that the quality of bond and, consequently, the quality of workmanship and construction can substantially affect the total energy dissipation capacity of a beam-column joint. On the other hand it seems that a variation in the history of loading (curve 5) in the range studied here does not affect much the total energy dissipated up to the moment of slip-through of the bottom reinforcing bars. This, however, does not allow any general conclusions, since the effect of the history of loading might be important in another range of cyclic excitations.

As already noted in Section 6.6, the full-scale model of the interior joint (curve 6) behaves almost identically to the half-scale model under the same conditions (curve 1), as long as bond is not severely damaged. However, under large deformation reversals the slip-through of bottom reinforcing bars is initiated at a much earlier stage in the case of the full-scale model and, consequently, the total energy dissipation differs substantially between half and full-scale models. It is therefore important to realize that the results from experiments on reduced scale subassemblages whose behavior is controlled by bond deterioration may have to be interpreted with caution when attempting to predict the behavior of full-scale members.

With respect to improving the seismic resistant design of beam-column joints, Fig. 6.7 indicates that equal amount of top and bottom reinforcement (curve 3) and reinforcing bars of lower yield strength or smaller bar diameter (curve 4) can offer considerable advantage. It should be noted in this context that the higher is the ratio between cumulative energy dissipation and cumulative fixed-end rotation ductility, the better is the hysteretic behavior of the members under consideration. It is therefore recommended to use equal amount of top and bottom reinforcement and a lower yield strength of reinforcing bars as a means of improving the hysteretic behavior of beam-column joints.

CHAPTER 7

SUMMARY, CONCLUSIONS AND RECOMMENDATIONS

7.1. Summary

The study presented herein has endeavored to develop an analytical model which describes the hysteretic behavior of reinforced concrete members under severe cyclic excitations. Special attention was devoted to the interaction of reinforcing steel and surrounding concrete through bond and the deterioration of such interaction under deformation reversals. The effects of cyclic bond deterioration on the hysteretic behavior of interior beam-column joints have been investigated and conclusions regarding the main factors affecting the hysteretic behavior of joints will be summarized in the following.

In developing an analytical model to describe the hysteretic behavior of R/C members special attention was devoted to material models describing the stress-strain relation of reinforcing steel and the bond stress-slip behavior along the anchorage length of reinforcing bars under arbitrary cyclic excitations.

The relative slip between reinforcing steel and surrounding concrete increases the size of cracks that have previously formed perpendicular to the axis of the member. The equilibrium of horizontal forces and bending moments must be introduced at the cracked R/C sections to complement the equations which describe the interaction of reinforcing steel and surrounding concrete. This necessitates the development of a new layer section model which takes into account the bond deterioration in the vicinity of the crack when establishing the contribution of reinforcing steel and concrete to the equilibrium of horizontal forces and bending moments at a cracked R/C section.

The developed model shows excellent agreement with available experimental evidence on the hysteretic behavior of interior R/C beam-column subassemblages.

7.2. Conclusions

After analyzing the results of the study presented herein the following conclusions can be drawn:

(1) The bond stress-slip behavior of reinforcing steel substantially affects the hysteretic behavior of reinforced concrete joints subjected to severe cyclic deformation reversals. An accurate bond stress-slip relation is the cornerstone of any attempt to accurately describe the hysteretic behavior of R/C joints.

(2) The relative contribution of reinforcing steel and concrete to the equilibrium of horizontal forces and bending moments at a cracked R/C section is not only controlled by the strains but also by the crack width at the top and bottom of the cross-section of interest. Any model of the hysteretic behavior of a cracked R/C section has to account for the effect of bond deterioration in the vicinity of the crack. This effect leads to an *incompatibility of strains* between reinforcing steel and surrounding concrete at a crack.

(3) From a series of analytical parametric studies on the hysteretic behavior of an interior joint the following conclusions were reached regarding the influence of different parameters:

(a) *the ratio of top to bottom reinforcement influences substantially the hysteretic behavior of interior joints.* If the area of the top and bottom reinforcing layers is equal, very stable hysteretic behavior is observed. In conformity with experiments, reducing the area of the bottom reinforcing layer with respect to that of the top, more pronounced pinching of hysteretic loops is observed resulting in a substantial reduction in energy dissipation capacity,

(b) *the hysteretic behavior of joints is very sensitive to the bond strength along the anchorage length of reinforcing bars. For example, a mere 15% reduction in bond strength along a bar results in a 30% reduction in total energy dissipation capacity.* This fact has important consequences in practice. Poor construction quality and poor workmanship can lead to diminished energy dissipation capacity of the joint,

(c) *increasing the number of anchored bars, reducing the bar diameter and reducing the yield strength of reinforcement improves the hysteretic behavior of joints,*

(d) *the time history of imposed deformations affects the hysteretic behavior of interior joints.* A small number of large deformation reversals inflicts more damage of bond along the anchorage length of reinforcing bars than a large number of small deformation reversals,

(e) *the scale of specimens* influences the hysteretic behavior of interior joints. By comparing the results of identical full and half scale interior joints it is concluded that the full scale joint exhibits complete bond damage earlier than the half scale model. This is due to the fact that bond damage in the joint directly depends on the slip imposed at the beam-column interface. The value of end slip transforms proportionately to the scale of the specimen between specimens of different scale. This can have important consequences regarding the interpretation of experimental results from reduced scale reinforced concrete models whose behavior is substantially affected by bond deterioration,

7.3. Recommendations for future research

The proposed model can be used in conducting additional investigations which go beyond the studies presented within the framework of this report. In this sense it is recommended:

(i) to extend the model for predicting the hysteretic behavior of critical regions of reinforced concrete columns, shear-walls and coupling beams in coupled shear-walls. The hysteretic behavior of critical regions in girders should also be investigated. These studies can help in developing analytical models which improve upon existing ones which are based on point plastic hinges or on distribution of curvatures along the empirically estimated length of the plastic hinges,

(ii) to derive simple analytical models which account for the effects of bond deterioration in the seismic response of moment resisting frames,

(iii) to use the proposed model in connection with cyclic shear models at a cracked reinforced concrete section, since it allows computation and tracing of crack width in time. As it is well established, the crack width is the main parameter which affects the contribution of aggregate interlock and of the dowel action of reinforcing bars to the shear resistance at crack interfaces,

(iv) to include the effect of joint shear and diagonal cracking in the hysteretic behavior of interior and exterior joints. In many cases the transfer of shear stresses in the joint can significantly affect the overall behavior of the member.

REFERENCES

[1] **"Finite Element Analysis of Reinforced Concrete"**, State-of-the-Art Report published by ASCE, New York, NY, 1982.

[2] **"Advanced Mechanics of Reinforced Concrete"**, IABSE Colloquium, Final Report, Delft, June 1981.

[3] Agrawal, G.L., Tulin, L.G., and Gerstle, K.H. "Response of Doubly Reinforced Concrete Beams to Cyclic Loading", *Journal of the American Concrete Institute,* Vol.62, No 7, July 1965.

[4] Anagnostopoulos, S.A., "Inelastic Beams for Inelastic Analyses of Structures", *ASCE, Journal of the Structural Division,* Vol.107, No ST7, July 1981.

[5] Anderson, J.C. and Townsend, W.H., "Models for RC Frames with Degrading Stiffness", *ASCE, Journal of the Structural Division,* Vol.103, No ST12, Dec. 1977.

[6] Aoyama, H., "Moment-Curvature Characteristics of Reinforced Concrete Members Subjected to Axial Load and Reversal of Bending", *Proceedings International Symposium on Flexural Mechanics of Reinforced Concrete,* ASCE-ACI, Florida 1964.

[7] Banon, H., Biggs, J.M. and Irvine, H.M., "Seismic Damage in Reinforced Concrete Frames", *ASCE, Journal of the Structural Division,* Vol.107, No ST9, Sept. 1981.

[8] Bažant, Z.P., and Bhat, P.D., "Prediction of Hysteresis of Reinforced Concrete Members", *ASCE, Journal of the Structural Division,* Vol.103, No ST1, Jan. 1977.

[9] Bertero, V.V., "Experimental Studies Concerning Reinforced, Prestressed and Partially Prestressed Concrete Structures and their Elements", *IABSE Symposium on Resistance and Ultimate Deformability of Structures Acted on by Well Defined Repeated Loads,* Introductory Report, Lisbon 1973.

[10] Bertero, V.V., "Seismic Behavior of Structural Concrete Linear Elements (Beams, Columns) and Their Connections", *AICAP-CEB Symposium, Structural Concrete Under Seismic Actions,* Introductory Report to Theme II, Comife Euro-International Du Beton, Bulletin D' Information No 131, Vol.1, pp.125-212, Rome 1979.

[11] Bertero, V.V., Bresler, B., "Seismic Behavior of Reinforced Concrete Framed Structures", *Proceedings Fourth World Conference on Earthquake Engineering,* Vol.1, B-3, pp.109-124, Chile 1969.

[12] Bertero, V.V., Bresler, B., and Liao, H., "Stiffness Degradation of Reinforced Concrete Members Subjected to Cyclic Flexural Moments", *Earthquake Engineering Research Center,* University of California, Berkeley, Report No EERC 69-12, Dec. 1969.

[13] Bertero, V.V. and Popov, E.P., "Hysteretic Behavior of Ductile Moment-Resisting Reinforced Concrete Frame Components", *Earthquake Engineering Research Center,* University of California, Berkeley, Report No EERC 75-16, April 1975.

[14] Bohong, Z., Mingshun, W. and Kunlian, Z., "A Study of Hysteretic Curve of Reinforced Concrete Members under Cyclic Loading", *Seventh World Conference on Earthquake Engineering,* Vol.6, Istanbul 1981.

[15] Brown, R.H. and Jirsa, J.O., "Reinforced Concrete Beams under Load Reversals", *ACI Journal,* Vol.68, May 1971.

[16] Capecchi, D., Ciampi, V. and Vestroni, "Numerical Studies on the Behavior of a Reinforced Concrete Beam Element under Repeated Loadings", *Bulletin D' Information No 132,* Comife Euro-International Du Beton, Paris, April 1979.

[17] Ciampi, V., Eligehausen, R., Bertero, V. and Popov, E., "Analytical Model for Deformed Bar Bond under Generalized Excitations", *IABSE Colloqium, Advanced Mechanics of Reinforced Concrete,* Final Report, Delft, June 1981.

[18] Ciampi, V., Eligehausen, R., Bertero, V.V. and Popov, E.P., "Analytical Model for Concrete Anchorages of Reinforcing Bars under Generalized Excitations", *Earthquake Engineering Research Center,* University of California, Berkeley, Report No EERC 82-23, Dec. 1982.

[19] Clough, R.W., "Effect of Stiffness Degradation on Earthquake Ductility Requirements", Report No 66-16, *Structural Engineering Laboratory,* University of California, Oct. 1966.

[20] Clough, R.W., Benuska, K.L. and Wilson, E.L., "Inelastic Earthquake Response of Tall Buildings", *Proceedings of the Third World Conference on Earthquake Engineering,* Vol.II, Session II, Wellington, New Zealand, 1965.

[21] Dafalias, Y.K. and Popov, E.P., "A Model for Nonlinearly Hardening Materials for Complex Loadings", *Acta Mechanica,* Vol.21, 1975.

[22] Darwin, D., and Pecknold, D.A., "Analysis of RC Shear Panels under Cyclic Loading", *ASCE, Journal of the Structural Division,* Vol.102, No ST2, Feb. 1976.

[23] Eligehausen, R., Bertero, V.V. and Popov, E.P., "Local Bond Stress-Slip Relationships of Deformed Bars under General Excitations- Tests and Analytical Model", *UCB-Report 1983,* University of California, Berkeley (to be published).

[24] Eligehausen, R., Bertero, V.V. and Popov, E.P., "Hysteretic Behavior of Reinforcing Deformed Hooked Bars in R/C Joints", *7th European Conference on Earthquake Engineering,* Athens, Sept. 1982.

[25] Emori, K. and Scnobrich, W.C., "Inelastic Behavior of Concrete Frame-Wall Structures", *ASCE, Journal of the Structural Division,* Vol.107, No ST1, Jan.1981.

[26] Giberson, "The Response of Nonlinear Multistory Structures Subjected to Earthquake Excitation", *Ph.D. Dissertation,* California Institute of Technology, Pasadena, 1967.

[27] Hanson, N.W., and Connor, H.W., "Seismic Resistance of Reinforced Concrete Beam-Column Joints", *ASCE, Journal of the Structural Division,* Vol.93, No ST5, Oct. 1967.

[28] Jirsa, J.O., "Behavior of Elements and Subassemblages-RC Frames", *Workshop on Earthquake Resistant Reinforced Concrete Building Construction,* Berkeley CA, July 1977.

[29] Karsan, I.D., and Jirsa, J.O., "Behavior of Concrete under Compressive Loadings", *ASCE, Journal of the Structural Division,* Vol.95, No ST12, Dec. 1969.

[30] Kent, D.C., and Park, R., "Flexural Members with Confined Concrete", *ASCE, Journal of the Structural Division,* Vol.97, No ST7, July 1971.

[31] Ma, S.Y.M, Bertero, V.V. and Popov, E.P., "Experimental and Analytical Studies on the Behavior of Reinforced Concrete Rectangular and T-Beams", *Earthquake Engineering Research Center,* Report No EERC 76-2, Univ. of California, Berkeley, May 1976.

[32] Mahin, S.A., and Bertero, V.V., "Problems in Establishing and Predicting Ductility in Aseismic Design", *Proceedings International Symposium on Earthquake Structural Engineering,* St. Louis, MO, Aug. 1976.

[33] Menegotto, M. and Pinto, P., "Method of Analysis for Cyclically Loaded Reinforced Concrete Plane Frames Including Changes in Geometry and Nonelastic Behavior of Elements under Combined Normal Force and Bending", *IABSE Symposium on Resistance and Ultimate Deformability of Structures Acted on by Well-Defined Repeated Loads,* Final Report, Lisbon, 1973.

[34] Noguchi, H., "Nonlinear Finite Element Analysis of Reinforced Concrete Beam-Column Joints", *IABSE Colloqium, Advanced Mechanics of Reinforced Concrete,* Final Report, Delft, June 1981.

[35] Ortega, J.M. and Rheinbold, W.C., **"Iterative Solution of Nonlinear Equations in Several Variables"**, Academic Press, 1970.

[36] Otani, S., "Inelastic Analysis of R/C Frame Structures", *ASCE, Journal of the Structural Division,* Vol.100, No ST7, July 1974.

[37] Park, R., Gaerty, L. and Stevenson, E.C., "Tests on an Interior Reinforced Concrete Beam-Column Joint", *Bulletin of the New Zealand National Society for Earthquake Engineering,* Vol.14, No 2, June 1981.

[38] Park, R., Kent, D.C., and Sampson, R.A., "Reinforced Concrete Members with Cyclic Loading", *ASCE, Journal of the Structural Division,* Vol.98, No ST7, July 1972.

[39] Popov, E.P., "Berkeley Re-Bar Bond Tests", *SEAOC Conference,* Sacramento CA, Oct. 1982.

[40] Scott, B.D., Park, R. and Priestley, M.J.N., "Stress-Strain Behavior of Concrete Confined by Overlapping Hoops at Low and High Strain Rates", *ACI Journal,* V.79, No 1, Jan-Feb. 1982.

[41] Sinha, B.P., Gerstle, K.H. and Tulin, L.G., "Response of Singly-Reinforced Beams to Cyclic Loading", *ACI Journal, Proceedings,* Vol.61, No 8, Aug. 1964.

[42] Soleimani, D., "Reinforced Concrete Ductile Frames under Earthquake Loadings with Stiffness Degradation", *Ph.D. Dissertation,* University of California, Berkeley, Dec. 1978.

[43] Soleimani, D., Popov, E.P. and Bertero, V.V., "Hysteretic Behavior of Reinforced Concrete Beam-Column Subassemblages", *ACI Journal,* Vol.76, No 11, Nov. 1979.

[44] Soleimani, D., Popov, E.P. and Bertero, V.V., "Nonlinear Beam Model for R/C Frame Analysis", *7th ASCE Conference on Electronic Computation,* St. Louis, MO, Aug. 1979.

[45] Stanton, J.F. and Mc Niven, H.D., "The Development of a Mathematical Model to Predict the Flexural Response of Reinforced Concrete Beams to Cyclic Loads, Using System Identification", *Earthquake Engineering Research Center,* Report No EERC 79-2, Univ. of California, Berkeley, Jan. 1979.

[46] Takeda, T., Sozen, M.A., and Nielsen, N.N., "Reinforced Concrete Response to Simulated Earthquakes", *ASCE, Journal of the Structural Division,* Vol.96, No ST12, Dec. 1970.

[47] Tassios, T.P., and Yannopoulos, P.J., "Analytical Studies on Reinforced Concrete Members Under Cyclic Loading Based on Bond Stress-Slip Relationships", *ACI Journal,* Vol.78, May-June 1981.

[48] Taylor, R.L. and Zienkiewicz, O,C., "Mixed Finite Element Solution of Fluid Flow Problems", Ch.1, Vol.4, **"Finite Elements in Fluids",** John Wiley & Sons 1982.

[49] Townsend, W.H. and Hanson, R.D., "Hysteretic Loops for Concrete Beam-Column Connections", *Fifth World Conference in Earthquake Engineering,* Paper 137, Session 3D, Rome 1973.

[50] Viwathanatepa, S., Popov, E.P. and Bertero, V.V., "Seismic Behavior of Reinforced Concrete Interior Beam-Column Subassemblages", *Earthquake Engineering Research Center,* Report No EERC 79-14, Univ. of California, Berkeley, June 1979.

[51] Viwathanatepa, S., Popov, E.P. and Bertero, V.V., "Effects of Generalized Loadings on Bond of Reinforcing Bars Embedded in Confined Concrete Blocks", *Earthquake Engineering Research Center,* Report No EERC 79-22, Univ. of California, Berkeley, Aug. 1979.

FIGURES

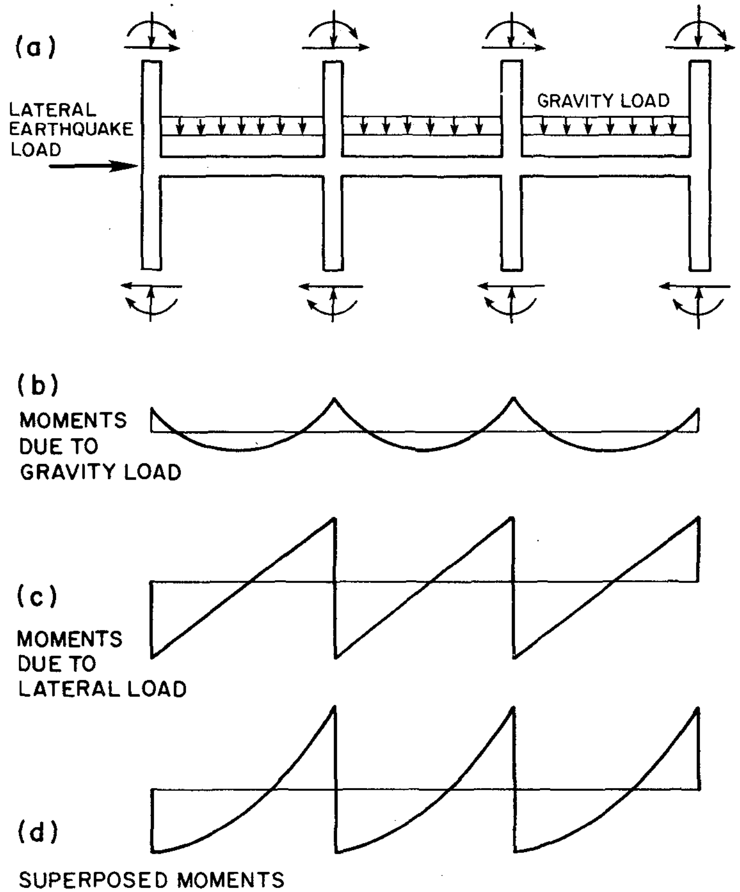

FIGURE 2.1

COMBINATION OF GRAVITY LOADS WITH LATERAL EARTHQUAKE LOAD EFFECTS IN A TYPICAL LOWER STORY OF A MOMENT RESISTING FRAME

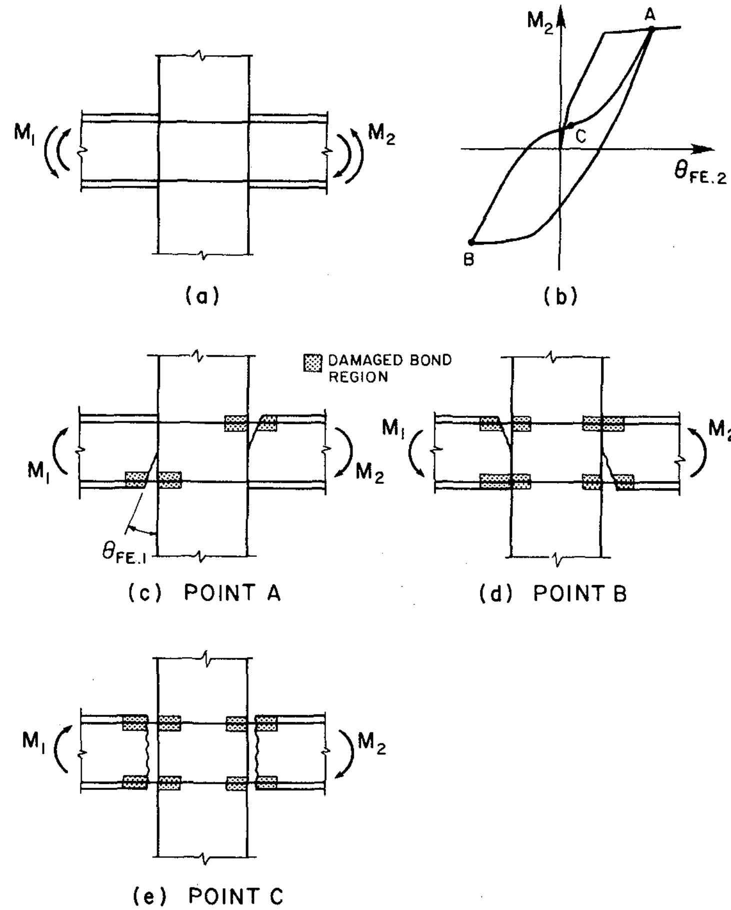

FIGURE 2.2

BEHAVIOR OF INTERIOR JOINT UNDER MOMENT REVERSALS

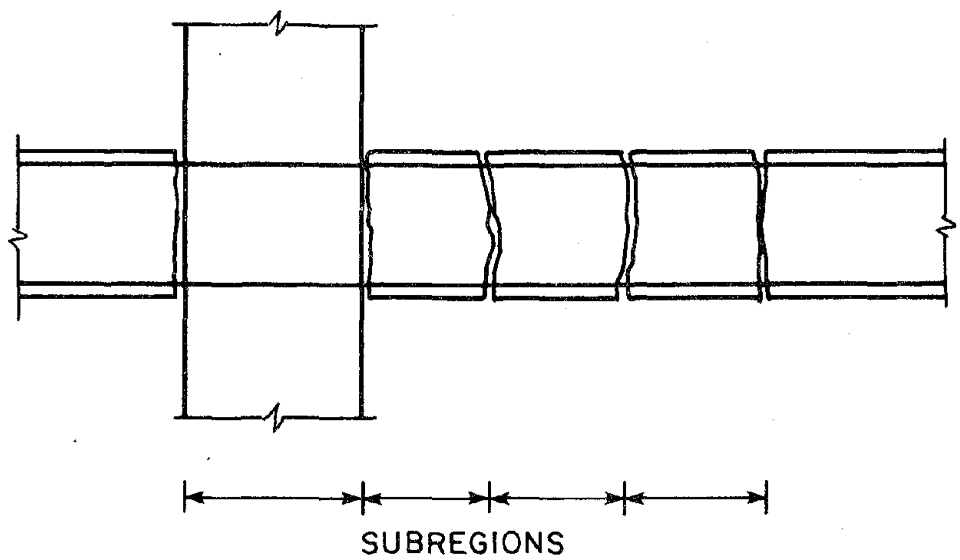

FIGURE 2.3 SUBDIVISION OF R/C MEMBER INTO SEVERAL SUBREGIONS

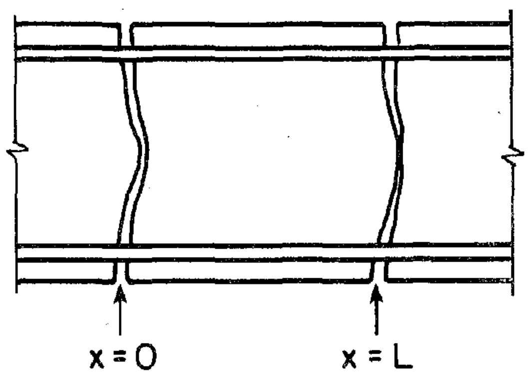

FIGURE 2.4a DEFINITION OF BOUNDARIES OF A SUBREGION

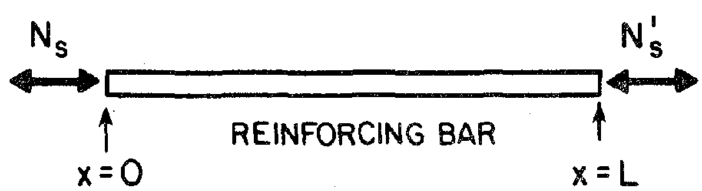

FIGURE 2.4b SINGLE REINFORCING BAR BETWEEN TWO ADJACENT CRACKS

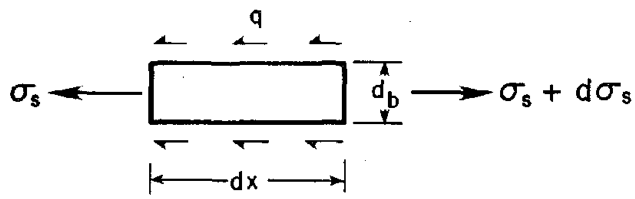

FIGURE 2.5a FORCES ACTING ON INFINITESIMAL BAR ELEMENT

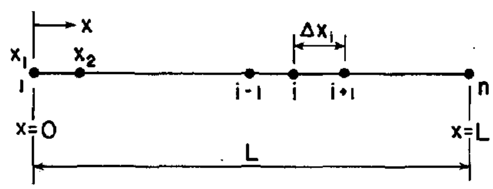

FIGURE 2.5b DISCRETIZATION ALONG A REINFORCING BAR

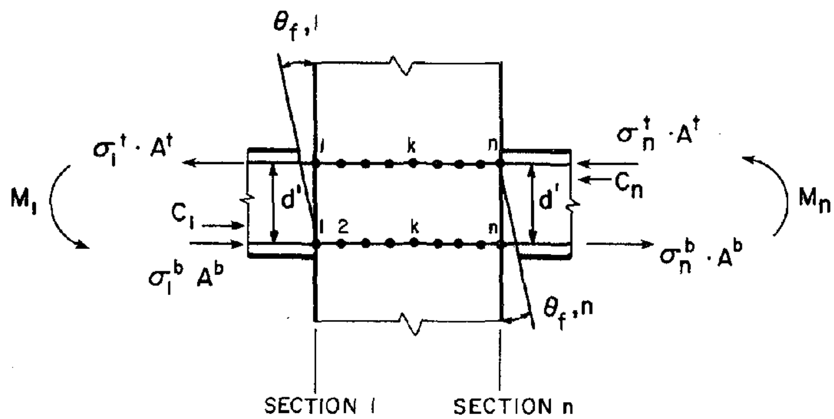

FIGURE 2.6 ANALYTICAL MODEL FOR INTERIOR BEAM-COLUMN JOINT

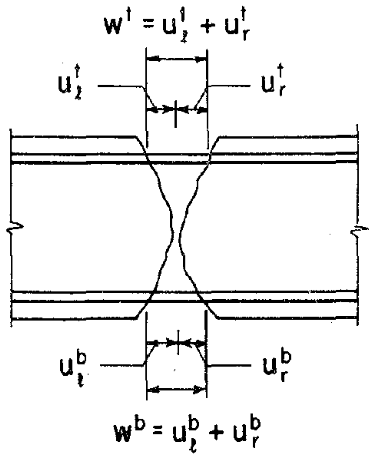

FIGURE 2.7 a DEFINITION OF RELATIVE SLIP AND CRACK WIDTH AT A CRACKED R/C SECTION

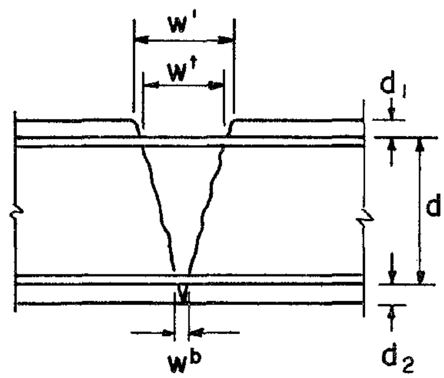

$$w' = w^t \frac{d_1 + d'}{d'} - w^b \frac{d_2}{d'}$$

$$w'' = w^b \frac{d_2 + d'}{d'} - w^t \frac{d_1}{d'}$$

FIGURE 2.7b COMPUTATION OF CRACK WIDTH AT THE TOP AND BOTTOM OF A CRACKED R/C SECTION

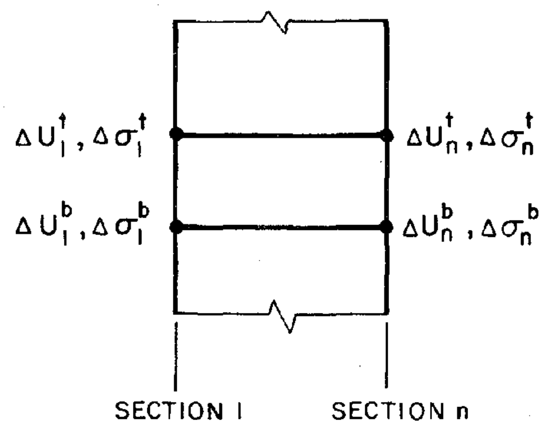

FIGURE 2.8 UNKNOWN VARIABLES AT JOINT END SECTIONS

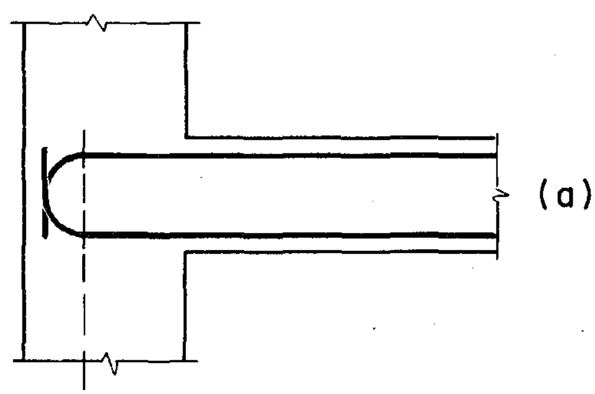

FIGURE 2.9a ACTUAL REINFORCEMENT ARRANGEMENT IN EXTERIOR JOINTS

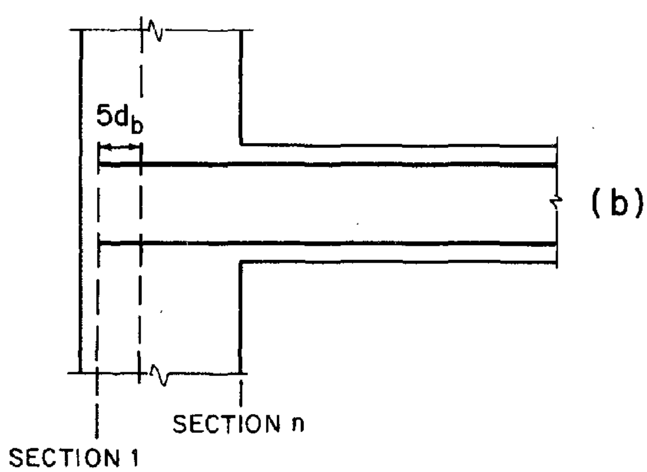

FIGURE 2.9b IDEALIZATION OF 90° HOOK ANCHORAGE AND DEFINITION OF END SECTIONS 1 AND n IN EXTERIOR JOINTS

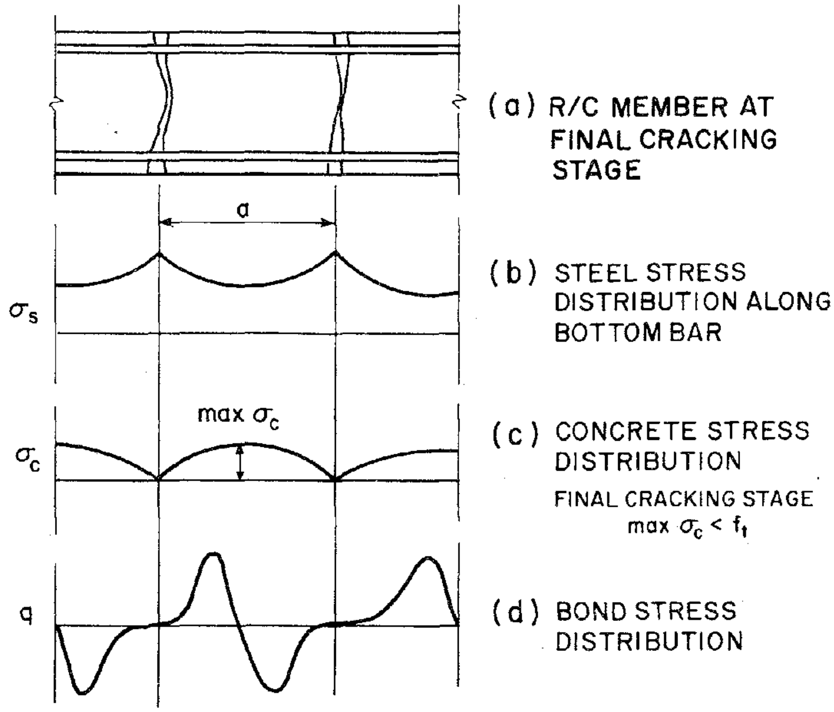

FIGURE 2.10 DISTRIBUTION OF STEEL, CONCRETE AND BOND STRESS ALONG BOTTOM REINFORCING BARS IN A GIRDER

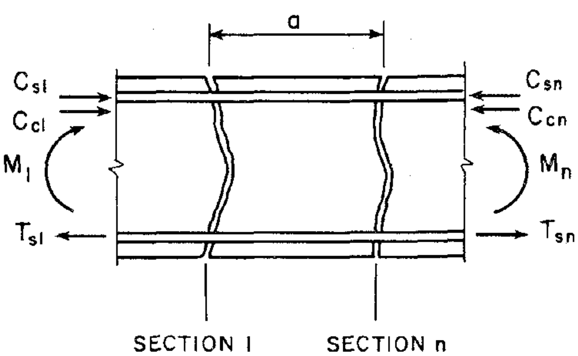

FIGURE 2.11 DEFINITION OF END SECTIONS AND BOUNDARY CONDITIONS IN THE CASE OF A GIRDER SUBREGION

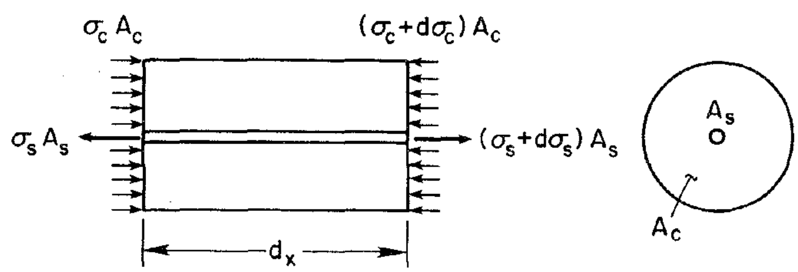

FIGURE 2.12 STRESS TRANSFER BETWEEN REINFORCING BAR AND SURROUNDING CONCRETE

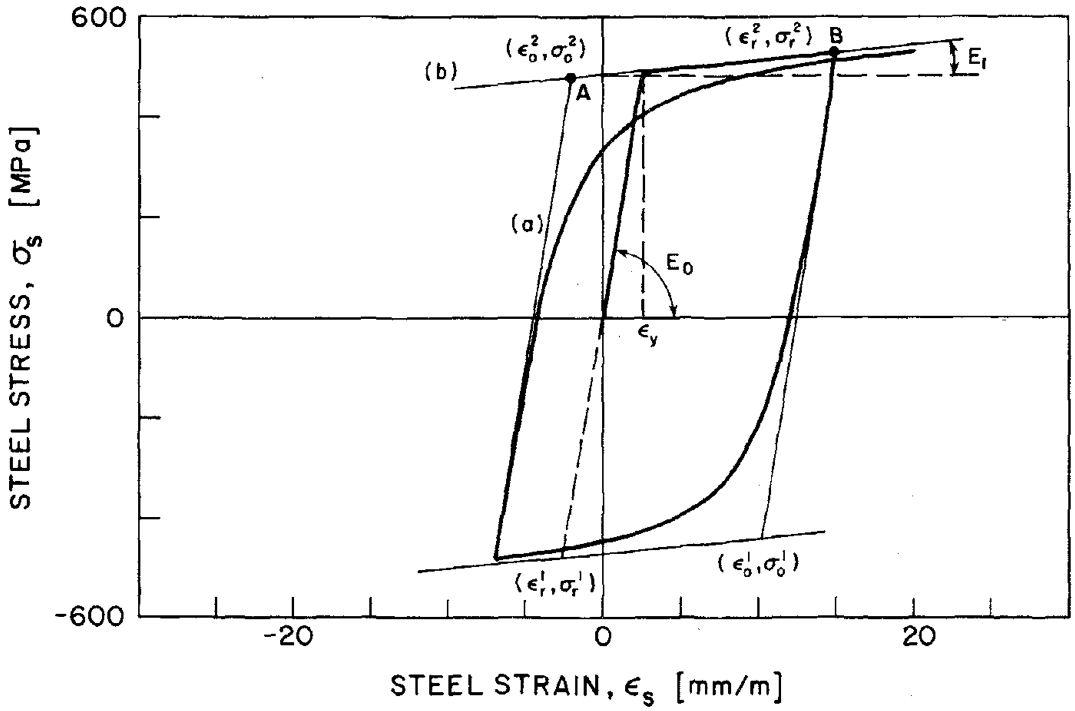

FIGURE 3.1 MENEGOTTO-PINTO STEEL MODEL

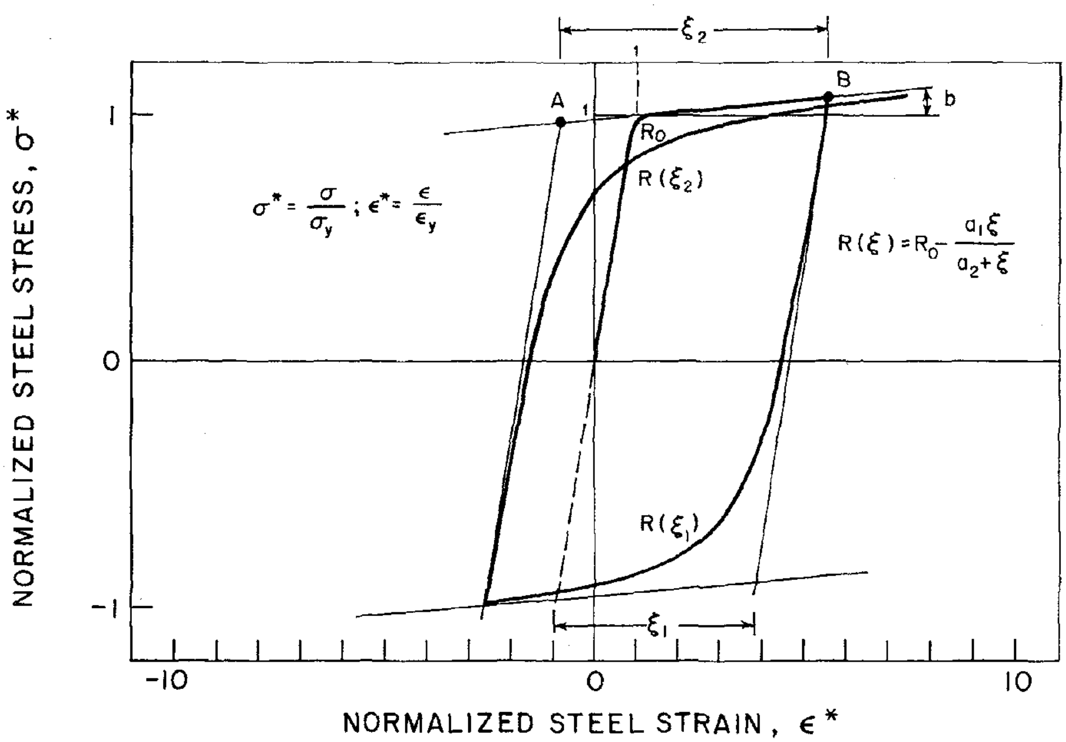

FIGURE 3.2 DEFINITION OF CURVATURE PARAMETER $R(\xi)$ IN MENEGOTTO-PINTO STEEL MODEL

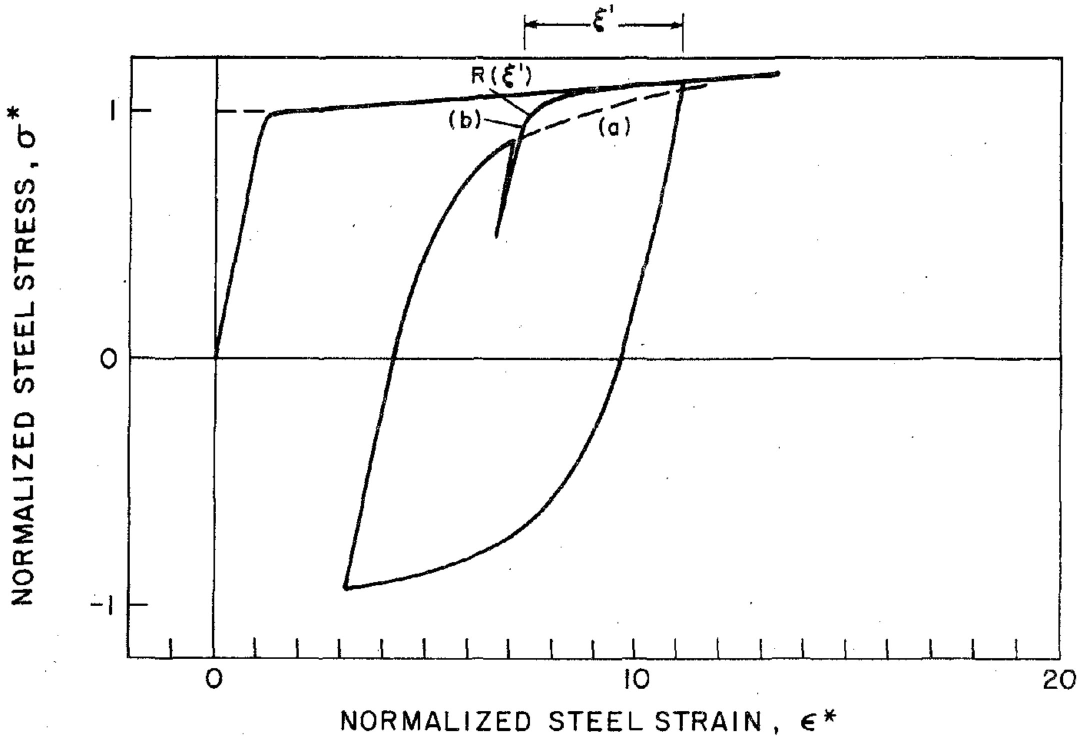

FIGURE 3.3 DEFINITION OF CURVATURE PARAMETER R (ξ) IN THE CASE OF PARTIAL UNLOADING AND RELOADING

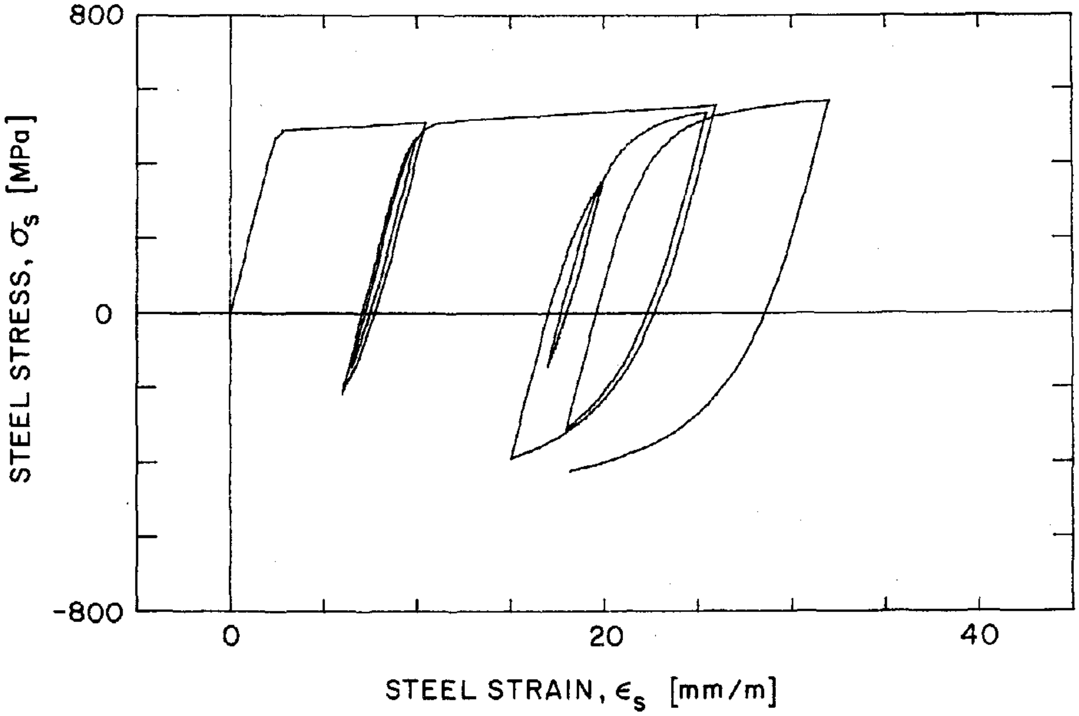

FIGURE 3.4a BEHAVIOR OF PROPOSED STEEL MODEL UNDER TYPICAL STRESS-STRAIN HISTORY

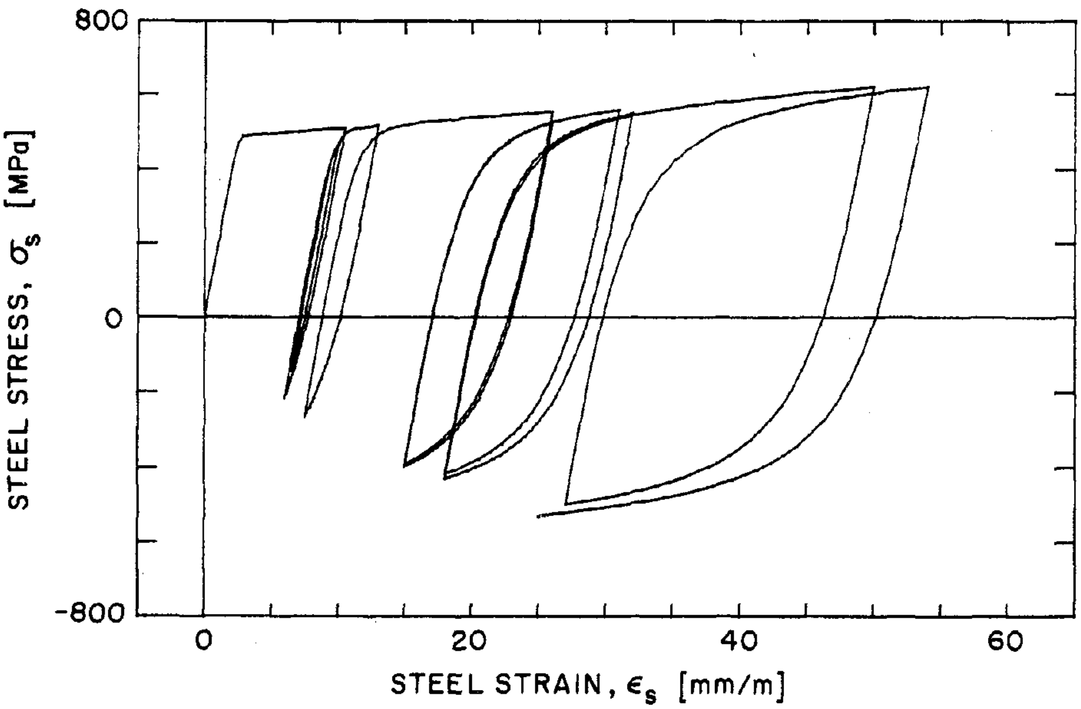

FIGURE 3.4b BEHAVIOR OF PROPOSED STEEL MODEL UNDER TYPICAL STRESS-STRAIN HISTORY

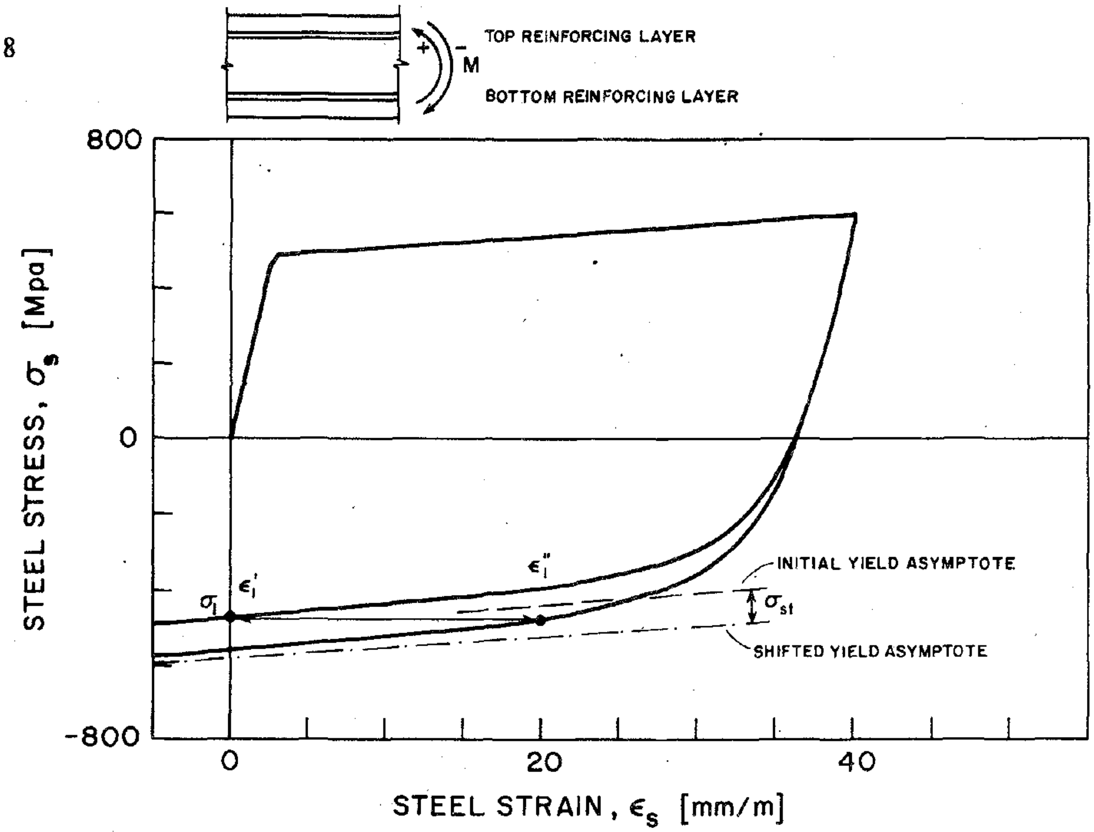

FIGURE 3.5 EFFECT OF ISOTROPIC STRAIN HARDENING ON THE STEEL STRAIN IN BOTTOM REINFORCING BARS DURING CRACK CLOSURE

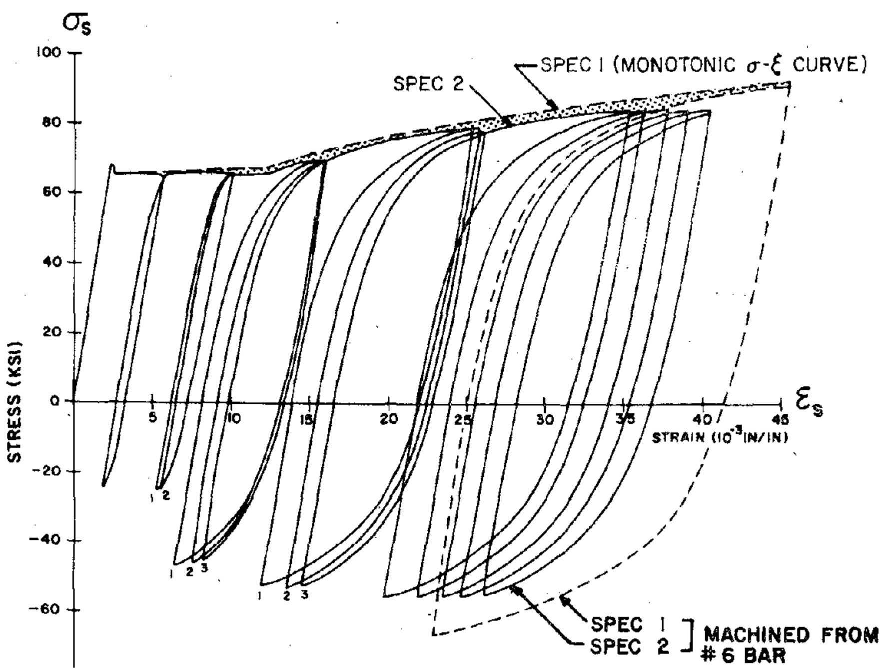

(a) EXPERIMENTAL RESULTS (SPECIMENS 1 AND 2 FROM REF.[31])

FIGURE 3.6 COMPARISON OF ANALYTICAL STEEL STRESS-STRAIN HISTORY WITH EXPERIMENTAL RESULTS (TOP REINFORCING BAR)

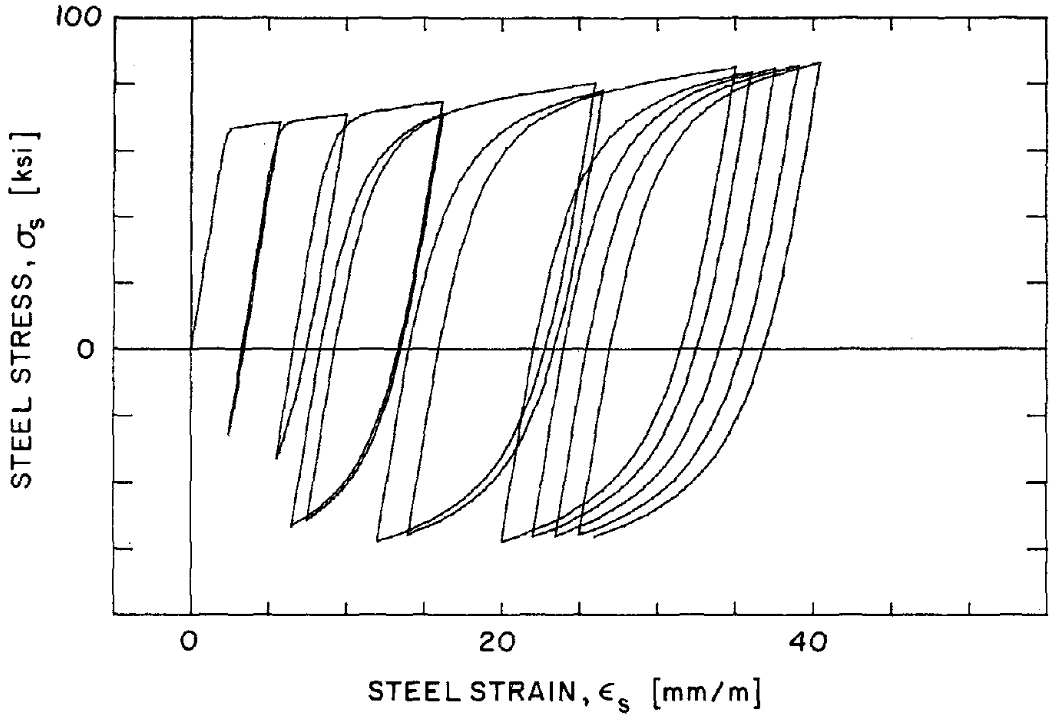

(b) MENEGOTTO-PINTO MODEL INCLUDING ISOTROPIC STRAIN HARDENING

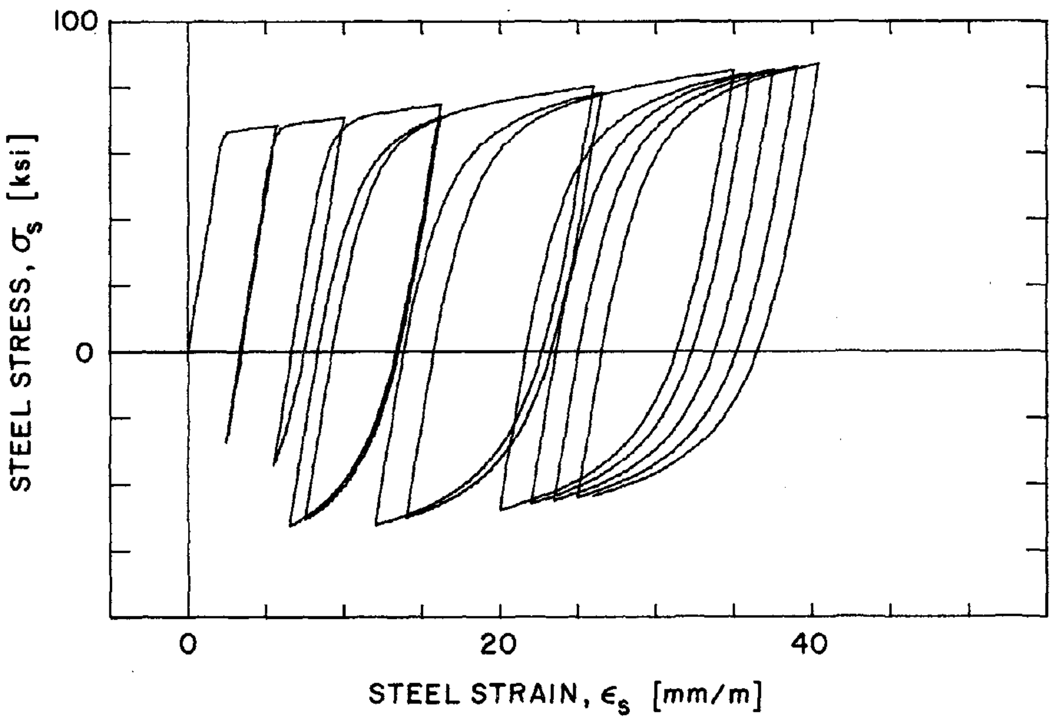

(c) MENEGOTTO-PINTO MODEL WITHOUT ISOTROPIC STRAIN HARDENING

FIGURE 3.6 COMPARISON OF ANALYTICAL STEEL STRESS-STRAIN HISTORY WITH EXPERIMENTAL RESULTS (TOP REINFORCING BAR)

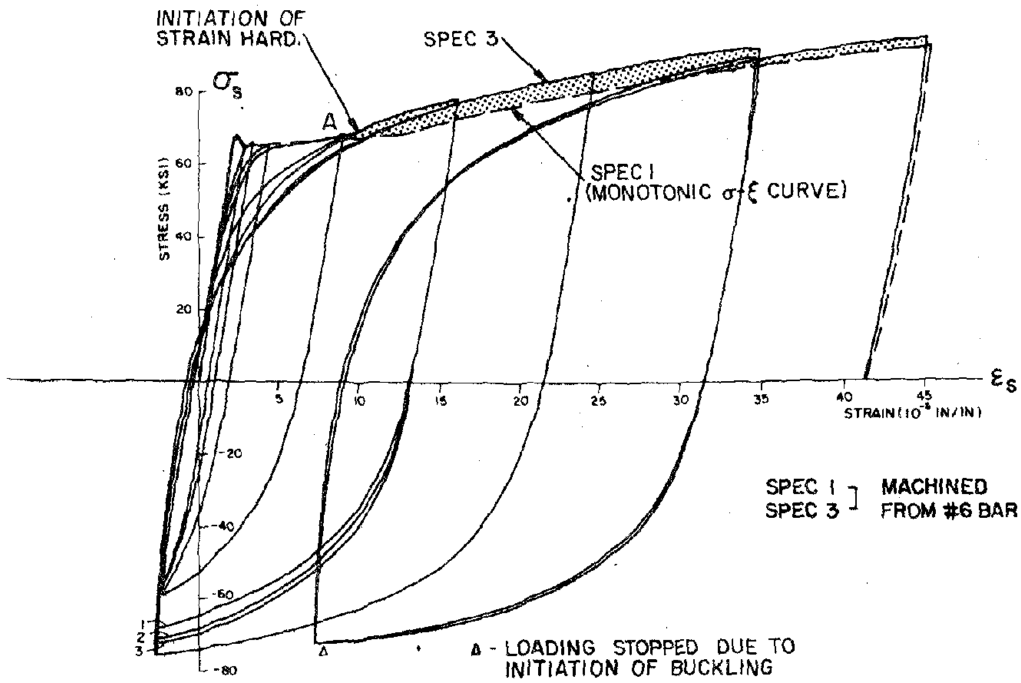

(a) EXPERIMENTAL RESULTS (SPECIMENS 1 AND 2 FROM REF.[31])

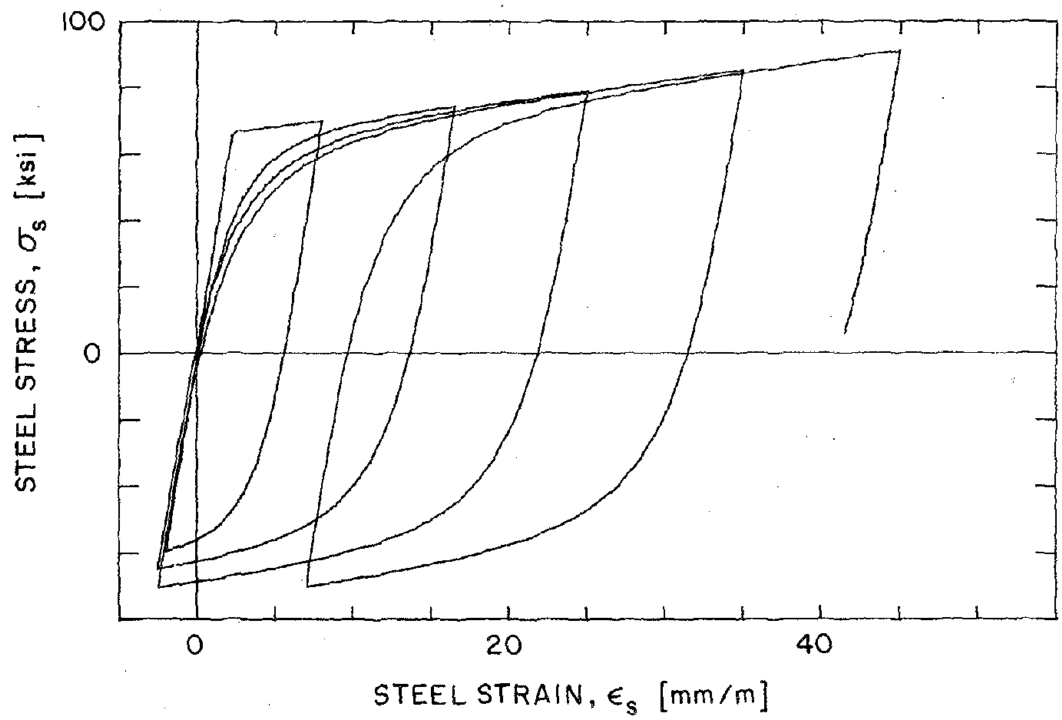

(b) MENEGOTTO-PINTO MODEL INCLUDING ISOTROPIC STRAIN HARDENING

FIGURE 3.7 COMPARISON OF ANALYTICAL STEEL STRESS-STRAIN HISTORY WITH EXPERIMENTAL RESULTS (BOTTOM REINFORCING BAR)

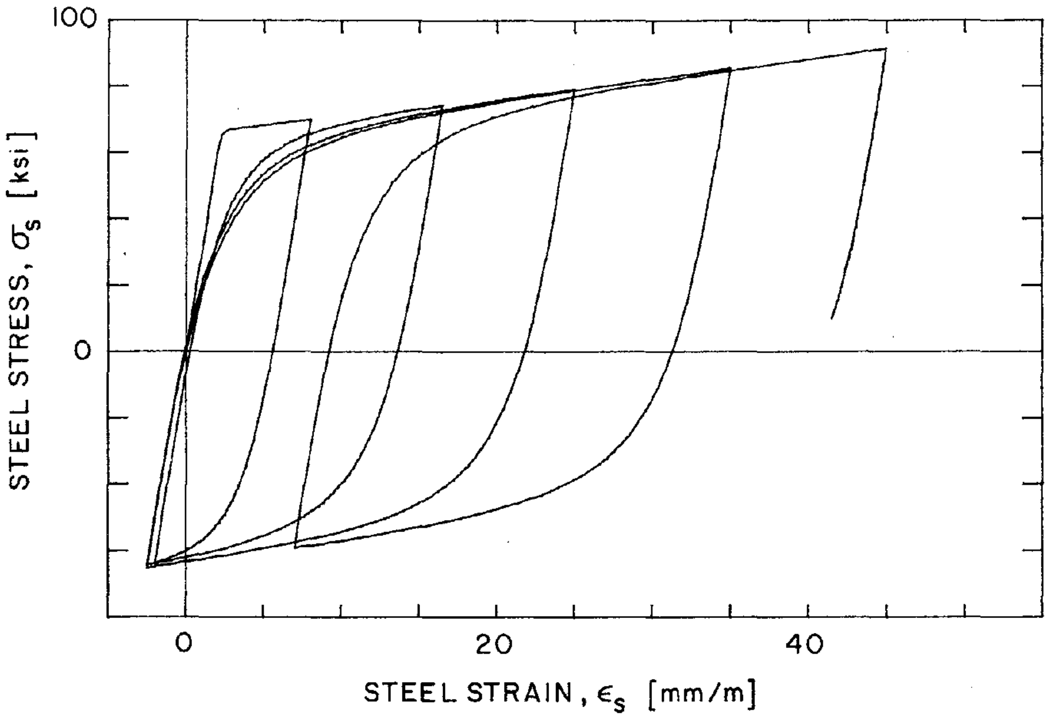

(c) MENEGOTTO-PINTO MODEL WITHOUT ISOTROPIC STRAIN HARDENING

FIGURE 3.7 COMPARISON OF ANALYTICAL STEEL STRESS-STRAIN HISTORY WITH EXPERIMENTAL RESULTS (BOTTOM REINFORCING BAR)

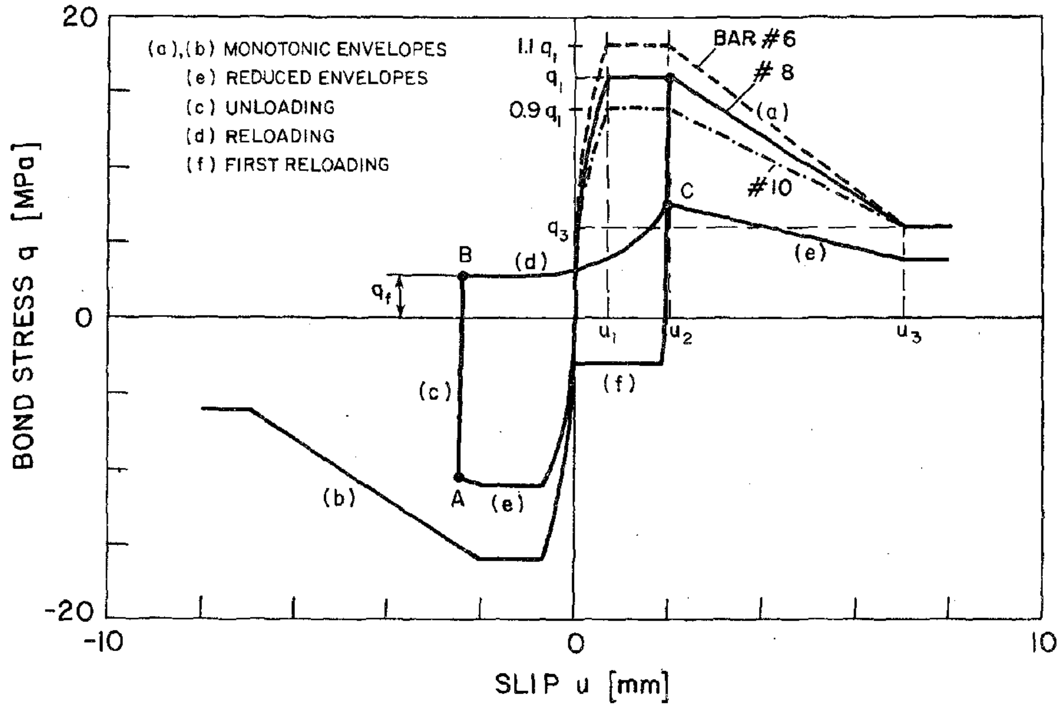

FIGURE 3.8 PROPOSED BOND STRESS-SLIP RELATION

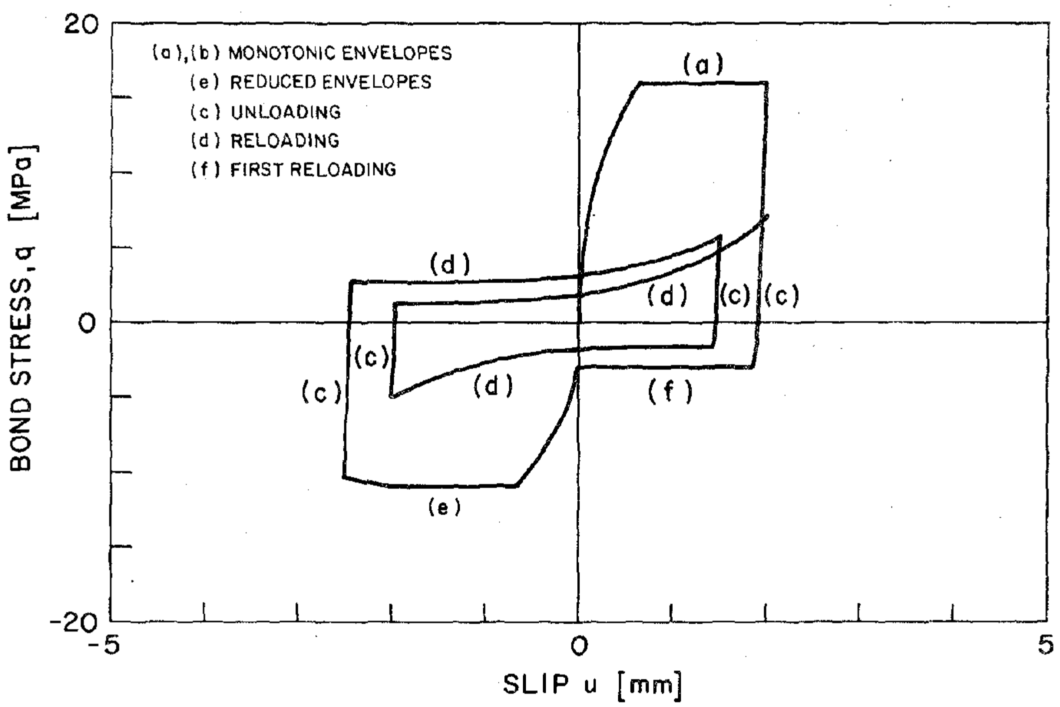

FIGURE 3.9 PROPOSED BOND STRESS-SLIP MODEL UNDER INCOMPLETE SLIP REVERSALS

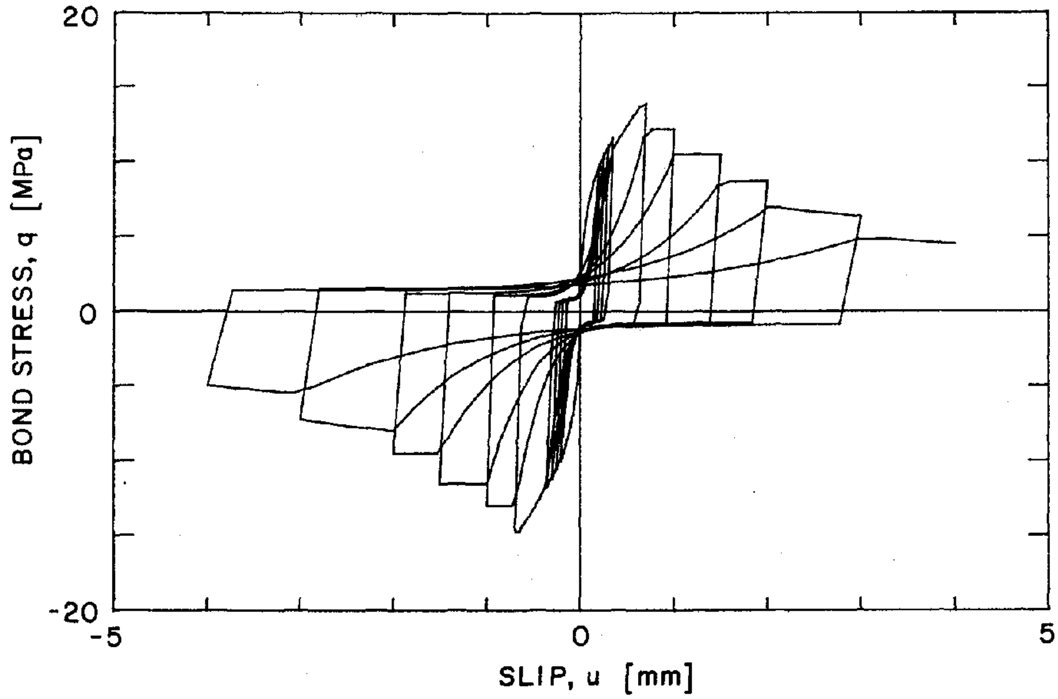

(a) PROPOSED MODEL

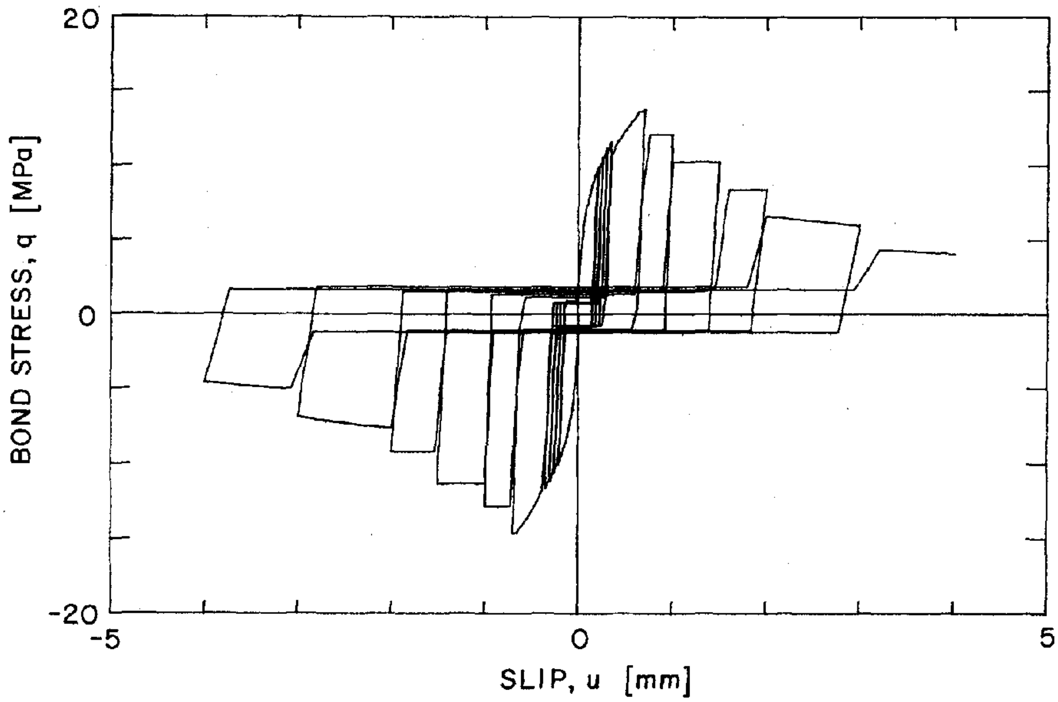

(b) ELIGEHAUSEN'S MODEL

FIGURE 3.10 COMPARISON OF HYSTERETIC BOND STRESS-SLIP BEHAVIOR BETWEEN PROPOSED MODEL AND ELIGEHAUSEN'S MODEL

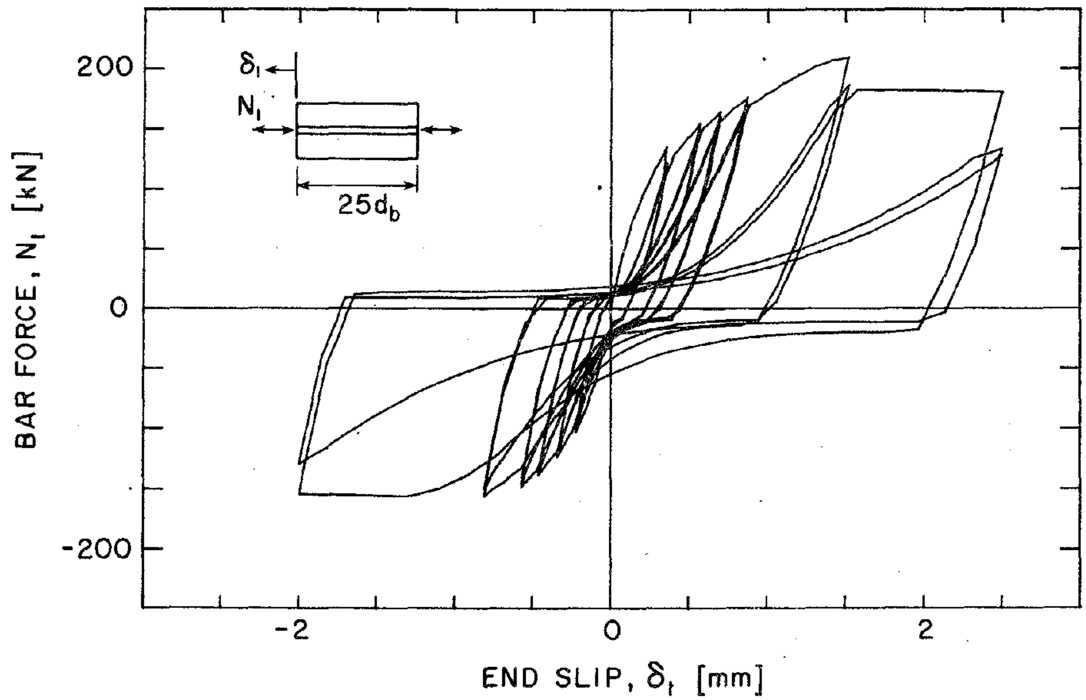

(a) USING PROPOSED BOND STRESS-SLIP MODEL

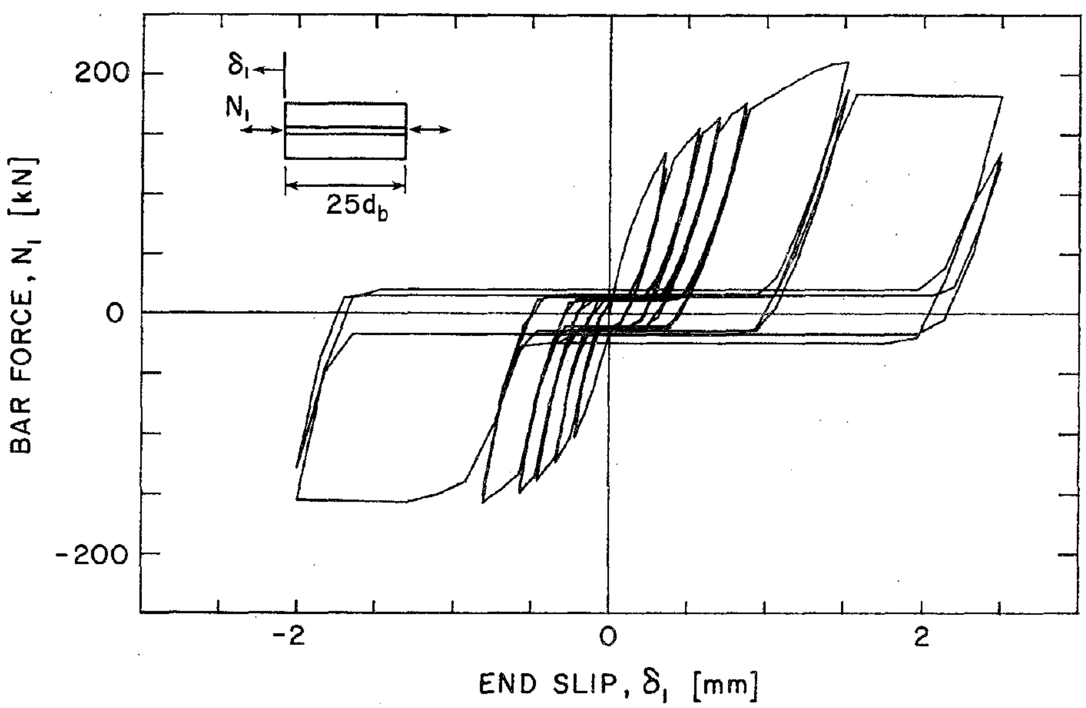

(b) USING ELIGEHAUSEN'S MODEL

FIGURE 3.11 COMPARISON OF HYSTERETIC STEEL FORCE-SLIP BEHAVIOR AT THE FREE END OF AN ANCHORED #8 REINFORCING BAR. ANCHORAGE LENGTH = 25 d_b

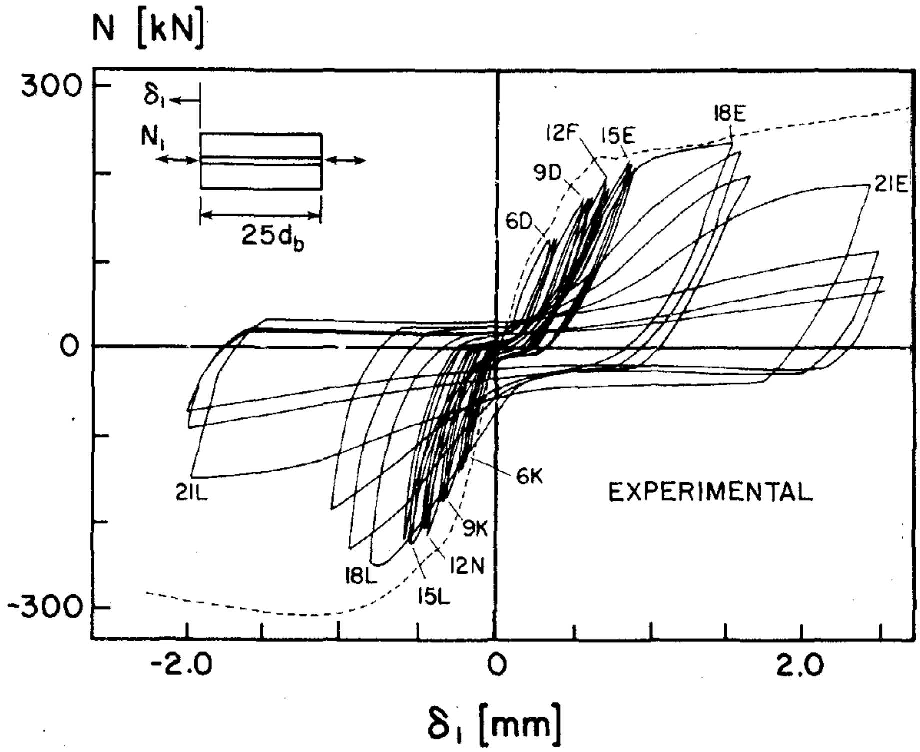

(c) EXPERIMENTAL RESULTS

FIGURE 3.11 COMPARISON OF HYSTERETIC STEEL FORCE-SLIP BEHAVIOR AT THE FREE END OF AN ANCHORED #8 REINFORCING BAR. ANCHORAGE LENGTH = 25 d_b

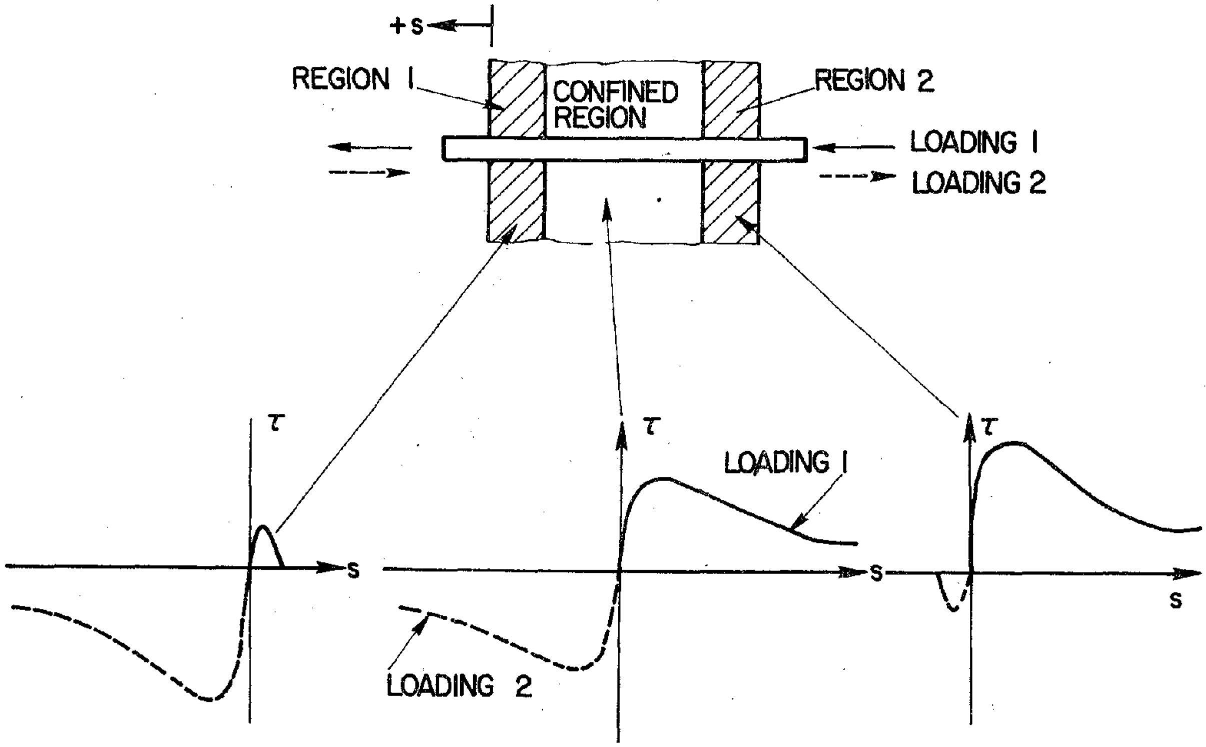

FIGURE 3.12 DIFFERENT REGIONS AND CORRESPONDING BOND STRESS-SLIP ENVELOPE CURVES IN AN INTERIOR JOINT

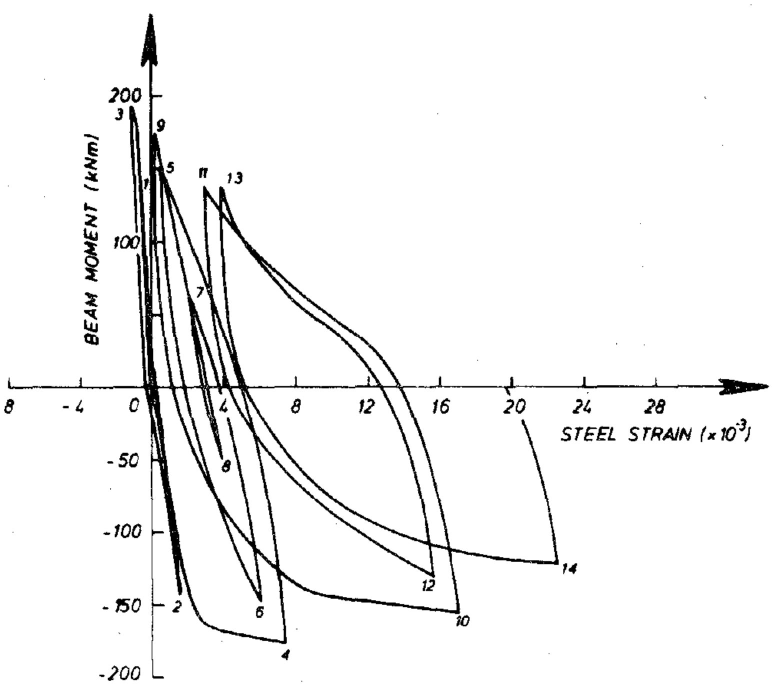

FIGURE 3.13 TYPICAL END MOMENT-STEEL STRAIN HISTORY OF BOTTOM REINFORCING BARS AT A BEAM-COLUMN INTERFACE (FROM REF.[37])

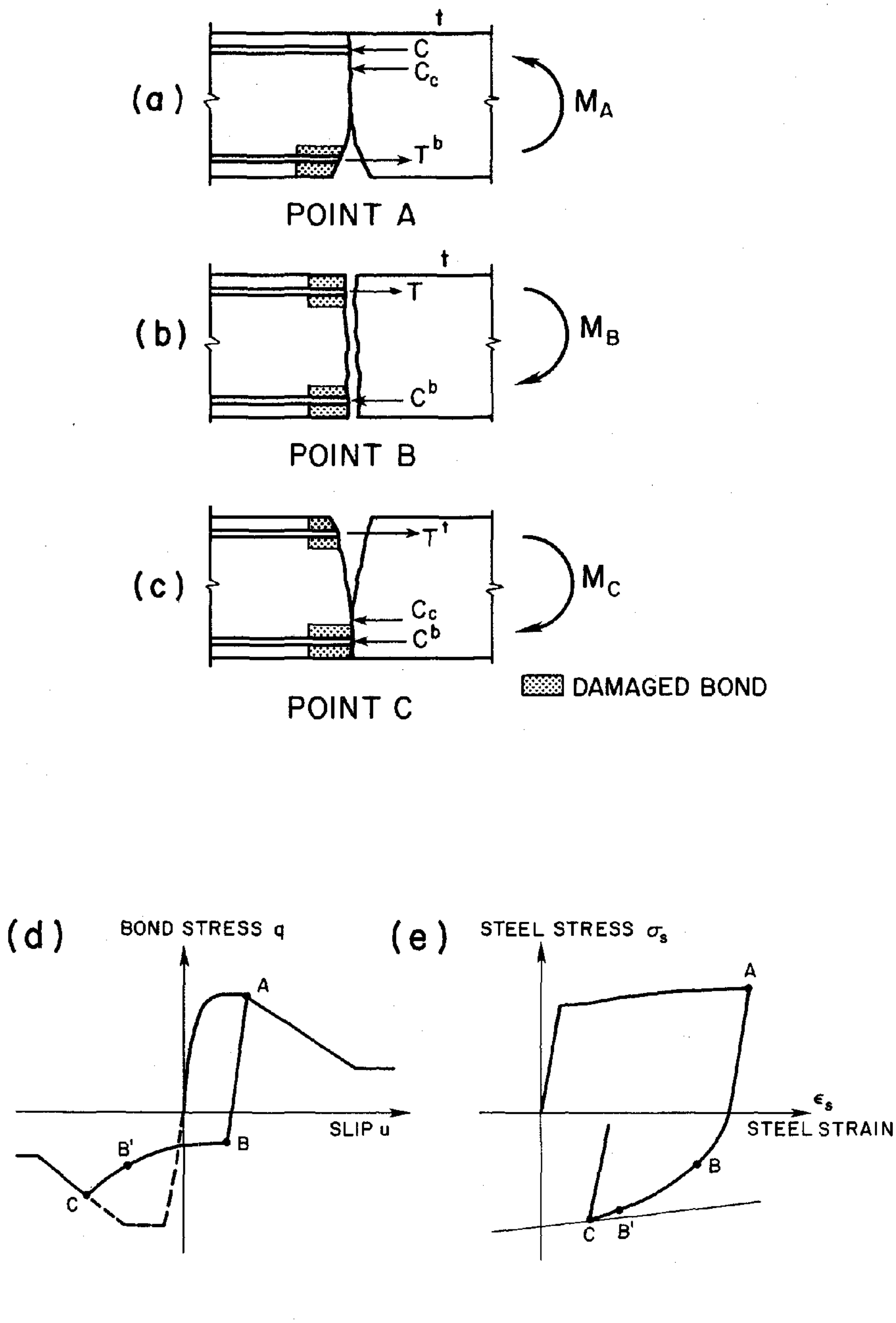

FIGURE 3.14 MECHANISM OF CRACK CLOSURE AT A CRACKED R/C SECTION TAKING INTO ACCOUNT CYCLIC BOND DETERIORATION

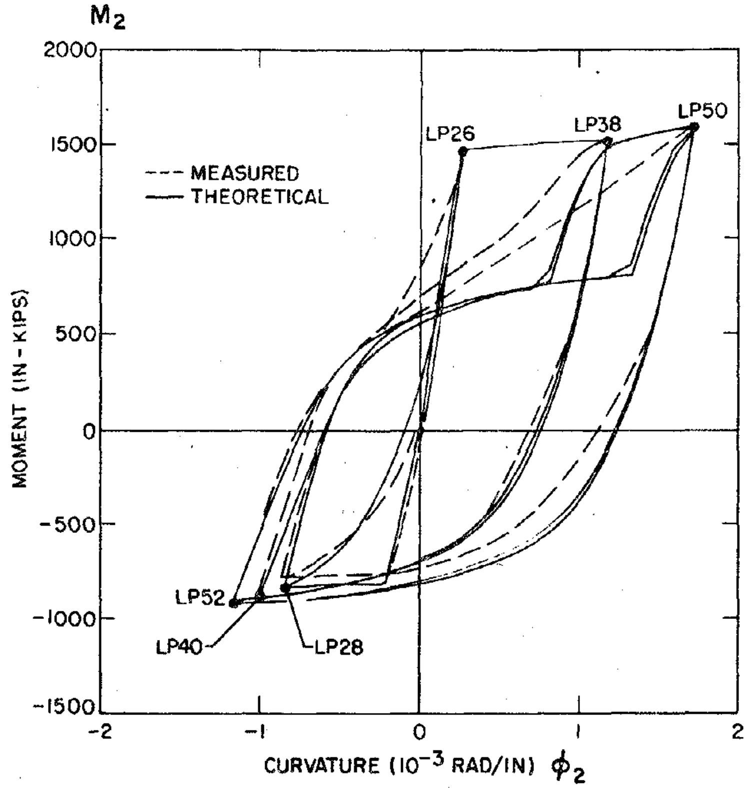

FIGURE 3.15 HYSTERETIC MOMENT-CURVATURE RELATION (FROM REF.[31])

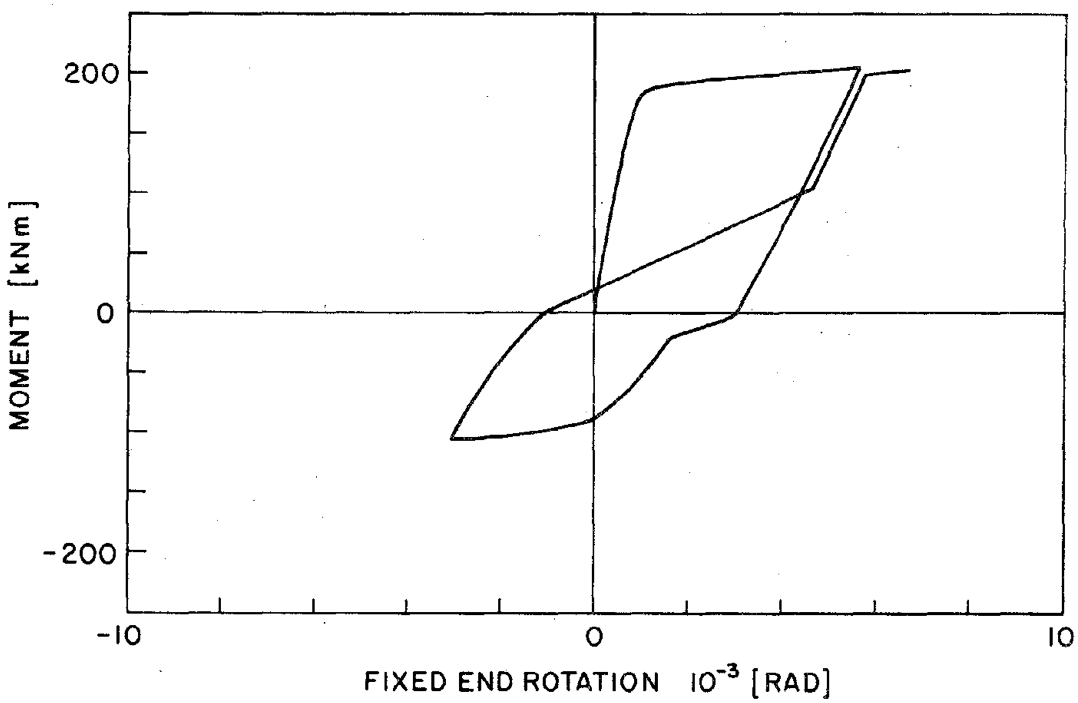

FIGURE 3.16 HYSTERETIC MOMENT-ROTATION RELATION ASSUMING STRAIN COMPATIBILITY BETWEEN STEEL AND CONCRETE

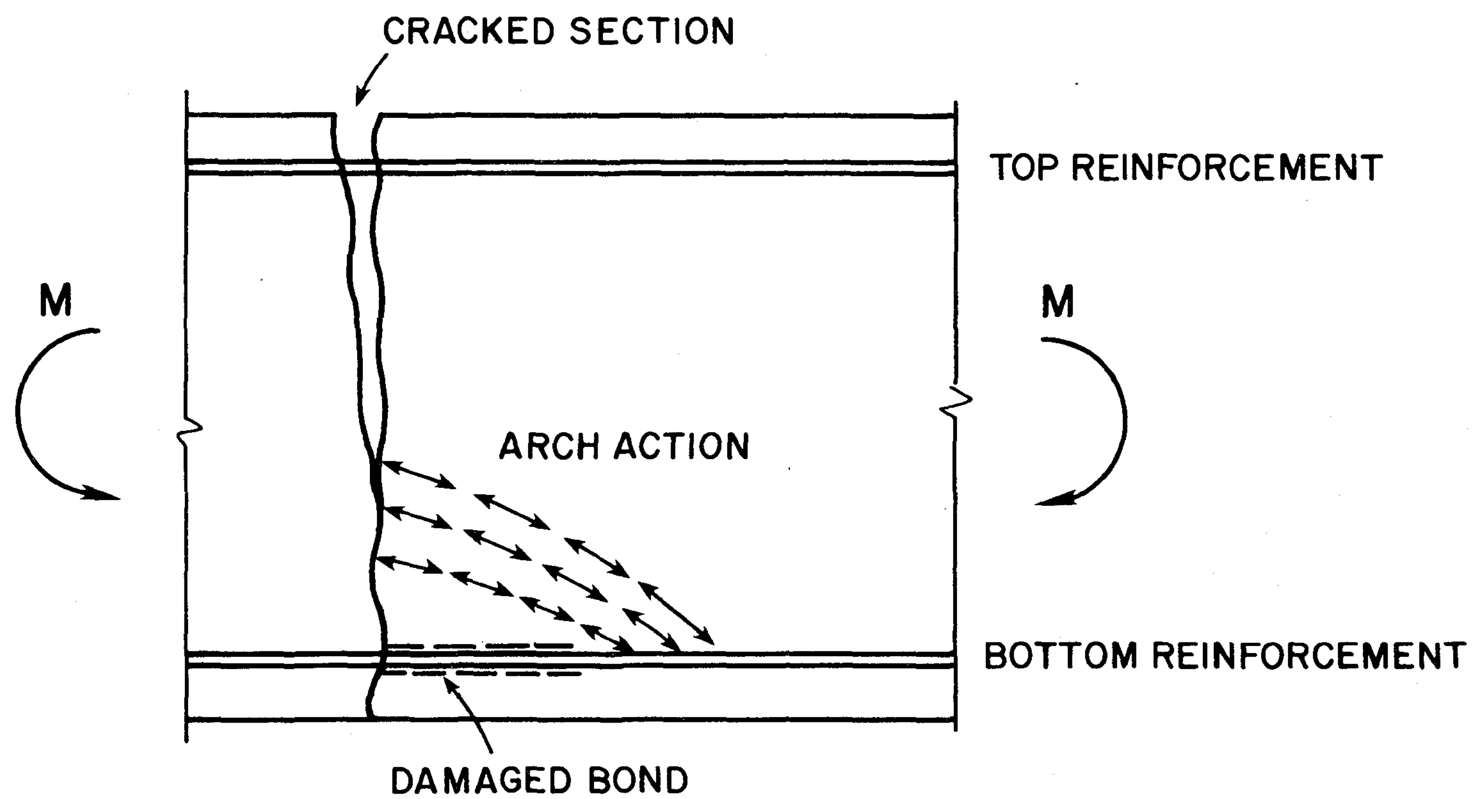

FIGURE 3.17 ARCH ACTION DURING CRACK CLOSURE AT A CRACKED R/C SECTION

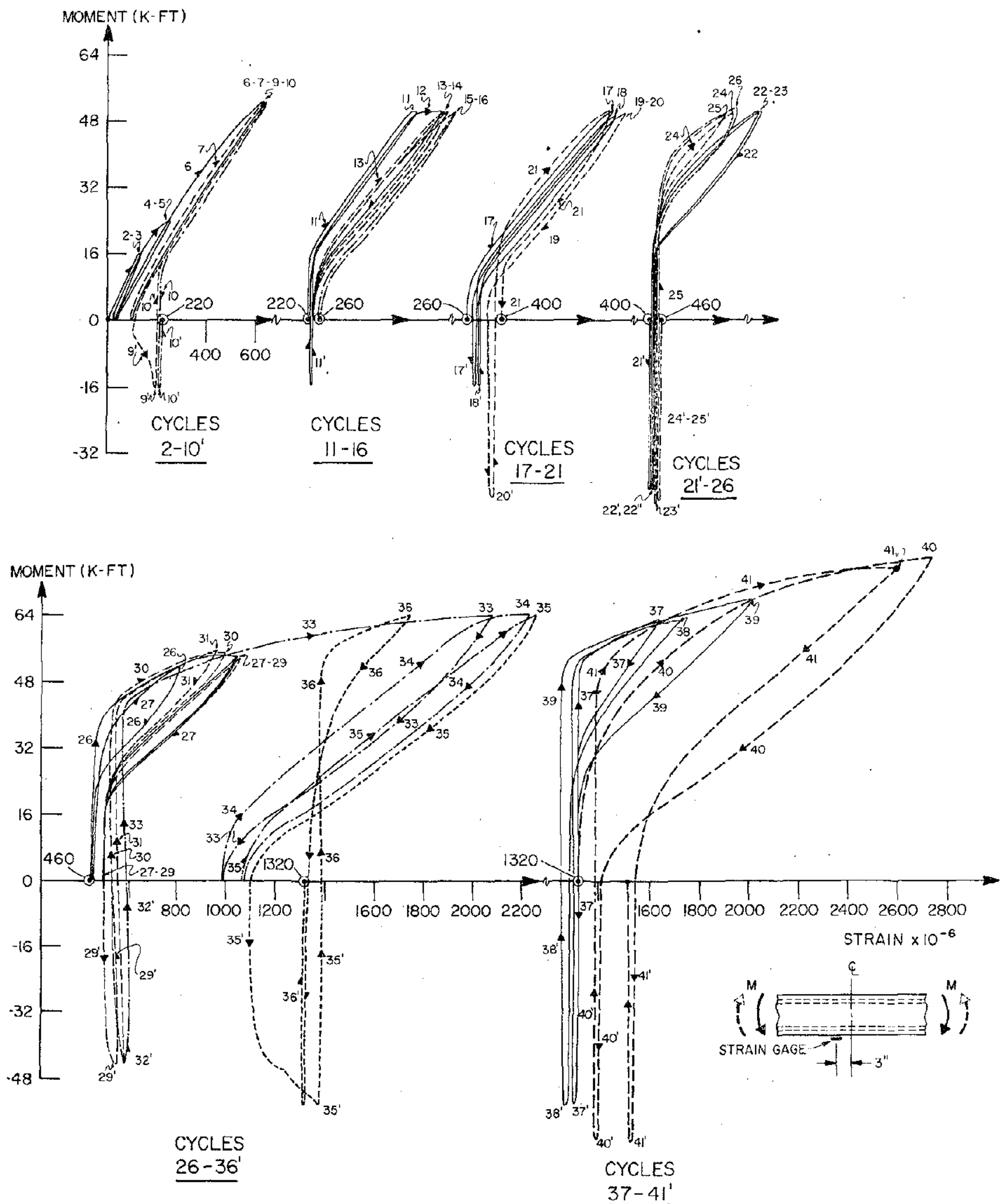

FIGURE 3.18 HISTORY OF CONCRETE STRAINS NEAR A CRACKED R/C SECTION (FROM REF. [12])

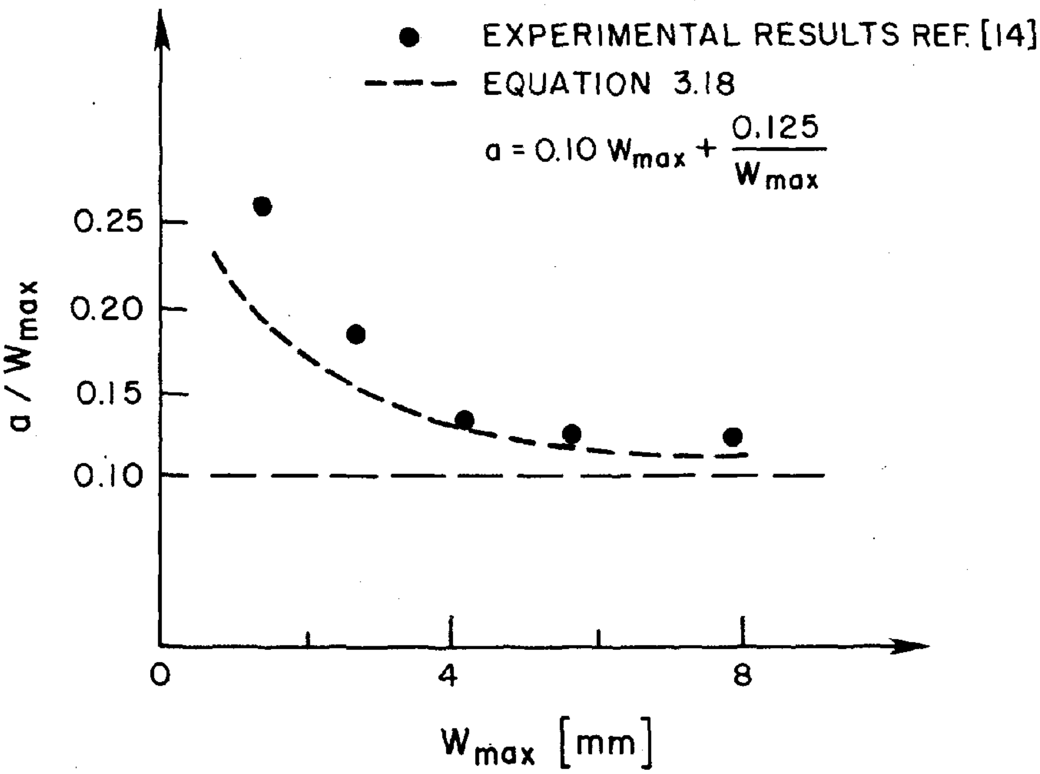

FIGURE 3.19 RELATION BETWEEN CRACK WIDTH AT CLOSURE a AND MAXIMUM PREVIOUS CRACK WIDTH w_{max} AT A CRACKED R/C SECTION

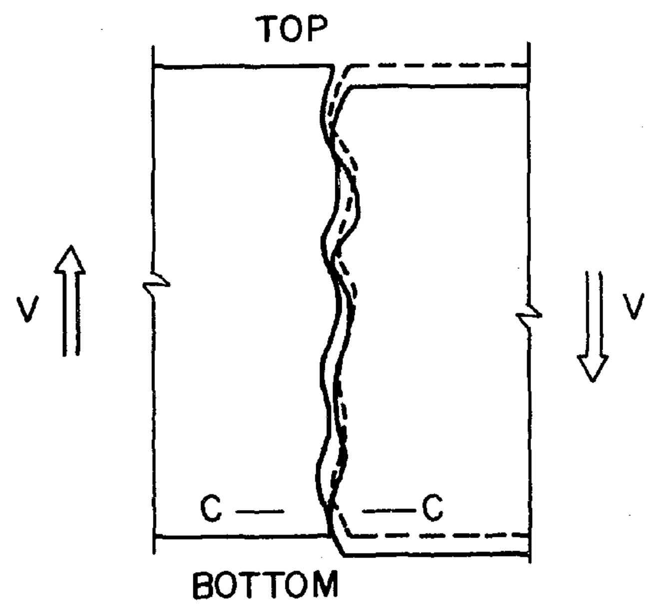

FIGURE 3.20 CONTACT OF CRACK SURFACES DUE TO SHEAR DISPLACEMENT

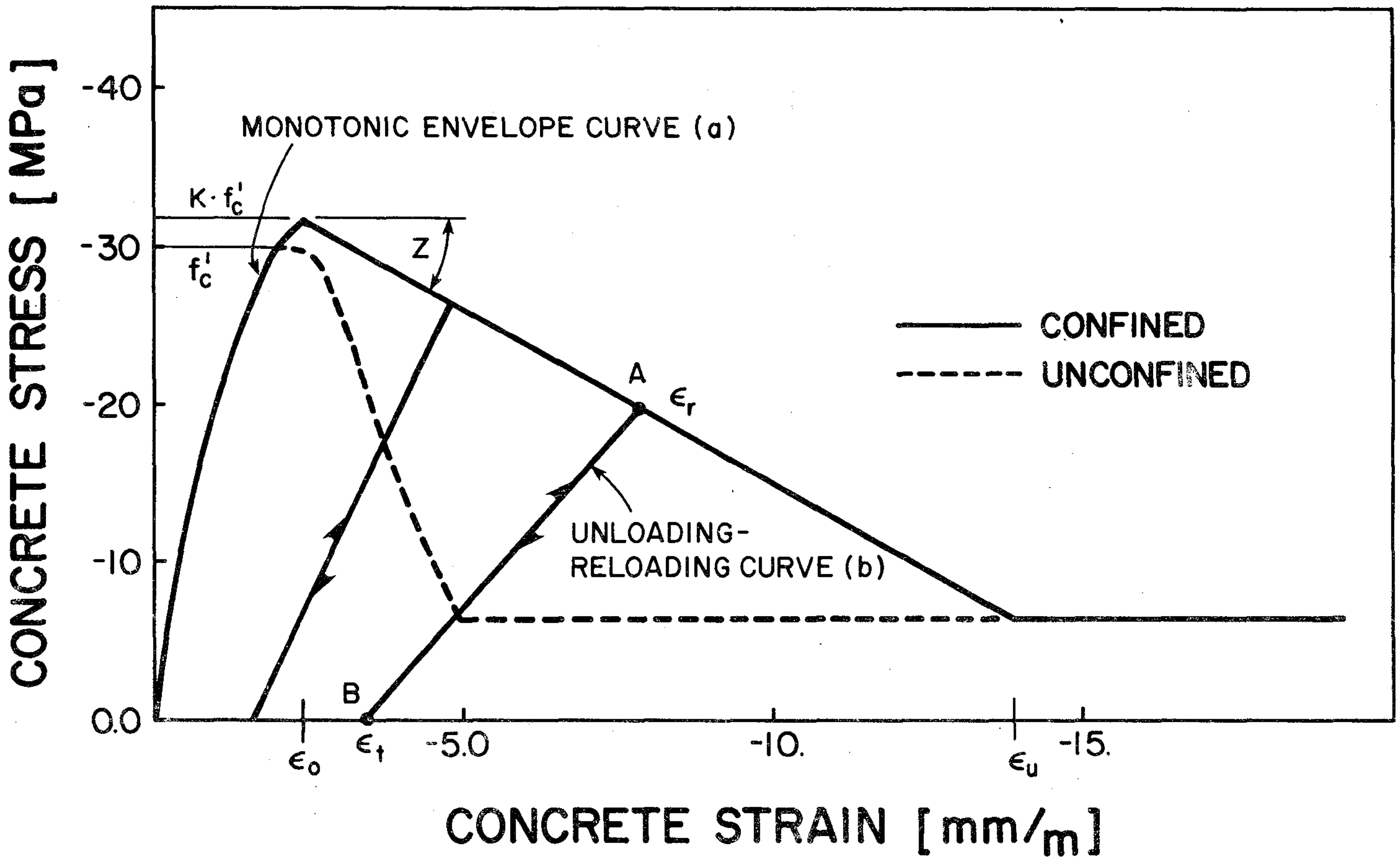

FIGURE 3.21 CYCLIC CONCRETE STRESS-STRAIN RELATION FOR CONFINED AND UNCONFINED CONCRETE

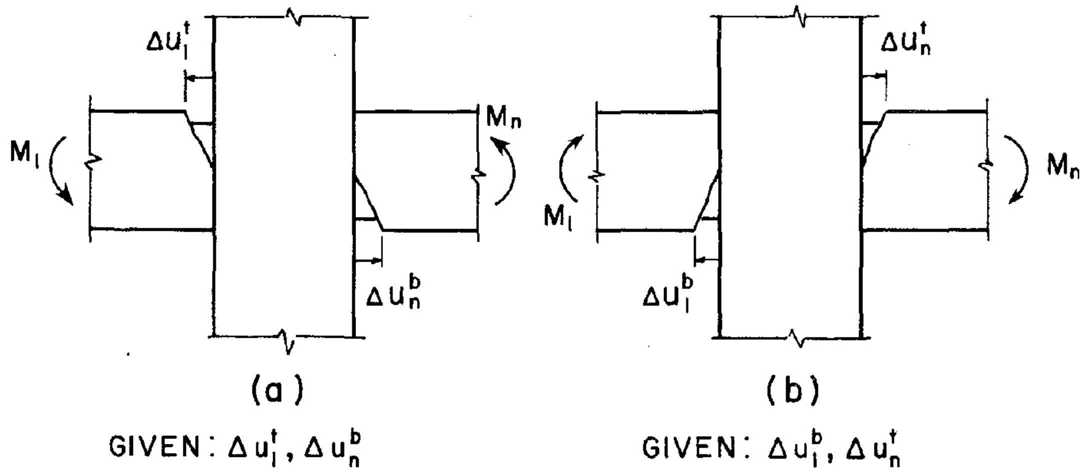

FIGURE 4.1 IMPOSED BOUNDARY CONDITIONS IN THE CASE OF INTERIOR JOINTS

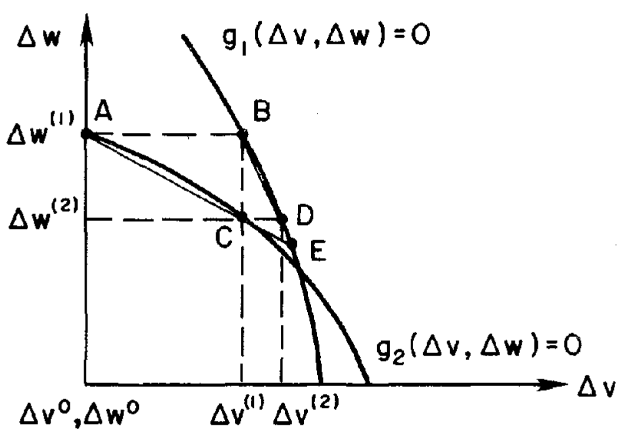

FIGURE 4.2 MODIFIED GAUSS-SEIDEL ALGORITHM FOR ITERATION LOOP (A)

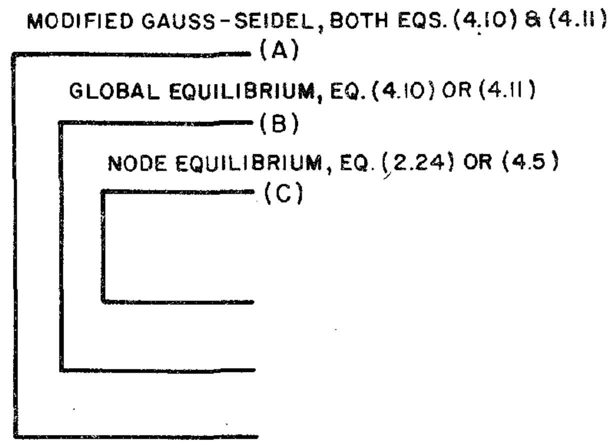

FIGURE 4.3 NESTED ITERATION LOOPS FOR INTERIOR JOINTS

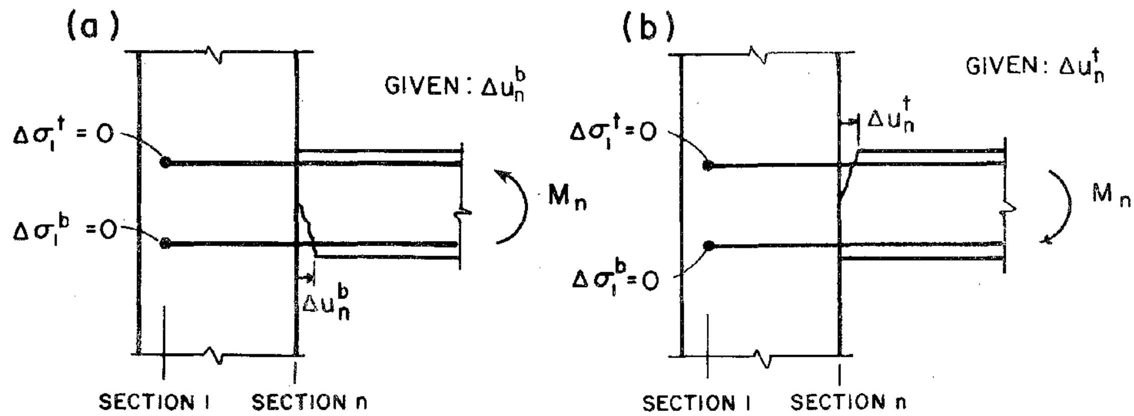

FIGURE 4.4 IMPOSED BOUNDARY CONDITIONS FOR EXTERIOR JOINTS

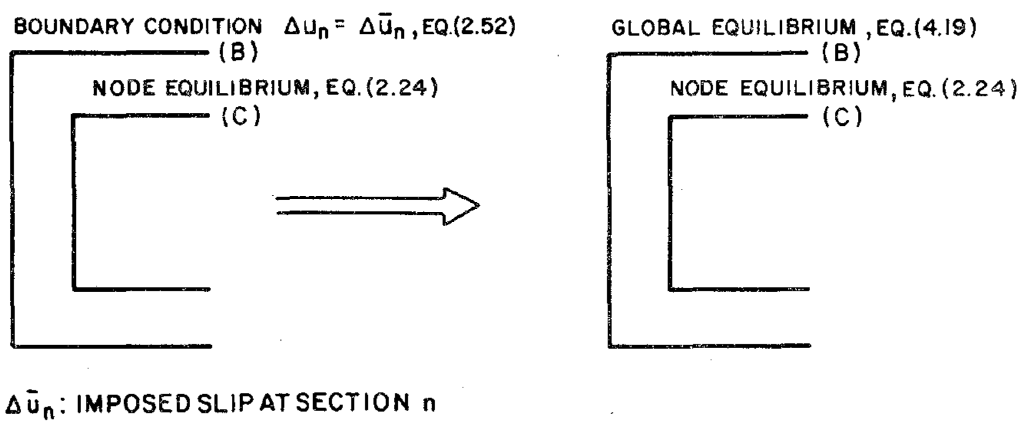

FIGURE 4.5 NESTED ITERATION LOOPS FOR EXTERIOR JOINTS

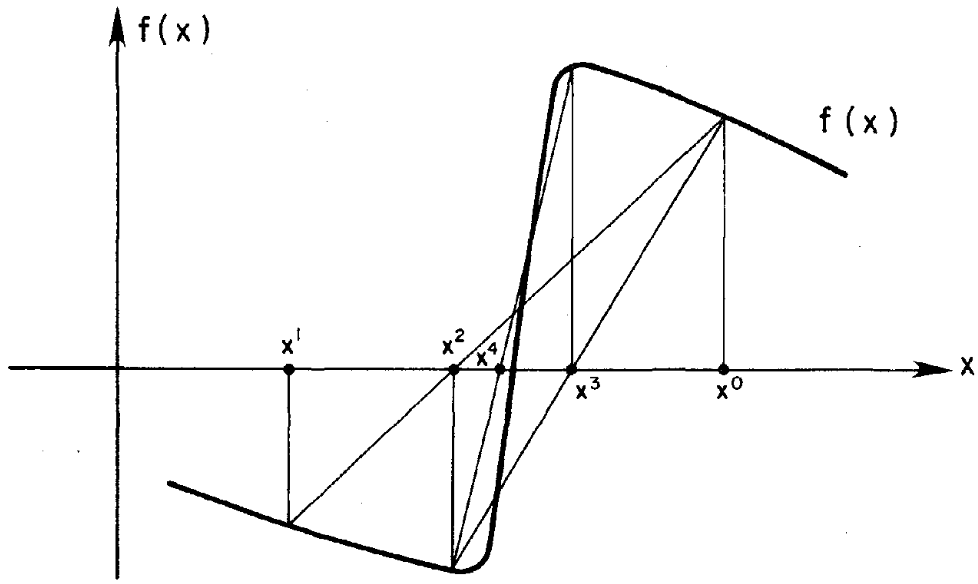

FIGURE 4.6a RESIDUAL FUNCTION $f(x)$ AND PROPOSED REGULA FALSI ALGORITHM

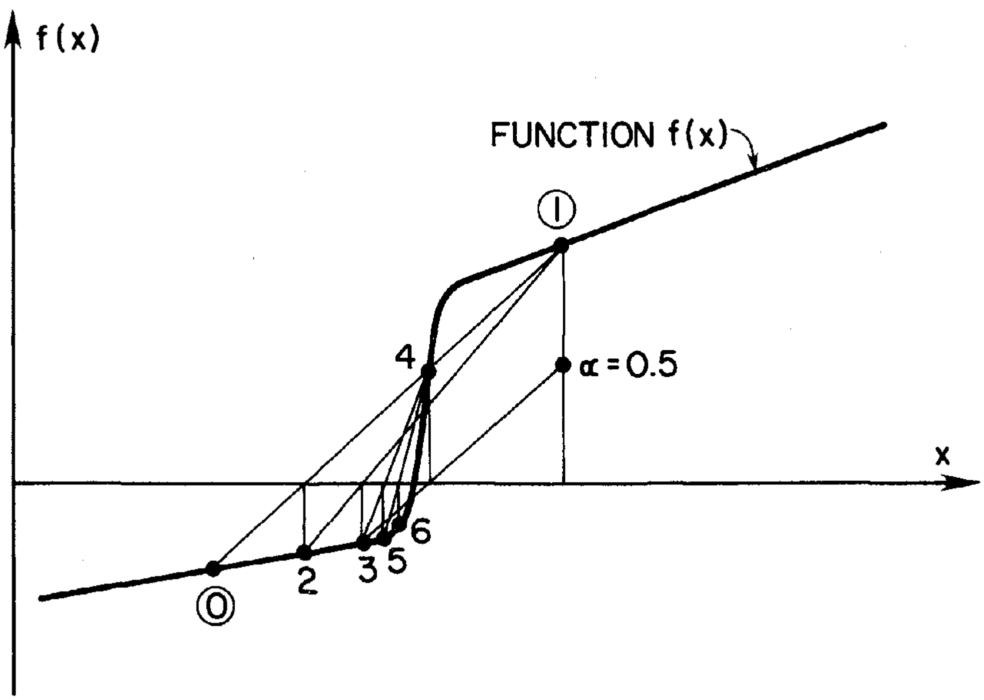

FIGURE 4.6b ACCELERATED REGULA FALSI OR ILLINOIS ALGORITHM

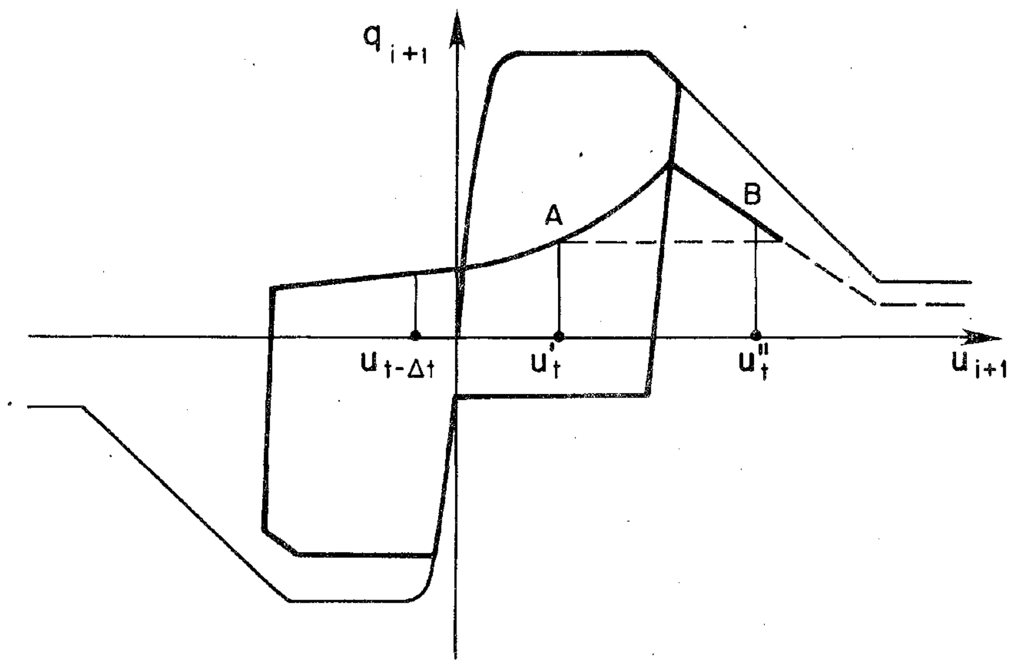

FIGURE 4.7 TWO POSSIBLE EQUILIBRIUM POSITIONS A AND B AT NODE $i+1$

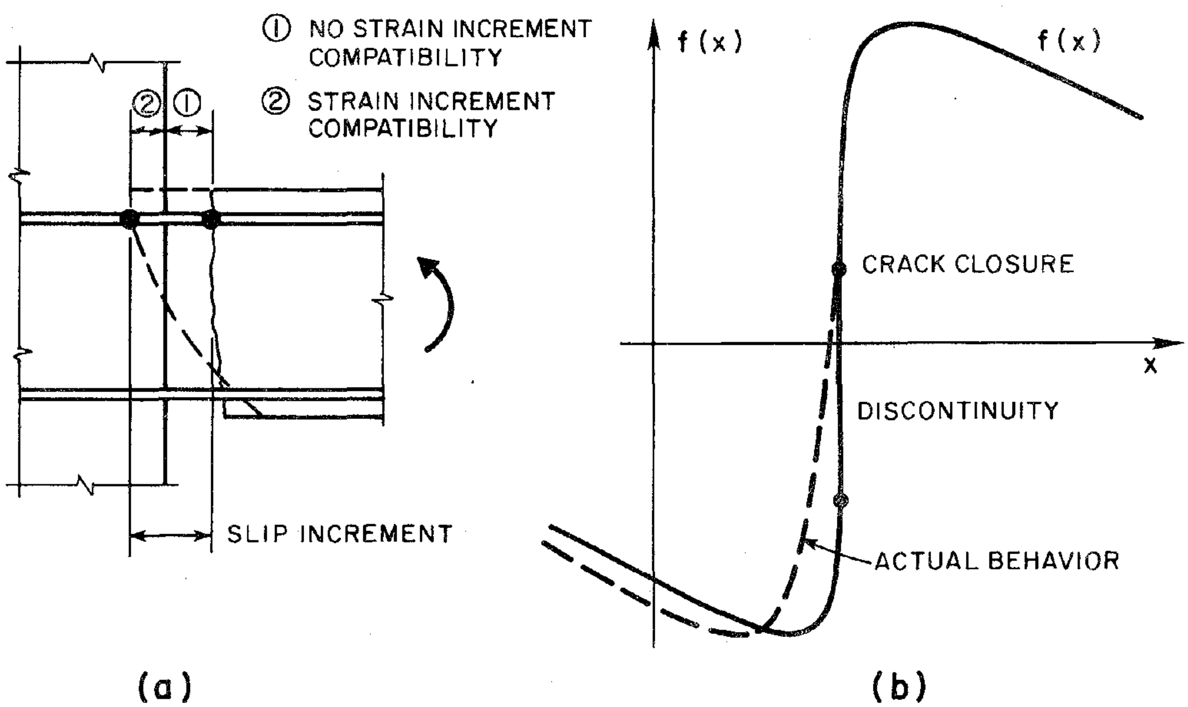

FIGURE 4.8 NUMERICAL PROBLEMS ASSOCIATED WITH CRACK CLOSURE

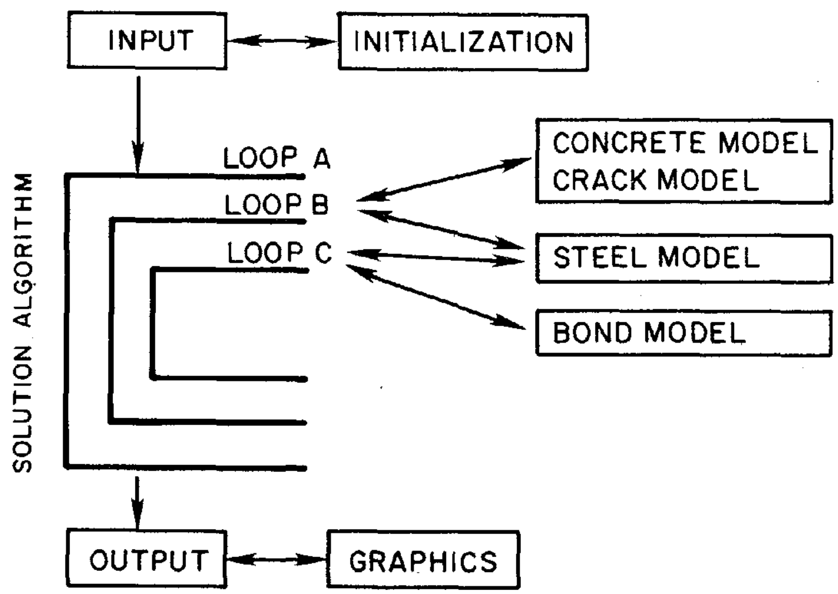

FIGURE 4.9 ORGANIZATION OF COMPUTER PROGRAM *JOINT*

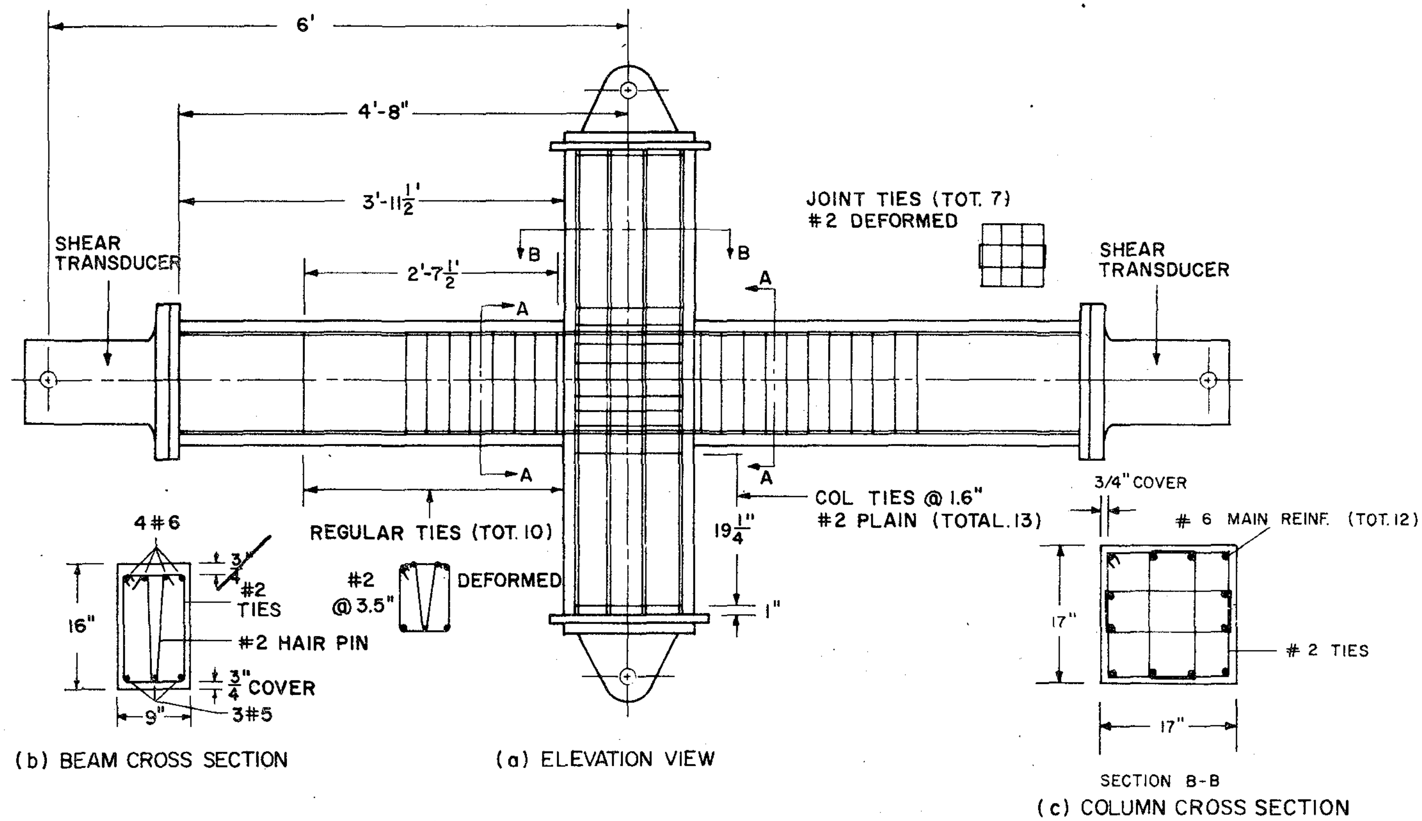

FIGURE 5.1 GEOMETRY AND REINFORCING DETAILS OF TEST SPECIMEN (REF.[50])

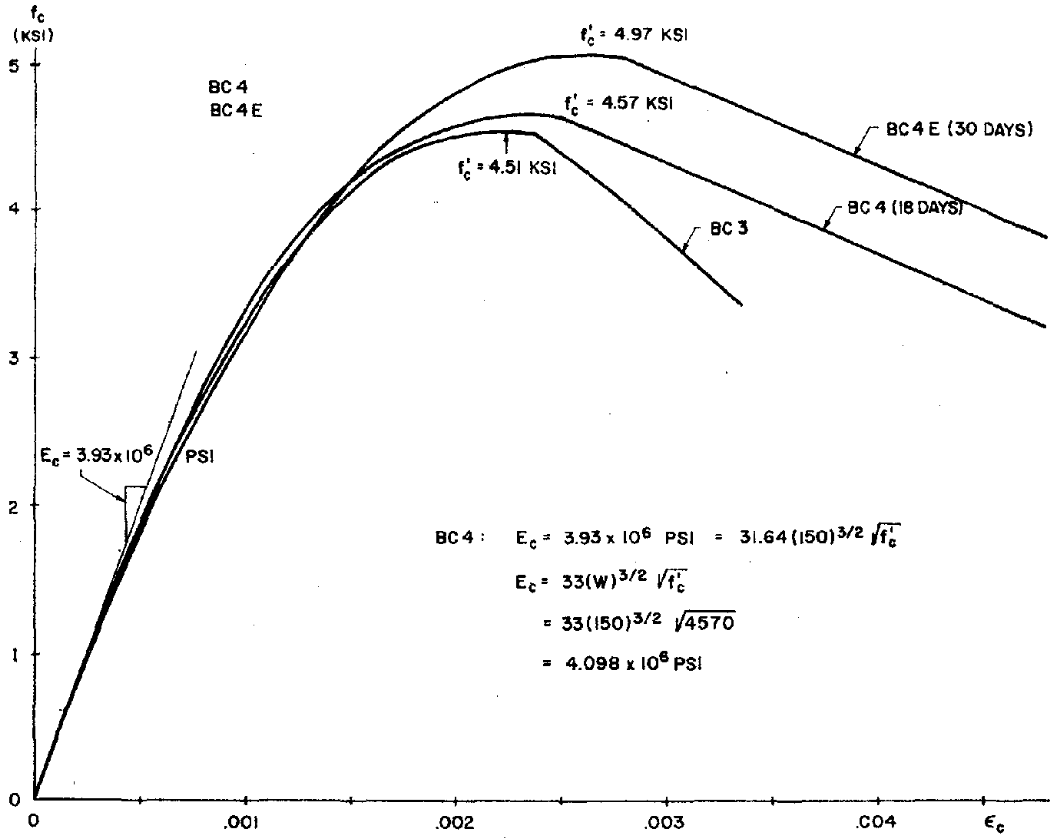

FIGURE 5.2a MEASURED STRESS-STRAIN RELATION FOR CONCRETE (REF.[50])

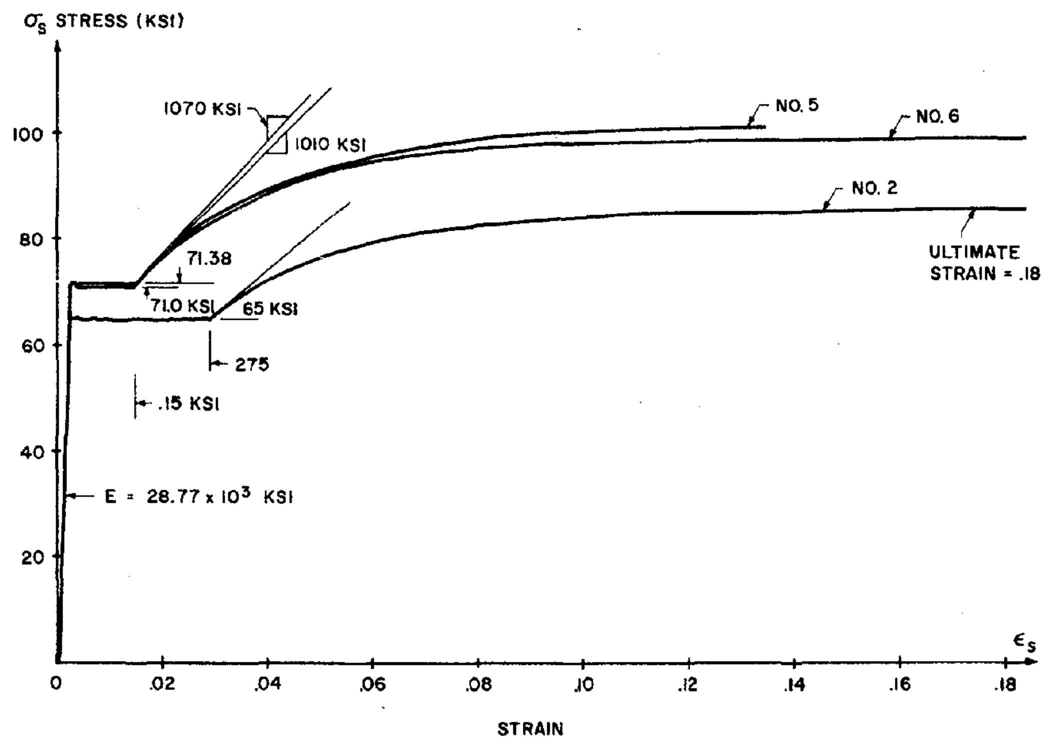

FIGURE 5.2b MEASURED STRESS-STRAIN RELATION FOR REINFORCING STEEL (REF.[50])

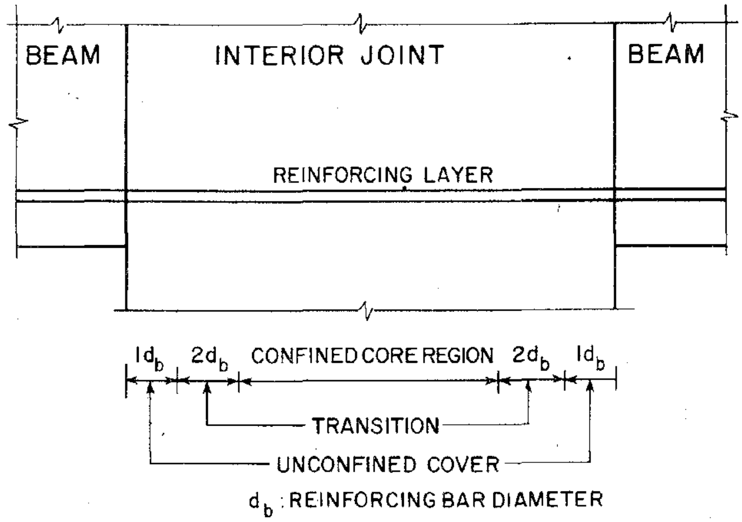

FIGURE 5.3 SUBVISION OF BAR ANCHORAGE LENGTH INTO DIFFERENT BOND REGIONS

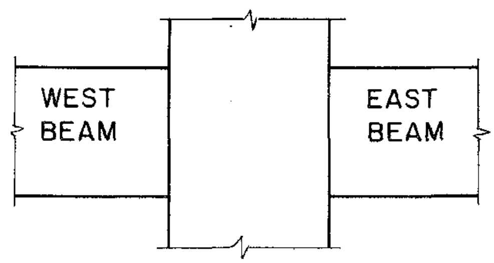

FIGURE 5.4 DEFINITION OF EAST AND WEST BEAM FOR TEST SPECIMEN

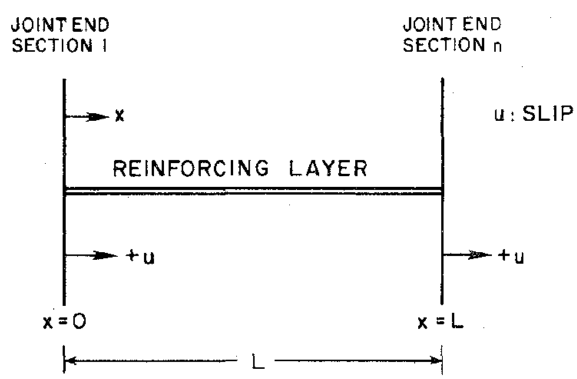

FIGURE 5.5 SIGN CONVENTION FOR RELATIVE SLIP VALUES

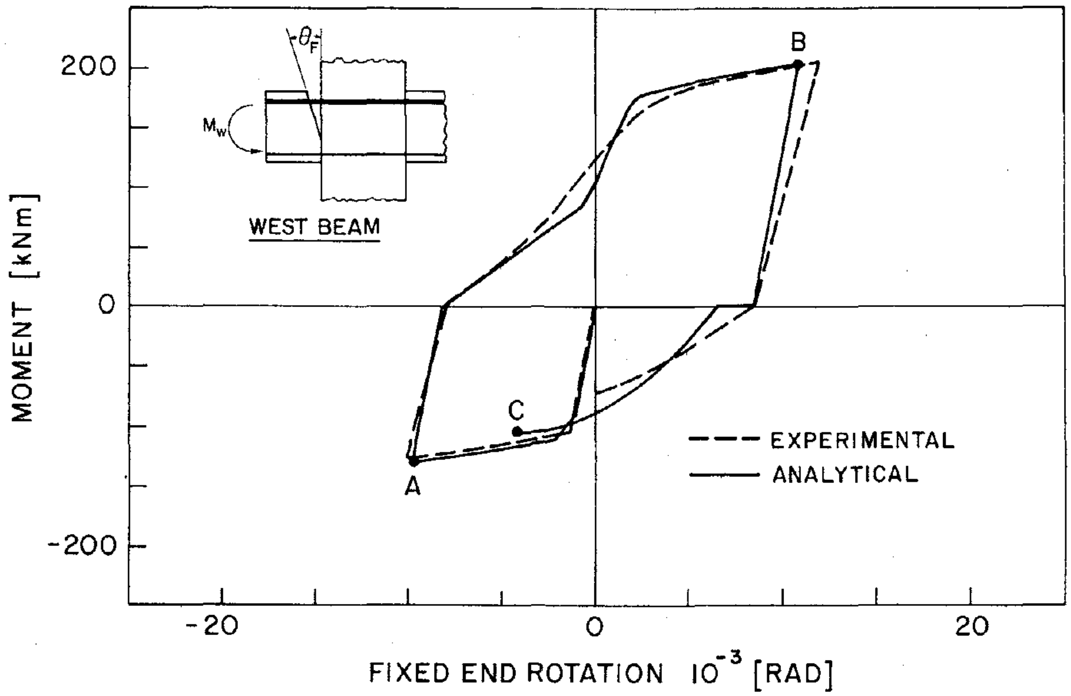

FIGURE 5.6a END MOMENT VERSUS FIXED-END ROTATION. SPECIMEN BC4

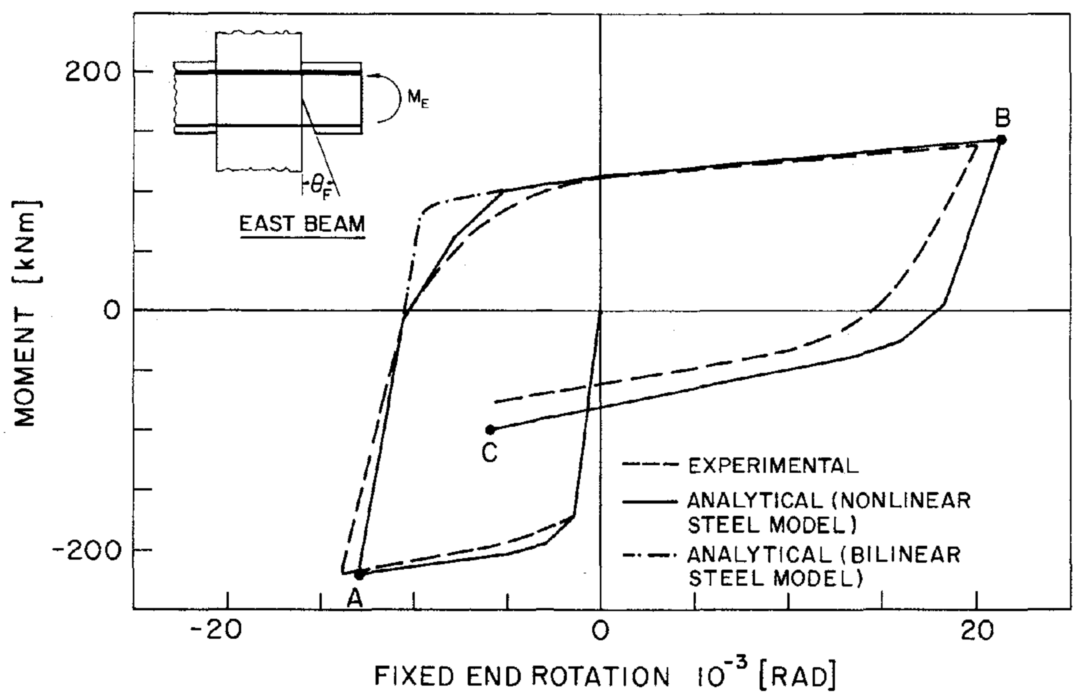

FIGURE 5.6b END MOMENT VERSUS FIXED-END ROTATION. SPECIMEN BC4

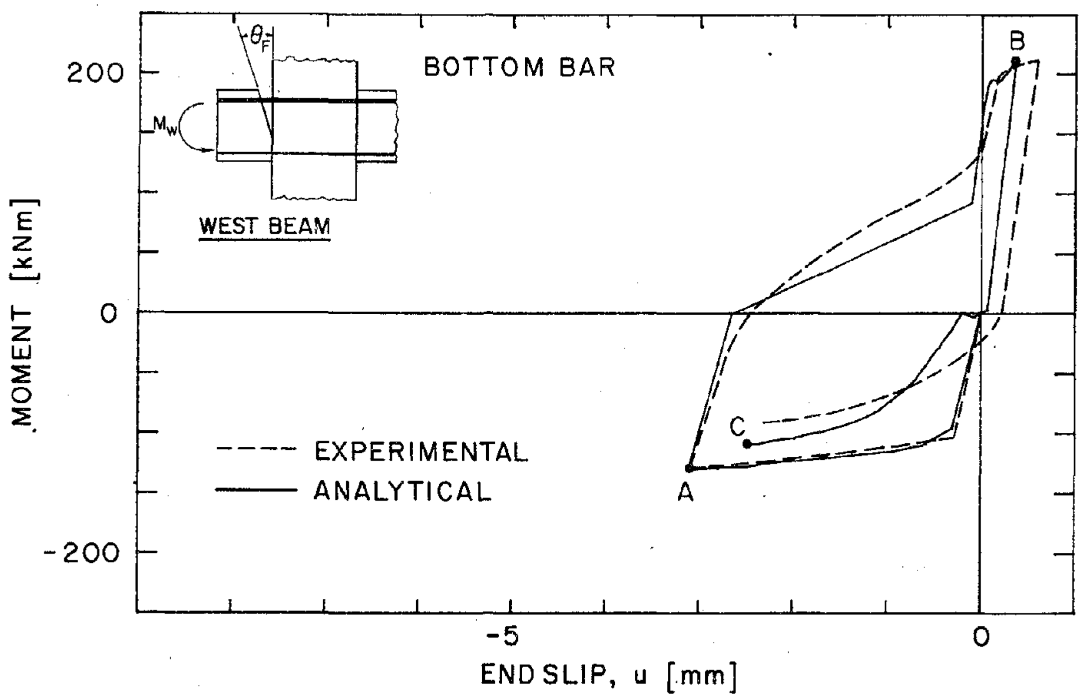

FIGURE 5.7a END MOMENT VERSUS RELATIVE BAR SLIPPAGE AT BEAM-COLUMN INTERFACE. SPECIMEN BC4

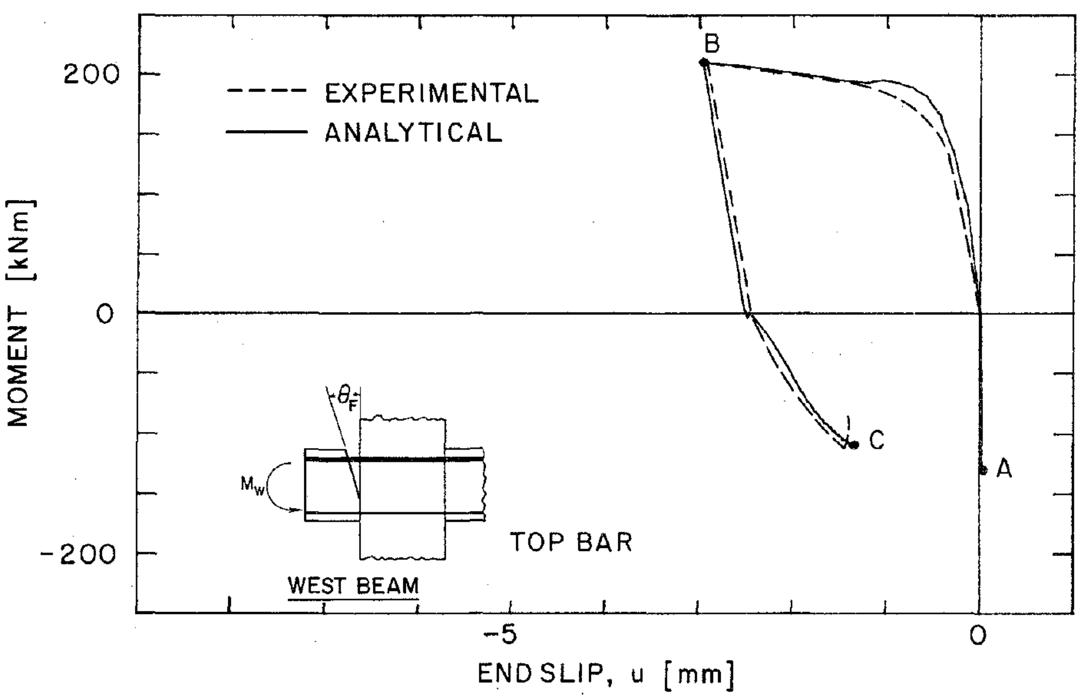

FIGURE 5.7b END MOMENT VERSUS RELATIVE BAR SLIPPAGE AT BEAM-COLUMN INTERFACE. SPECIMEN BC4

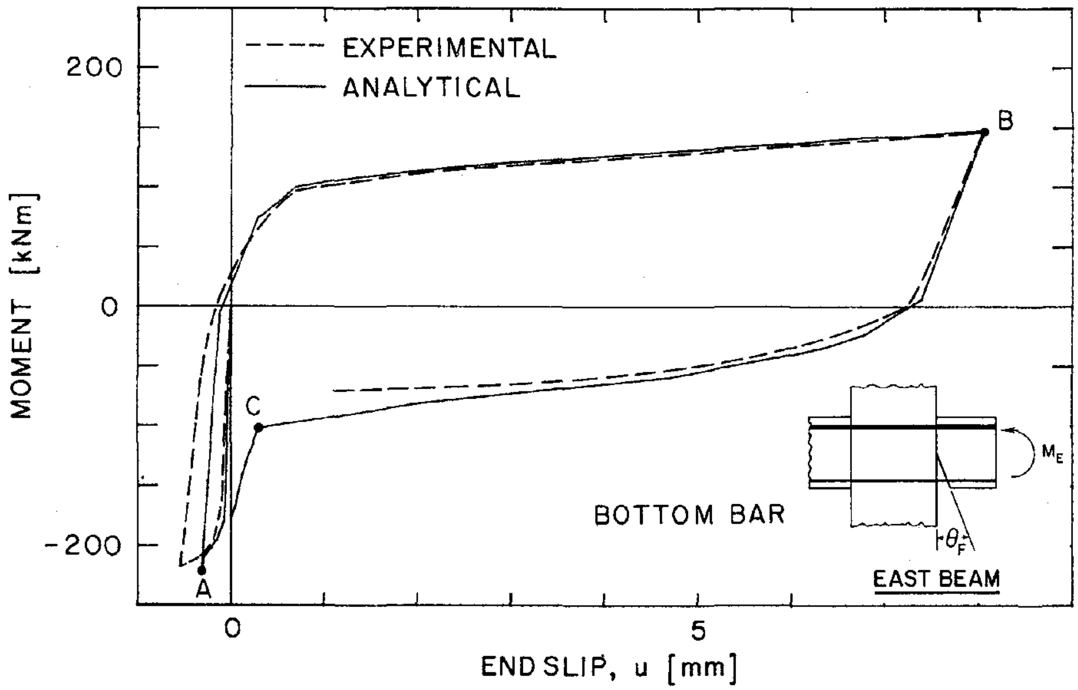

FIGURE 5.7c END MOMENT VERSUS RELATIVE BAR SLIPPAGE AT BEAM-COLUMN INTERFACE. SPECIMEN BC4

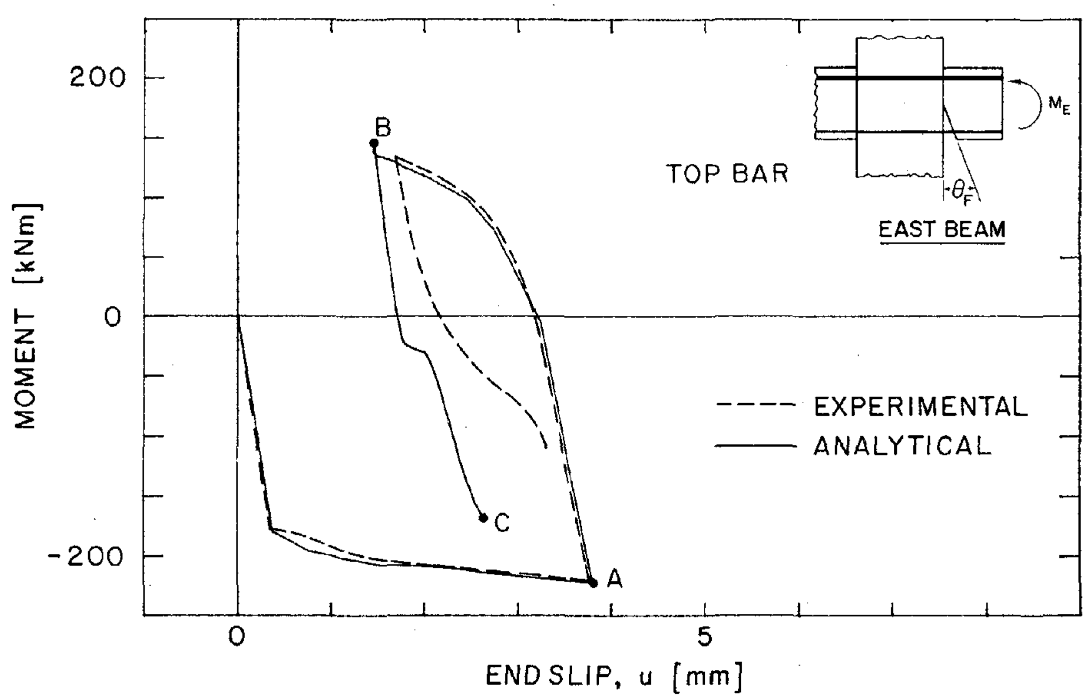

FIGURE 5.7d END MOMENT VERSUS RELATIVE BAR SLIPPAGE AT BEAM-COLUMN INTERFACE. SPECIMEN BC4

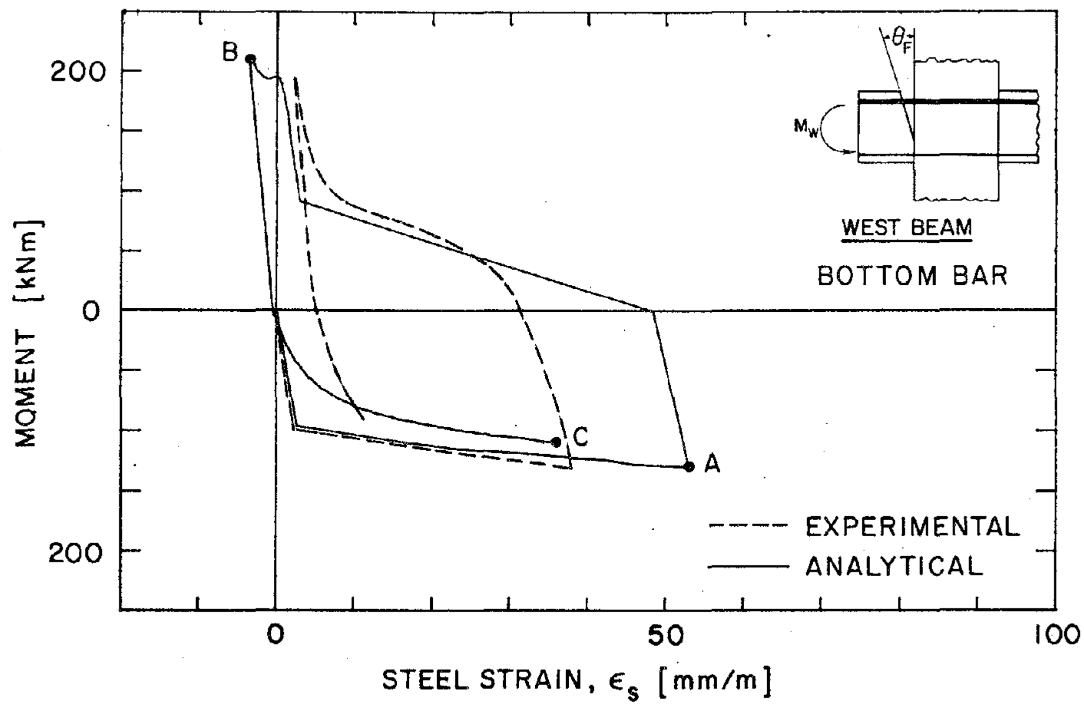

FIGURE 5.8a END MOMENT VERSUS REINFORCING STEEL STRAIN AT BEAM-COLUMN INTERFACE. SPECIMEN BC4

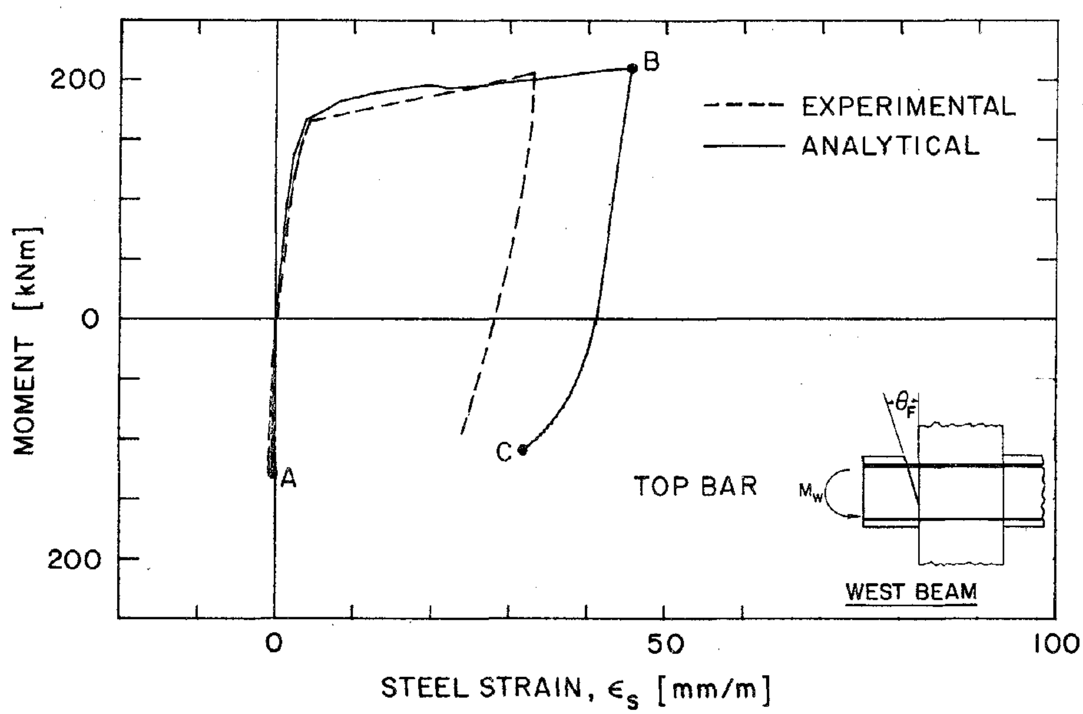

FIGURE 5.8b END MOMENT VERSUS REINFORCING STEEL STRAIN AT BEAM-COLUMN INTERFACE. SPECIMEN BC4

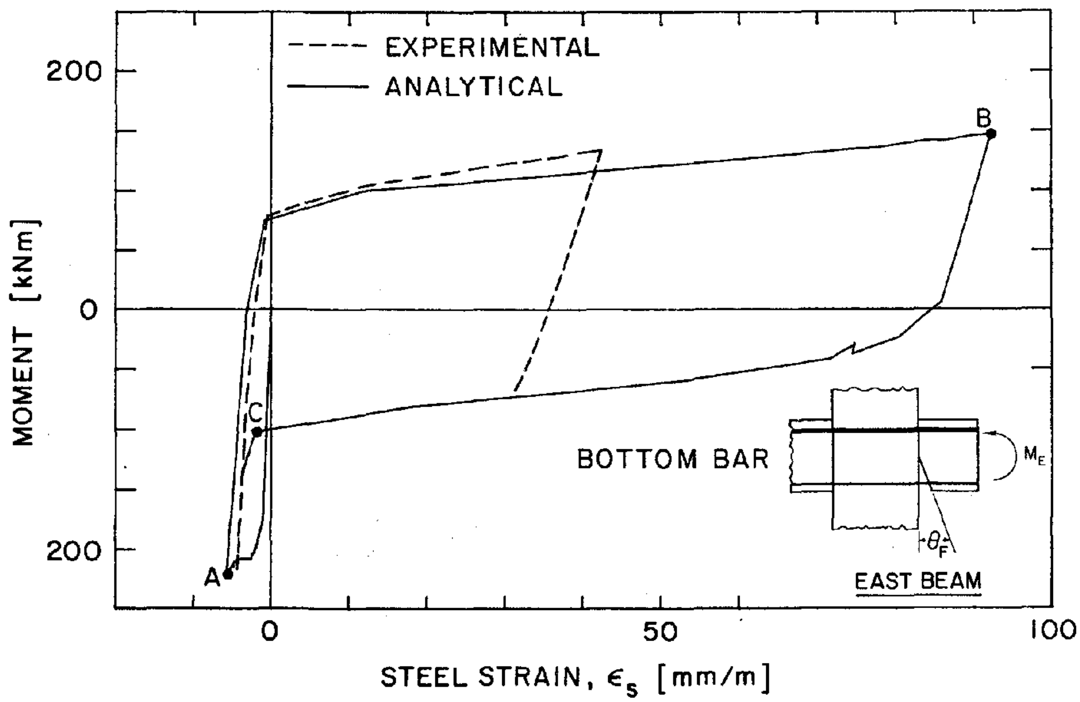

FIGURE 5.8c END MOMENT VERSUS REINFORCING STEEL STRAIN AT BEAM-COLUMN INTERFACE. SPECIMEN BC4

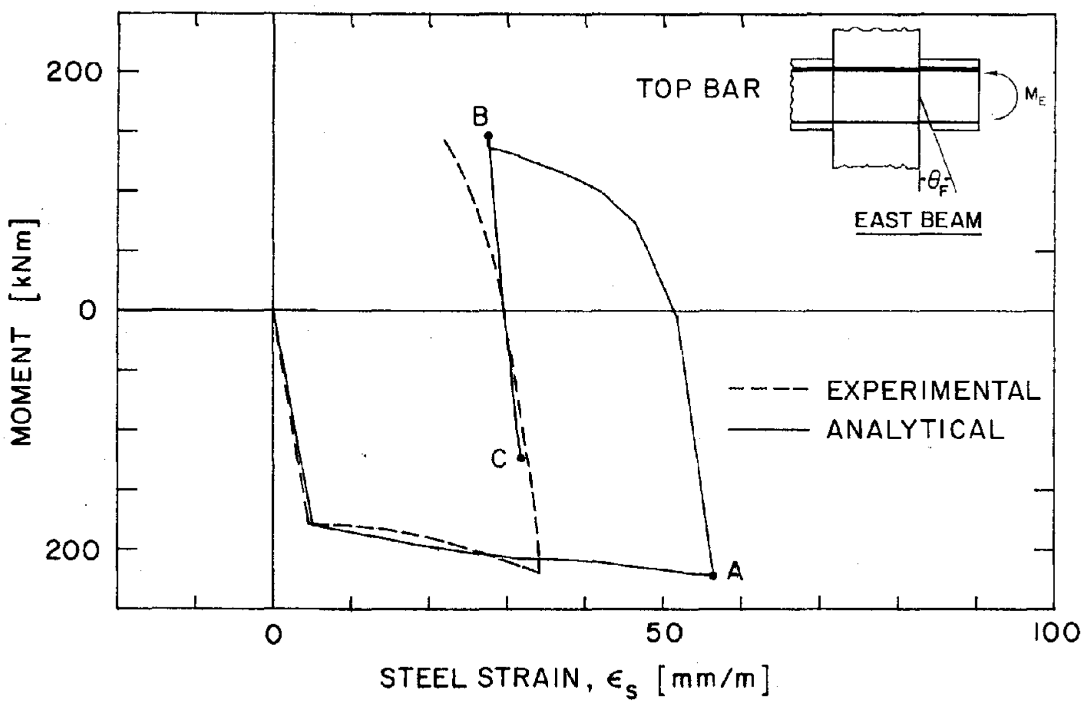

FIGURE 5.8d END MOMENT VERSUS REINFORCING STEEL STRAIN AT BEAM-COLUMN INTERFACE. SPECIMEN BC4

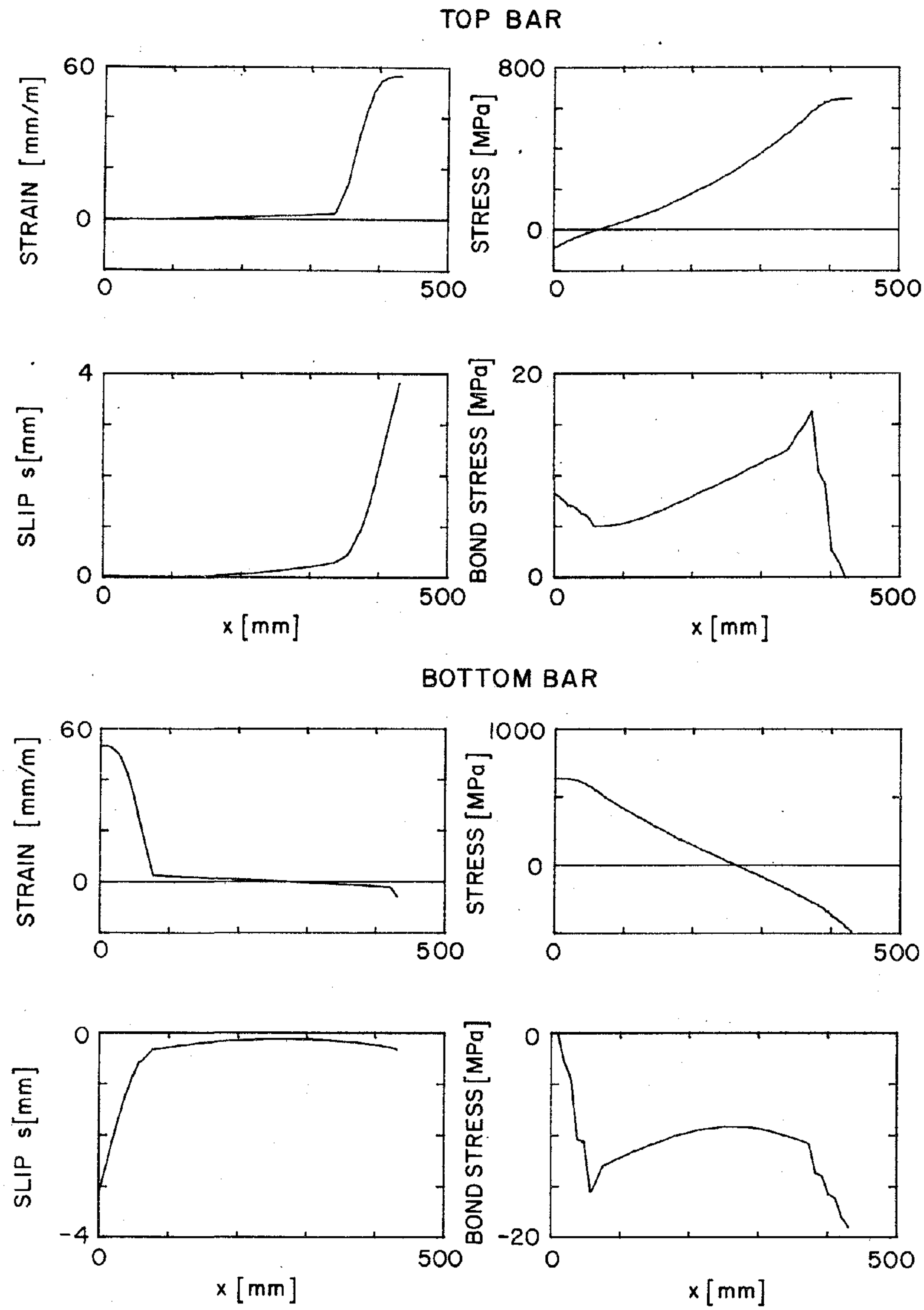

FIGURE 5.9a DISTRIBUTION OF STEEL STRAIN, BAR SLIP, STEEL STRESS AND BOND STRESS ALONG EMBEDDED BARS AT LOAD POINT A. COLUMN WIDTH = 430 mm

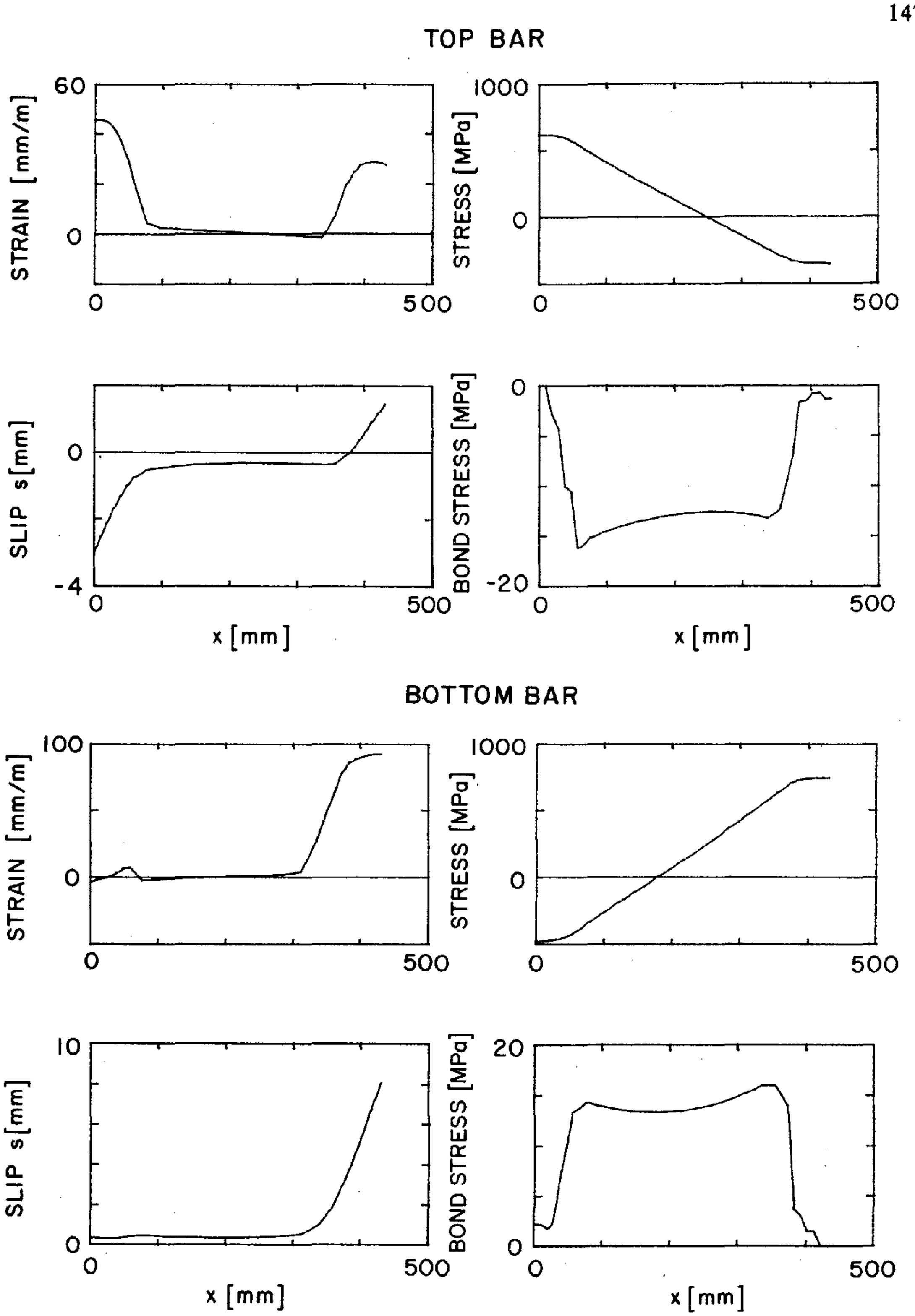

FIGURE 5.9b DISTRIBUTION OF STEEL STRAIN, BAR SLIP, STEEL STRESS AND BOND STRESS ALONG EMBEDDED BARS AT LOAD POINT B. COLUMN WIDTH = 430 mm

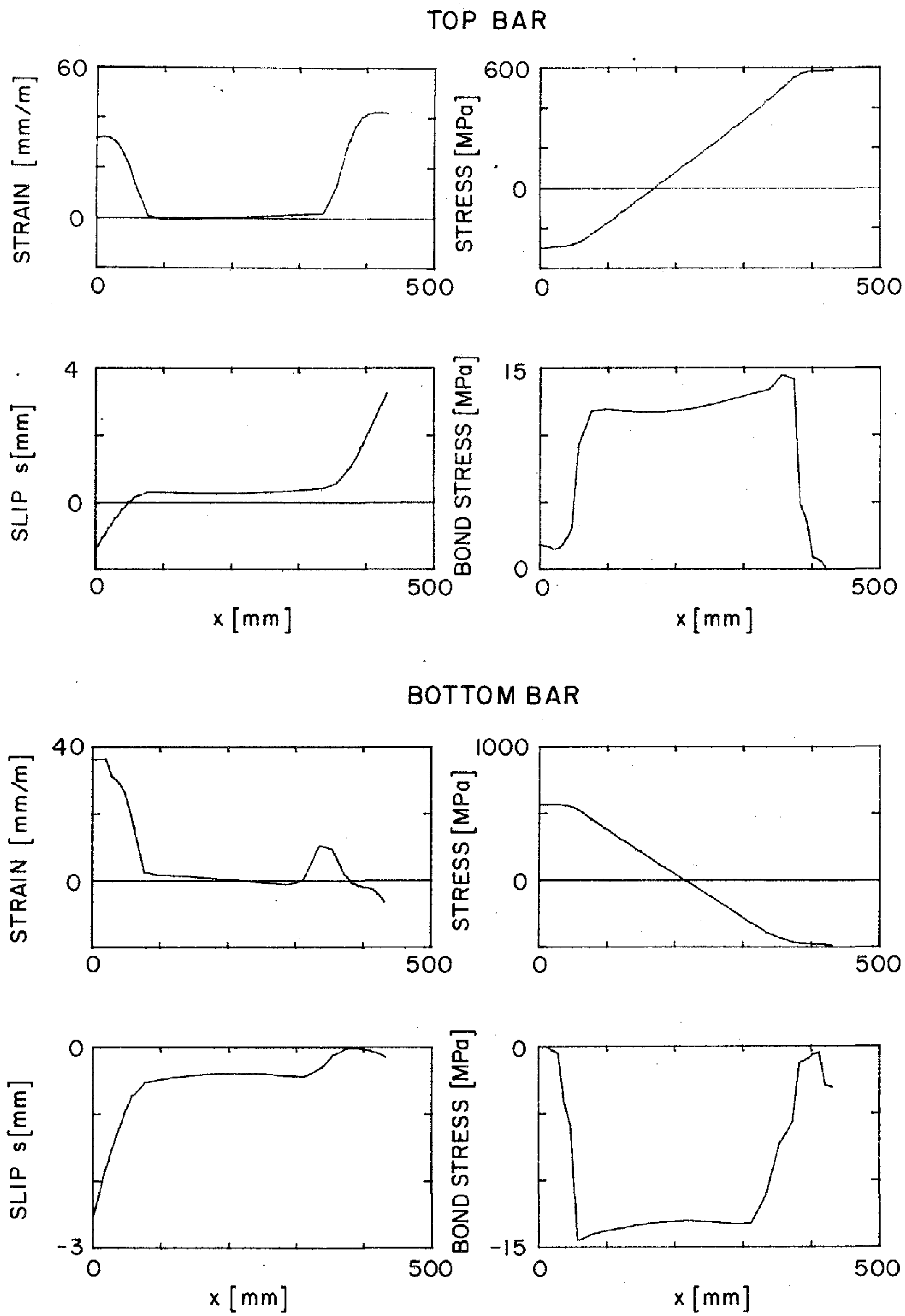

FIGURE 5.9c DISTRIBUTION OF STEEL STRAIN, BAR SLIP, STEEL STRESS AND BOND STRESS ALONG EMBEDDED BARS AT LOAD POINT C. COLUMN WIDTH = 430 mm

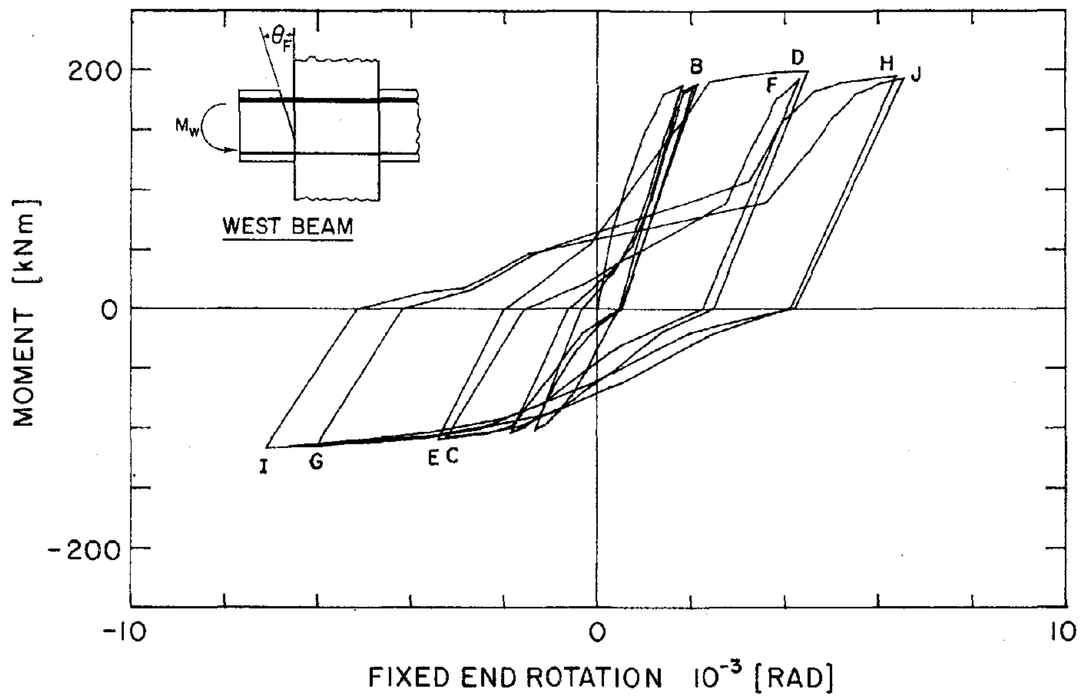

FIGURE 5.10a END MOMENT VERSUS FIXED-END ROTATION. SPECIMEN BC3

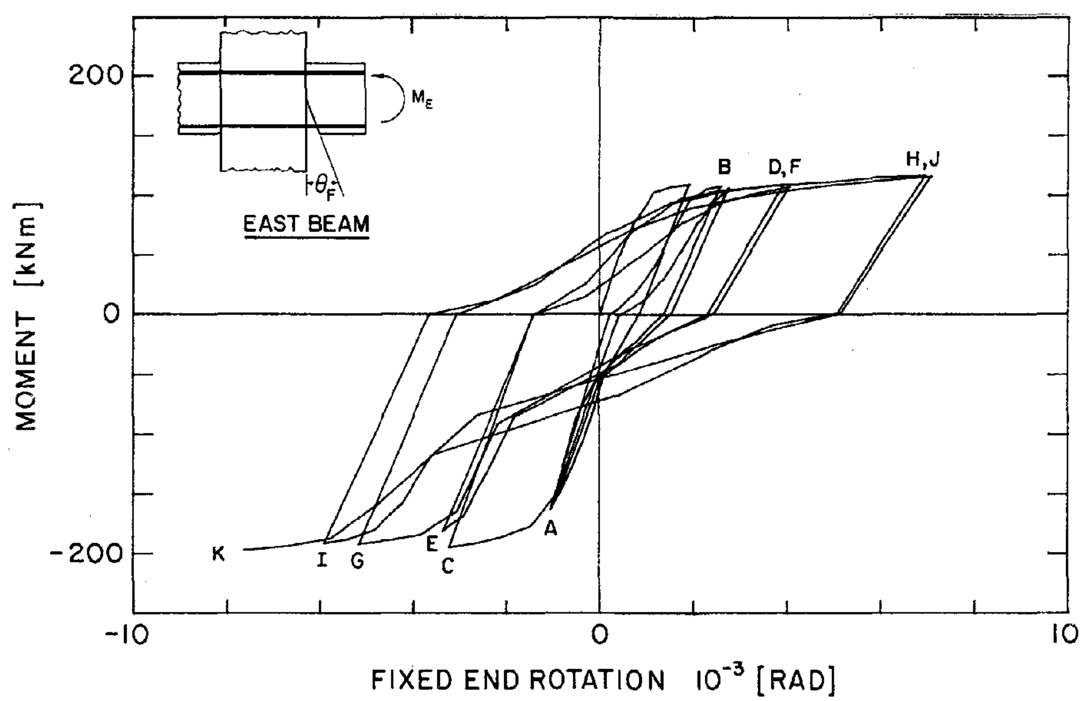

FIGURE 5.10b END MOMENT VERSUS FIXED-END ROTATION. SPECIMEN BC3

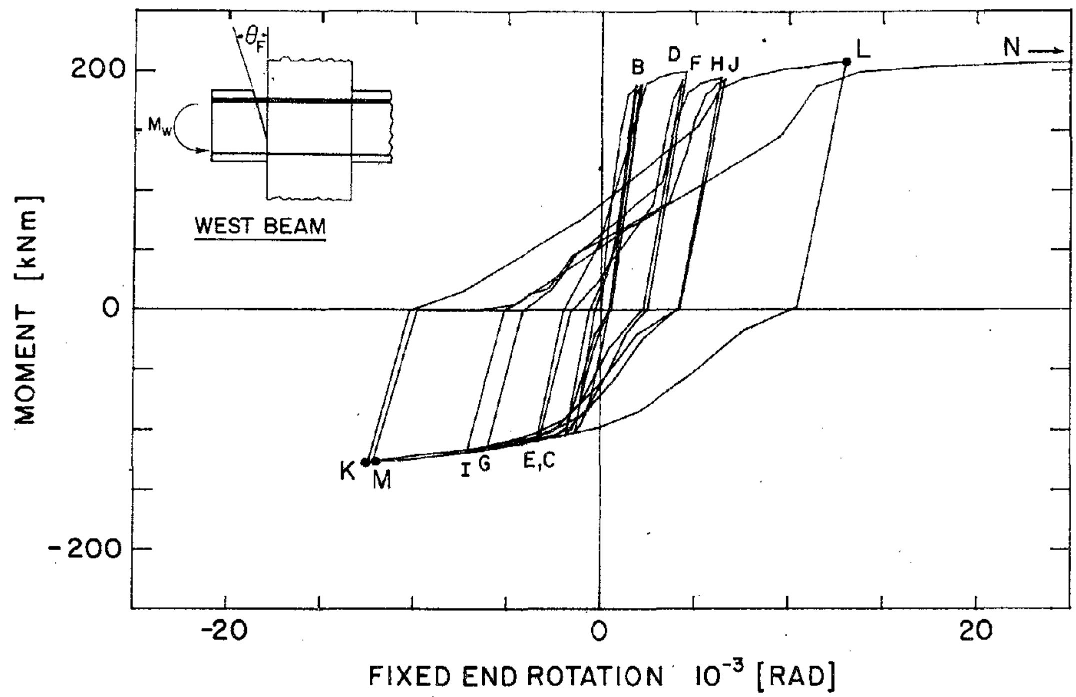

FIGURE 5.11a END MOMENT VERSUS FIXED-END ROTATION. SPECIMEN BC3

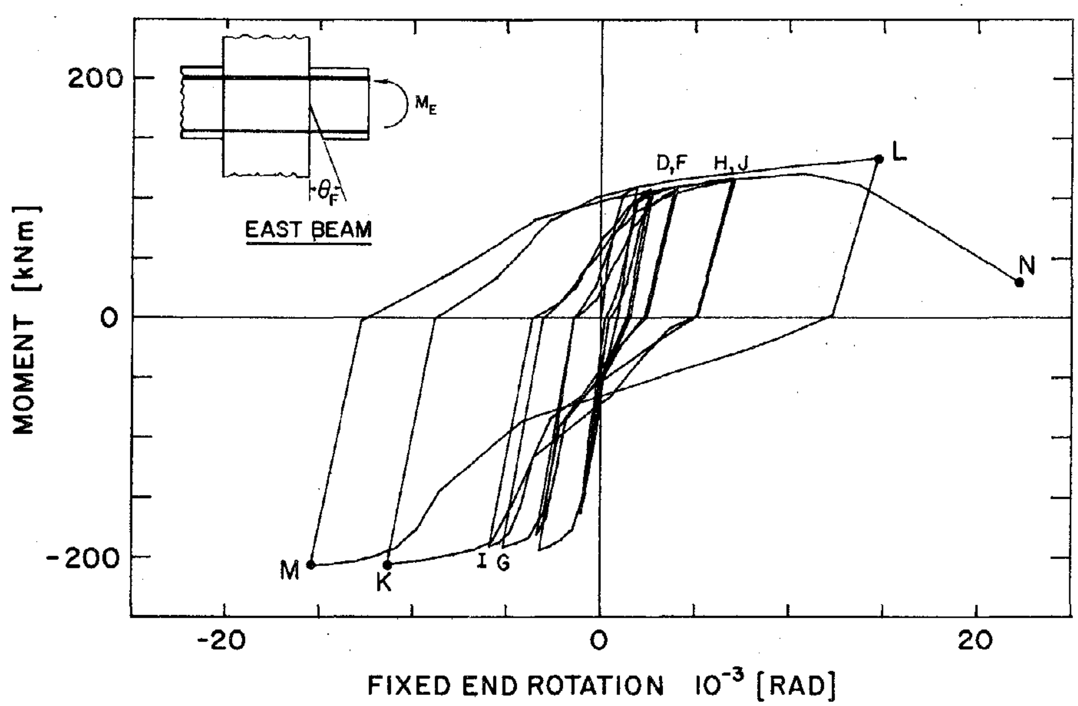

FIGURE 5.11b END MOMENT VERSUS FIXED-END ROTATION. SPECIMEN BC3

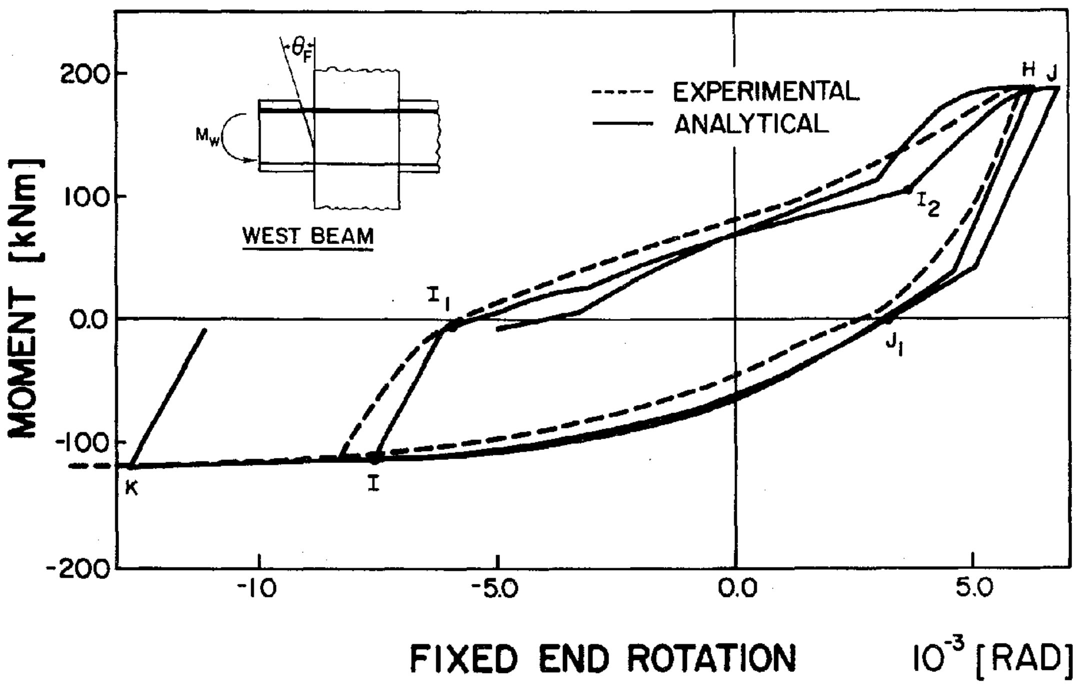

FIGURE 5.12a END MOMENT VERSUS FIXED-END ROTATION. SPECIMEN BC3

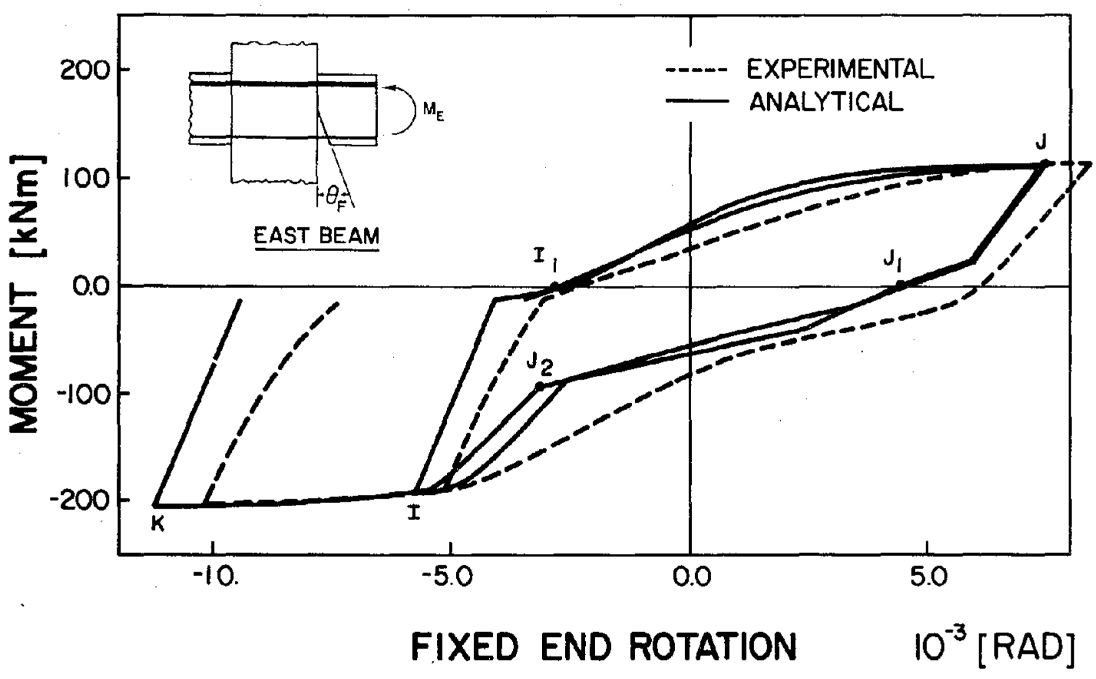

FIGURE 5.12b END MOMENT VERSUS FIXED-END ROTATION. SPECIMEN BC3

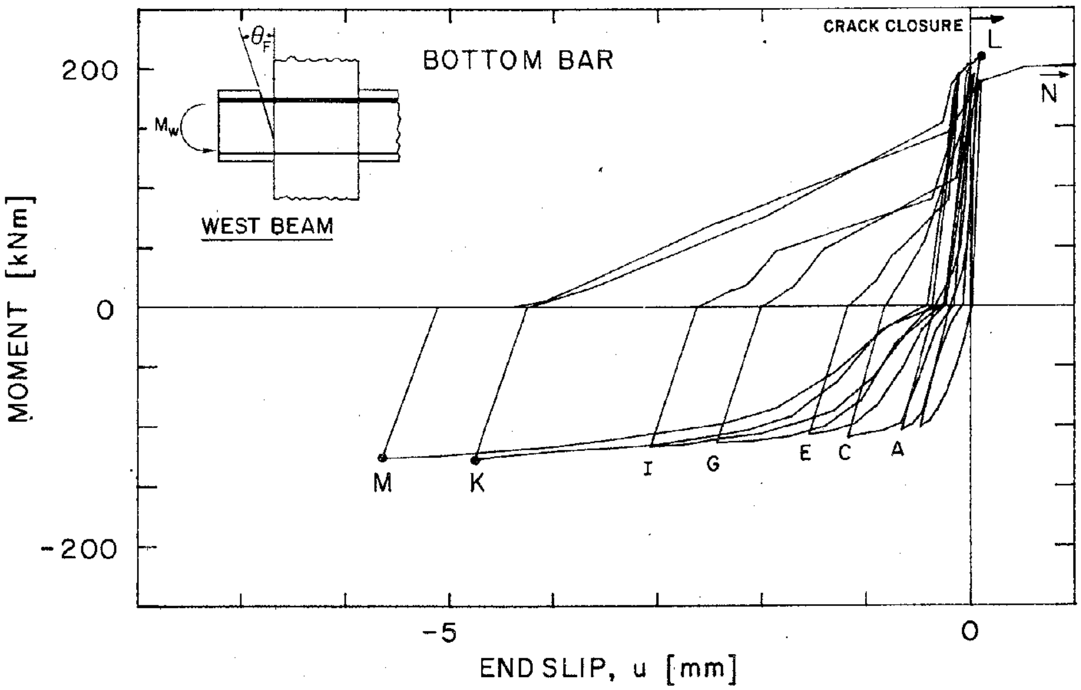

FIGURE 5.13a END MOMENT VERSUS RELATIVE BAR SLIPPAGE AT BEAM-COLUMN INTERFACE. SPECIMEN BC3

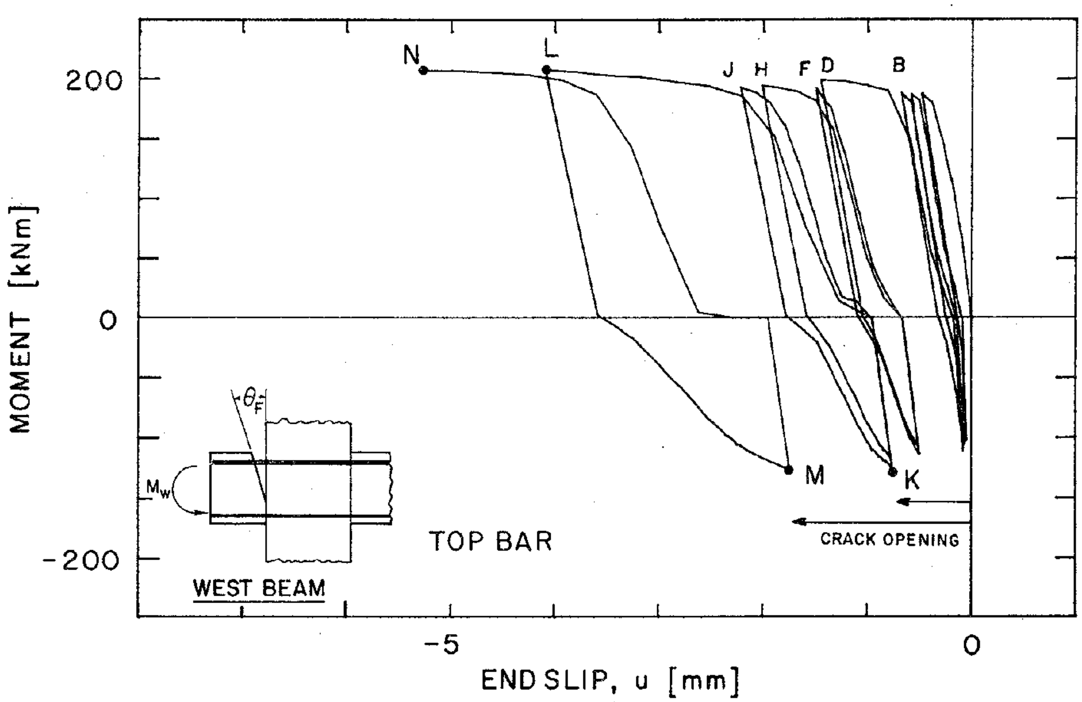

FIGURE 5.13b END MOMENT VERSUS RELATIVE BAR SLIPPAGE AT BEAM-COLUMN INTERFACE. SPECIMEN BC3

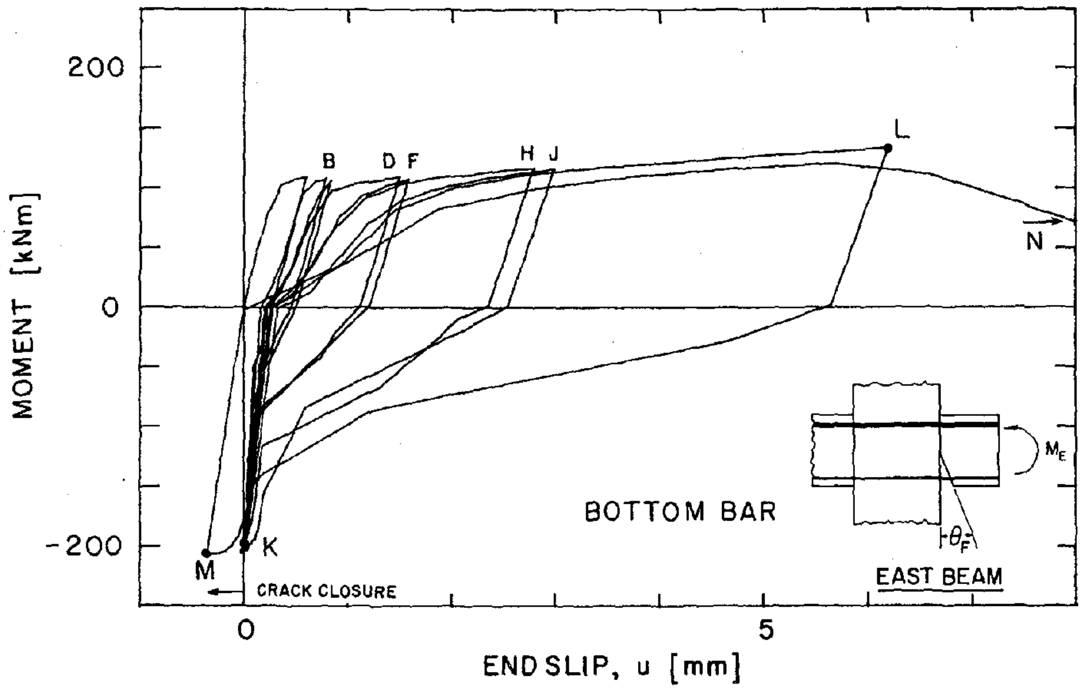

FIGURE 5.13c END MOMENT VERSUS RELATIVE BAR SLIPPAGE AT BEAM-COLUMN INTERFACE. SPECIMEN BC3

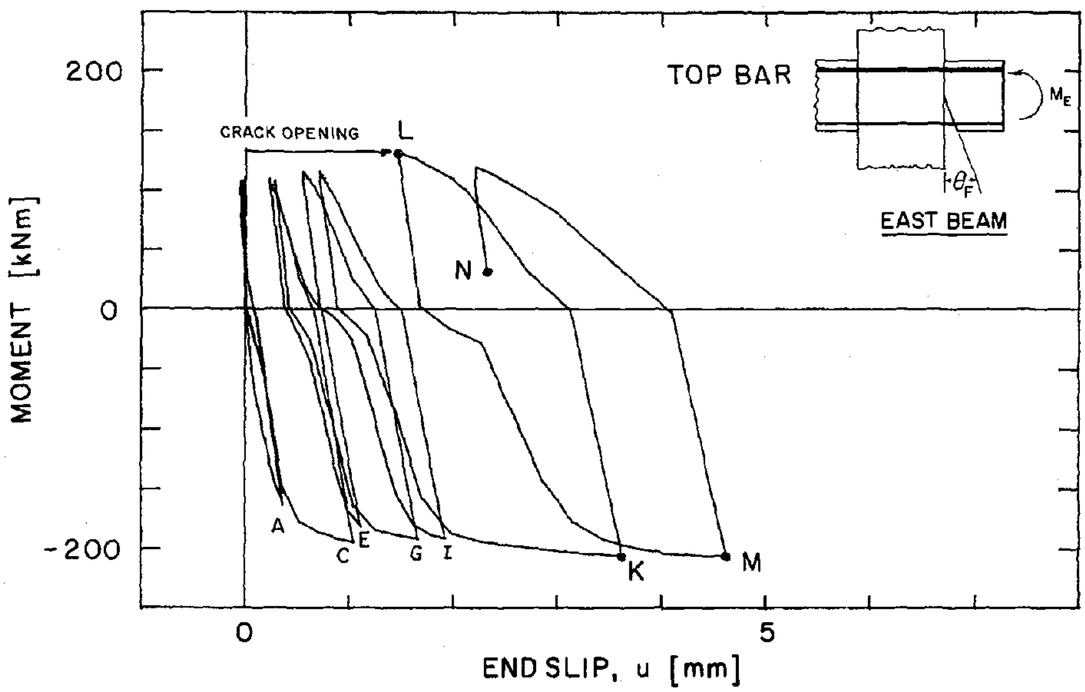

FIGURE 5.13d END MOMENT VERSUS RELATIVE BAR SLIPPAGE AT BEAM-COLUMN INTERFACE. SPECIMEN BC3

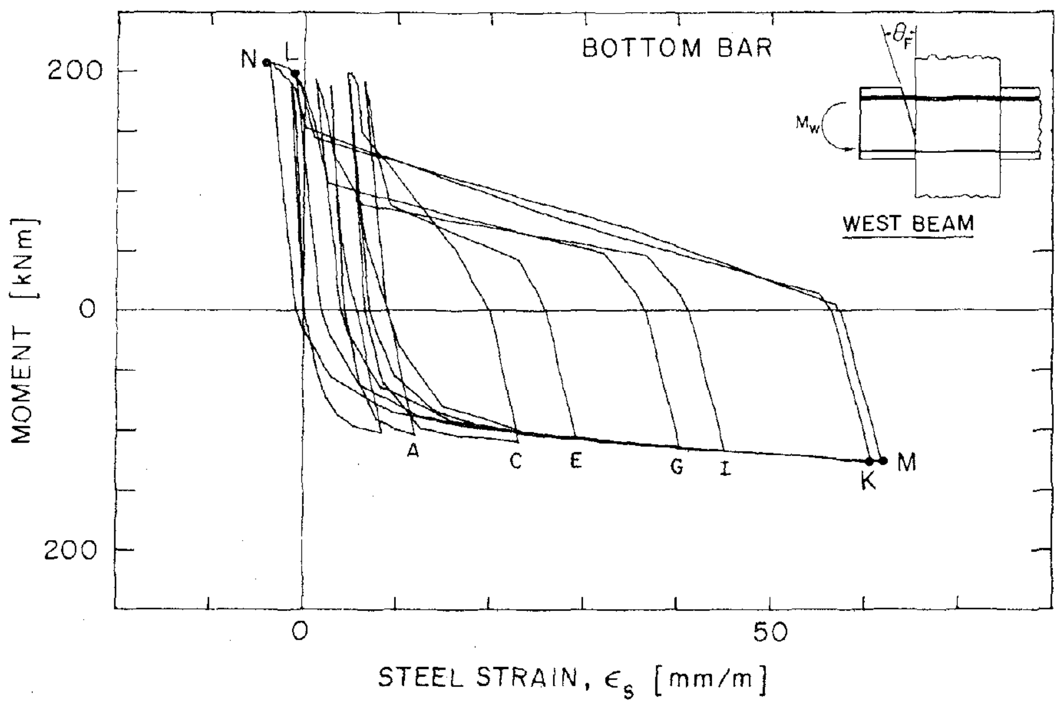

FIGURE 5.14a END MOMENT VERSUS REINFORCING STEEL STRAIN AT BEAM-COLUMN INTERFACE. SPECIMEN BC3

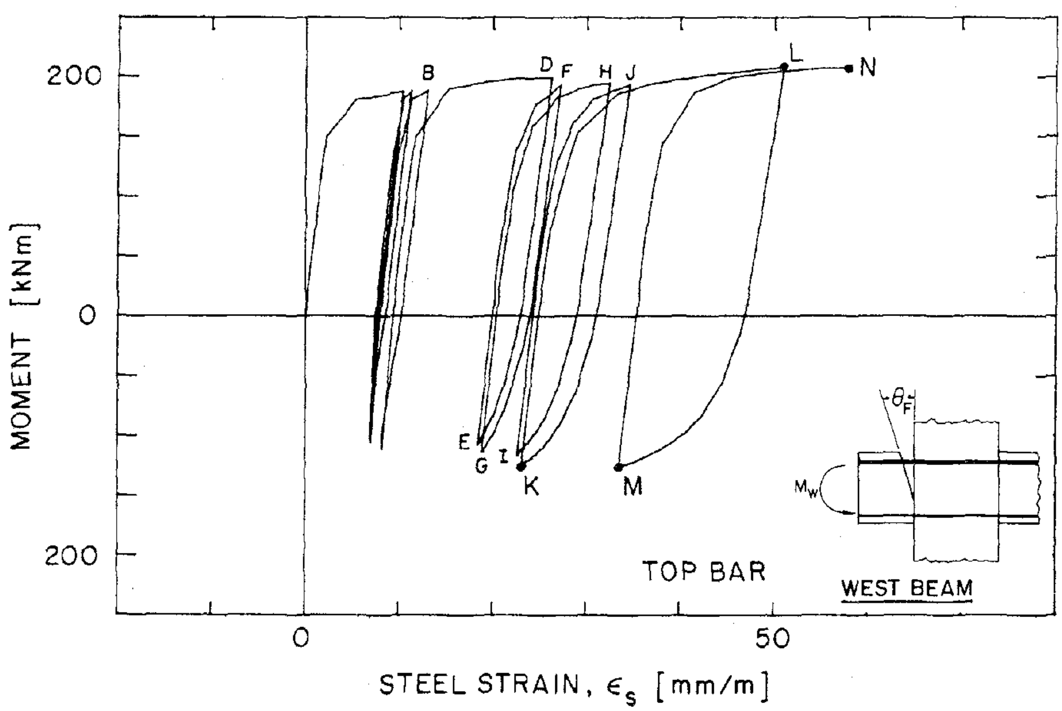

FIGURE 5.14b END MOMENT VERSUS REINFORCING STEEL STRAIN AT BEAM-COLUMN INTERFACE. SPECIMEN BC3

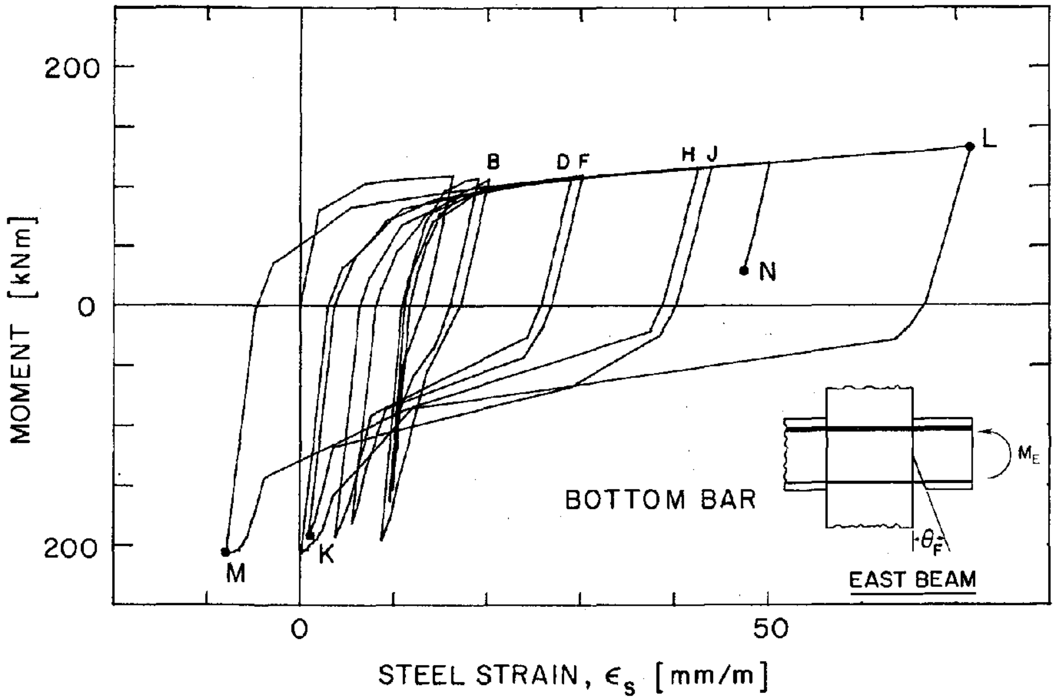

FIGURE 5.14c END MOMENT VERSUS REINFORCING STEEL STRAIN AT BEAM-COLUMN INTERFACE. SPECIMEN BC3

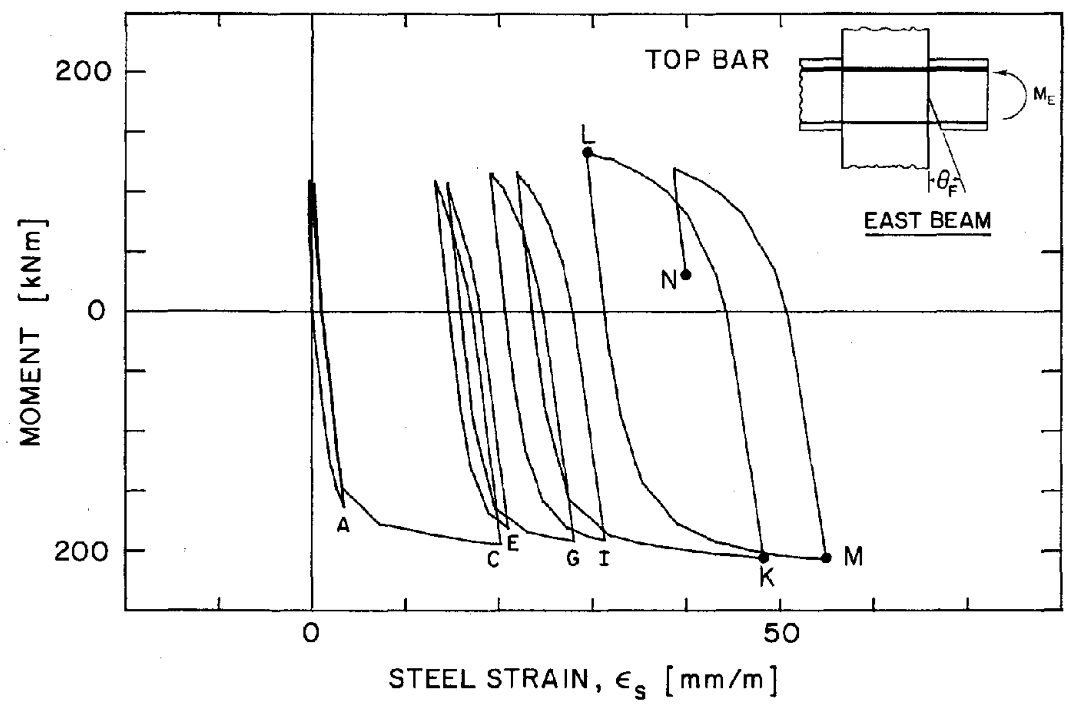

FIGURE 5.14d END MOMENT VERSUS REINFORCING STEEL STRAIN AT BEAM-COLUMN INTERFACE. SPECIMEN BC3

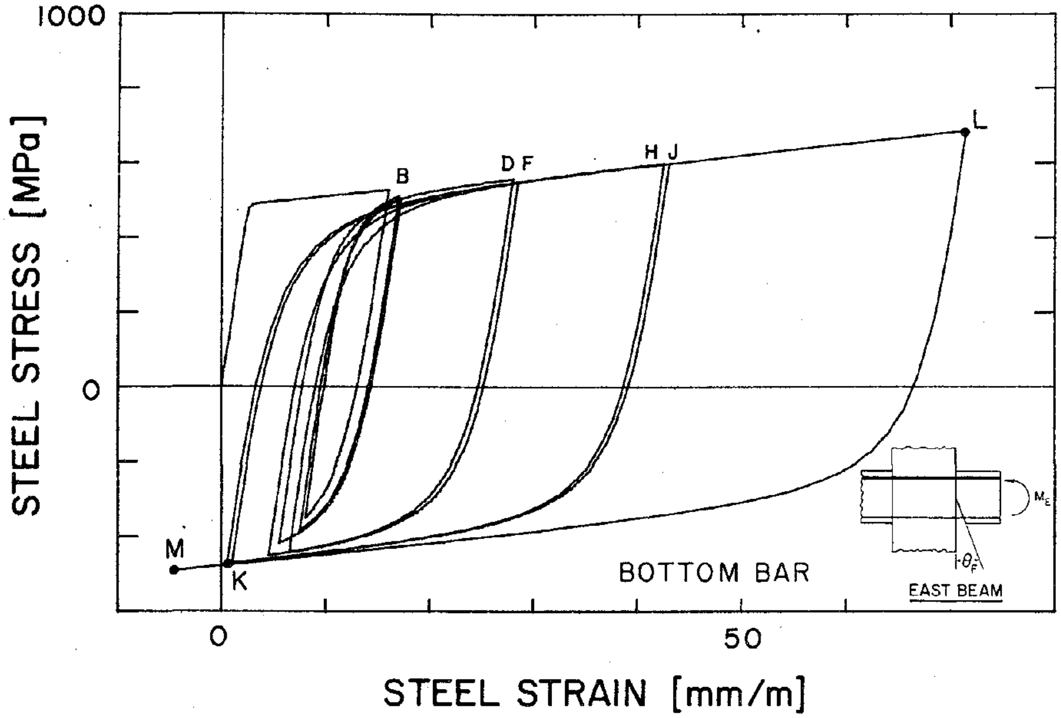

FIGURE 5.15a STEEL STRESS VERSUS STEEL STRAIN AT BEAM-COLUMN INTERFACE. SPECIMEN BC3

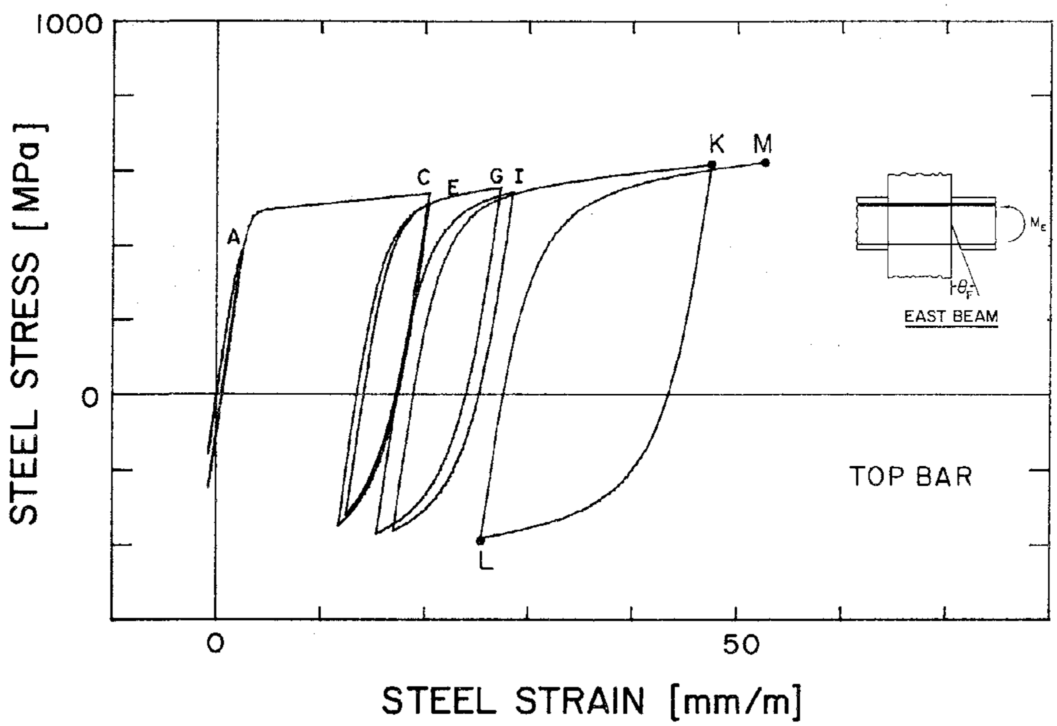

FIGURE 5.15b STEEL STRESS VERSUS STEEL STRAIN AT BEAM-COLUMN INTERFACE. SPECIMEN BC3

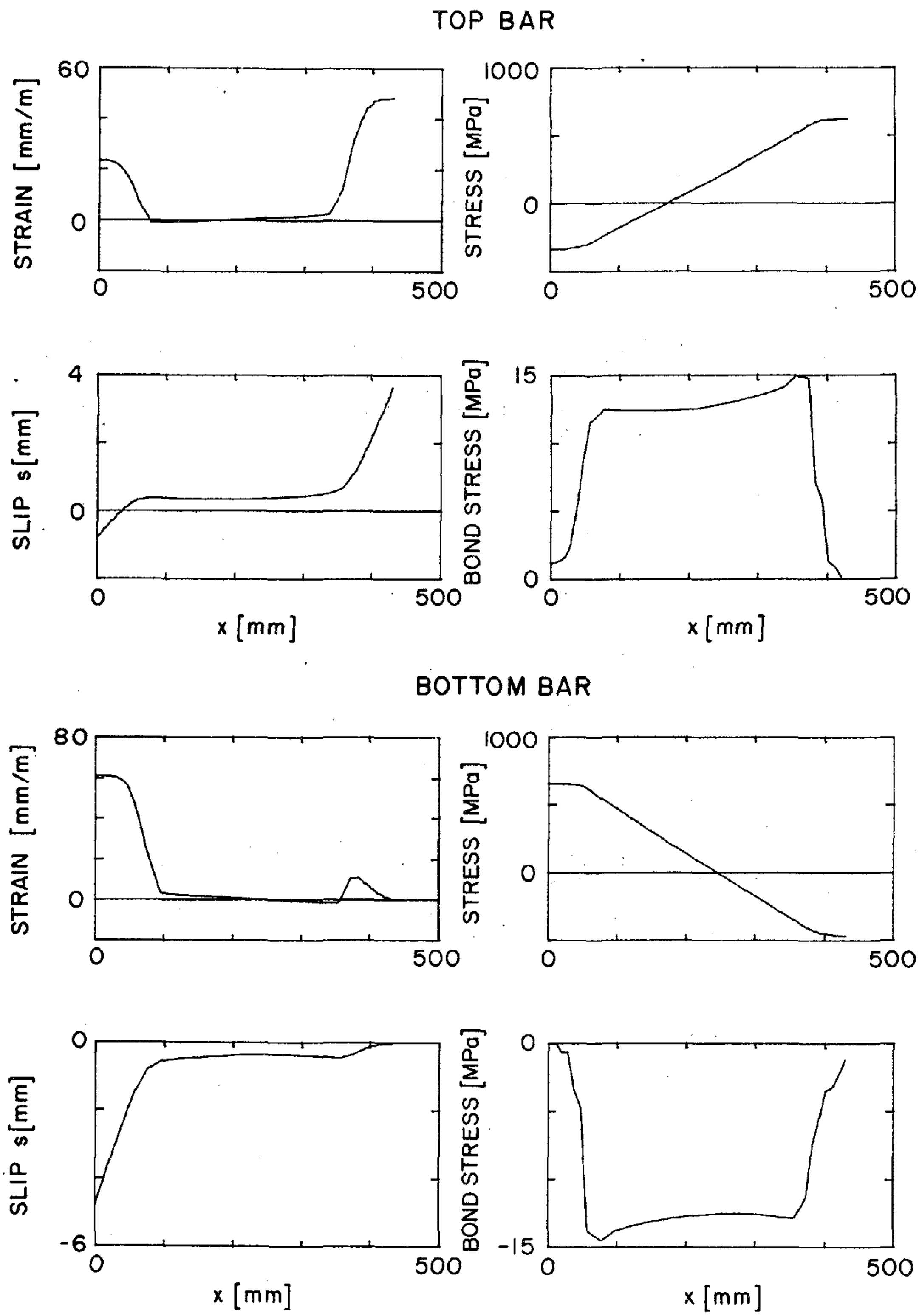

FIGURE 5.16a DISTRIBUTION OF STEEL STRAIN, BAR SLIP, STEEL STRESS AND BOND STRESS ALONG EMBEDDED BARS AT LOAD POINT K. COLUMN WIDTH = 430 mm

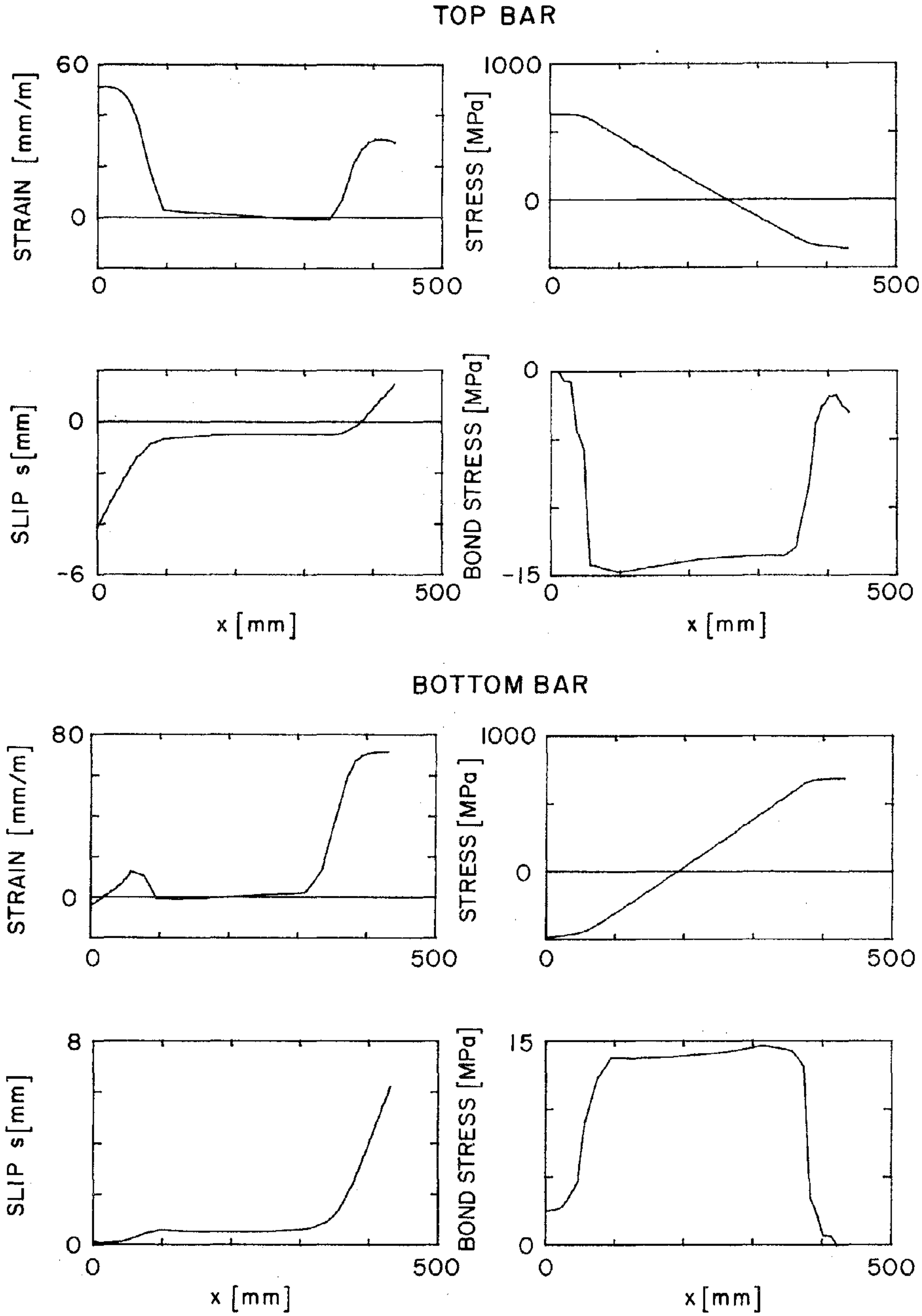

FIGURE 5.16b DISTRIBUTION OF STEEL STRAIN, BAR SLIP, STEEL STRESS AND BOND STRESS ALONG EMBEDDED BARS AT LOAD POINT L. COLUMN WIDTH = 430 mm

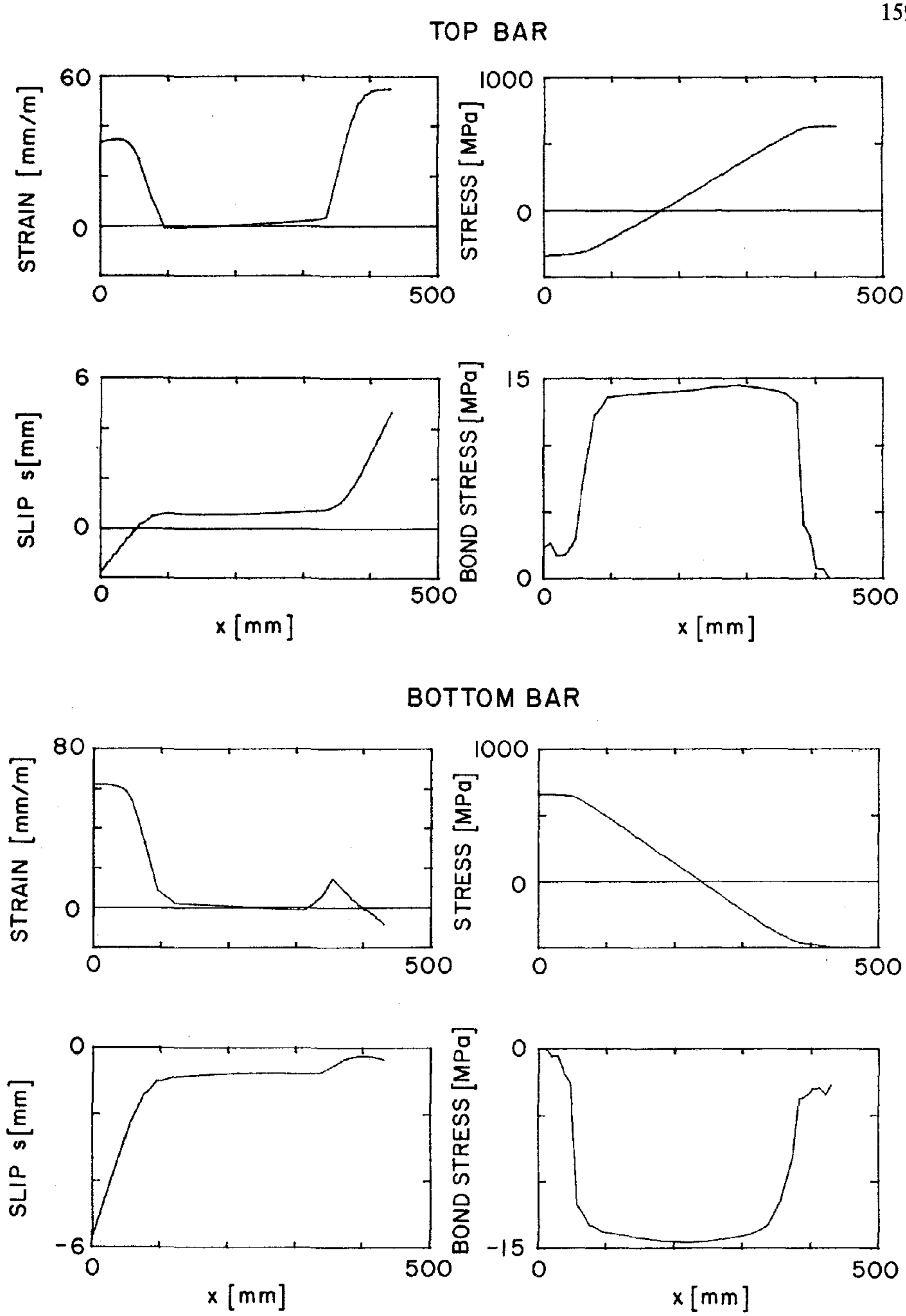

FIGURE 5.16c DISTRIBUTION OF STEEL STRAIN, BAR SLIP, STEEL STRESS AND BOND STRESS ALONG EMBEDDED BARS AT LOAD POINT M. COLUMN WIDTH = 430 mm

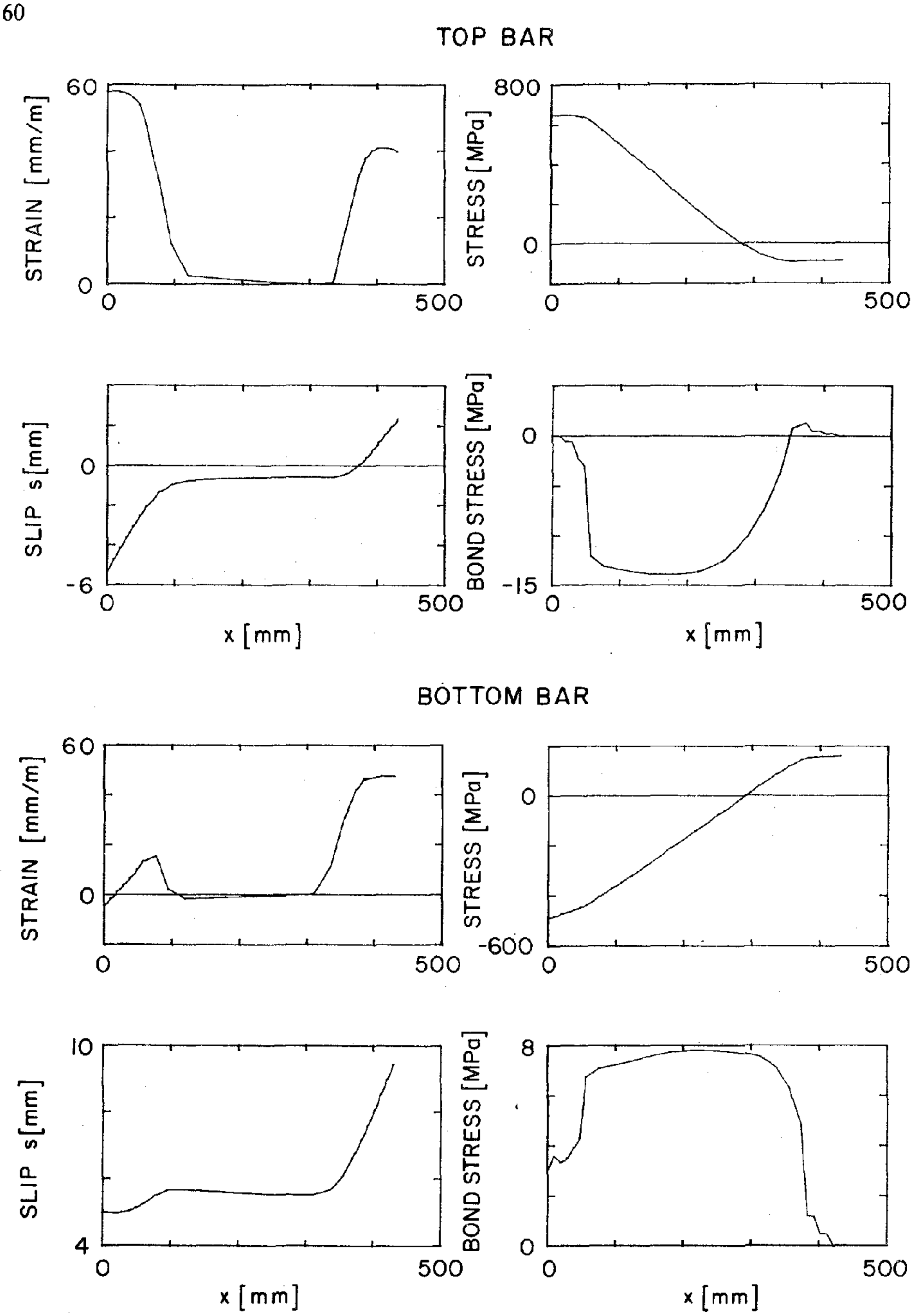

FIGURE 5.16d DISTRIBUTION OF STEEL STRAIN, BAR SLIP, STEEL STRESS AND BOND STRESS ALONG EMBEDDED BARS AT LOAD POINT N. COLUMN WIDTH = 430 mm

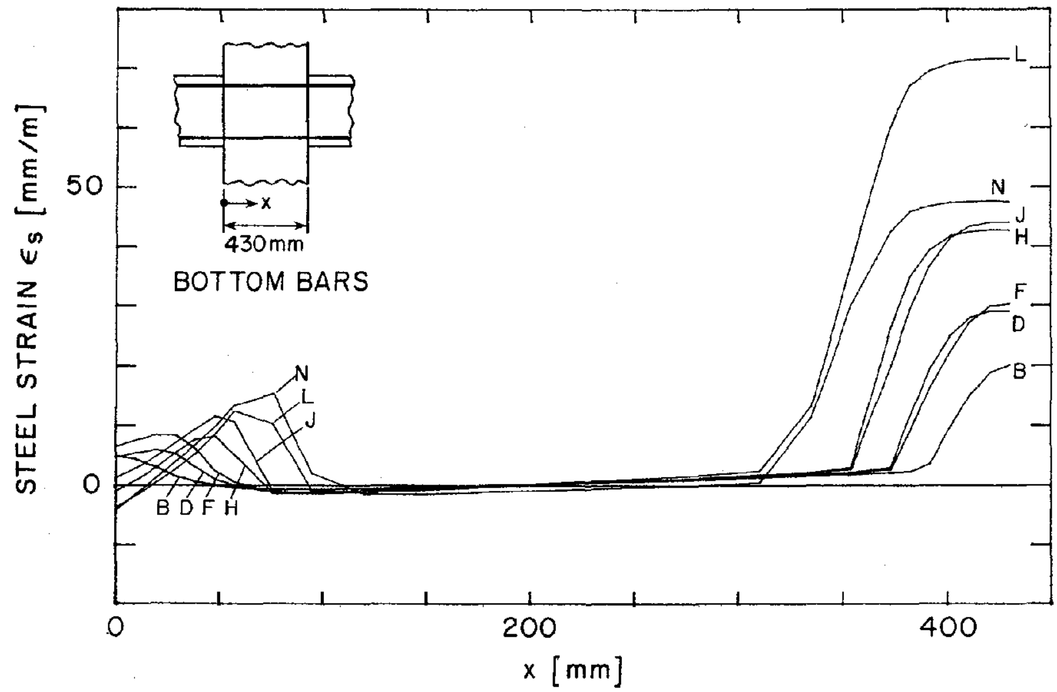

FIGURE 5.17a DISTRIBUTION OF STEEL STRAIN ALONG THE BOTTOM REINFORCING BARS WITH INCREASING MAGNITUDE OF END SLIP

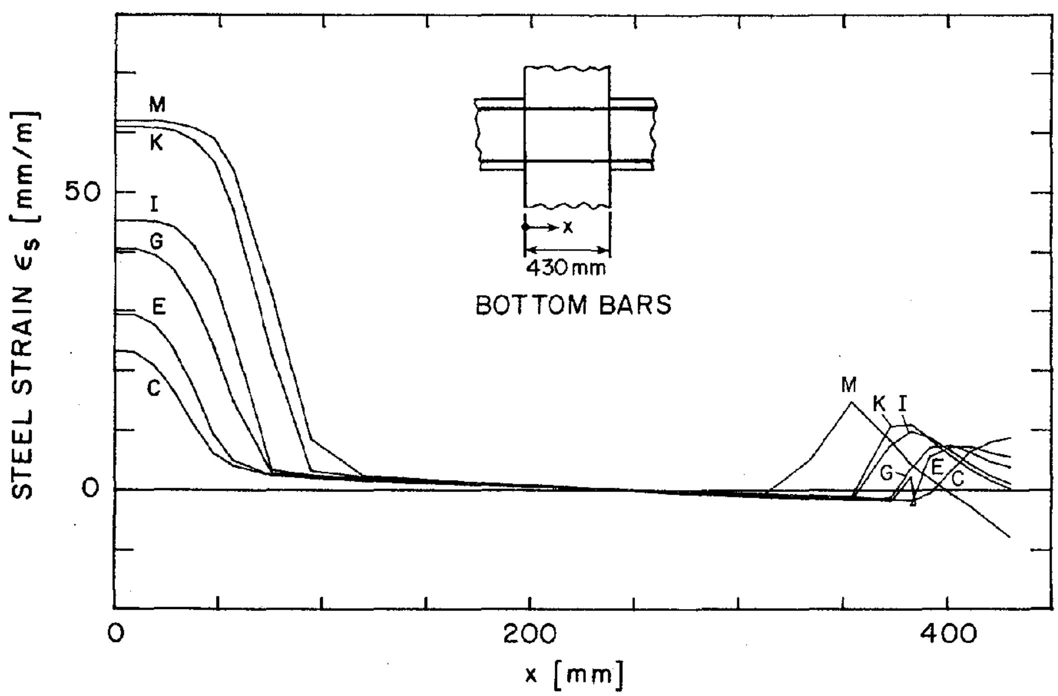

FIGURE 5.18a DISTRIBUTION OF STEEL STRAIN ALONG THE BOTTOM REINFORCING BARS WITH INCREASING MAGNITUDE OF END SLIP

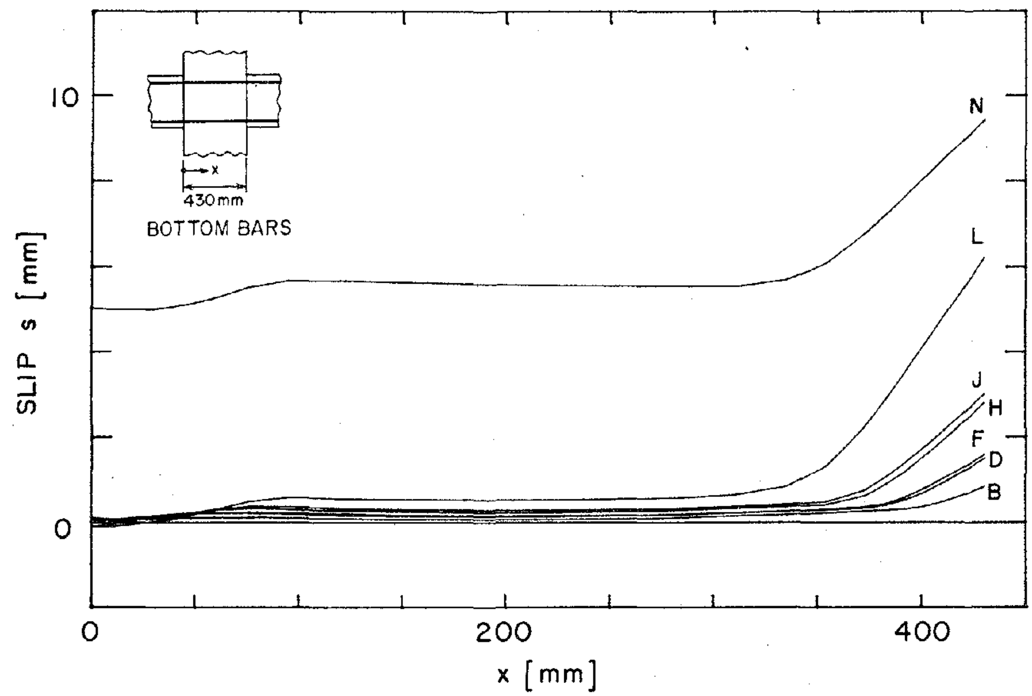

FIGURE 5.17b DISTRIBUTION OF RELATIVE SLIP ALONG THE BOTTOM REINFORCING BARS WITH INCREASING MAGNITUDE OF END SLIP

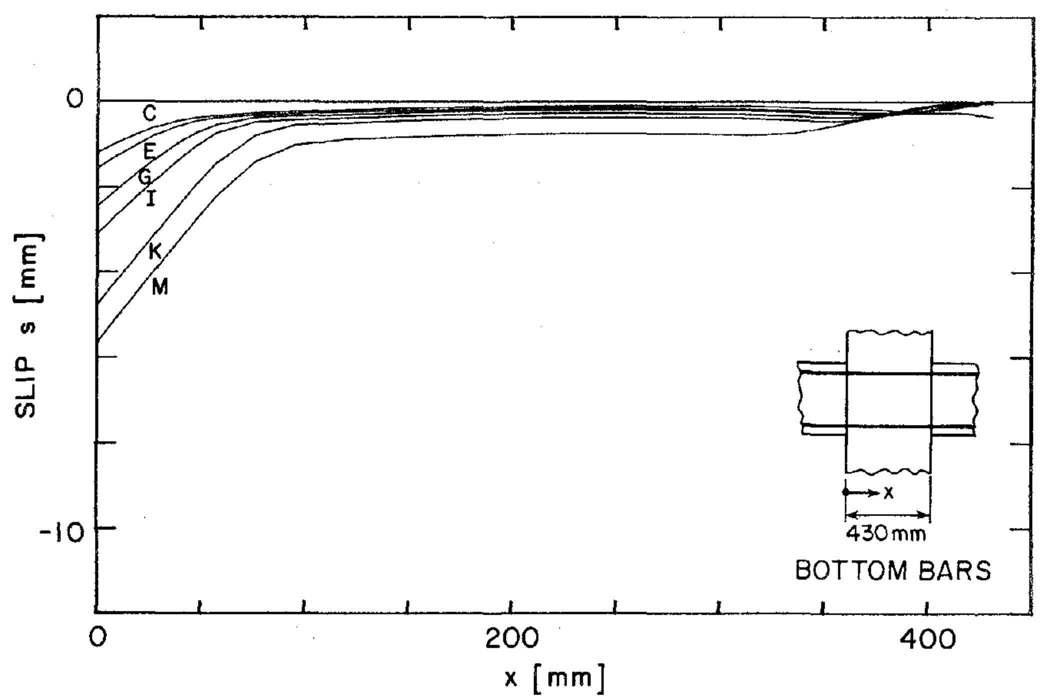

FIGURE 5.18b DISTRIBUTION OF RELATIVE SLIP ALONG THE BOTTOM REINFORCING BARS WITH INCREASING MAGNITUDE OF END SLIP

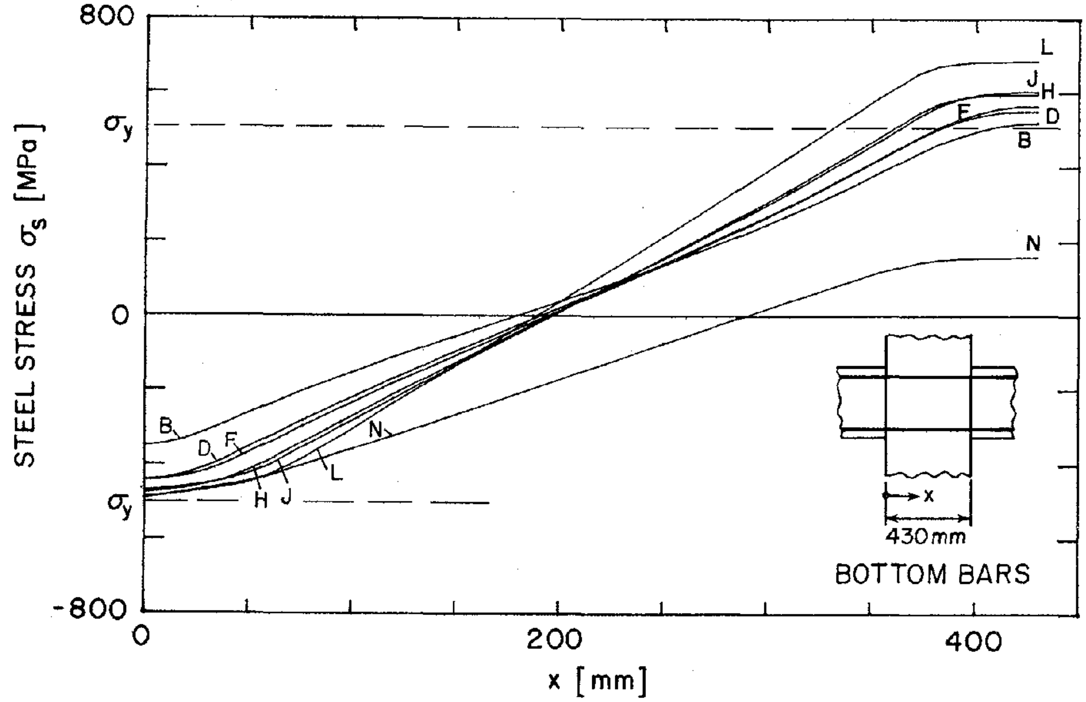

FIGURE 5.17c DISTRIBUTION OF STEEL STRESS ALONG THE BOTTOM REINFORCING BARS WITH INCREASING MAGNITUDE OF END SLIP

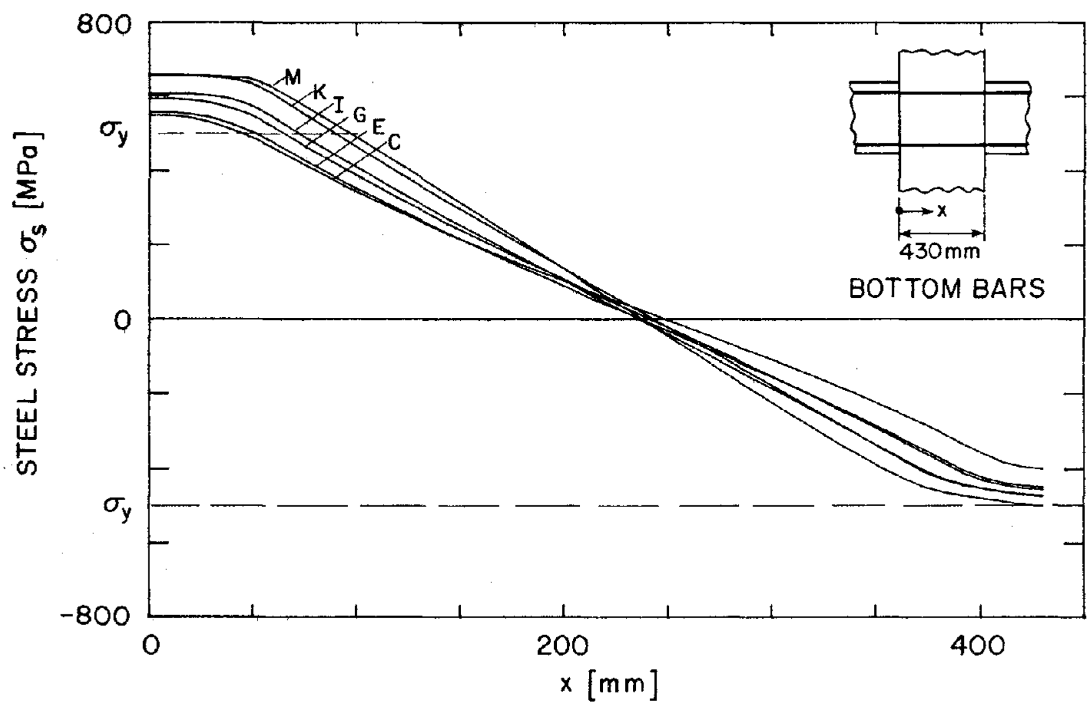

FIGURE 5.18c DISTRIBUTION OF STEEL STRESS ALONG THE BOTTOM REINFORCING BARS WITH INCREASING MAGNITUDE OF END SLIP

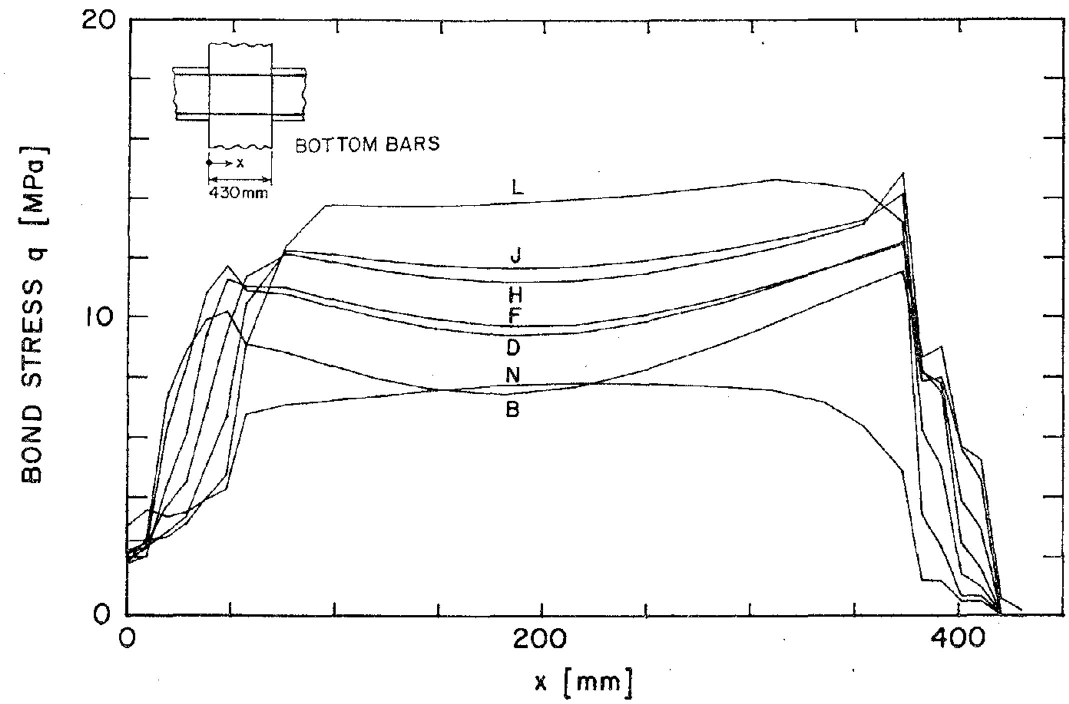

FIGURE 5.17d DISTRIBUTION OF BOND STRESS ALONG THE BOTTOM REINFORCING BARS WITH INCREASING MAGNITUDE OF END SLIP

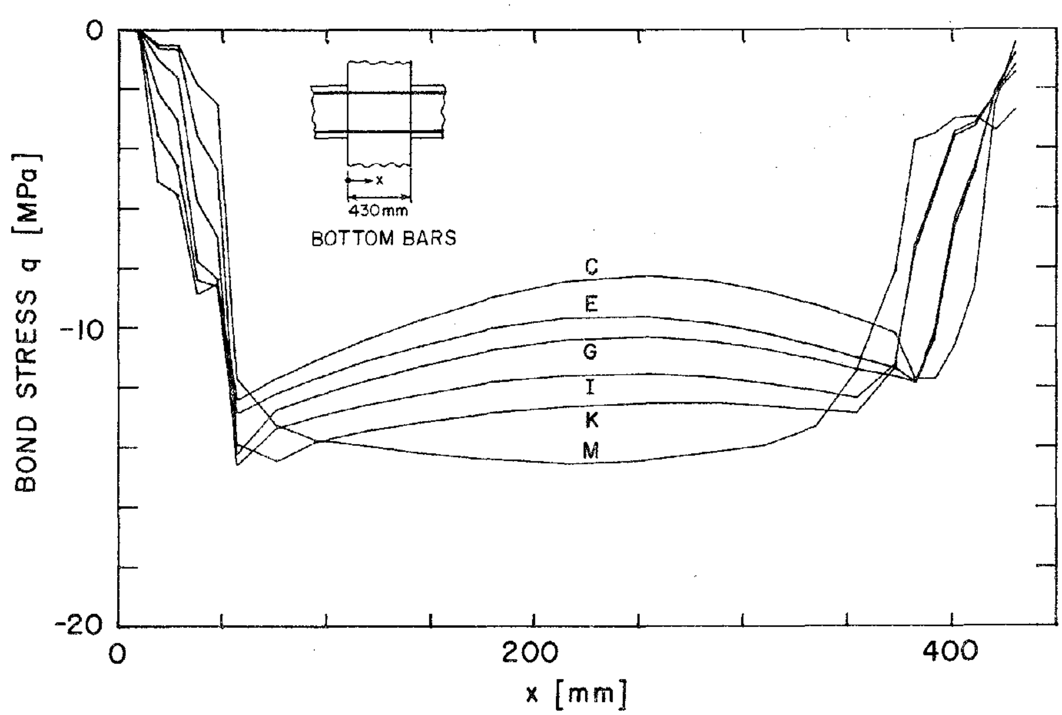

FIGURE 5.18d DISTRIBUTION OF BOND STRESS ALONG THE BOTTOM REINFORCING BARS WITH INCREASING MAGNITUDE OF END SLIP

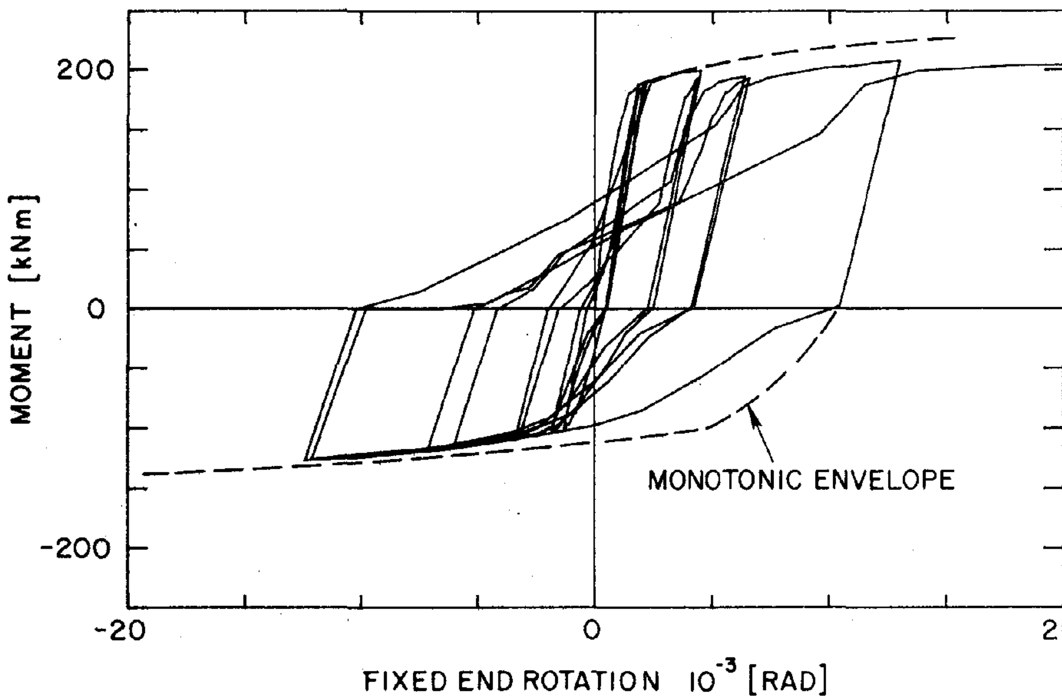

FIGURE 5.19 COMPARISON OF MONOTONIC AND CYCLIC ENVELOPE CURVES

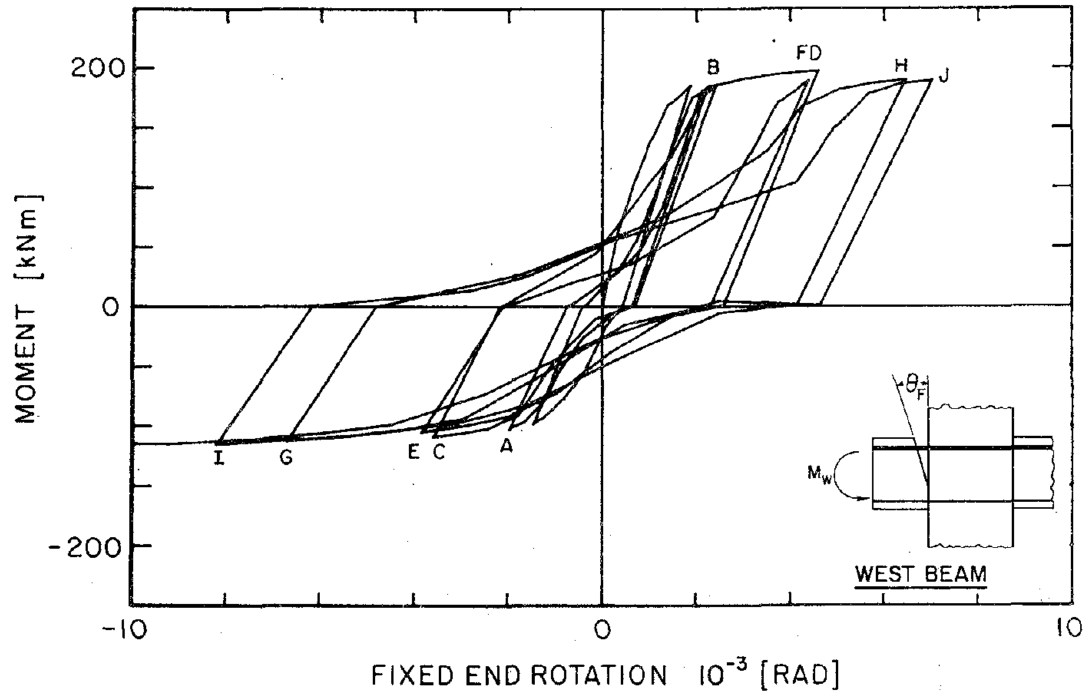

FIGURE 6.1a END MOMENT VERSUS FIXED-END ROTATION
BOND STRENGTH REDUCED BY 15% ALONG REINFORCING BARS

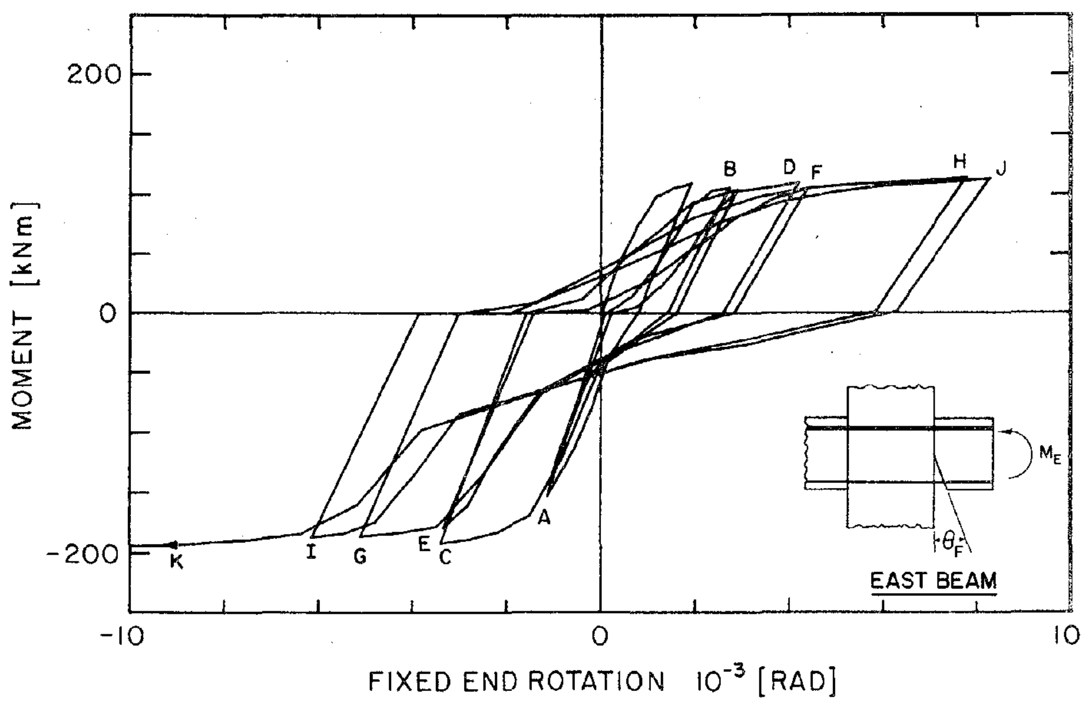

FIGURE 6.1b END MOMENT VERSUS FIXED-END ROTATION
BOND STRENGTH REDUCED BY 15% ALONG REINFORCING BARS

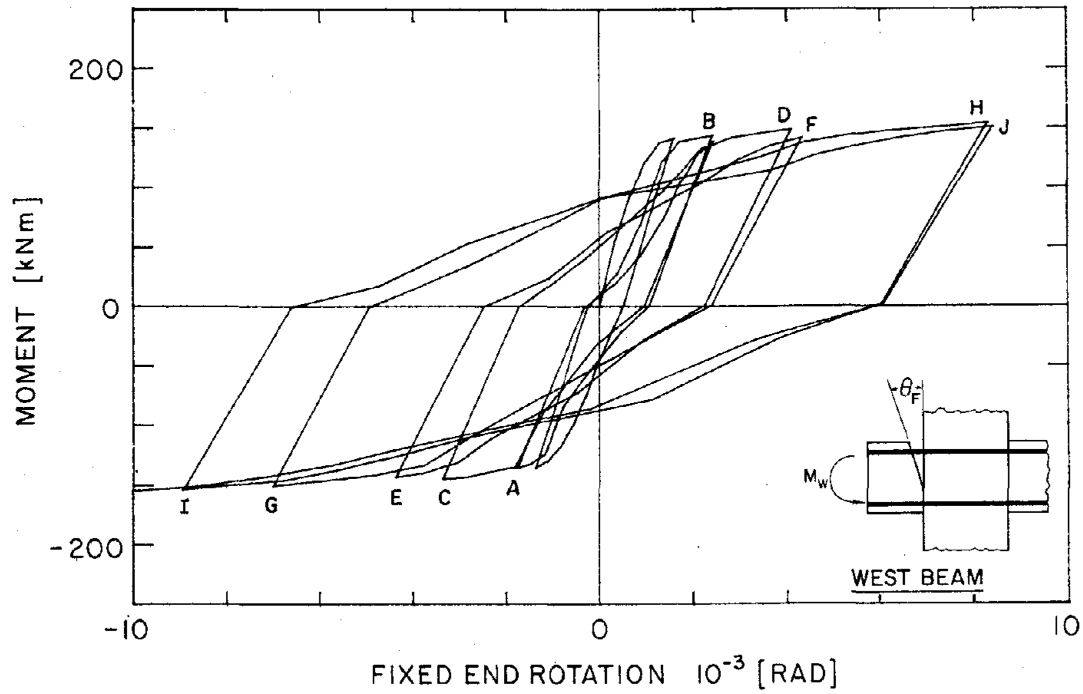

FIGURE 6.2a END MOMENT VERSUS FIXED-END ROTATION
EQUAL RATIO OF TOP TO BOTTOM REINFORCEMENT

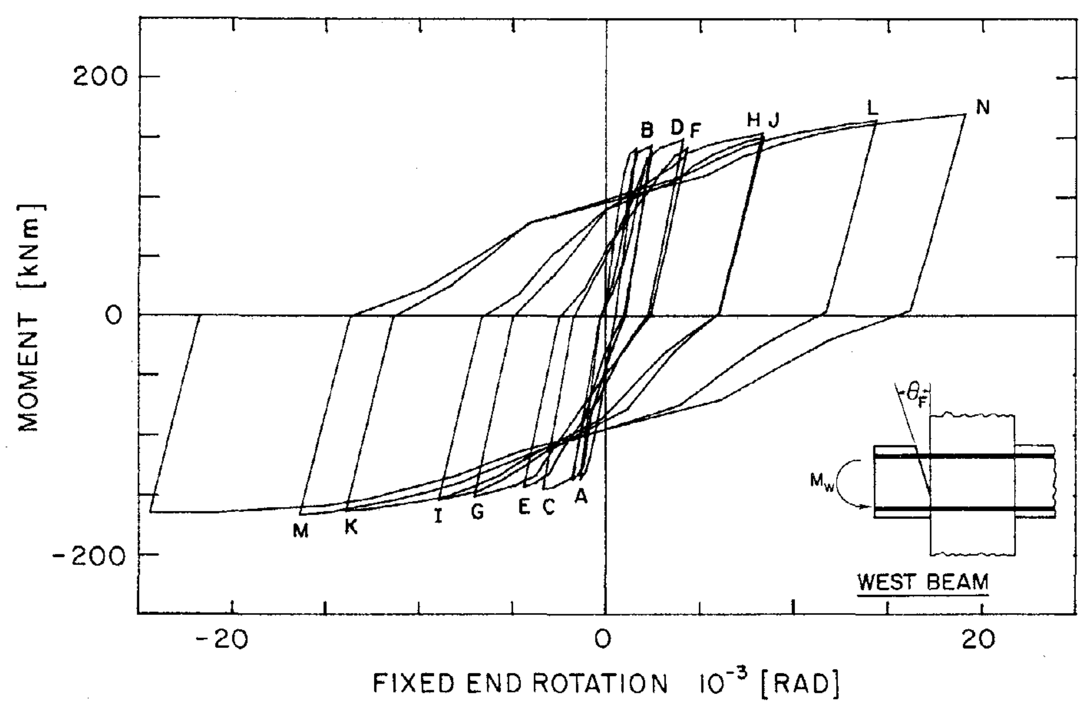

FIGURE 6.2b END MOMENT VERSUS FIXED-END ROTATION
EQUAL RATIO OF TOP TO BOTTOM REINFORCEMENT

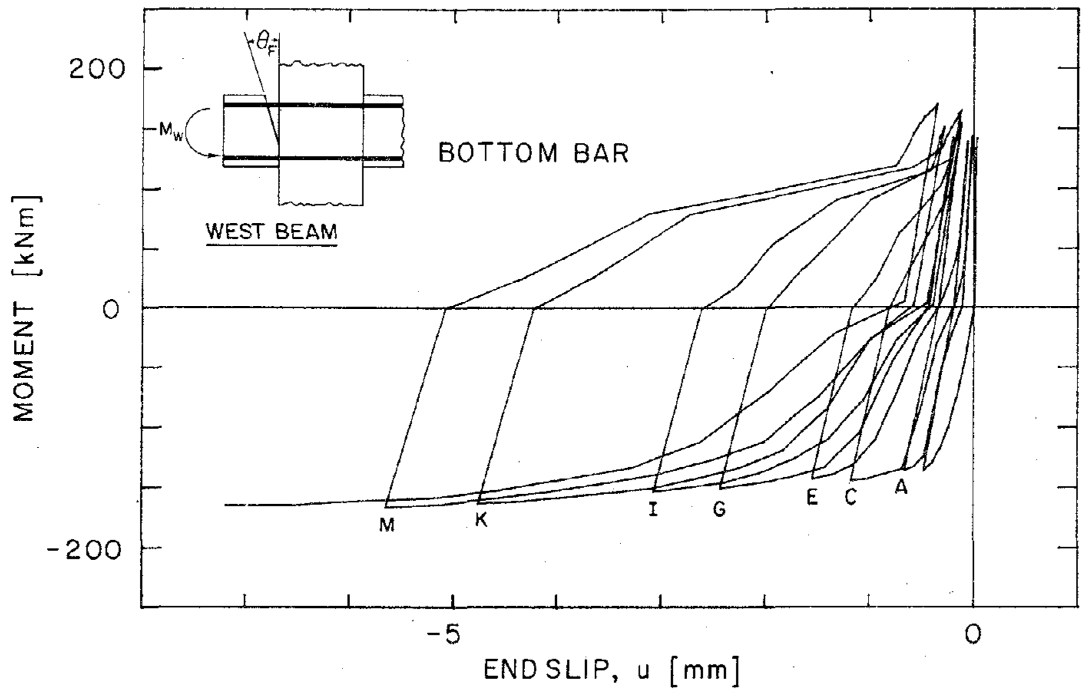

FIGURE 6.2c END MOMENT VERSUS RELATIVE BAR SLIPPAGE AT BEAM-COLUMN INTERFACE. EQUAL RATIO OF TOP TO BOTTOM REINFORCEMENT

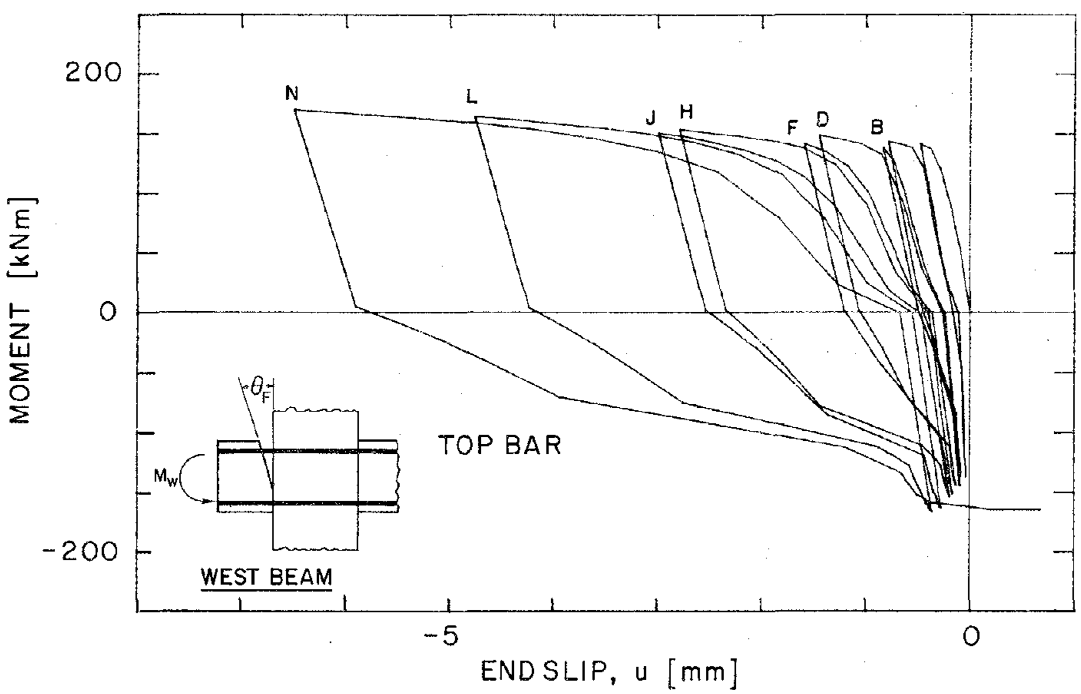

FIGURE 6.2d END MOMENT VERSUS RELATIVE BAR SLIPPAGE AT BEAM-COLUMN INTERFACE. EQUAL RATIO OF TOP TO BOTTOM REINFORCEMENT

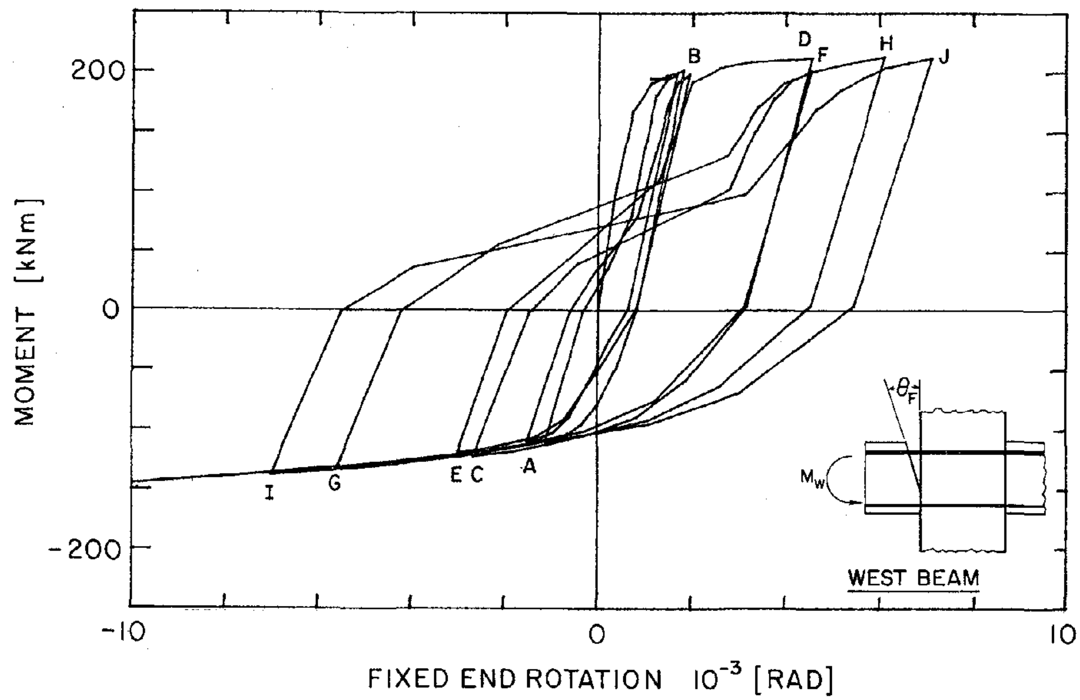

FIGURE 6.3a END MOMENT VERSUS FIXED-END ROTATION
YIELD STRENGTH OF REINFORCEMENT $= 326\ MPa$

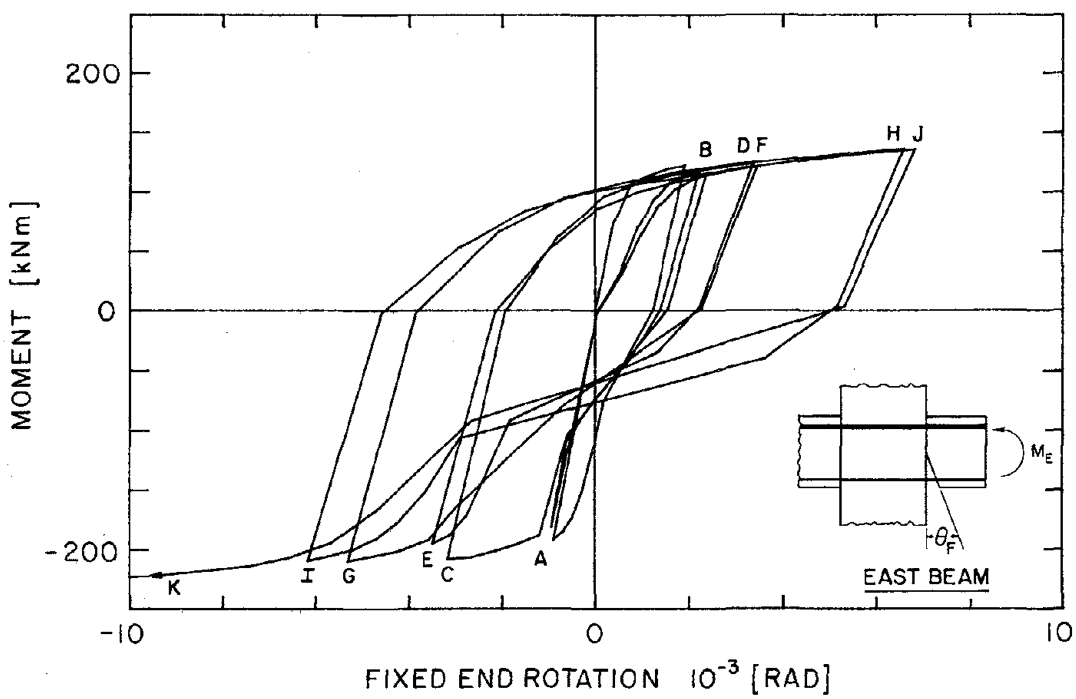

FIGURE 6.3b END MOMENT VERSUS FIXED-END ROTATION
YIELD STRENGTH OF REINFORCEMENT $= 326\ MPa$

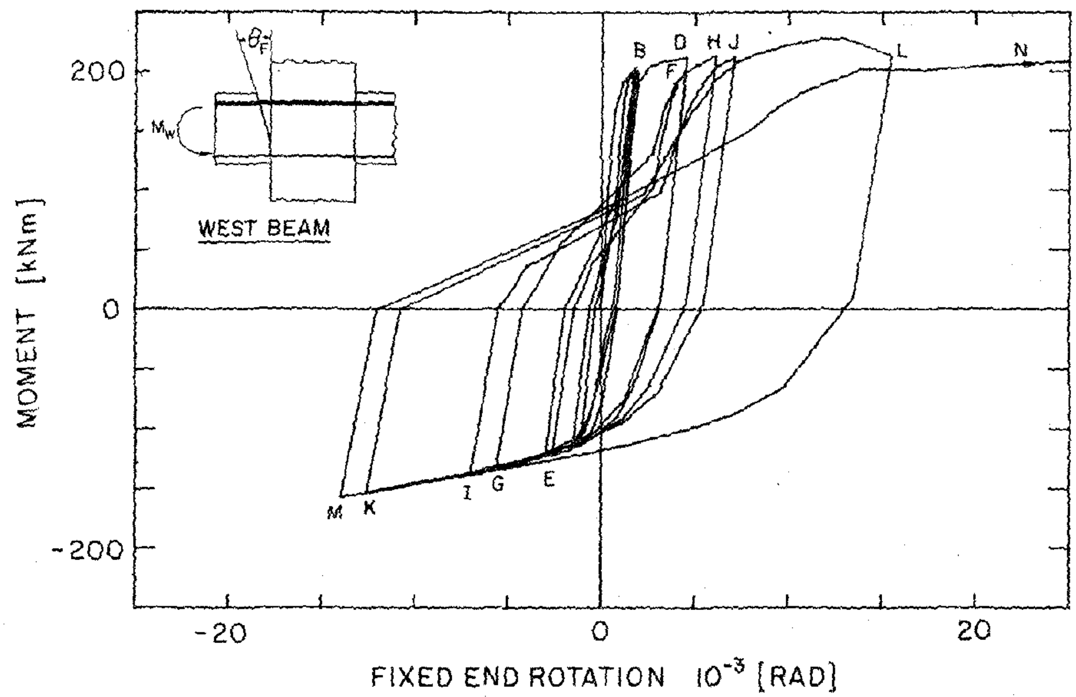

FIGURE 6.3c END MOMENT VERSUS FIXED-END ROTATION
YIELD STRENGTH OF REINFORCEMENT = 326 *MPa*

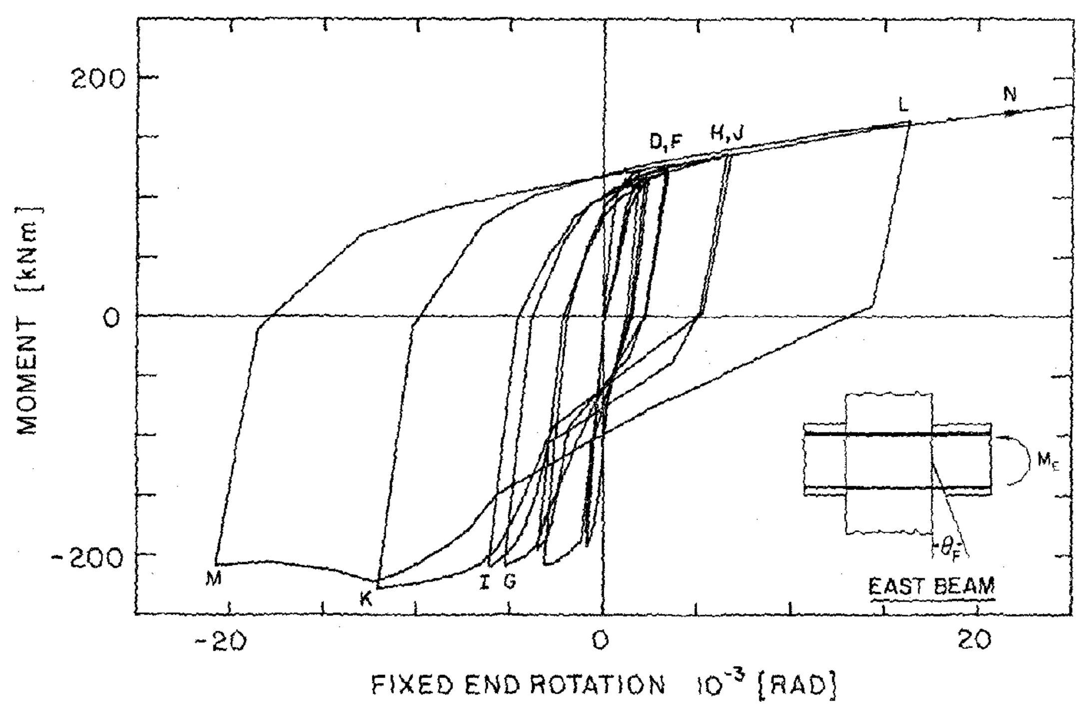

FIGURE 6.3d END MOMENT VERSUS FIXED-END ROTATION
YIELD STRENGTH OF REINFORCEMENT = 326 *MPa*

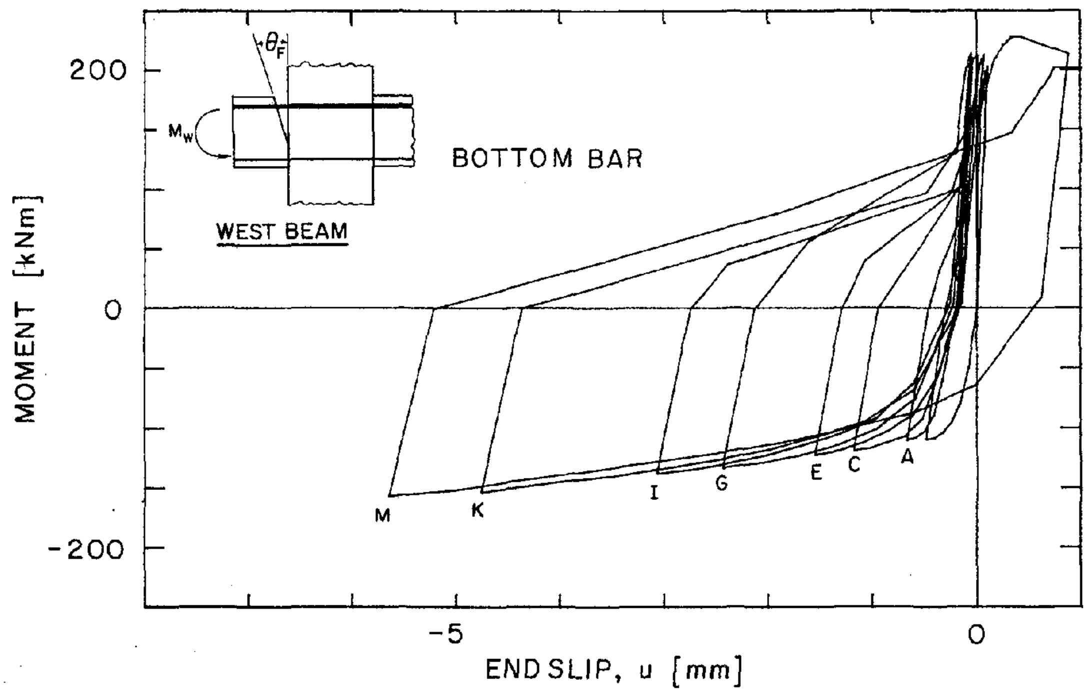

FIGURE 6.4a END MOMENT VERSUS RELATIVE BAR SLIPPAGE AT BEAM-COLUMN INTERFACE. YIELD STRENGTH OF REINFORCEMENT = 326 *MPa*

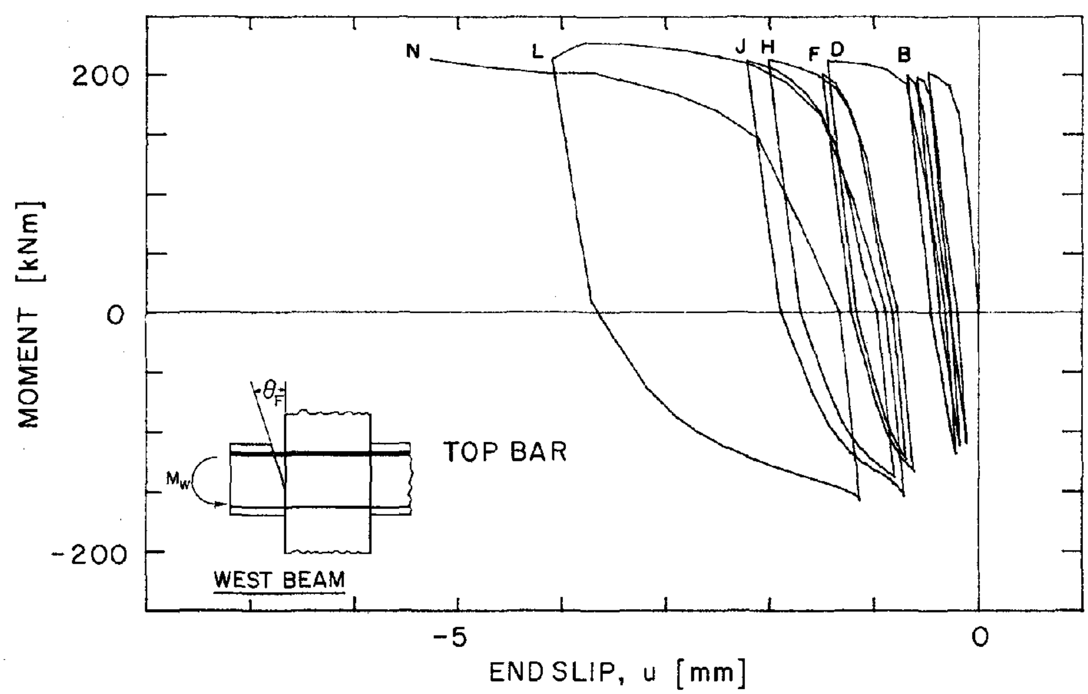

FIGURE 6.4b END MOMENT VERSUS RELATIVE BAR SLIPPAGE AT BEAM-COLUMN INTERFACE. YIELD STRENGTH OF REINFORCEMENT = 326 *MPa*

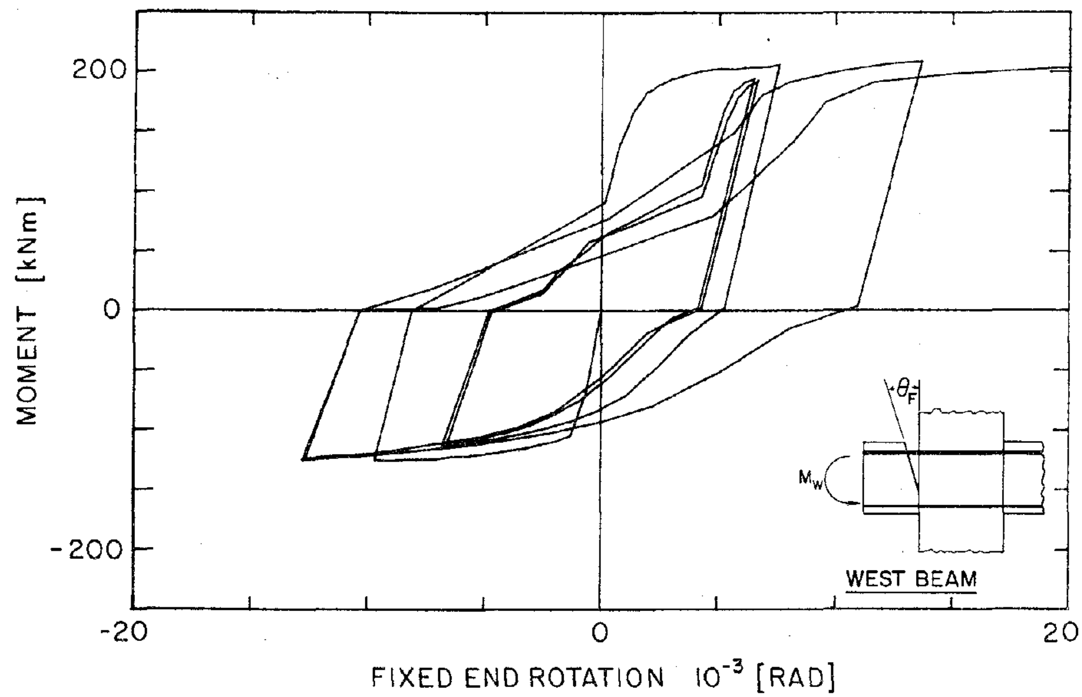

FIGURE 6.5a END MOMENT VERSUS FIXED-END ROTATION VARIATION IN HISTORY OF LOADING

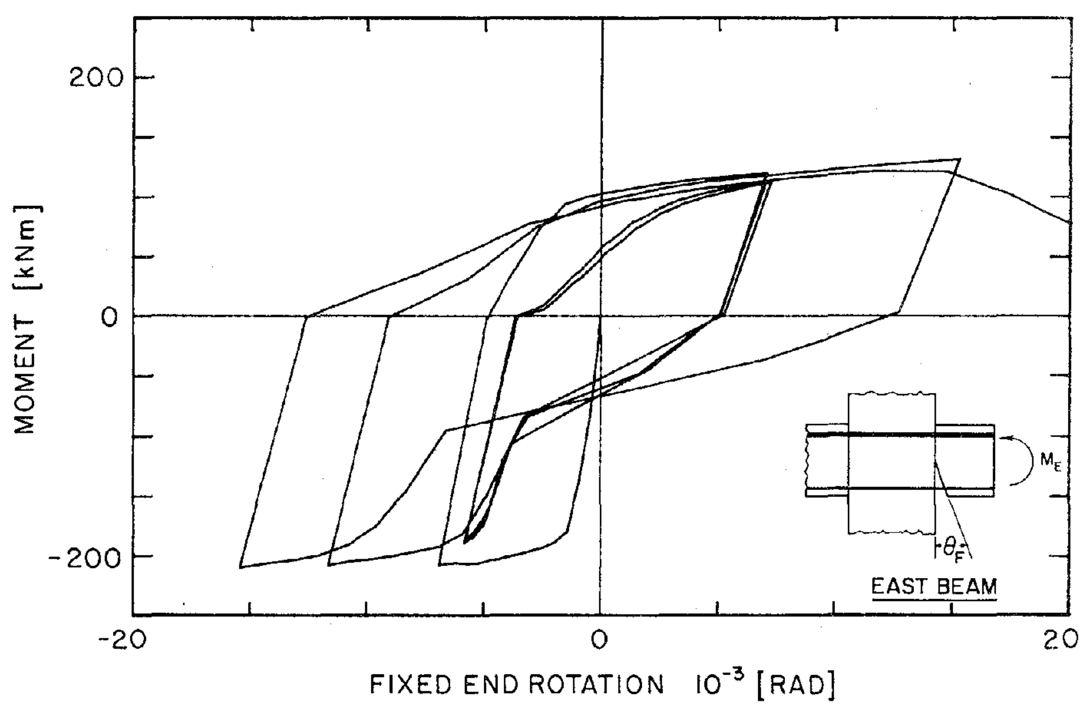

FIGURE 6.5b END MOMENT VERSUS FIXED-END ROTATION VARIATION IN HISTORY OF LOADING

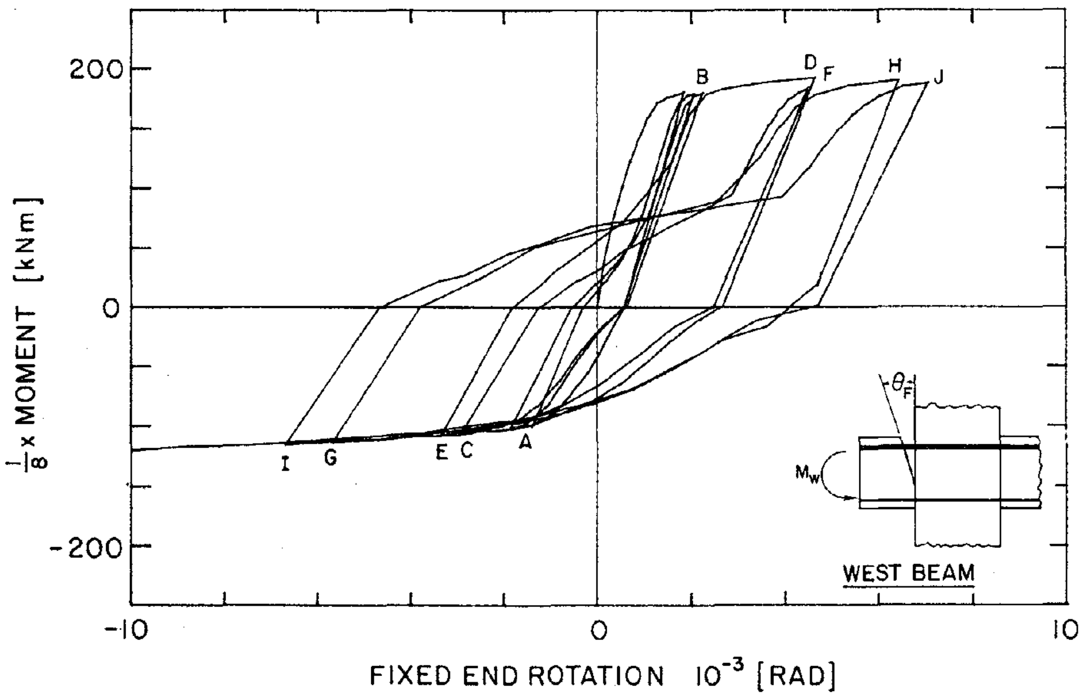

FIGURE 6.6a END MOMENT VERSUS FIXED-END ROTATION FULL-SCALE INTERIOR BEAM-COLUMN JOINT

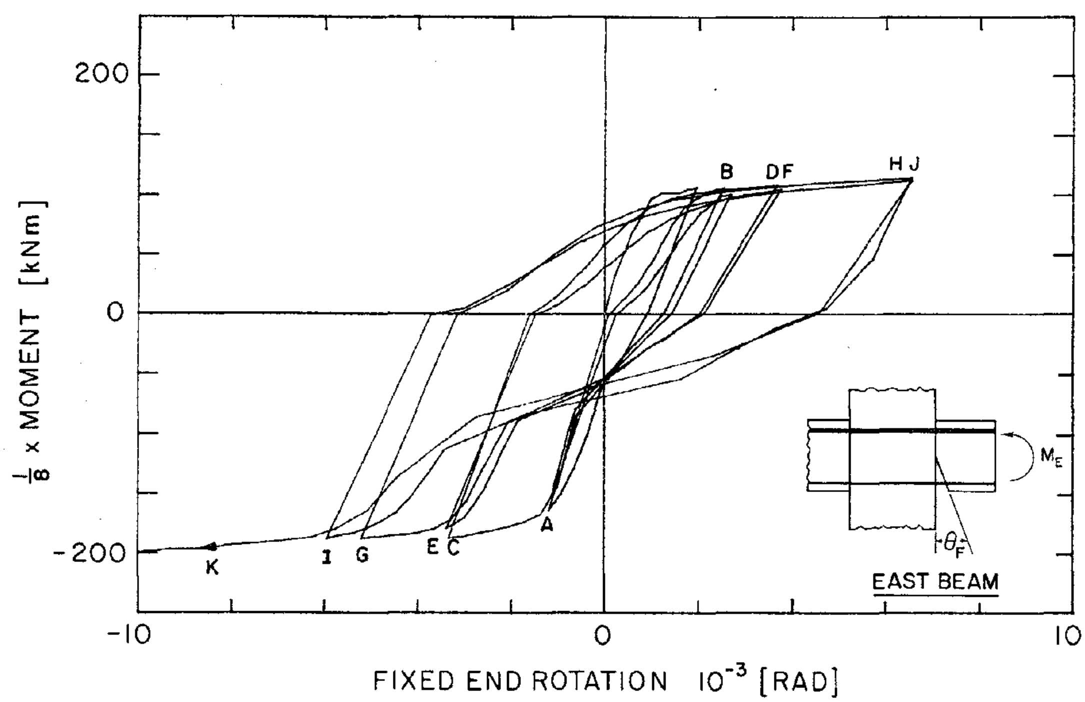

FIGURE 6.6b END MOMENT VERSUS FIXED-END ROTATION FULL-SCALE INTERIOR BEAM-COLUMN JOINT

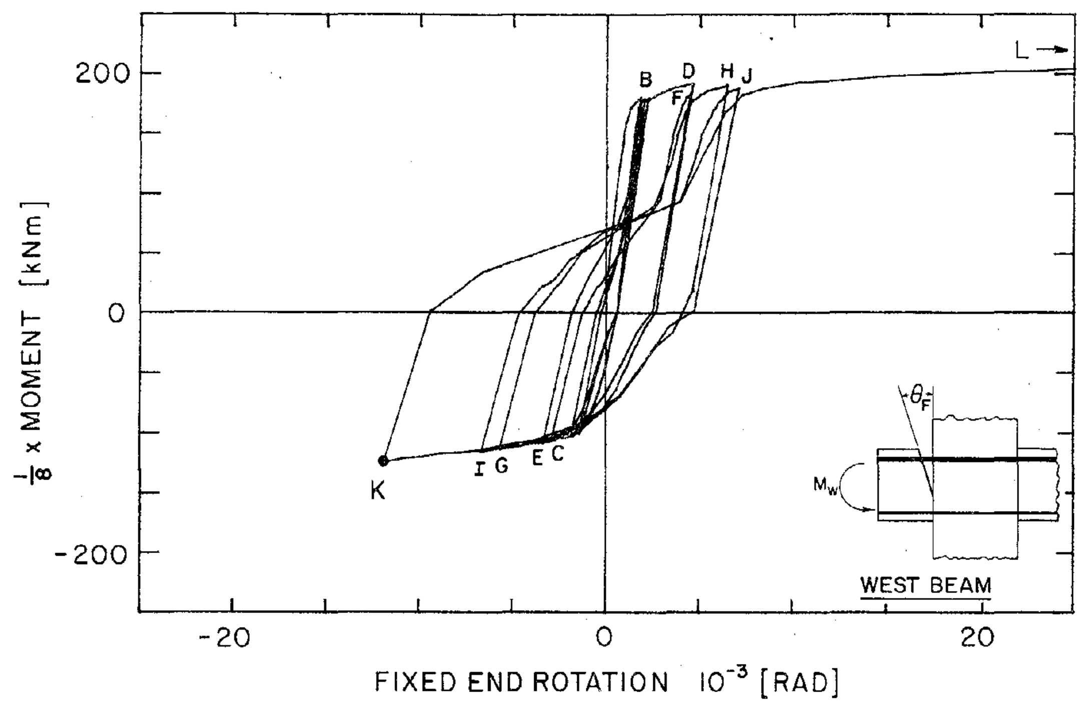

FIGURE 6.6c END MOMENT VERSUS FIXED-END ROTATION FULL-SCALE INTERIOR BEAM-COLUMN JOINT

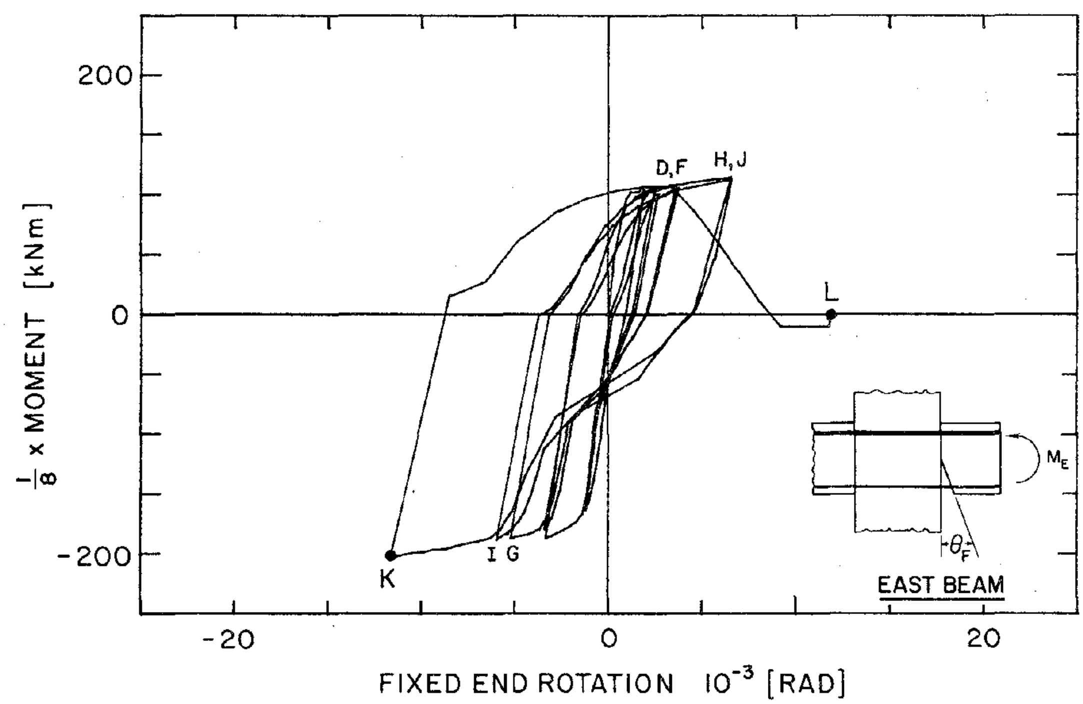

FIGURE 6.6d END MOMENT VERSUS FIXED-END ROTATION FULL-SCALE INTERIOR BEAM-COLUMN JOINT

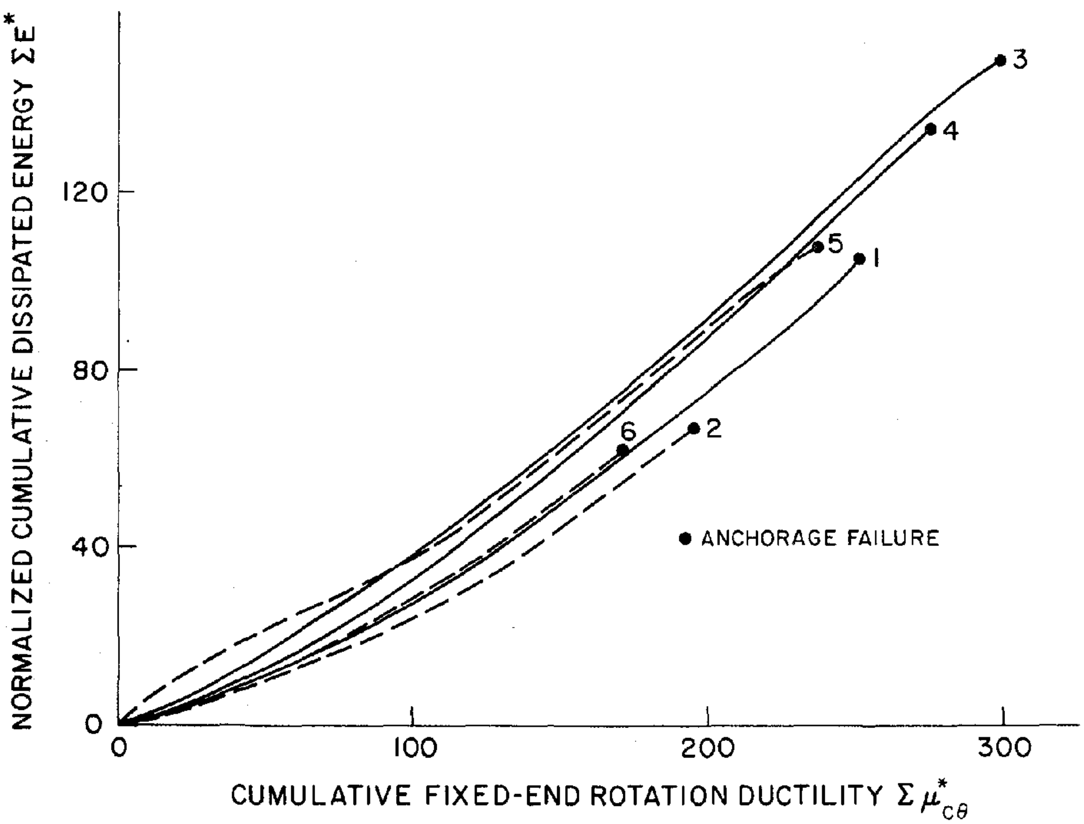

FIGURE 6.7 NORMALIZED TOTAL ENERGY DISSIPATION VERSUS CUMULATIVE FIXED-END ROTATION DUCTILITY FOR INTERIOR BEAM-COLUMN JOINT UNDER VARIATION OF PARAMETERS

EARTHQUAKE ENGINEERING RESEARCH CENTER REPORTS

NOTE: Numbers in parentheses are Accession Numbers assigned by the National Technical Information Service; these are followed by a price code. Copies of the reports may be ordered from the National Technical Information Service, 5285 Port Royal Road, Springfield, Virginia, 22161. Accession Numbers should be quoted on orders for reports (PB --- ---) and remittance must accompany each order. Reports without this information were not available at time of printing. The complete list of EERC reports (from EERC 67-1) is available upon request from the Earthquake Engineering Research Center, University of California, Berkeley, 47th Street and Hoffman Boulevard, Richmond, California 94804.

UCB/EERC-77/01 "PLUSH - A Computer Program for Probabilistic Finite Element Analysis of Seismic Soil-Structure Interaction," by M.P. Romo Organista, J. Lysmer and H.B. Seed - 1977 (PB81 177 651)A05

UCB/EERC-77/02 "Soil-Structure Interaction Effects at the Humboldt Bay Power Plant in the Ferndale Earthquake of June 7, 1975," by J.E. Valera, H.B. Seed, C.F. Tsai and J. Lysmer - 1977 (PB 265 795)A04

UCB/EERC-77/03 "Influence of Sample Disturbance on Sand Response to Cyclic Loading," by K. Mori, H.B. Seed and C.K. Chan - 1977 (PB 267 352)A04

UCB/EERC-77/04 "Seismological Studies of Strong Motion Records," by J. Shoja-Taheri - 1977 (PB 269 655)A10

UCB/EERC-77/05 Unassigned

UCB/EERC-77/06 "Developing Methodologies for Evaluating the Earthquake Safety of Existing Buildings," by No. 1 - B. Bresler; No. 2 - B. Bresler, T. Okada and D. Zisling; No. 3 - T. Okada and B. Bresler; No. 4 - V.V. Bertero and B. Bresler - 1977 (PB 267 354)A08

UCB/EERC-77/07 "A Literature Survey - Transverse Strength of Masonry Walls," by Y. Omote, R.L. Mayes, S.W. Chen and R.W. Clough - 1977 (PB 277 933)A07

UCB/EERC-77/08 "DRAIN-TABS: A Computer Program for Inelastic Earthquake Response of Three Dimensional Buildings," by R. Guendelman-Israel and G.H. Powell - 1977 (PB 270 693)A07

UCB/EERC-77/09 "SUBWALL: A Special Purpose Finite Element Computer Program for Practical Elastic Analysis and Design of Structural Walls with Substructure Option," by D.Q. Le, H. Peterson and E.P. Popov - 1977 (PB 270 567)A05

UCB/EERC-77/10 "Experimental Evaluation of Seismic Design Methods for Broad Cylindrical Tanks," by D.P. Clough (PB 272 280)A13

UCB/EERC-77/11 "Earthquake Engineering Research at Berkeley - 1976," - 1977 (PB 273 507)A09

UCB/EERC-77/12 "Automated Design of Earthquake Resistant Multistory Steel Building Frames," by N.D. Walker, Jr. - 1977 (PB 276 526)A09

UCB/EERC-77/13 "Concrete Confined by Rectangular Hoops Subjected to Axial Loads," by J. Vallenas, V.V. Bertero and E.P. Popov - 1977 (PB 275 165)A06

UCB/EERC-77/14 "Seismic Strain Induced in the Ground During Earthquakes," by Y. Sugimura - 1977 (PB 284 201)A04

UCB/EERC-77/15 Unassigned

UCB/EERC-77/16 "Computer Aided Optimum Design of Ductile Reinforced Concrete Moment Resisting Frames," by S.W. Zagajeski and V.V. Bertero - 1977 (PB 280 137)A07

UCB/EERC-77/17 "Earthquake Simulation Testing of a Stepping Frame with Energy-Absorbing Devices," by J.M. Kelly and D.F. Tsztoo - 1977 (PB 273 506)A04

UCB/EERC-77/18 "Inelastic Behavior of Eccentrically Braced Steel Frames under Cyclic Loadings," by C.W. Roeder and E.P. Popov - 1977 (PB 275 526)A15

UCB/EERC-77/19 "A Simplified Procedure for Estimating Earthquake-Induced Deformations in Dams and Embankments," by F.I. Makdisi and H.B. Seed - 1977 (PB 276 820)A04

UCB/EERC-77/20 "The Performance of Earth Dams during Earthquakes," by H.B. Seed, F.I. Makdisi and P. de Alba - 1977 (PB 276 821)A04

UCB/EERC-77/21 "Dynamic Plastic Analysis Using Stress Resultant Finite Element Formulation," by P. Lukkunapvasit and J.M. Kelly - 1977 (PB 275 453)A04

UCB/EERC-77/22 "Preliminary Experimental Study of Seismic Uplift of a Steel Frame," by R.W. Clough and A.A. Huckelbridge 1977 (PB 278 769)A08

UCB/EERC-77/23 "Earthquake Simulator Tests of a Nine-Story Steel Frame with Columns Allowed to Uplift," by A.A. Huckelbridge - 1977 (PB 277 944)A09

UCB/EERC-77/24 "Nonlinear Soil-Structure Interaction of Skew Highway Bridges," by M.-C. Chen and J. Penzien - 1977 (PB 276 176)A07

UCB/EERC-77/25 "Seismic Analysis of an Offshore Structure Supported on Pile Foundations," by D.D.-N. Liou and J. Penzien 1977 (PB 283 180)A06

UCB/EERC-77/26 "Dynamic Stiffness Matrices for Homogeneous Viscoelastic Half-Planes," by G. Dasgupta and A.K. Chopra - 1977 (PB 279 654)A06

Preceding page blank

UCB/EERC-77/27 "A Practical Soft Story Earthquake Isolation System," by J.M. Kelly, J.M. Eidinger and C.J. Derham - 1977 (PB 276 814)A07

UCB/EERC-77/28 "Seismic Safety of Existing Buildings and Incentives for Hazard Mitigation in San Francisco: An Exploratory Study," by A.J. Meltsner - 1977 (PB 281 970)A05

UCB/EERC-77/29 "Dynamic Analysis of Electrohydraulic Shaking Tables," by D. Rea, S. Abedi-Hayati and Y. Takahashi 1977 (PB 282 569)A04

UCB/EERC-77/30 "An Approach for Improving Seismic - Resistant Behavior of Reinforced Concrete Interior Joints," by B. Galunic, V.V. Bertero and E.P. Popov - 1977 (PB 290 870)A06

UCB/EERC-78/01 "The Development of Energy-Absorbing Devices for Aseismic Base Isolation Systems," by J.M. Kelly and D.F. Tsztoo - 1978 (PB 284 978)A04

UCB/EERC-78/02 "Effect of Tensile Prestrain on the Cyclic Response of Structural Steel Connections, by J.G. Bouwkamp and A. Mukhopadhyay - 1978

UCB/EERC-78/03 "Experimental Results of an Earthquake Isolation System using Natural Rubber Bearings," by J.M. Eidinger and J.M. Kelly - 1978 (PB 281 686)A04

UCB/EERC-78/04 "Seismic Behavior of Tall Liquid Storage Tanks," by A. Niwa - 1978 (PB 284 017)A14

UCB/EERC-78/05 "Hysteretic Behavior of Reinforced Concrete Columns Subjected to High Axial and Cyclic Shear Forces," by S.W. Zagajeski, V.V. Bertero and J.G. Bouwkamp - 1978 (PB 283 858)A13

UCB/EERC-78/06 "Three Dimensional Inelastic Frame Elements for the ANSR-I Program," by A. Riahi, D.G. Row and G.H. Powell - 1978 (PB 295 755)A04

UCB/EERC-78/07 "Studies of Structural Response to Earthquake Ground Motion," by O.A. Lopez and A.K. Chopra - 1978 (PB 282 790)A05

UCB/EERC-78/08 "A Laboratory Study of the Fluid-Structure Interaction of Submerged Tanks and Caissons in Earthquakes," by R.C. Byrd - 1978 (PB 284 957)A08

UCB/EERC-78/09 Unassigned

UCB/EERC-78/10 "Seismic Performance of Nonstructural and Secondary Structural Elements," by I. Sakamoto - 1978 (PB81 154 593)A05

UCB/EERC-78/11 "Mathematical Modelling of Hysteresis Loops for Reinforced Concrete Columns," by S. Nakata, T. Sproul and J. Penzien - 1978 (PB 298 274)A05

UCB/EERC-78/12 "Damageability in Existing Buildings," by T. Blejwas and B. Bresler - 1978 (PB 80 166 978)A05

UCB/EERC-78/13 "Dynamic Behavior of a Pedestal Base Multistory Building," by R.M. Stephen, E.L. Wilson, J.G. Bouwkamp and M. Button - 1978 (PB 286 650)A08

UCB/EERC-78/14 "Seismic Response of Bridges - Case Studies," by R.A. Imbsen, V. Nutt and J. Penzien - 1978 (PB 286 503)A10

UCB/EERC-78/15 "A Substructure Technique for Nonlinear Static and Dynamic Analysis," by D.G. Row and G.H. Powell - 1978 (PB 288 077)A10

UCB/EERC-78/16 "Seismic Risk Studies for San Francisco and for the Greater San Francisco Bay Area," by C.S. Oliveira - 1978 (PB 81 120 115)A07

UCB/EERC-78/17 "Strength of Timber Roof Connections Subjected to Cyclic Loads," by P. Gülkan, R.L. Mayes and R.W. Clough - 1978 (HUD-000 1491)A07

UCB/EERC-78/18 "Response of K-Braced Steel Frame Models to Lateral Loads," by J.G. Bouwkamp, R.M. Stephen and E.P. Popov - 1978

UCB/EERC-78/19 "Rational Design Methods for Light Equipment in Structures Subjected to Ground Motion," by J.L. Sackman and J.M. Kelly - 1978 (PB 292 357)A04

UCB/EERC-78/20 "Testing of a Wind Restraint for Aseismic Base Isolation," by J.M. Kelly and D.E. Chitty - 1978 (PB 292 833)A03

UCB/EERC-78/21 "APOLLO - A Computer Program for the Analysis of Pore Pressure Generation and Dissipation in Horizontal Sand Layers During Cyclic or Earthquake Loading," by P.P. Martin and H.B. Seed - 1978 (PB 292 835)A04

UCB/EERC-78/22 "Optimal Design of an Earthquake Isolation System," by M.A. Bhatti, K.S. Pister and E. Polak - 1978 (PB 294 735)A06

UCB/EERC-78/23 "MASH - A Computer Program for the Non-Linear Analysis of Vertically Propagating Shear Waves in Horizontally Layered Deposits," by P.P. Martin and H.B. Seed - 1978 (PB 293 101)A05

UCB/EERC-78/24 "Investigation of the Elastic Characteristics of a Three Story Steel Frame Using System Identification," by I. Kaya and H.D. McNiven - 1978 (PB 296 225)A06

UCB/EERC-78/25 "Investigation of the Nonlinear Characteristics of a Three-Story Steel Frame Using System Identification," by I. Kaya and H.D. McNiven - 1978 (PB 301 363)A05

UCB/EERC-78/26 "Studies of Strong Ground Motion in Taiwan," by Y.M. Hsiung, B.A. Bolt and J. Penzien - 1978 (PB 298 436)A06

UCB/EERC-78/27 "Cyclic Loading Tests of Masonry Single Piers: Volume 1 - Height to Width Ratio of 2," by P.A. Hidalgo, R.L. Mayes, H.D. McNiven and R.W. Clough - 1978 (PB 296 211)A07

UCB/EERC-78/28 "Cyclic Loading Tests of Masonry Single Piers: Volume 2 - Height to Width Ratio of 1," by S.-W.J. Chen, P.A. Hidalgo, R.L. Mayes, R.W. Clough and H.D. McNiven - 1978 (PB 296 212)A09

UCB/EERC-78/29 "Analytical Procedures in Soil Dynamics," by J. Lysmer - 1978 (PB 298 445)A06

UCB/EERC-79/01 "Hysteretic Behavior of Lightweight Reinforced Concrete Beam-Column Subassemblages," by B. Forzani, E.P. Popov and V.V. Bertero - April 1979(PB 298 267)A06

UCB/EERC-79/02 "The Development of a Mathematical Model to Predict the Flexural Response of Reinforced Concrete Beams to Cyclic Loads, Using System Identification," by J. Stanton & H. McNiven - Jan. 1979(PB 295 875)A10

UCB/EERC-79/03 "Linear and Nonlinear Earthquake Response of Simple Torsionally Coupled Systems," by C.L. Kan and A.K. Chopra - Feb. 1979(PB 298 262)A06

UCB/EERC-79/04 "A Mathematical Model of Masonry for Predicting its Linear Seismic Response Characteristics," by Y. Mengi and H.D. McNiven - Feb. 1979(PB 298 266)A06

UCB/EERC-79/05 "Mechanical Behavior of Lightweight Concrete Confined by Different Types of Lateral Reinforcement," by M.A. Manrique, V.V. Bertero and E.P. Popov - May 1979(PB 301 114)A06

UCB/EERC-79/06 "Static Tilt Tests of a Tall Cylindrical Liquid Storage Tank," by R.W. Clough and A. Niwa - Feb. 1979 (PB 301 167)A06

UCB/EERC-79/07 "The Design of Steel Energy Absorbing Restrainers and Their Incorporation into Nuclear Power Plants for Enhanced Safety: Volume 1 - Summary Report," by P.N. Spencer, V.F. Zackay, and E.R. Parker - Feb. 1979(UCB/EERC-79/07)A09

UCB/EERC-79/08 "The Design of Steel Energy Absorbing Restrainers and Their Incorporation into Nuclear Power Plants for Enhanced Safety: Volume 2 - The Development of Analyses for Reactor System Piping,""Simple Systems" by M.C. Lee, J. Penzien, A.K. Chopra and K, Suzuki "Complex Systems" by G.H. Powell, E.L. Wilson, R.W. Clough and D.G. Row - Feb. 1979(UCB/EERC-79/08)A10

UCB/EERC-79/09 "The Design of Steel Energy Absorbing Restrainers and Their Incorporation into Nuclear Power Plants for Enhanced Safety: Volume 3 - Evaluation of Commercial Steels," by W.S. Owen, R.M.N. Pelloux, R.O. Ritchie, M. Faral, T. Ohhashi, J. Toplosky, S.J. Hartman, V.F. Zackay and E.R. Parker - Feb. 1979(UCB/EERC-79/09)A04

UCB/EERC-79/10 "The Design of Steel Energy Absorbing Restrainers and Their Incorporation into Nuclear Power Plants for Enhanced Safety: Volume 4 - A Review of Energy-Absorbing Devices," by J.M. Kelly and M.S. Skinner - Feb. 1979(UCB/EERC-79/10)A04

UCB/EERC-79/11 "Conservatism In Summation Rules for Closely Spaced Modes," by J.M. Kelly and J.L. Sackman - May 1979(PB 301 328)A03

UCB/EERC-79/12 "Cyclic Loading Tests of Masonry Single Piers; Volume 3 - Height to Width Ratio of 0.5," by P.A. Hidalgo, R.L. Mayes, H.D. McNiven and R.W. Clough - May 1979(PB 301 321)A08

UCB/EERC-79/13 "Cyclic Behavior of Dense Course-Grained Materials in Relation to the Seismic Stability of Dams," by N.G. Banerjee, H.B. Seed and C.K. Chan - June 1979(PB 301 373)A13

UCB/EERC-79/14 "Seismic Behavior of Reinforced Concrete Interior Beam-Column Subassemblages," by S. Viwathanatepa, E.P. Popov and V.V. Bertero - June 1979(PB 301 326)A10

UCB/EERC-79/15 "Optimal Design of Localized Nonlinear Systems with Dual Performance Criteria Under Earthquake Excitations," by M.A. Bhatti - July 1979(PB 80 167 109)A06

UCB/EERC-79/16 "OPTDYN - A General Purpose Optimization Program for Problems with or without Dynamic Constraints," by M.A. Bhatti, E. Polak and K.S. Pister - July 1979(PB 80 167 091)A05

UCB/EERC-79/17 "ANSR-II, Analysis of Nonlinear Structural Response, Users Manual," by D.P. Mondkar and G.H. Powell July 1979(PB 80 113 301)A05

UCB/EERC-79/18 "Soil Structure Interaction in Different Seismic Environments," A. Gomez-Masso, J. Lysmer, J.-C. Chen and H.B. Seed - August 1979(PB 80 101 520)A04

UCB/EERC-79/19 "ARMA Models for Earthquake Ground Motions," by M.K. Chang, J.W. Kwiatkowski, R.F. Nau, R.M. Oliver and K.S. Pister - July 1979(PB 301 166)A05

UCB/EERC-79/20 "Hysteretic Behavior of Reinforced Concrete Structural Walls," by J.M. Vallenas, V.V. Bertero and E.P. Popov - August 1979(PB 80 165 905)A12

UCB/EERC-79/21 "Studies on High-Frequency Vibrations of Buildings - 1: The Column Effect," by J. Lubliner - August 1979 (PB 80 158 553)A03

UCB/EERC-79/22 "Effects of Generalized Loadings on Bond Reinforcing Bars Embedded in Confined Concrete Blocks," by S. Viwathanatepa, E.P. Popov and V.V. Bertero - August 1979(PB 81 124 018)A14

UCB/EERC-79/23 "Shaking Table Study of Single-Story Masonry Houses, Volume 1: Test Structures 1 and 2," by P. Gülkan, R.L. Mayes and R.W. Clough - Sept. 1979 (HUD-000 1763)A12

UCB/EERC-79/24 "Shaking Table Study of Single-Story Masonry Houses, Volume 2: Test Structures 3 and 4," by P. Gülkan, R.L. Mayes and R.W. Clough - Sept. 1979 (HUD-000 1836)A12

UCB/EERC-79/25 "Shaking Table Study of Single-Story Masonry Houses, Volume 3: Summary, Conclusions and Recommendations," by R.W. Clough, R.L. Mayes and P. Gülkan - Sept. 1979 (HUD-000 1837)A06

UCB/EERC-79/26 "Recommendations for a U.S.-Japan Cooperative Research Program Utilizing Large-Scale Testing Facilities," by U.S.-Japan Planning Group - Sept. 1979(PB 301 407)A06

UCB/EERC-79/27 "Earthquake-Induced Liquefaction Near Lake Amatitlan, Guatemala," by H.B. Seed, I. Arango, C.K. Chan, A. Gomez-Masso and R. Grant de Ascoli - Sept. 1979(NUREG-CR1341)A03

UCB/EERC-79/28 "Infill Panels: Their Influence on Seismic Response of Buildings," by J.W. Axley and V.V. Bertero Sept. 1979(PB 80 163 371)A10

UCB/EERC-79/29 "3D Truss Bar Element (Type 1) for the ANSR-II Program," by D.P. Mondkar and G.H. Powell - Nov. 1979 (PB 80 169 709)A02

UCB/EERC-79/30 "2D Beam-Column Element (Type 5 - Parallel Element Theory) for the ANSR-II Program," by D.G. Row, G.H. Powell and D.P. Mondkar - Dec. 1979(PB 80 167 224)A03

UCB/EERC-79/31 "3D Beam-Column Element (Type 2 - Parallel Element Theory) for the ANSR-II Program," by A. Riahi, G.H. Powell and D.P. Mondkar - Dec. 1979(PB 80 167 216)A03

UCB/EERC-79/32 "On Response of Structures to Stationary Excitation," by A. Der Kiureghian - Dec. 1979(PB 80166 929)A03

UCB/EERC-79/33 "Undisturbed Sampling and Cyclic Load Testing of Sands," by S. Singh, H.B. Seed and C.K. Chan Dec. 1979(ADA 087 298)A07

UCB/EERC-79/34 "Interaction Effects of Simultaneous Torsional and Compressional Cyclic Loading of Sand," by P.M. Griffin and W.N. Houston - Dec. 1979(ADA 092 352)A15

UCB/EERC-80/01 "Earthquake Response of Concrete Gravity Dams Including Hydrodynamic and Foundation Interaction Effects," by A.K. Chopra, P. Chakrabarti and S. Gupta - Jan. 1980(AD-A087297)A10

UCB/EERC-80/02 "Rocking Response of Rigid Blocks to Earthquakes," by C.S. Yim, A.K. Chopra and J. Penzien - Jan. 1980 (PB80 166 002)A04

UCB/EERC-80/03 "Optimum Inelastic Design of Seismic-Resistant Reinforced Concrete Frame Structures," by S.W. Zagajeski and V.V. Bertero - Jan. 1980(PB80 164 635)A06

UCB/EERC-80/04 "Effects of Amount and Arrangement of Wall-Panel Reinforcement on Hysteretic Behavior of Reinforced Concrete Walls," by R. Iliya and V.V. Bertero - Feb. 1980(PB81 122 525)A09

UCB/EERC-80/05 "Shaking Table Research on Concrete Dam Models," by A. Niwa and R.W. Clough - Sept. 1980(PB81 122 368)A06

UCB/EERC-80/06 "The Design of Steel Energy-Absorbing Restrainers and their Incorporation into Nuclear Power Plants for Enhanced Safety (Vol 1A): Piping with Energy Absorbing Restrainers: Parameter Study on Small Systems," by G.H. Powell, C. Oughourlian and J. Simons - June 1980

UCB/EERC-80/07 "Inelastic Torsional Response of Structures Subjected to Earthquake Ground Motions," by Y. Yamazaki April 1980(PB81 122 327)A08

UCB/EERC-80/08 "Study of X-Braced Steel Frame Structures Under Earthquake Simulation," by Y. Ghanaat - April 1980 (PB81 122 335)A11

UCB/EERC-80/09 "Hybrid Modelling of Soil-Structure Interaction," by S. Gupta, T.W. Lin, J. Penzien and C.S. Yeh May 1980(PB81 122 319)A07

UCB/EERC-80/10 "General Applicability of a Nonlinear Model of a One Story Steel Frame," by B.I. Sveinsson and H.D. McNiven - May 1980(PB81 124 877)A06

UCB/EERC-80/11 "A Green-Function Method for Wave Interaction with a Submerged Body," by W. Kioka - April 1980 (PB81 122 269)A07

UCB/EERC-80/12 "Hydrodynamic Pressure and Added Mass for Axisymmetric Bodies," by F. Nilrat - May 1980(PB81 122 343)A08

UCB/EERC-80/13 "Treatment of Non-Linear Drag Forces Acting on Offshore Platforms," by B.V. Dao and J. Penzien May 1980(PB81 153 413)A07

UCB/EERC-80/14 "2D Plane/Axisymmetric Solid Element (Type 3 - Elastic or Elastic-Perfectly Plastic) for the ANSR-II Program," by D.P. Mondkar and G.H. Powell - July 1980(PB81 122 350)A03

UCB/EERC-80/15 "A Response Spectrum Method for Random Vibrations," by A. Der Kiureghian - June 1980(PB81 122 301)A03

UCB/EERC-80/16 "Cyclic Inelastic Buckling of Tubular Steel Braces," by V.A. Zayas, E.P. Popov and S.A. Mahin June 1980(PB81 124 885)A10

UCB/EERC-80/17 "Dynamic Response of Simple Arch Dams Including Hydrodynamic Interaction," by C.S. Porter and A.K. Chopra - July 1980(PB81 124 000)A13

UCB/EERC-80/18 "Experimental Testing of a Friction Damped Aseismic Base Isolation System with Fail-Safe Characteristics," by J.M. Kelly, K.E. Beucke and M.S. Skinner - July 1980(PB81 148 595)A04

UCB/EERC-80/19 "The Design of Steel Energy-Absorbing Restrainers and their Incorporation into Nuclear Power Plants for Enhanced Safety (Vol 1B): Stochastic Seismic Analyses of Nuclear Power Plant Structures and Piping Systems Subjected to Multiple Support Excitations," by M.C. Lee and J. Penzien - June 1980

UCB/EERC-80/20 "The Design of Steel Energy-Absorbing Restrainers and their Incorporation into Nuclear Power Plants for Enhanced Safety (Vol 1C): Numerical Method for Dynamic Substructure Analysis," by J.M. Dickens and E.L. Wilson - June 1980

UCB/EERC-80/21 "The Design of Steel Energy-Absorbing Restrainers and their Incorporation into Nuclear Power Plants for Enhanced Safety (Vol 2): Development and Testing of Restraints for Nuclear Piping Systems," by J.M. Kelly and M.S. Skinner - June 1980

UCB/EERC-80/22 "3D Solid Element (Type 4-Elastic or Elastic-Perfectly-Plastic) for the ANSR-II Program," by D.P. Mondkar and G.H. Powell - July 1980(PB81 123 242)A03

UCB/EERC-80/23 "Gap-Friction Element (Type 5) for the ANSR-II Program," by D.P. Mondkar and G.H. Powell - July 1980 (PB81 122 285)A03

UCB/EERC-80/24 "U-Bar Restraint Element (Type 11) for the ANSR-II Program," by C. Oughourlian and G.H. Powell July 1980(PB81 122 293)A03

UCB/EERC-80/25 "Testing of a Natural Rubber Base Isolation System by an Explosively Simulated Earthquake," by J.M. Kelly - August 1980(PB81 201 360)A04

UCB/EERC-80/26 "Input Identification from Structural Vibrational Response," by Y. Hu - August 1980(PB81 152 308)A05

UCB/EERC-80/27 "Cyclic Inelastic Behavior of Steel Offshore Structures," by V.A. Zayas, S.A. Mahin and E.P. Popov August 1980(PB81 196 180)A15

UCB/EERC-80/28 "Shaking Table Testing of a Reinforced Concrete Frame with Biaxial Response," by M.G. Oliva October 1980(PB81 154 304)A10

UCB/EERC-80/29 "Dynamic Properties of a Twelve-Story Prefabricated Panel Building," by J.G. Bouwkamp, J.P. Kollegger and R.M. Stephen - October 1980(PB82 117 128)A06

UCB/EERC-80/30 "Dynamic Properties of an Eight-Story Prefabricated Panel Building," by J.G. Bouwkamp, J.P. Kollegger and R.M. Stephen - October 1980(PB81 200 313)A05

UCB/EERC-80/31 "Predictive Dynamic Response of Panel Type Structures Under Earthquakes," by J.P. Kollegger and J.G. Bouwkamp - October 1980(PB81 152 316)A04

UCB/EERC-80/32 "The Design of Steel Energy-Absorbing Restrainers and their Incorporation into Nuclear Power Plants for Enhanced Safety (Vol 3): Testing of Commercial Steels in Low-Cycle Torsional Fatigue," by P. Spencer, E.R. Parker, E. Jongewaard and M. Drory

UCB/EERC-80/33 "The Design of Steel Energy-Absorbing Restrainers and their Incorporation into Nuclear Power Plants for Enhanced Safety (Vol 4): Shaking Table Tests of Piping Systems with Energy-Absorbing Restrainers," by S.F. Stiemer and W.G. Godden - Sept. 1980

UCB/EERC-80/34 "The Design of Steel Energy-Absorbing Restrainers and their Incorporation into Nuclear Power Plants for Enhanced Safety (Vol 5): Summary Report," by P. Spencer

UCB/EERC-80/35 "Experimental Testing of an Energy-Absorbing Base Isolation System," by J.M. Kelly, M.S. Skinner and K.E. Beucke - October 1980(PB81 154 072)A04

UCB/EERC-80/36 "Simulating and Analyzing Artificial Non-Stationary Earthquake Ground Motions," by R.F. Nau, R.M. Oliver and K.S. Pister - October 1980(PB81 153 397)A04

UCB/EERC-80/37 "Earthquake Engineering at Berkeley - 1980," - Sept. 1980(PB81 205 874)A09

UCB/EERC-80/38 "Inelastic Seismic Analysis of Large Panel Buildings," by V. Schricker and G.H. Powell - Sept. 1980 (PB81 154 338)A13

UCB/EERC-80/39 "Dynamic Response of Embankment, Concrete-Gravity and Arch Dams Including Hydrodynamic Interaction," by J.F. Hall and A.K. Chopra - October 1980(PB81 152 324)A11

UCB/EERC-80/40 "Inelastic Buckling of Steel Struts Under Cyclic Load Reversal," by R.G. Black, W.A. Wenger and E.P. Popov - October 1980(PB81 154 312)A08

UCB/EERC-80/41 "Influence of Site Characteristics on Building Damage During the October 3, 1974 Lima Earthquake," by P. Repetto, I. Arango and H.B. Seed - Sept. 1980(PB81 161 739)A05

UCB/EERC-80/42 "Evaluation of a Shaking Table Test Program on Response Behavior of a Two Story Reinforced Concrete Frame," by J.M. Blondet, R.W. Clough and S.A. Mahin

UCB/EERC-80/43 "Modelling of Soil-Structure Interaction by Finite and Infinite Elements," by F. Medina - December 1980(PB81 229 270)A04

UCB/EERC-81/01 "Control of Seismic Response of Piping Systems and Other Structures by Base Isolation," edited by J.M. Kelly - January 1981 (PB81 200 735)A05

UCB/EERC-81/02 "OPTNSR - An Interactive Software System for Optimal Design of Statically and Dynamically Loaded Structures with Nonlinear Response," by M.A. Bhatti, V. Ciampi and K.S. Pister - January 1981 (PB81 218 851)A09

UCB/EERC-81/03 "Analysis of Local Variations in Free Field Seismic Ground Motions," by J.-C. Chen, J. Lysmer and H.B. Seed - January 1981 (AD-A099508)A13

UCB/EERC-81/04 "Inelastic Structural Modeling of Braced Offshore Platforms for Seismic Loading," by V.A. Zayas, P.-S.B. Shing, S.A. Mahin and E.P. Popov - January 1981(PB82 138 777)A07

UCB/EERC-81/05 "Dynamic Response of Light Equipment in Structures," by A. Der Kiureghian, J.L. Sackman and B. Nour-Omid - April 1981 (PB81 218 497)A04

UCB/EERC-81/06 "Preliminary Experimental Investigation of a Broad Base Liquid Storage Tank," by J.G. Bouwkamp, J.P. Kollegger and R.M. Stephen - May 1981(PB82 140 385)A03

UCB/EERC-81/07 "The Seismic Resistant Design of Reinforced Concrete Coupled Structural Walls," by A.E. Aktan and V.V. Bertero - June 1981(PB82 113 358)A11

UCB/EERC-81/08 "The Undrained Shearing Resistance of Cohesive Soils at Large Deformations," by M.R. Pyles and H.B. Seed - August 1981

UCB/EERC-81/09 "Experimental Behavior of a Spatial Piping System with Steel Energy Absorbers Subjected to a Simulated Differential Seismic Input," by S.F. Stiemer, W.G. Godden and J.M. Kelly - July 1981

UCB/EERC-81/10 "Evaluation of Seismic Design Provisions for Masonry in the United States," by B.I. Sveinsson, R.L. Mayes and H.D. McNiven - August 1981

UCB/EERC-81/11 "Two-Dimensional Hybrid Modelling of Soil-Structure Interaction," by T.-J. Tzong, S. Gupta and J. Penzien - August 1981(PB82 142 118)A04

UCB/EERC-81/12 "Studies on Effects of Infills in Seismic Resistant R/C Construction," by S. Brokken and V.V. Bertero - September 1981

UCB/EERC-81/13 "Linear Models to Predict the Nonlinear Seismic Behavior of a One-Story Steel Frame," by H. Valdimarsson, A.H. Shah and H.D. McNiven - September 1981(PB82 138 793)A07

UCB/EERC-81/14 "TLUSH: A Computer Program for the Three-Dimensional Dynamic Analysis of Earth Dams," by T. Kagawa, L.H. Mejia, H.B. Seed and J. Lysmer - September 1981(PB82 139 940)A06

UCB/EERC-81/15 "Three Dimensional Dynamic Response Analysis of Earth Dams," by L.H. Mejia and H.B. Seed - September 1981 (PB82 137 274)A12

UCB/EERC-81/16 "Experimental Study of Lead and Elastomeric Dampers for Base Isolation Systems," by J.M. Kelly and S.B. Hodder - October 1981 (PB82 166 182)A05

UCB/EERC-81/17 "The Influence of Base Isolation on the Seismic Response of Light Secondary Equipment," by J.M. Kelly - April 1981 (PB82 255 266)A04

UCB/EERC-81/18 "Studies on Evaluation of Shaking Table Response Analysis Procedures," by J. Marcial Blondet - November 1981 (PB82 197 278)A10

UCB/EERC-81/19 "DELIGHT.STRUCT: A Computer-Aided Design Environment for Structural Engineering," by R.J. Balling, K.S. Pister and E. Polak - December 1981 (PB82 218 496)A07

UCB/EERC-81/20 "Optimal Design of Seismic-Resistant Planar Steel Frames," by R.J. Balling, V. Ciampi, K.S. Pister and E. Polak - December 1981 (PB82 220 179)A07

UCB/EERC-82/01 "Dynamic Behavior of Ground for Seismic Analysis of Lifeline Systems," by T. Sato and A. Der Kiureghian January 1982 (PB82 218 926)A05

UCB/EERC-82/02 "Shaking Table Tests of a Tubular Steel Frame Model," by Y. Ghanaat and R. W. Clough - January 1982 (PB82 220 161)A07

UCB/EERC-82/03 "Experimental Behavior of a Spatial Piping System with Shock Arrestors and Energy Absorbers under Seismic Excitation," by S. Schneider, H.-M. Lee and G. W. Godden - May 1982

UCB/EERC-82/04 "New Approaches for the Dynamic Analysis of Large Structural Systems," by E. L. Wilson - June 1982 (PB83 148 080)A05

UCB/EERC-82/05 "Model Study of Effects of Damage on the Vibration Properties of Steel Offshore Platforms," by F. Shahrivar and J. G. Bouwkamp - June 1982

UCB/EERC-82/06 "States of the Art and Practice in the Optimum Seismic Design and Analytical Response Prediction of R/C Frame-Wall Structures," by A. E. Aktan and V. V. Bertero - July 1982 (PB83 147 736)A05

UCB/EERC-82/07 "Further Study of the Earthquake Response of a Broad Cylindrical Liquid-Storage Tank Model," by G. C. Manos and R. W. Clough - July 1982 (PB83 147 744)A11

UCB/EERC-82/08 "An Evaluation of the Design and Analytical Seismic Response of a Seven Story Reinforced Concrete Frame - Wall Structure," by F. A. Charney and V. V. Bertero - July 1982

UCB/EERC-82/09 "Fluid-Structure Interactions: Added Mass Computations for Incompressible Fluid," by J. S.-H. Kuo - August 1982

UCB/EERC-82/10 "Joint-Opening Nonlinear Mechanism: Interface Smeared Crack Model," by J. S.-H. Kuo - August 1982 (PB83 149 195)A05

UCB/EERC-82/11 "Dynamic Response Analysis of Techi Dam," by R. W. Clough, R. M. Stephen and J. S.-H. Kuo - August 1982 (PB83 147 496)A06

UCB/EERC-82/12 "Prediction of the Seismic Responses of R/C Frame-Coupled Wall Structures," by A. E. Aktan, V. V. Bertero and M. Piazza - August 1982 (PB83 149 203)A09

UCB/EERC-82/13 "Preliminary Report on the SMART 1 Strong Motion Array in Taiwan," by B. A. Bolt, C. H. Loh, J. Penzien, Y. B. Tsai and Y. T. Yeh - August 1982

UCB/EERC-82/14 "Shaking-Table Studies of an Eccentrically X-Braced Steel Structure," by M. S. Yang - September 1982

UCB/EERC-82/15 "The Performance of Stairways in Earthquakes," by C. Roha, J. W. Axley and V. V. Bertero - September 1982

UCB/EERC-82/16 "The Behavior of Submerged Multiple Bodies in Earthquakes," by W.-G. Liao - September 1982

UCB/EERC-82/17 "Effects of Concrete Types and Loading Conditions on Local Bond-Slip Relationships," by A. D. Cowell, E. P. Popov and V. V. Bertero - September 1982 (PB83 153 577)A04

UCB/EERC-82/18 "Mechanical Behavior of Shear Wall Vertical Boundary Members: An Experimental Investigation," by M. T. Wagner and V. V. Bertero - October 1982 (PB83 159 764)A05

UCB/EERC-82/19 "Experimental Studies of Multi-support Seismic Loading on Piping Systems," by J. M. Kelly and A. D. Cowell - November 1982

UCB/EERC-82/20 "Generalized Plastic Hinge Concepts for 3D Beam-Column Elements," by P. F.-S. Chen and G. H. Powell - November 1982

UCB/EERC-82/21 "ANSR-III: General Purpose Computer Program for Nonlinear Structural Analysis," by C. V. Oughourlian and G. H. Powell - November 1982

UCB/EERC-82/22 "Solution Strategies for Statically Loaded Nonlinear Structures," by J. W. Simons and G. H. Powell - November 1982

UCB/EERC-82/23 "Analytical Model of Deformed Bar Anchorages under Generalized Excitations," by V. Ciampi, R. Eligehausen, V. V. Bertero and E. P. Popov - November 1982 (PB83 169 532)A06

UCB/EERC-82/24 "A Mathematical Model for the Response of Masonry Walls to Dynamic Excitations," by H. Sucuoğlu, Y. Mengi and H. D. McNiven - November 1982 (PB83 169 011)A07

UCB/EERC-82/25 "Earthquake Response Considerations of Broad Liquid Storage Tanks," by F. J. Cambra - November 1982

UCB/EERC-82/26 "Computational Models for Cyclic Plasticity, Rate Dependence and Creep," by B. Mosaddad and G. H. Powell - November 1982

UCB/EERC-82/27 "Inelastic Analysis of Piping and Tubular Structures," by M. Mahasuverachai and G. H. Powell - November 1982

UCB/EERC-83/01 "The Economic Feasibility of Seismic Rehabilitation of Buildings by Base Isolation," by J. M. Kelly - January 1983

UCB/EERC-83/02 "Seismic Moment Connections for Moment-Resisting Steel Frames," by E. P. Popov - January 1983

UCB/EERC-83/03 "Design of Links and Beam-to-Column Connections for Eccentrically Braced Steel Frames," by E. P. Popov and J. O. Malley - January 1983

UCB/EERC-83/04 "Numerical Techniques for the Evaluation of Soil-Structure Interaction Effects in the Time Domain," by E. Bayo and E. L. Wilson - February 1983

UCB/EERC-83/05 "A Transducer for Measuring the Internal Forces in the Columns of a Frame-Wall Reinforced Concrete Structure," by R. Sause and V. V. Bertero - May 1983

UCB/EERC-83/06 "Dynamic Interactions between Floating Ice and Offshore Structures," by P. Croteau - May 1983

UCB/EERC-83/07 "Dynamic Analysis of Multiply Tunnelled and Arbitrarily Supported Secondary Systems," by T. Igusa and A. Der Kiureghian - June 1983

UCB/EERC-83/08 "A Laboratory Study of Submerged Multi-body Systems in Earthquakes," by G. R. Ansari - June 1983

UCB/EERC-83/09 "Effects of Transient Foundation Uplift on Earthquake Response of Structures," by C.-S. Yim and A. K. Chopra - June 1983

UCB/EERC-83/10 "Optimal Design of Friction-Braced Frames under Seismic Loading," by M. A. Austin and K. S. Pister - June 1983

UCB/EERC-83/11 "Shaking Table Study of Single-Story Masonry Houses: Earthquake Performance under Three Component Simulated Seismic Input and Recommendations," by G. C. Manos, R. W. Clough and R. L. Mayes - June 1983

UCB/EERC-83/12 "Experimental Error Propagation in Pseudodynamic Testing," by P. B. Shing and S. A. Mahin - June 1983

UCB/EERC-83/13 "Experimental and Analytical Predictions of the Mechanical Characteristics of a 1/5-scale Model of a 7-story R/C Frame-Wall Building Structure," by A. E. Aktan, V. V. Bertero, A. A. Chowdhury and T. Nagashima - August 1983

UCB/EERC-83/14 "Shaking Table Tests of Large-Panel Precast Concrete Building System Assemblages," by M. G. Oliva and R. W. Clough - August 1983

UCB/EERC-83/15 "Seismic Behavior of Active Beam Links in Eccentrically Braced Frames," by K. D. Hjelmstad and E. P. Popov - July 1983

UCB/EERC-83/16 "System Identification of Structures with Joint Rotation," by J. S. Dimsdale and H. D. McNiven - July 1983

UCB/EERC-83/17 "Construction of Inelastic Response Spectra for Single-Degree-of-Freedom Systems", by S. Mahin and J. Lin - July 1983

UCB/EERC-83/18 "Interactive Computer Analysis Methods for Predicting the Inelastic Cyclic Behavior of Sections," by S. Kaba and S. Mahin - July 1983

UCB/EERC-83/19 "Effects of Bond Deterioration on Hysteretic Behavior of Reinforced Concrete Joints," by F. C. Filippou, E. P. Popov and V. V. Bertero - August 1983